Interplay between TPS proteins and the SnRK1 kinase in the regulation of plant growth and development

Diana Reis-Barata

Dissertation presented to obtain the Ph.D degree in Plant Sciences – Plants for Life

Instituto de Tecnologia Química e Biológica António Xavier | Universidade Nova de Lisboa

Research work coordinated by: INSTITUTO GULBENKIAN DE CIÊNCIA; Max Planck Institute of Molecular Plant Physiology

Oeiras, June, 2025

ITQB UNIVERSIDADE NOVA DE LISBOA

Financial support from Fundação para a Ciência e a Tecnologia, Portugal, through grant PD/BD/150239/2019 awarded to Diana Reis Barata

Supervisors: Elena Baena-González
John E. Lunn

Co-Supervisor: Mark Stitt

Jury Members

Supervisors:

Dr. Elena Baena-González
University of Oxford, Department of Biology
Oxford, United Kingdom

Dr. John E. Lunn
Max Planck Institute of Molecular Plant Physiology
Golm, Germany

Co-supervisor:

Prof. Dr. Dr. h.c. Mark Stitt em.
Max Planck Institute of Molecular Plant Physiology
Golm, Germany

Examiners:

Prof. Dr. Alisdair Fernie
Max Planck Institute of Molecular Plant Physiology
Golm, Germany

PD Dr. Christoph Weiste
University of Wuerzburg
Würzburg, Germany

Dr. Jörg Becker
Instituto de Tecnologia Química e Biológica António Xavier
Oeiras, Portugal

Dr. Rita Abranches
Instituto de Tecnologia Química e Biológica António Xavier
Oeiras, Portugal

Acknowledgments

As I reach the end of my journey as a PhD student, I often think of an image that kept me going during the hardest moments: a climber facing a steep mountain, still far from the summit, with a caption that reads “when what’s ahead feels daunting...” In the second panel, the perspective shifts, revealing the vast distance the climber has already covered. That simple change in view reminded me, time and again, to pause and acknowledge how far I’d come, even when the peak still felt out of reach. This thesis is not just the result of academic effort, but of resilience, countless compromises, and the support of many people who helped me keep climbing and who made this journey an incredibly meaningful experience.

To all members of the Plant Stress Signaling group, I am deeply grateful. Your enthusiasm and support have made the lab a place I genuinely love and hold dear. A special mention to Ana and Leonor, from whom I’ve learned so much and who also helped keep my health in check with our weekly running sessions. To all members of the Plant Molecular Biology and Plant Genomics groups who shared lab space with us at IGC, thank you warmly for the laughs, the memories, and the invaluable help.

I would especially like to acknowledge Mónica, Bruno, Joana, Rui, and Clarisse. Their presence brought immense joy to my time in the lab, and their friendship continues to uplift my days. They are truly some of the greatest gifts this PhD journey has given me.

To my supervisor Elena, I extend my deepest gratitude for guiding me from a baby master’s student into a fully grown PhD researcher. Thank you for your constant enthusiasm, patience, unwavering support, and for believing in me, especially in the moments I doubted myself. Your mentorship has shaped not only my research but also the way I approach challenges, and I will carry those lessons with me far beyond this thesis.

I would like to thank the IGC and ITQB, along with all their staff and facilities, for the invaluable help and for providing me the opportunity to work in such a welcoming and stimulating environment.

I truly thank Vera for always keeping my plants alive and healthy, and for being such a wonderful (peculiar but adorable) friend and companion throughout this adventure.

My thanks to my thesis committee members, Isabel Abreu and Tiago Lourenço, for accompanying me throughout this journey, always making time to discuss my work, and offering valuable input along the way.

To all the members of the AG Stitt group at the MPI thank you for welcoming me so warmly. You made this part of the journey not only easier but also genuinely exciting. To Regina and Steph, whose technical expertise was essential for the success of this work – thank you!

To Mark and John, a huge thank you for giving me the opportunity to work with you. I'm grateful for your enthusiasm, support, and the stimulating scientific discussions. Your expertise and willingness to share knowledge have been crucial to my academic growth.

I extend my gratitude to Ina, coordinator of the PhD program IMPRS, who always made me feel fully supported as a member of the institute.

My thanks to the MPI's facilities and staff, especially the green team and the media and labware preparation teams, for their invaluable help throughout my time there.

To all my friends at the MPI and those I met outside the institute during my time in Germany, thank you for making me feel at home despite being so far away. There are far too many to mention by name, but to Vittoria, Sofia, Eleftheria, Enrique, Zac, Fabio, Rishabh, the cool kids, the Köhler's and Figueiredo's, I send a very warm hug.

To Juju, Sara, Cátia, and all my long-term friends (too many to list) thank you for being there for me, for caring, for encouraging me, and for patiently waiting through my hermit phase until I came back around.

To my best friend and partner in life, Jota, thank you for standing by me through the good, the bad, and the ugly. Thank you for believing in me, sometimes more than I do, for your support, your warmth, and for bringing light to my darkest days. I'll never forget the quiet nights when you fell asleep on the couch across from me, just to keep me company while I worked late into the night – a silent reassurance that, even in solitude, I was never truly alone.

I would also like to dedicate this work to my mom, my dad, and my sister, without whom I would never have made it this far. Thank you for checking on me every day, for your constant care, for always being proud of me, and for encouraging me with words like, "Keep going, you're nearly there," especially when I needed it most.

While I cannot name everyone who has been part of my journey, I want to express my heartfelt thanks to all who have supported me along the way. Your presence has been invaluable in reaching this milestone.

With that, all I have left to say is… VAMOOOOOSSS!

Resumo

Para assegurar a sua adaptação e sobrevivência, é crucial que as plantas consigam monitorizar as suas reservas de carbono e ajustar dinamicamente o seu crescimento através de vias integradas de sinalização de açúcares. Um dos componentes essenciais destas vias é a molécula sinalizadora trealose 6-fosfato (T6P), cujo modo de ação integra duas funções principais. Por um lado, a T6P atua como sinalizadora da disponibilidade de sacarose e, por outro, contribui ativamente para a homeostasia deste açúcar, regulando, de forma coordenada, a sua síntese, distribuição e utilização. Consequentemente, a T6P desempenha um papel fundamental como indutora do crescimento e das transições de desenvolvimento em tecidos-dreno altamente dependentes de sacarose.

A T6P exerce parte das suas funções através da inibição da quinase SnRK1 (Sucrose Non-Fermenting 1-related Kinase 1), um complexo de proteínas extremamente conservado que atua como sensor energético e regulador de respostas ao stress e do crescimento de plantas. A SnRK1 é ativada em condições de baixa energia celular e, através de uma extensa reprogramação metabólica e transcricional, estimula o catabolismo e inibe o anabolismo, com o objetivo final de restabelecer a homeostasia energética. Deste modo, nos tecidos em crescimento, a acumulação de T6P, induzida pela sacarose, inibe a SnRK1, reduzindo a sua repressão sobre os processos anabólicos e promovendo o desenvolvimento. Em contraste, quando os níveis de sacarose diminuem, a correspondente queda nos níveis de T6P alivia a inibição da SnRK1, que, por sua vez, ativa vias catabólicas e restringe o crescimento celular dependente de energia. No entanto, os mecanismos moleculares subjacentes à perceção da T6P e à consequente inibição da SnRK1 permanecem por esclarecer.

Estudos recentes em *Arabidopsis thaliana* demonstraram que proteínas T6P-sintetase da classe II (AtTPS5-11; TPS-II), embora cataliticamente inativas, interagem fisicamente com todas as subunidades da SnRK1 e reprimem a atividade quinase da subunidade catalítica SnRK1α1. Contudo, a relevância funcional das proteínas TPS-II e das suas interações com a SnRK1 in planta, incluindo se estas interações são mediadas pela T6P, continua por determinar.

Neste estudo, utilizei uma abordagem de mutagénese combinatória, acompanhada de análises genéticas, bioquímicas, imagiológicas e fenotípicas, para investigar o papel das proteínas TPS-II no crescimento e desenvolvimento das plantas, assim como a sua influência na função da SnRK1. Os meus resultados mostram que as proteínas TPS5/6/7 são essenciais para que a T6P possa coordenar o crescimento e o desenvolvimento em função da disponibilidade de carbono. Plantas de Arabidopsis desprovidas das proteínas TPS5/6/7 apresentam um atraso na floração e defeitos acentuados no crescimento radicular, associados a um perfil metabólico indicativo de perturbações na utilização de açúcares e na sinalização de T6P. Especificamente, o mutante *tps5/6/7* acumula níveis anormalmente elevados de T6P e de açúcares solúveis, apresenta reservas de aminoácidos reduzidas, um consumo de oxigénio aumentado e uma regulação pós-translacional alterada da fosfoenolpiruvato carboxilase (PEPC) e da nitrato redutase (NR). Os meus dados sugerem ainda que estes fenótipos são dependentes da SnRK1 e provavelmente resultam de uma atividade desregulada desta quinase na ausência das proteínas TPS5/6/7. Importa salientar que os meus resultados comprovam que a T6P promove a interação entre as proteínas TPS-II e a SnRK1 de modo específico e dose-dependente, sugerindo que as TPS5/6/7 atuam como sensores de T6P que regulam a atividade da SnRK1 de acordo com a disponibilidade de carbono.

Em suma, este trabalho fornece uma compreensão mecanística de como as plantas ajustam a sua fisiologia e crescimento em função dos recursos de carbono disponíveis, estabelecendo as TPS-II como componentes essenciais da via de sinalização T6P-SnRK1.

Abstract

The ability to sense carbon availability and dynamically adjust growth through integrated sugar-sensing pathways is essential for plant adaptation and survival. A key component of these pathways is the signaling molecule trehalose 6-phosphate (T6P). T6P reflects sucrose availability and maintains sucrose homeostasis by coordinating its synthesis, allocation, and utilization. Accordingly, T6P is a key positive regulator of growth and developmental transitions in sucrose-demanding sink tissues.

T6P exerts its regulatory functions in part by inhibiting Sucrose Non-Fermenting 1-related Kinase 1 (SnRK1), a highly conserved energy-sensing protein kinase complex that governs plant stress responses and growth. SnRK1 is activated under conditions of low energy, upregulating catabolism and downregulating anabolism through a vast metabolic and transcriptional reprogramming to ultimately restore energy homeostasis. In growing tissues, sucrose-induced T6P accumulation inhibits SnRK1, releasing its brake on anabolic processes to promote growth. When sucrose is scarce, falling T6P levels relieve SnRK1 inhibition, activating catabolic pathways and restraining energy-demanding growth. However, the precise molecular mechanisms underlying T6P perception and subsequent SnRK1 inhibition remain unresolved.

Recent research in *Arabidopsis thaliana* revealed that catalytically inactive class II T6P-synthase proteins (AtTPS5-11; TPS-II) physically interact with all SnRK1 subunits and functionally repress the kinase activity of the SnRK1α1 catalytic subunit. Nevertheless, the broader functional relevance of TPS-II proteins and their interactions with SnRK1 *in planta*, including whether these interactions are driven by T6P, remain elusive.

In this study, I employed a combinatorial knockout approach together with genetic, biochemical, imaging, and phenotypic analyses to investigate the role of TPS-II proteins in plant growth and development, and their influence on SnRK1 function. My findings demonstrate that TPS5/6/7 are essential for T6P-mediated coordination of carbon availability with developmental progression and growth. Arabidopsis plants lacking TPS5/6/7 exhibit delayed flowering and pronounced root growth defects,

accompanied by a metabolic signature indicative of impaired sugar utilization and disrupted T6P signaling. Specifically, the *tps5/6/7* mutant accumulates abnormally high levels of T6P and soluble sugars, shows depleted amino acid pools, elevated oxygen consumption, and altered post-translational regulation of phosphoenolpyruvate carboxylase (PEPC) and nitrate reductase (NR). My data further suggest that these phenotypes are SnRK1-dependent and likely arise from deregulated SnRK1 activity in the absence of TPS5/6/7. Importantly, I show that T6P promotes the interaction between TPS-II proteins and SnRK1 in a specific and dose-dependent manner, suggesting that TPS5/6/7 act as T6P sensors that repress SnRK1 activity in response to carbon availability.

Altogether, this work provides mechanistic insight into how plants adjust their physiology and growth according to available carbon resources and redefines the catalytically inactive TPS-II proteins as key regulators within the T6P–SnRK1 signaling network.

Table of Contents

List of Abbreviations

2-OG	2-oxoglutarate
3-PGA	3-phosphoglyceric acid
ABA	Abscisic acid
ACC	Acetyl-CoA carboxylase
Ala	Alanine
ATP	Adenosine Triphosphate
BCAA	Branched-chain amino acids
BiFC	Bimolecular Fluorescence Complementation
CL	Control Light
CLSM	Confocal Laser Scanning Microscopy
CoA	Coenzyme A
ED	End of Day
EN	End of Night
ER	Endoplasmic Reticulum
FC	Fold change
FDR	False Discovery Rate
Fru1,6BP	Fructose 1,6-bisphosphate
Fru6P	Fructose 6-phosphate
G1P	Glucose 1-phosphate
G6P	Glucose 6-phosphate
GFP	Green Fluorescent Protein
Gln	Glutamine
Glu	Glutamate
HL	High Light
Iso	Isoleucine
Leu	Leucine
LFQ	Label-Free Quantification
Lys	Lysine

LR	Lateral Root
MD	Middle of Day
MN	Middle of Night
NLS	Nuclear Localization Signal
NR	Nitrate Reductase
O_2	Oxygen
OAA	Oxaloacetate
PEP	Phospho*enol* Pyruvate
PEPC	Phospho*enol* Pyruvate Carboxylase
PI	Propidium Iodide
PR	Primary Root
Pro	Proline
RAM	Root Apical Meristem
RFP	Red Fluorescent Protein
ROS	Reactive Oxygen Species
S6P	Sucrose 6-phosphate
SAM	Shoot Apical Meristem
SnAK	SnRK1 Activating Kinase
SnRK	Sucrose non-fermenting Related Kinase
Suc	Sucrose
SWEET	Sugars Will Eventually Be Exported Transporter
T6P	Trehalose 6-phosphate
TCA	Tricarboxylic Acid
TOR	Target of Rapamycin
TPP	Trehalose 6-phosphate phosphatase
TPS	Trehalose 6-phosphate synthase
UDPG	Uridine diphosphate glucose
Val	Valine
ZT	Zeitgeber time

List of Figures

List of Tables

CHAPTER 1

General Introduction

1.1. Carbon allocation

Energy acquisition and management are central to the biology of all life forms. In plants, this process begins with photosynthesis and involves the distribution of carbon resources to different cellular processes and to different non-photosynthetic organs like roots, flowers and seeds. Adequate carbon management is crucial for normal growth and development and for optimal stress responses, enabling plants to finely adjust their growth and development to changes in the environment (Smith and Stitt 2007). During photosynthesis, sun light is captured by pigments like chlorophylls and carotenoids, initiating an electron transport chain that reduces $NADP^+$ to NADPH and generates a proton gradient used to produce ATP. These energy carriers then power the Calvin-Benson-Bassham cycle to produce triose phosphates, which serve as central precursors for sugars (the plant's primary energy currency) and nearly all other organic compounds (Stitt et al. 2010). In Arabidopsis and other species (Caspar et al. 1985; Geiger and Servaites 1994; Geiger et al. 2000; Gibon et al. 2004; Lu et al. 2005), triose phosphates are partitioned between sucrose, readily available for growth, and starch, which is transiently stored in leaf chloroplasts (Geiger and Servaites 1994; Geiger et al. 2000) and later reconverted to sucrose when the demand for carbon exceeds the photosynthetic supply, such as during the night (Smith and Stitt 2007).

1.2. Trehalose 6-Phosphate as a key regulator of sucrose metabolism and homeostasis

Newly synthesized sucrose can be stored in vacuoles or used for local metabolic needs, but it is predominantly exported through the phloem from autotrophic source tissues to heterotrophic sink organs, where it provides energy and carbon skeletons to support growth and development (Lunn 2016). In addition to its role as a metabolic substrate, sucrose functions as a key signaling molecule that regulates numerous metabolic and developmental processes, including floral induction, shoot

branching, vascular differentiation and root architecture (Lastdrager et al. 2014; Mason et al. 2014; Göbel and Fichtner 2023). Therefore, sucrose metabolism must be tightly regulated to ensure that sucrose synthesis, export, and accumulation of carbon reserves meet the competing demands of immediate energy needs, storage, and growth while maintaining cellular homeostasis (Smith and Stitt 2007; Lastdrager et al. 2014). This regulation of sugar allocation becomes particularly important under stress conditions, when ATP production through photosynthesis and respiration is often compromised, significantly limiting plant growth (De Block and Van Lijsebettens 2011). Given these challenges, plants have evolved integrated sensing and signaling networks that monitor local sucrose availability and relay this information systemically, enabling dynamic coordination of carbon allocation with developmental and environmental cues. Trehalose 6-phosphate (T6P), the intermediate in trehalose biosynthesis, has emerged as a central sugar signaling metabolite in these networks, linking sucrose availability with growth regulation (Figueroa and Lunn 2016).

1.2.1. The T6P pathway

Trehalose is a non-reducing disaccharide composed of two glucose molecules linked by an α-α-1,1-glycosidic bond. It is ubiquitously present in prokaryotes and eukaryotes but absent in vertebrates. In plants, trehalose serves important physiological functions, being implicated in responses to both biotic (e.g. acting as a signal in plant interactions with micro-organisms and herbivorous insects) and abiotic stresses (e.g. drought, salinity, cold) (Lunn et al. 2014; Kosar et al. 2019; Hassan et al. 2023).

Trehalose synthesis in plants occurs via a conserved two-step pathway: trehalose 6-phosphate synthase (TPS) catalyzes the transfer of a glucose moiety from uridine diphosphate glucose (UDPG) to glucose 6-phosphate (G6P), forming T6P, which is subsequently dephosphorylated by trehalose 6-phosphate phosphatase (TPS) to yield trehalose (Avonce et al. 2006). *TPS* and *TPP* genes are present in all major groups of land plants, and their origin traces back to before the divergence of

streptophyte and chlorophyte evolutionary branches, indicating that the pathway was already established at the onset of the green lineage (Avonce et al. 2006; Lunn 2007). Both families have expanded during the evolution of terrestrial plants (Lunn 2007). The *Arabidopsis thaliana* genome encodes eleven *TPS* (*TPS1-11*) and ten *TPP* (*TPPA-J*) genes. Phylogenetic analyses further divide the TPS family into two distinct clades: Class I (TPS1-4; hereafter TPS-I) and Class II (TPS5-11; hereafter TPS-II) (Kaul et al. 2000; Leyman et al. 2001).

1.2.2. T6P synthase enzymes – Catalytically active TPS-I

In Arabidopsis, all TPS proteins share a common structure with a glycosyltransferase domain and a TPP-like C-terminal domain (Lunn 2007; Figure 1.1). However, only TPS-I enzymes retain catalytic activity (Delorge et al., 2015), except for TPS3, which is likely a pseudogene (Lunn 2007). TPS1, the predominant T6P-synthesizing enzyme, is crucial for plant viability, as *tps1-1* null mutants are embryo-lethal (Eastmond et al. 2002). Embryo arrest of *tps1* can be overcome by dexamethasone-inducible expression of *TPS1* during embryogenesis (Dijken et al. 2004) or expression of *TPS1* under the control of an embryo-specific (ABSCISIC ACID INSENSITIVE 3 – *ABI3*) promoter (Gómez et al. 2010). Nonetheless, the resulting plants are dwarfed and fail to flower, indicating that TPS1 is pivotal throughout all stages of plant development. This pivotal role likely stems from the absence of T6P synthesis rather than TPS1-specific signalling, as *tps1-1* null mutants complemented with a bacterial *TPS* (*OtsA)* driven by the *TPS1* promoter can complete embryogenesis and flower concurrently with wild-type (WT) plants (Fichtner et al. 2020). In contrast to TPS1, the functional significance of *TPS2* and *TPS4* remains unclear. Although both isoforms exhibit TPS activity, demonstrated by their ability to complement the yeast *tps1Δ tps2Δ* mutant (Delorge et al. 2015), they fail to compensate for the loss of *TPS1* in developing seeds of the *tps1-1* null mutant.

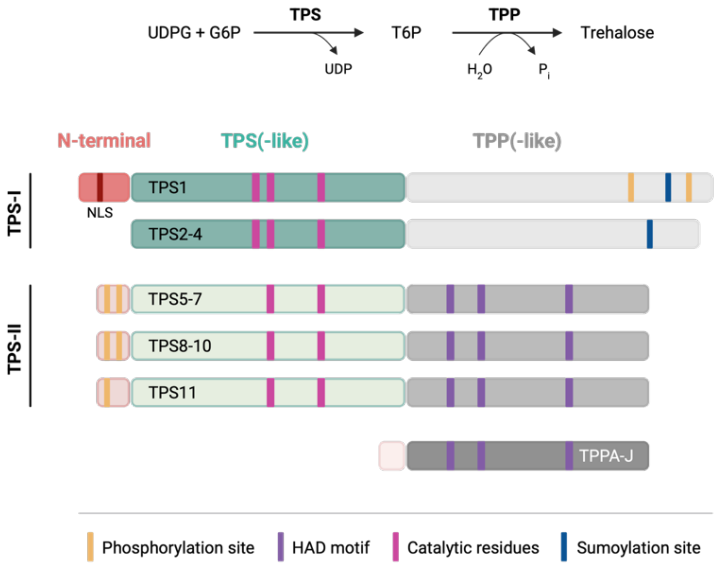

Figure 1.1. Trehalose Biosynthesis Pathway and Enzymes.
Trehalose 6-phosphate synthase (TPS) uses UDP-glucose (UDPG) and glucose 6-phosphate (G6P) to synthesize trehalose 6-phosphate (T6P), which is subsequently dephosphorylated to trehalose by trehalose 6-phosphate phosphatase (TPP). The *Arabidopsis thaliana* genome encodes 11 *TPS* genes and 10 *TPP* genes. The TPS family is subdivided into two main clades: TPS-I (*AtTPS1-AtTPS4*) and TPS-II (*AtTPS5-AtTPS11*). Only TPS-I proteins are catalytically active, with AtTPS1 functioning as the primary enzyme responsible for T6P synthesis in Arabidopsis. AtTPS1 consists of three protein domains: an N-terminal extension containing a nuclear localization signal (NLS) that directs most of the protein to the nucleus, a glycosyltransferase (TPS-like) domain, and a C-terminal domain structurally similar to TPP enzymes but lacking TPP activity. The latter, which includes a putative SUMOylation site (dark blue bar) and two phosphorylation sites (yellow bars), appears critical for catalytic fidelity. AtTPS2 and AtTPS4 also exhibit TPS activity but lack the N-terminal extension. TPS-I proteins contain a catalytic triad – Arg (R), Lys (K), and Glu (E) – required for T6P synthesis (pink bars), which is less conserved in TPS-II proteins. TPS-II proteins contain TPS- and TPP-like domains with several conserved phosphorylation sites (yellow bars) but lack enzymatic activity and their biological functions are not yet understood. Phylogenetically, *AtTPS5-7* form one subgroup, while *AtTPS8-11* cluster separately, with some studies further distinguishing *AtTPS11* from *AtTPS8-10*. All 10 *AtTPP* genes encode catalytically active TPP enzymes. Both TPS-II and TPP proteins have three conserved peptide motifs with active site residues (purple bars) in their TPP(-like) domain, characteristic of the haloacid dehalogenase (HAD) phosphatase superfamily. Adapted from Fichtner and Lunn, 2020.

The predominant role of TPS1 may potentially be explained by its unique structural features, as well as its spatiotemporal expression and tissue-specific protein distribution. In addition to the glycosyltransferase and TPP-like C-terminal domains shared among all TPS proteins, TPS1 contains an N-terminal extension (Van Dijck et al. 2002; Lunn 2007) with a putative nuclear localization signal (NLS), which targets most of the protein to the nucleus in various cell types (Fichtner et al. 2020). This N-

terminal region also harbors a putative autoinhibitory motif, demonstrated to repress enzyme activity when expressed in yeast (Van Dijck et al. 2002). Furthermore, while *TPS2* and *TPS4* are mostly expressed in developing seeds (Vandesteene et al. 2010), *TPS1* is expressed in all major tissues of the plant (Schmid et al. 2005). At the protein levels, complementation of the *tps1-1* null mutant with a GFP-tagged TPS1 protein, driven by its endogenous regulatory elements, revealed that TPS1 primarily localizes to the phloem loading zone and guard cells of leaves, the root vasculature, and the shoot apical meristem – key sites for systemic signalling and source-sink communication (Fichtner et al. 2020).

1.2.3. T6P synthase enzymes – Catalytically inactive TPS-II

Although TPS-II proteins share structural similarity with TPS-I (Figure 1.1), featuring both N-terminal TPS-like and C-terminal TPP-like domains, they appear catalytically inactive, as they cannot consistently complement the yeast *tps1Δ* mutant (Ramon et al. 2009; Vandesteene et al. 2010; Delorge et al. 2015). This lack of T6P-synthesizing activity has been attributed to variations in key active site residues within their glycosyltransferase domain (Lunn 2007). Surprisingly, despite the high conservation of active site residues in their TPP-like domain, TPS-II proteins lack TPP activity as well, failing to complement the yeast *tps2Δ* mutant (Vogel et al. 2001; Ramon et al. 2009). Consequently, the precise biological roles of TPS-II proteins remain largely elusive.

Nonetheless, the stringent purifying selection (Avonce et al. 2006) and distinct transcriptional regulation of TPS-II genes, characterized by tissue-specific expression and sensitivity to carbon, nitrogen and phytohormones (Ramon et al. 2009; Persyn et al. 2024), strongly suggests they play important regulatory roles in plant development and growth. This proposal is further reinforced by loss- and gain-of-function studies of individual *TPS-II* genes in Arabidopsis and other plant species. For example, in Arabidopsis, *TPS5* alters ABA signaling (Tian et al. 2019), pathogen defense (Wang et al. 2019), and thermotolerance (Suzuki et al. 2008), while *TPS6* influences cell

shape (Chary et al. 2008), *TPS9* impacts root development and salt tolerance (Vishal et al. 2024), and *TPS11* mediates aphid resistance (Singh et al. 2011). Overexpression of *BnaC02.TPS8* in *Brassica napus*, the orthologue of *AtTPS8*, leads to increased photosynthesis, elevated sugar levels and improved seed yield (Yuan et al. 2024). In addition, *OsTPS8* improves salt stress tolerance in rice (Vishal et al. 2019) and wheat *TPS11* confers cold tolerance when overexpressed in *A. thaliana* (Liu et al. 2019). Nevertheless, for most of these studies, the underlying molecular mechanisms remain poorly understood. Furthermore, it remains unclear whether these roles are directly mediated by TPS-II proteins, result indirectly from functions downstream of T6P or involve a combination of both.

Consistent with this, the conservation of key T6P-binding residues in TPS-II proteins suggests their function may be related to the sensing and relay of the T6P signal (Lunn 2007). Further supporting a regulatory role within the T6P pathway, yeast two-hybrid (Y2H) and bimolecular fluorescence complementation (BiFC) assays in rice demonstrate that TPS-II proteins physically interact with TPS-I proteins (Zang et al. 2011). Additionally, their structural similarity to non-catalytic subunits of the trehalose-synthesizing complex in yeast suggests they may modulate TPS-I enzyme activity (Lunn 2007).

Notably, emerging evidence on TPS-II protein localization and protein-protein interactions provides promising avenues for elucidating their mode of action. Localization studies using mCherry-tagged constructs transiently expressed in tobacco leaves have shown that all Arabidopsis TPS-II proteins localize to the endoplasmic reticulum (ER) (Van Leene et al. 2022), a central hub for nutrient and stress signaling (Liu and Li 2019). Furthermore, interactome analysis in Arabidopsis cell cultures indicates that TPS-II proteins form complexes both among themselves and with key regulators of carbon metabolism, including members of the FLZ (FCS-like zinc finger) protein family and the evolutionarily conserved SNF1-related protein kinase 1 (SnRK1) (Van Leene et al. 2022) (see sections 1.3.1 and 1.3.3 for more details on the interaction with SnRK1).

1.2.4. T6P phosphatase enzymes

The Arabidopsis genome harbors ten *TPP* genes, all encoding catalytically active enzymes capable of complementing the yeast *tps2Δ* mutant (Vogel et al. 1998; Vandesteene et al. 2012). These genes exhibit differential expression across various cell types, tissues, and developmental stages, based on a promoter-reporter gene approach, suggesting that individual TPPs have evolved distinct functions (Vandesteene et al. 2012; Van Houtte et al. 2013). Moreover, TPP proteins display a broad subcellular distribution. Some localize to specific organelles, such as chloroplasts (TPPD and TPPE) and the nucleus (TPPG, TPPI, and TPPJ), while others are distributed across two subcellular compartments: the cytosol and nuclei (TPPA, TPPB, TPPC, TPPF, and TPPH), or peroxisomes and nuclei (TPPI) (Krasensky et al. 2014; Kataya et al. 2020).

Several *TPP* genes are involved in responses to abiotic stress. In Arabidopsis, loss-of-function mutants for *TPPD* or *TPPI* are hypersensitive to salt stress (Krasensky et al. 2014; Kataya et al. 2020), whereas overexpression of *TPPF* or *TPPI* enhances drought tolerance (Lin et al. 2019, 2020). Additionally, overexpressing *TPPI* improves resistance to cold in Arabidopsis, potentially by regulating jasmonic acid (JA) synthesis and accumulation of soluble sugars (Lin et al. 2023b).

TPP proteins also play important functions in plant growth and development. For instance, auxin-dependent downregulation of TPPB is essential for normal lateral root (LR) formation (Morales-Herrera et al. 2023), and TPPI is implicated both in the control of flowering time (Kataya et al. 2020) and in the regulation of primary root (PR) growth and LR elongation, potentially by modulating auxin transport through PIN1 and PIN3 efflux carriers (Lin et al. 2020, 2023a). Moreover, in maize, loss-of-function mutations in *RAMOSA3* (*RA3*) or *ZmTPP4*, two catalytically active TPPs expressed in specific inflorescence primordia regions, result in reduced meristem determinacy and increased ear and tassel branching (Satoh-Nagasawa et al. 2006; Claeys et al. 2019). Surprisingly, the *ra3* mutant phenotype could be substantially rescued by complementation with an inactive form of *RA3*, suggesting that the branching effect

stems from a moonlighting role rather than RA3's catalytic function (Claeys et al. 2019).

1.2.5. The Suc-T6P impact on metabolic regulation

In plants, T6P and sucrose levels are positively correlated across different tissues, developmental stages, and in various species (for example, as observed in Martínez-Barajas et al. 2011; Wingler et al. 2012; Carillo et al. 2013; Martins et al. 2013; Nunes et al. 2013; Wahl et al. 2013; Henry et al. 2014; Sulpice et al. 2014; Yadav et al. 2014; Zhang et al. 2015; Fichtner et al. 2020). This correlation was initially detected in carbon-starved Arabidopsis seedlings, where endogenous sucrose and T6P levels rose in parallel upon sucrose supplementation (Lunn et al. 2006). Subsequently, Yadav et al. (2014) demonstrated that T6P levels appear to respond specifically to sucrose, with changes induced by other sugars (e.g. glucose or fructose) or nitrogen likely occurring indirectly through their conversion to sucrose. However, the precise molecular mechanisms driving the dynamic response of T6P to fluctuations in sucrose levels remain poorly elucidated. In Arabidopsis seedlings, inhibitor studies revealed that the increase in T6P levels following sucrose feeding could not be attributed to enhanced availability of the substrates for T6P synthesis (G6P and UDPG), nor changes in TPS1 protein levels. Instead, the response of T6P to exogenous sucrose supply was found to be reliant on *de novo* translation of an unidentified protein or proteins, but not on transcription (Yadav et al. 2014). A recent study demonstrated that TPS1 itself has a role in linking T6P and sucrose. Complementation of the Arabidopsis *tps1-1* null mutant with wild-type or modified variants of *TPS1* successfully rescued the mutant through embryogenesis, with T6P levels highly correlating with those of sucrose in rosettes of most of the resulting plants (Fichtner et al. 2020). However, complementation with a bacterial TPS (OtsA), a full-length TPS1 with a point mutation (A119W) in the catalytic domain, or a truncated TPS1 lacking the C-terminal domain, disrupted the T6P-sucrose correlation. This indicates that inherent properties of TPS1 might be important for the correct

functioning of the signaling pathways that link sucrose and T6P (Fichtner et al. 2020; Fichtner and Lunn 2021).

The observation that altering T6P levels through *TPS* or *TPP* overexpression in Arabidopsis resulted in changes in sucrose levels opposite to those of T6P prompted the formulation of the sucrose-T6P nexus model (Yadav et al. 2014; Figure 1.2). This model proposes that T6P serves as both an indicator of sucrose availability and a negative feedback regulator of sucrose levels, stimulating sucrose synthesis or consumption to maintain its levels within an ideal range for optimal plant function (Yadav et al. 2014; Figueroa and Lunn 2016). Such homeostatic regulation of sucrose levels by T6P involves multiple mechanisms across different tissues. During the day, an inducible rise in T6P levels in Arabidopsis leaves leads to a decrease in sucrose content via the redirection of photoassimilates away from sucrose synthesis towards the synthesis of organic and amino acids (Figueroa et al. 2016). This shift in photoassimilate partitioning is achieved by the post-translational activation of phosphoenolpyruvate carboxylase (PEPC) and nitrate reductase (NR), thereby stimulating carbon flow to the tricarboxylic acid (TCA) cycle and increasing the availability of carbon skeletons and reduced nitrogen for amino acid synthesis (Figueroa et al. 2016). Conversely, during the night or late in the day, increased levels of T6P restrict the mobilization of transitory starch reserves in Arabidopsis leaves, resulting in incomplete exhaustion of starch by dawn and accumulation of sucrose in the leaf due to slowed export (Martins et al. 2013; dos Anjos et al. 2018; Ishihara et al. 2022). Though the molecular mechanism remains unclear, this restriction is thought to operate in a step preceding maltose production while integrating inputs from the circadian clock and the measurement of time to dawn (Martins et al. 2013; dos Anjos et al. 2018; Ishihara et al. 2022).

Additional mechanisms by which T6P regulates sucrose utilization have been reported. In pea plants, T6P acts upstream of auxin biosynthesis during seed filling to promote sucrose-to-starch conversion and cell differentiation within the developing embryo (Meitzel et al. 2021). Similarly, a transient increase in T6P levels in *Nicotiana benthamiana* leaves or *Brassica napus* suspension cells induces *de novo* fatty acid

synthesis through stabilization of the WRINKLED1 (WRI1) transcription factor (Zhai et al. 2018). T6P also plays a role in sucrose allocation. Maize plants engineered to express rice *OsTPP1* during the flowering period exhibit higher yields compared to wild-type plants (Nuccio et al. 2015). Surprisingly, despite having low T6P levels in reproductive tissues, these transgenic plants display contrasting metabolite patterns in pith and florets, with reduced and increased assimilate content, respectively (Oszvald et al. 2018). These differences likely reflect the context-specific effects of T6P. In reproductive tissues, low T6P levels create a demand for sucrose that stimulates source leaves to increase photosynthesis, whereas in florets, low T6P triggers upregulation of SWEET genes in the pith, enhancing sucrose transport from the pith to the florets (Oszvald et al. 2018).

In addition to functions related to metabolism, T6P also influences gene expression, contributing to a broad shift in the balance between sucrose production and sucrose utilization for growth (Avidan et al. 2024; see Section 1.2.7).

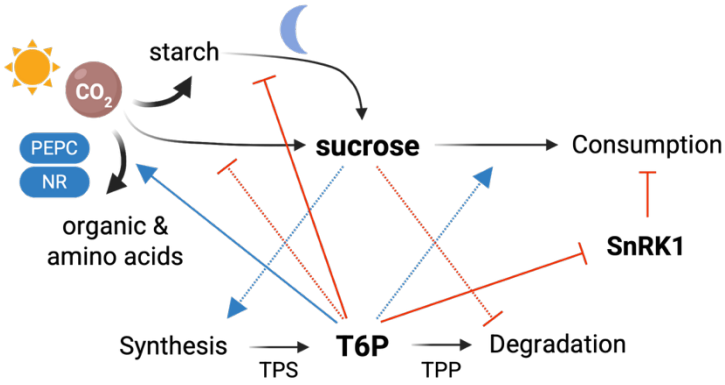

Figure 1.2. Overview of the sucrose-T6P nexus model.
During the light period, T6P controls the distribution of photoassimilates between sucrose synthesis and the production of organic acids and amino acids, partly through post-translational regulation of PEPC and NR activities (Figueroa et al., 2016). During the dark period, T6P restricts transitory starch degradation, limiting carbon availability for sucrose synthesis. T6P regulates carbon metabolism in a broadly similar manner in both source leaves during the night and sink tissues. However, the key distinction is that source leaves primarily rely on mobilizing transitory starch at night, whereas sink tissues also utilize carbon imported via the phloem. T6P enhances sucrose utilization in sink tissues, in part through the inhibition of SnRK1. Blue and red lines represent positive and negative interactions, respectively. Solid lines indicate confirmed interactions, whereas dashed lines indicate hypothetical interactions. Adapted from Baena-González and Lunn, 2020.

1.2.6. T6P impact on growth and development

Plant developmental transitions often mark the beginning of new growth phases, reliant on a substantial investment of sucrose and essential nutrients. In meristematic and dormant tissues, T6P is proposed to report the plants' sucrose status, influencing developmental decisions and sustaining subsequent growth accordingly (reviewed in Fichtner and Lunn 2021). Consistent with this, disrupting the trehalose biosynthesis pathway through changes in T6P, rather than trehalose itself, profoundly affects plant growth and development, as evidenced by the opposing phenotypes of Arabidopsis plants engineered to overexpress bacterial TPS (OtsA) or TPP (OtsB) enzymes constitutively (Schluepmann et al. 2003). Building on this foundational evidence, a growing number of studies have further highlighted the critical role of T6P in regulating various developmental transitions, such as germination, vegetative phase change, shoot and root branching, and flowering (reviewed in Göbel and Fichtner 2023).

During germination, Arabidopsis *tps1-1* embryos become arrested at the torpedo stage (Eastmond et al. 2002). Restoring the T6P synthesizing activity of TPS1 proved to be both sufficient and necessary to rescue the mutant through seed development, showing that embryogenesis is highly dependent on T6P (Fichtner et al. 2020).

T6P has also been linked to the control of vegetative phase change in Arabidopsis (Ponnu et al. 2020). Inducible expression of *TPS1* in *tps1-2;GVG::TPS1* seedlings successfully rescued the delayed vegetative phase change phenotype of the mutant and restored microRNA (miRNA) miR156 to WT-like levels, suggesting that the T6P pathway influences vegetative phase transition through the miR156-mediated age pathway (Ponnu et al. 2020).

An early indication of the significance of T6P in flowering was observed when the overexpression of heterologous *TPS* or *TPP* in Arabidopsis resulted in early or delayed flowering phenotypes, respectively (Schluepmann et al. 2003). Subsequent research by Wahl et al. (2013) revealed that TPS1 is essential for the timely onset of

flowering. Under long-day conditions, T6P signalling controls the expression of *FLOWERING LOCUS T* (*FT*) in leaves and the subsequent movement of the FT protein to the shoot apical meristem (SAM). In contrast, under short-day conditions, T6P regulates the miR156/SPL pathway within the SAM (Wahl et al. 2013). Moreover, localized overexpression of *TPS* (*OtsA*) in the vasculature resulted in increased expression of *CONSTANS* (*CO*), *FT*, and *TWIN SISTER OF FT* (*TSF*) – central regulators of the flowering process – and led to enhanced branching and early flowering. Conversely, localized overexpression of *TPP* (*OtsB*) in the vasculature resulted in decreased branching and delayed flowering. These observations collectively suggest that elevated T6P levels in the vasculature promote branching and induce flowering via *FT* expression, thus providing further support for previous findings (Fichtner et al. 2021).

Similar to its role in shoot branching, T6P also appears to regulate lateral root branching in Arabidopsis, as inducible release of T6P *in planta* or localized overexpression of a heterologous TPS (E. coli otsA) in LR primordia increased LR branching density (Morales-Herrera et al. 2023).

1.2.7. T6P impact on gene expression

In addition to its roles in metabolism and development, T6P also influences gene expression (Zhang et al. 2009; Paul et al. 2010; Avidan et al. 2024). A recent study using an inducible *OtsA* overexpressor demonstrated that transient increases in T6P levels repress genes associated with photosynthesis and gluconeogenesis, while upregulating genes involved in growth-related processes such as nucleotide biosynthesis and ribosome biogenesis in both the cytosol and mitochondria (Avidan et al. 2024). Although many differentially expressed genes identified in this study did not overlap with those reported in a previous microarray analysis of Arabidopsis seedlings with constitutive *TPS* overexpression (Zhang et al. 2009), approximately 1,500 transcripts responded robustly to elevation of T6P across both inducible and constitutive systems (Avidan et al. 2024). This partial overlap likely reflects the indirect

effects of long-term T6P elevation, which may trigger extensive metabolic and developmental reprogramming that shapes the transcriptome beyond the immediate targets of T6P signalling.

Notably, these and other studies have revealed a link between T6P and SnRK1, with several SnRK1-regulated genes responding inversely to changes in T6P levels (Baena-González et al. 2007; Zhang et al. 2009; Nunes et al. 2013a; Peixoto et al. 2021; Avidan et al. 2024). Furthermore, T6P has been shown to inhibit SnRK1 activity *in vitro* and in extracts of Arabidopsis seedlings (Zhang et al. 2009; Nunes et al. 2013b; Zhai et al. 2018; Blanford et al. 2024). Consequently, T6P is believed to modulate sucrose levels primarily by regulating its utilization for growth, partly through inhibition of SnRK1 (Figures 1.2 and 1.4). A more detailed discussion of the relationship between T6P and SnRK1 can be found in section 1.3.3.

1.3. SnRK1 kinase complex: subunit composition, domain architecture, and spatiotemporal expression

SnRK1 is an evolutionarily conserved protein kinase and the plant ortholog of the mammalian AMP-activated protein kinase (AMPK) and the yeast Sucrose Non-Fermenting 1 (Snf1). All three kinases exhibit similar domain architectures, forming heterotrimeric complexes composed of a catalytic α subunit and regulatory β and γ subunits. In addition to their structural similarity, they share a function as central regulators of metabolism and energy homeostasis across eukaryotes, integrating information about nutrient availability and stress signals (Polge and Thomas 2007; Broeckx et al. 2016). In Arabidopsis, the SnRK1 complex is encoded by three α subunit genes (*SnRK1α1/α2/α3*), three β subunit genes (*SnRK1β1/β2/β3*), and a single βγ hybrid subunit gene (*SnRK1βγ*) (Kleinow et al. 2000; Lumbreras et al. 2001; Ramon et al. 2013; Emanuelle et al. 2015; Figure 1.3).

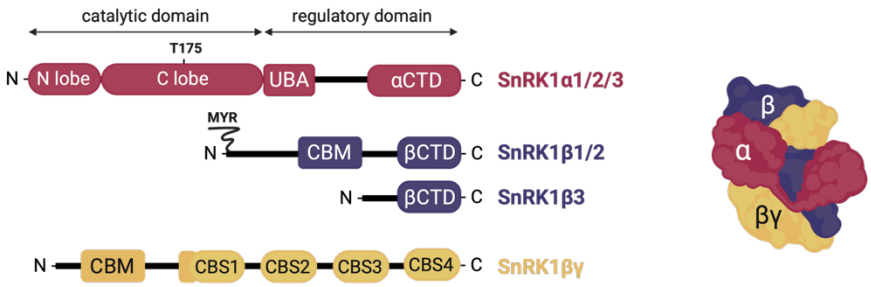

Figure 1.3. Structure of the SnRK1 heterotrimeric kinase complex.
The SnRK1α subunits (red) are composed of a catalytic (kinase) domain, harbouring the active site (between the N and C lobes) and the regulatory T-loop with the conserved threonine residue (T175), and a regulatory domain, containing the Ubiquitin-Associated (UBA) and the far α C-terminal domain (αCTD), which mediates interactions with the regulatory SnRK1β and SnRK1βγ subunits, as well as with type 2C phosphatases (PP2Cs). The SnRK1β subunits (purple) consist of an N-terminal variable region that is myristoylated at Gly2 (MYR), a central carbohydrate-binding module (CBM) – which is missing in SnRK1β3 due to an N-terminal truncation – and a C-terminal domain (βCTD) involved in interactions with SnRK1α and SnRK1βγ subunits. The hybrid SnRK1βγ subunit (yellow) contains an N-terminal carbohydrate-binding module (CBM), four cystathionine β-synthase (CBS) domains, and a small pre-CBS domain essential for complex formation. Adapted from Broeckx et al., 2016.

The α subunits comprise an N-terminal catalytic kinase domain and a C-terminal regulatory domain (Broeckx et al. 2016). The N-terminal catalytic domain is highly conserved across eukaryotes. It contains the kinase active site, located in a cleft between the N-terminal β-sheet lobe (N-lobe) and C-terminal α-helical lobe (C-lobe) (Hanks and Hunter 1995; Huse and Kuriyan 2002), as well as the T-loop region harboring a conserved threonine (T175 and T176 for SnRK1α1 and SnRK1α2, respectively), whose phosphorylation is required for kinase activity (Estruch et al. 1992; Hawley et al. 1996; Baena-González et al. 2007). The less conserved C-terminal regulatory domain facilitates heterotrimer assembly via interactions with the β and βγ regulatory subunits and contributes to interactions with upstream phosphatases – a function mediated by the far α C-terminal subdomain (αCTD) (Kleinow et al. 2000; Rodrigues et al. 2013). Among the α isoforms, SnRK1α3 is the most divergent, with N-terminal substitutions and deletions in its C-terminal regulatory domain that may impair interactions with regulatory subunits, despite a conserved catalytic core (Bhalerao et al. 1999). Furthermore, its expression appears limited to pollen grains and seeds (Schmid et al. 2005; Le et al. 2011), suggesting very specialized functions.

The regulatory β-subunits serve a scaffolding role and are proposed to influence kinase activity, subcellular localization of the complex, and substrate recognition (Hedbacker et al. 2004; Polge and Thomas 2007; Ghillebert et al. 2011; Hardie et al. 2012; Emanuelle et al. 2015; Ramon et al. 2019). SnRK1β1 and SnRK1β2 possess a conserved N-terminal domain that undergoes myristoylation *in planta*, facilitating membrane association (Pierre et al. 2007; Wang et al. 2020). They also contain a carbohydrate-binding module (CBM) and a β C-terminal domain (βCTD), the later necessary for association with the α and βγ subunits (Broeckx et al. 2016). Notably, the β1 subunit has also been linked to the regulation of organic acid metabolism and widespread transcriptional changes affecting carbon, lipid, and nitrogen metabolism (Wang et al. 2020). The plant specific SnRK1β3 subunit is highly divergent, lacking the typical CBM domain and myristoylation site due to N-terminal truncation. However, it remains capable of interacting with both yeast and plant α subunits (Gissot et al. 2004; Emanuelle et al. 2015).

Unique to plants, the atypical SnRK1βγ subunit combines features of both γ and β subunits, including four C-terminal cystathionine-β-synthase (CBS) domains and an N-terminal CBM (Lumbreras et al. 2001; Gissot et al. 2006; Broeckx et al. 2016). Despite its chimeric architecture, SnRK1βγ clusters phylogenetically with yeast and animal γ subunits, interacts with β subunits, assembles into heterotrimeric complexes, and can complement the yeast *snf4* mutant (Ramon et al. 2013; Emanuelle et al. 2015). Thus far, efforts to obtain a homozygous *snrk1βγ* loss-of-function mutant in Arabidopsis have been unsuccessful, suggesting that the mutant is embryo lethal (Ramon et al. 2013). An additional barrier for obtaining such mutant is parental transmission, with the *snrk1βγ* mutation causing defects in pollen hydration and germination (Gao et al. 2016).

Importantly, the presence of multiple subunit isoforms enables the formation of at least six distinct SnRK1 heterotrimeric complexes (2α × 3β × 1βγ) in Arabidopsis (Emanuelle et al. 2015), with further diversity potentially arising from alternative splicing (Gissot et al. 2004; López-Paz et al. 2009; Steinberg and Kemp 2009; Ghillebert et al. 2011). However, there is limited understanding of how these isoforms

assemble into complexes *in vivo*, and their distinct cellular localizations and functions. Still, subunit expression patterns may provide preliminary insight into the spatial and temporal assembly of specific SnRK1 complexes.

SnRK1α1 shows broad spatiotemporal expression patterns, consistent with this subunit accounting for most of the SnRK1 enzymatic activity *in vivo* (Jossier et al. 2009) – from early embryogenesis throughout later developmental stages – with ubiquitous tissue distribution and particular enrichment in leaf primordia, root tips, and vasculature (Williams et al. 2014). Unlike *SnRK1α1*, *SnRK1α2* shows a more restricted spatiotemporal expression pattern, being predominantly localized to the hydathodes and the bases of newly developing leaves (Williams et al. 2014; O'Brien et al. 2015). Notably, simultaneous loss of *SnRK1α1* and *SnRK1α2* appears lethal in higher plants (Baena-González et al. 2007), highlighting their essential, potentially redundant roles and the limited compensatory capacity of the weakly expressed *SnRK1α3* gene, which is only detected in pollen grains, developing embryos, and seeds (Baena-González et al. 2007; Fragoso et al. 2009). Moreover, SnRK1α1 and SnRK1βγ are enriched in the meristematic, elongation, and differentiation zones of primary and lateral roots, as well as in young leaf primordia, based on findings using tagged proteins (Bitrián et al. 2011; Belda-Palazón et al. 2020). Regarding the β-subunits, all are expressed in roots and mature rosettes, with *SnRK1β3* particularly enriched in reproductive tissues such as developing pollen grains, ovules, and seeds (Polge et al. 2008). Additionally, *SnRK1β1* is induced under carbon starvation conditions (Usadel et al. 2008) and, along with *SnRK1β2*, shows reciprocal responses to transient elevations of T6P (Avidan et al. 2024).

1.3.1. Regulation of SnRK1 by post-translational modifications and protein interactions

Although the SnRK1 complex composition remains poorly characterized *in vivo*, several post-translational modifications regulating its activity have been identified (Broeckx et al. 2016; Jamsheer K et al. 2021). Among these, phosphorylation of a

conserved threonine residue within the T-loop is required for SnRK1α activation (Hey et al. 2007; Shen et al. 2009), reflecting a regulatory mechanism shared with AMPK and Snf1 (Sugden et al. 1999a; Baena-González et al. 2007). This phosphorylation is mediated by SnRK1-activating kinases 1 and 2 (SnAK1/GRIK2 and SnAK2/GRIK1) in a Ca^{2+}-independent manner upon interaction with SnRK1 catalytic subunits (Shen et al. 2009). However, whereas AMPK activity in animals typically correlates with increased T-loop phosphorylation both *in vitro* and *in vivo*, making it a reliable indicator of kinase activation (Herzig and Shaw 2018; Lin and Hardie 2018), the relationship between *in vivo* SnRK1 activity and T-loop phosphorylation appears less consistent. Except in plants exposed to flooding, where a clear correlation has been reported (Cho et al. 2016), several studies have found no change in T-loop phosphorylation despite activation of SnRK1 signaling under stress (Baena-González et al. 2007; Fragoso et al. 2009; Rodrigues et al. 2013; Emanuelle et al. 2015), suggesting the involvement of additional regulatory layers. Intriguingly, the reduced T-loop phosphorylation in SnRK1α1 K48M kinase-dead mutants suggests this modification requires functional catalytic activity (Ramon et al. 2019), potentially through either direct autophosphorylation or conformational changes facilitating upstream kinase access. T-loop dephosphorylation via PP2C phosphatases, on the other hand, appears conserved across AMPK, Snf1 and SnRK1(Davies et al. 1995; Rodrigues et al. 2013; Ruiz et al. 2013), enabling kinase inactivation under energy-replete conditions. Moreover, in plants, clade A PP2C phosphatases also form repressor complexes with SnRK2 kinases that physically sequester SnRK1α, inhibiting its function in the absence of abscisic acid (ABA) (Figure 1.4). Conversely, when ABA levels rise, these complexes dissociate, releasing active SnRK1α to coordinate metabolic adaptation with ABA-dependent stress signaling (Rodrigues et al. 2013; Belda-Palazón et al. 2020).

Beyond phosphorylation, SnRK1 activity is modulated by other post-translational modifications, including ubiquitination, SUMOylation, and myristoylation (Ananieva et al. 2008; Lee et al. 2008; Carvalho et al. 2016; Crozet et al. 2016). Conserved among eukaryotes, β-subunit myristoylation plays a key role in regulating AMPK, Snf1, and SnRK1 complexes by facilitating their association with

membranes, thereby influencing their subcellular localization and enzymatic activity (Warden et al. 2001; Lin et al. 2003; Hedbacker et al. 2004; Pierre et al. 2007; Oakhill et al. 2010; Ramon et al. 2019). Consistent with this, N-myristoylation of SnRK1β2 in Arabidopsis promotes membrane association of the complex and retention of the catalytic subunit outside the nucleus, thereby limiting its impact on transcription (Pierre et al. 2007; Ramon et al. 2019). In contrast, defective N-myristoyltransferase activity in Arabidopsis *nmt1-1* mutants disrupts the myristoylation of a small number of proteins, including SnRK1β1 and SnRK1β2, resulting in severe developmental defects that correlate with increased SnRK1 kinase activity (Pierre et al. 2007). Notably, a similar increase in kinase activity has been reported for AMPK in animals following G2A substitutions that abolish β-subunit myristoylation (Warden et al. 2001; Oakhill et al. 2010). Although SnRK1 activity was not assessed in Arabidopsis lines carrying analogous G2A substitutions, these mutations caused relocalization of SnRK1β1 and SnRK1β2 from the plasma membrane to the nucleus and cytoplasm, respectively, providing a plausible explanation for the increased SnRK1 activity observed in *nmt1-1* mutants (Pierre et al. 2007).

In addition to post-translational modifications, SnRK1 stability and activity are further modulated by various interacting partners, several of which are discussed here. One such protein is PLEIOTROPIC REGULATORY LOCUS 1 (PRL1), a WD40-repeat protein that is part of the nuclear spliceosome-activating NTC complex (Koncz et al. 2012). PRL1 binds SnRK1α1 and SnRK1α2 *in vitro*, inhibiting their catalytic activity (Bhalerao et al. 1999). Consistent with its inhibitory role, *prl1* mutants exhibit increased SnRK1 activity, growth defects, anthocyanin accumulation, and heightened sensitivity to sugars, ABA, and cytokinin, likely due to elevated SnRK1α1 levels (Bhalerao et al. 1999; Lee et al. 2008). While the precise mechanism of PRL1-mediated inhibition remains unclear, genetic evidence suggests that PRL1, as part of the CUL4-DDB1 E3 ubiquitin ligase complex, promotes SnRK1α1 degradation (Lee et al. 2008).

The inositol polyphosphate 5-phosphatase 5PTase13, a component of the myoinositol signaling pathway, exhibits context-dependent effects on SnRK1. Under nutrient or sugar scarcity, it stabilizes SnRK1α1 by blocking its proteasomal

degradation, thereby enhancing SnRK1 activity (Ananieva et al. 2008). Paradoxically, 5PTase13 suppresses SnRK1 activity under severe starvation conditions. Although the mechanistic basis for this dual role remains unresolved, these findings point to 5PTase13 as a key factor in adapting SnRK1 signaling to fluctuating metabolic demands (Ananieva et al. 2008).

SnRK1-interacting negative regulators (SKINs), a class of stress-induced proteins first identified in rice, inhibit SnRK1(A) by blocking its nuclear translocation (Lin et al. 2014). While homologues of rice SKINs interact with Arabidopsis SnRK1α1 and SnRK1α2 in Y2H assays (Nietzsche et al. 2016) and are among the most strongly enriched SnRK1-associated proteins in Arabidopsis cell cultures (Van Leene et al. 2022), their functional conservation as negative regulators in Arabidopsis remains to be experimentally confirmed.

SnRK1 activity is also modulated through interactions with FLZ proteins (FCS-like zinc fingers) – a land plant-specific zinc finger family previously annotated as DUF581 (Domain of Unknown Function 581) (Figure 1.4; K and Laxmi 2014; Nietzsche et al. 2014, 2016; Jamsheer K et al. 2018). Arabidopsis FLZs interact with both SnRK1α isoforms in Y2H, BiFC, and interactome studies and are believed to act as scaffolds that recruit target proteins to the SnRK1 complex in a tissue- and stimulus-specific manner (Nietzsche et al. 2014, 2016; Jamsheer K et al. 2018b; Van Leene et al. 2022). Notably, FLZs also interact with components of the target of rapamycin (TOR) complex, another highly conserved eukaryotic kinase complex that plays largely antagonistic functions to SnRK1, positively regulating growth and developmental progression (see section 4.4 of the General Discussion; Margalha et al. 2019; Artins et al. 2024). FLZs also share several interactors with SnRK1, positioning them as potential integrators of multiple signaling pathways, including MAPK- and DELLA-related networks (Broeckx et al. 2016; Nietzsche et al. 2016; Jamsheer K et al. 2021). However, how FLZs influence SnRK1 signaling dynamics is not fully understood, though emerging evidence points to functional divergence. Whereas FLZ6 and FLZ10 negatively regulate SnRK1α1 stability during sugar starvation (Jamsheer K et al. 2018a), FLZ8 positively regulates SnRK1 signaling under nutrient-replete conditions

by promoting T-loop phosphorylation and facilitating its interaction with RAPTOR1B, thereby antagonizing TOR activity (Jamsheer K et al. 2022). Furthermore, a subset of ATG8-interacting FLZs directly inhibits SnRK1α1 activity by binding to the UBIQUITIN ASSOCIATED (UBA) domain and preventing T-loop phosphorylation, ultimately suppressing autophagy (Yang et al. 2023). Thus, FLZ proteins are thought to fine-tune SnRK1 and TOR signaling by preventing their excessive activation, thereby enabling a coordinated response to the plant energy status (Artins and Fernie 2023; Feng et al. 2025).

Lastly, all TPS-II proteins have been shown to interact with SnRK1 and appear to negatively regulate its kinase activity and nuclear signaling (Figure 1.4), as demonstrated by *in vitro* and transient luciferase assays, respectively (Van Leene et al. 2022). Consistent with this, TPS5-11 co-purified with all tested SnRK1 subunits in Arabidopsis culture cells. Moreover, co-expression of SnRK1α1-GFP with either TPS5, TPS8 or TPS9 in tobacco leaves reduced SnRK1α1 nuclear localization and induced pronounced co-localization with these TPSs at the endoplasmic reticulum (ER) perinuclear ring, an effect observed exclusively in young but not mature leaves (Van Leene et al. 2022). These findings led the authors to propose that TPS-II proteins may regulate SnRK1 activity *in vivo*. Notably, several TPS-II members have also been identified as SnRK1 substrates (Harthill et al. 2006; Cho et al. 2016; Nukarinen et al. 2016). Though the biological role of this phosphorylation is unclear, it may provide negative feedback to modulate TPS-mediated regulation of SnRK1 (see Chapter 3).

1.3.2. SnRK1 as a central energy sensor coordinating metabolism, growth and development

As sessile organisms, plants face fluctuating environmental conditions that often impair photosynthetic carbon fixation and respiratory ATP synthesis, depleting cellular energy and carbon reserves (Gururani et al. 2015; Muhammad et al. 2020). SnRK1 is activated under these energy-depleted conditions, thereby triggering a

coordinated transcriptional and metabolic reprogramming to restore energy homeostasis and support plant survival.

As part of this energy-saving program, SnRK1 phosphorylates and inactivates key metabolic enzymes, such as 3-hydroxy-3-methylglutaryl-coenzyme A reductase (HMGR), sucrose phosphate synthase (SPS) and nitrate reductase (NR) (Sugden et al. 1999b; Nukarinen et al. 2016; Robertlee et al. 2017). SnRK1 also targets enzymes involved in the T6P pathway and glycolysis. These include the catalytically inactive TPS5 and TPS7 (Harthill et al. 2006; Nukarinen et al. 2016); the central glycolytic enzyme cytosolic pyruvate kinase (PKc) (Beczner et al. 2010); non-phosphorylating glyceraldehyde-3-phosphate dehydrogenase (np-Ga3PDHase) (Piattoni et al. 2011) that participates in an ATP-independent glycolytic bypass; and the bifunctional enzyme fructose 6-phosphate2-kinase/fructose-2,6-bisphosphatase (F2KP) (Kulma et al. 2004), which controls fructose-2,6-bisphosphate (Fru-2,6bP) levels. Fru-2,6bP, in turn, inhibits fructose-1,6-bisphosphatase (FBPase), a key regulatory enzyme in sucrose biosynthesis (Stitt 1987), and activates pyrophosphate fructose 6-phosphate phosphotransferase (PFP). This likely contributes to the flexible regulation of glycolysis, gluconeogenesis, and pyrophosphate homeostasis, thereby supporting sucrose mobilization and the provision of precursors for diverse biosynthetic pathways (Hatzfeld et al. 1990; Stitt 1990, 1998; Plaxton 1996).

For NR, F2KP, np-Ga3PDHase, and TPS5, SnRK1-mediated phosphorylation serves as a signal that promotes the recruitment of 14-3-3 proteins to these targets (Moorhead et al. 1996; Ikeda et al. 2000; Bustos and Iglesias 2003; Kulma et al. 2004; Harthill et al. 2006; Piattoni et al. 2011). This interaction has been shown to lead to the inactivation of NR and np-Ga3PDHase (McMichael Jr et al. 1995; Moorhead et al. 1996; Piattoni et al. 2011), suggesting that this could be a general principle by which SnRK1 represses metabolic enzymes. Additionally, 14-3-3 binding has been implicated in targeting associated proteins for proteolytic degradation, particularly under sugar starvation conditions (Cotelle et al. 2000; Huber et al. 2002). Thus, 14-3-3 proteins may act as key mediators of SnRK1-induced metabolic reprogramming,

coupling phosphorylation-dependent recognition to both enzymatic inhibition and protein turnover.

Beyond direct metabolic control, SnRK1α translocates to the nucleus upon activation (Ramon et al. 2019), where it drives widespread transcriptional changes to restore energy homeostasis by coordinately suppressing anabolic processes and activating catabolic pathways (Baena-González et al. 2007; Baena-González and Sheen 2008; Sheen 2014). Specifically, SnRK1 upregulates genes involved in nutrient recycling via autophagy, gluconeogenesis, and the breakdown of cell wall components, starch, amino acids, proteins, and lipids, while downregulating genes associated with protein synthesis, glycolysis, and the TCA cycle (Baena-González et al. 2007; Baena-González and Sheen 2008). This transcriptional rewiring is partly achieved through SnRK1-mediated phosphorylation of C- and S1-class bZIP transcription factors (Ma et al. 2011; Mair et al. 2015; Dröge-Laser and Weiste 2018; Pedrotti et al. 2018). Particularly, phosphorylation of bZIP63 enhances its ability to homo- and heterodimerize with S1 bZIPs and to bind DNA (Mair et al. 2015). This subsequently leads to recruitment of SnRK1 to target promoters, where C/S1-bZIP-SnRK1 complexes associate with the histone acetylation machinery to remodel chromatin and activate gene expression. A key outcome is the induction of branched-chain amino acid catabolism, providing an alternative energy source to support mitochondrial respiration under carbon starvation (Pedrotti et al. 2018).

Importantly, SnRK1 further restricts growth under energy-limiting conditions through multiple regulatory routes: it phosphorylates and inhibits translation initiation factors eIF4E and eIFiso4E to suppress protein synthesis (Bruns et al. 2019), destabilizes the cell cycle regulator E2Fa to block cell proliferation (Son et al. 2023), and directly phosphorylates core ATG proteins to promote autophagy (Chen et al. 2017; Huang et al. 2019). In parallel, evidence from *in vitro* and transient co-expression assays suggests that SnRK1 may inhibit the TOR pathway (Figure 1.4; see also section 4.4 of the General Discussion) via phosphorylation of the RAPTOR1B subunit (Nukarinen et al. 2016).

In plants, the conserved TOR kinase forms a heterotrimeric complex with the regulatory associated protein of TOR (RAPTOR) and lethal with SEC thirteen protein 8 (LST8) (van Dam et al. 2011). In contrast to SnRK1, TOR is typically suppressed during nutrient scarcity and activated under nutrient-rich conditions, thereby promoting cell proliferation, growth, and developmental progression (Dobrenel et al. 2013; Shi et al. 2018; Caldana et al. 2019; Artins and Caldana 2022). Accordingly, TOR signaling is strongly stimulated by photosynthesis-derived glucose and sucrose in root and shoot meristems (Xiong et al. 2013; Li et al. 2017), and is also activated by light in the shoot apical meristem via auxin signaling (Pfeiffer et al. 2016; Li et al. 2017). The auxin-dependent activation of TOR extends to roots as well and, in both tissues, likely occurs via a direct interaction between TOR and the small GTPase Rho-related protein 2 (ROP2) (Schepetilnikov et al. 2013, 2017; Li et al. 2017). Once activated, TOR promotes growth by stimulating anabolic processes, such as protein synthesis and cell division, while repressing catabolism and nutrient recycling through both direct phosphorylation of target proteins and transcriptional reprogramming (Burkart and Brandizzi 2021). Among its best-characterized downstream targets is S6 kinase (S6K), whose phosphorylation by TOR is a key step in activating protein synthesis via downstream phosphorylation of ribosomal protein S6 (RPS6). As such, phosphorylation of S6K and RPS6 (though the latter is an indirect target) has been widely used as a readout of TOR activity in plants (see Chapter 2; Mahfouz et al. 2006; Schepetilnikov et al. 2011, 2013; Dobrenel et al. 2016; Li et al. 2017; Wang et al. 2018).

Given SnRK1's pivotal regulatory functions, it is unsurprising that altering its activity profoundly impacts plant growth and development. A consistent pattern across multiple studies indicates that elevated SnRK1 activity typically delays developmental transitions, while reduced activity tends to accelerate them (Baena-González and Hanson 2017). Accordingly, SnRK1α1 overexpression in Arabidopsis delays germination, flowering, and senescence (Baena-González et al. 2007; Tsai and Gazzarrini 2012), partly through phosphorylation of specific transcription factors. These include FUSCA3 (FUS3), which mediates SnRK1's repression of germination and flowering (Tsai and Gazzarrini 2012); INDETERMINATE DOMAIN-8 (IDD8),

whose phosphorylation by SnRK1 reduces its transcriptional activity also contributing to delayed flowering (Jeong et al. 2015); and ETHYLENE INSENSITIVE3 (EIN3), which is destabilized by SnRK1 to delay senescence progression (Kim et al. 2017). In contrast, post-embryonic silencing of SnRK1α in pea causes premature germination, abnormal cotyledon development, and defective seed maturation (Radchuk et al. 2009). Moreover, Arabidopsis plants expressing inactive forms of SnRK1 show accelerated senescence (Cho et al. 2012).

In line with its role as a central regulator affecting many processes, the complete knockout of SnRK1α1/α2 in higher plants appears to be embryo lethal (Ramon et al. 2019), and systemic silencing through virus-induced gene silencing (VIGS) results in irreversible growth arrest (Baena-González et al. 2007). This shows that, although SnRK1 generally restricts development, it is also indispensable for proper growth and viability. Consistent with this, mounting evidence highlights critical roles for SnRK1 even under non-stress conditions (Radchuk et al. 2009; Nukarinen et al. 2016; Li et al. 2020; Liang et al. 2021; Peixoto et al. 2021; Wang et al. 2021; Henninger et al. 2022; Lopes et al. 2024), suggesting that both its activation and repression may be required at specific developmental stages and in distinct tissues to guide proper growth and development. This is exemplified by SnRK1's dual role in the SAM, where it suppresses meristem activity under unfavorable conditions by inhibiting SHOOT MERISTEMLESS (STM), a key regulator of meristem function. Meanwhile, under favorable conditions, SnRK1 is also required to maintain meristem integrity, as SAM-specific silencing of SnRK1α leads to meristem dysfunction and severe developmental abnormalities (Lopes et al. 2024).

1.3.3. The convergence of SnRK1 and T6P pathways in plant metabolic regulation and growth

Although SnRK1 retains the conserved energy-sensing function of eukaryotic AMPK/Snf1 kinases, its regulation has diverged significantly in plants. AMPK and Snf1 are allosterically activated by AMP and/or ADP. These nucleotides compete with ATP

for binding to the γ-subunit, thereby inhibiting T-loop dephosphorylation and promoting kinase activation (Hardie and Carling 1997; Hardie et al. 1998; Mayer et al. 2011; Oakhill et al. 2011). In contrast, plant SnRK1 appears unresponsive to changes in nucleotide charge (Wilson et al. 1996; Sugden et al. 1999a; Emanuelle et al. 2015). Moreover, unlike AMPK and Snf1, which function exclusively as obligate heterotrimers requiring α, β and γ subunits, SnRK1 catalytic α-subunits display intrinsic kinase activity independent of regulatory subunits (Ramon et al. 2019). This suggests that SnRK1 is active by default, with signaling suppressed under energy-replete conditions. Consistent with this, sugar phosphates such as glucose 1-phosphate, G6P, and T6P have been shown to inhibit SnRK1 (Figure 1.4; Toroser et al. 2000; Zhang et al. 2009; Nunes et al. 2013b; Zhai et al. 2018; Avidan et al. 2023; Blanford et al. 2024), indicating that SnRK1 activity in plants is regulated primarily through changes in metabolite levels rather than adenylate charge, thereby linking its inhibition to energy-rich conditions rather than activation during energy shortage.

Especially T6P has emerged as a physiologically relevant inhibitor of SnRK1, suppressing its kinase activity *in vitro* across Arabidopsis tissues, developmental stages and various plant species (Zhang et al. 2009, 2015; Debast et al. 2011; Delatte et al. 2011; Martínez-Barajas et al. 2011; Nunes et al. 2013b; Coello and Martínez-Barajas 2014; Nuccio et al. 2015; Griffiths et al. 2016). *In vitro* studies demonstrate that T6P-mediated inhibition of SnRK1 requires an as-yet unidentified proteinaceous factor present in growing tissues but either absent or no longer effective in mature leaf extracts (Figure 1.4; Zhang et al. 2009; Martins et al. 2013; Nunes et al. 2013b). More recent work has shown that T6P can also directly bind with very high affinity to the SnRK1 catalytic α-subunit at a different site to that of ATP, preventing its phosphorylation and activation by upstream SnAK kinases (Figure 1.4; Zhai et al. 2018; Blanford et al. 2024). Given the broad expression of SnAKs, including mature leaves (Zhai et al. 2018), they are unlikely to be the unknown factor described by Zhang et al. (2009). This suggests that T6P modulates SnRK1 activity through multiple, distinct mechanisms. Importantly, catalytically inactive TPS-II proteins have been identified as strong interactors and negative regulators of SnRK1 (Van Leene et al. 2022; see above for details), making them promising candidates for the elusive

factor mediating T6P-dependent SnRK1 inhibition. However, their potential role as intermediaries in this pathway remains unexplored and warrants further investigation.

An anti-correlation between T6P levels and SnRK1-responsive gene expression has also been frequently reported, with elevated T6P associated with reduced expression of SnRK1-induced genes and, more variably, with enhanced expression of SnRK1-repressed genes (Baena-González et al. 2007; Zhang et al. 2009; Oszvald et al. 2018; Avidan et al. 2024). This relationship has been observed across several plant species, tissues, developmental stages, and in response to stress conditions (Debast et al. 2011; Martínez-Barajas et al. 2011; Nunes et al. 2013a; Henry et al. 2014, 2015; Bledsoe et al. 2017; Oszvald et al. 2018; Peixoto et al. 2021), with some of these changes also reproduced upon treatment with membrane-permeable T6P analogs (Griffiths et al. 2016; Morales-Herrera et al. 2023). However, caution is advised when interpreting these data, as many studies rely on correlative evidence and typically assess only a limited subset of SnRK1-responsive genes. In line with this, transcriptional responses do not always align with measurable differences in total SnRK1 kinase activity *in vitro* (Martínez-Barajas et al. 2011; Oszvald et al. 2018; Baena-González and Lunn 2020). Furthermore, diel changes in *in vivo* SnRK1 activity, inferred from the phosphorylation status of an *in vivo* reporter protein, do not consistently correlate with T6P levels (Avidan et al. 2023). Meanwhile, these *in vivo* SnRK1 activity fluctuations also do not always correlate with the abundance of SnRK1 transcripts (Avidan et al. 2023), suggesting that transcript levels are not always a reliable proxy for SnRK1 activity. The implication is that T6P likely modulates spatially or functionally distinct SnRK1 pools in a context-dependent manner and/or that other factors regulate SnRK1 activity alongside T6P.

In any case, T6P-mediated inhibition of *in vitro* SnRK1 activity is typically strongest in extracts from young, actively growing tissues (Zhang et al. 2009), where elevated T6P levels and reduced SnRK1 activity correlate with developmental progression and sucrose-driven biosynthetic processes (Baena-González and Lunn 2020). Consistently, T6P and SnRK1 often exert opposing influences on developmental transitions. A clear example is flowering, which is accelerated by high

T6P levels (Schluepmann et al. 2003; Fichtner et al. 2017, 2021) but delayed by SnRK1 overexpression (Baena-González et al. 2007). Notably, loss-of-function mutations in SnRK1α1 and SnRK1βγ restore embryogenesis and flowering in *tps1* mutants, supporting the idea that T6P drives development partly by restraining SnRK1, whose unchecked activity interferes with normal growth and development (Zacharaki et al. 2022). Nevertheless, although SnRK1 typically blocks developmental progression, its activity becomes crucial to sustain new sink growth once a developmental transition is initiated. Such a role may involve the remobilization of nutrients to the growing sinks, as shown in germinating rice seedlings (Lee et al. 2009). This is further supported by findings in potato tubers, where reduced T6P, driven by OtsB (TPP) overexpression, led to increased sugar accumulation and premature sprouting, whereas antisense-mediated repression of SnRK1 markedly delayed sprouting (Debast et al. 2011), suggesting that low T6P facilitates reserve mobilization via SnRK1.

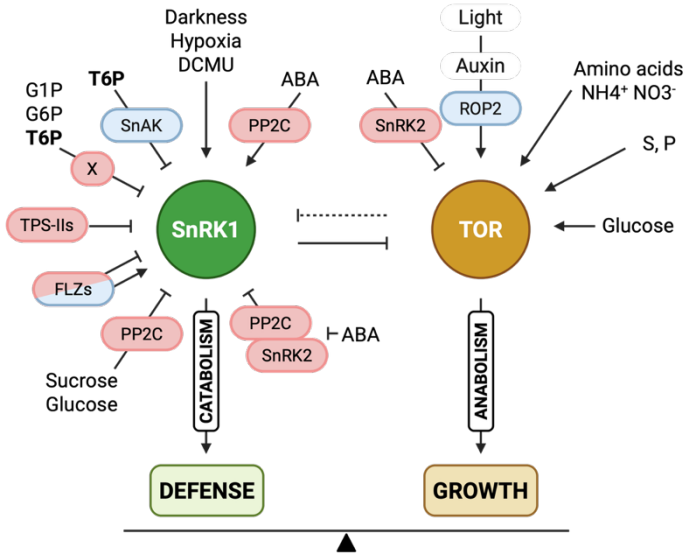

Figure 1.4. SnRK1 and TOR are key metabolic regulators that antagonistically control growth-defense trade-offs in plants.
Plants adjust their metabolism in response to environmental conditions through the opposing actions of SnRK1 and TOR. When biotic or abiotic stresses limit energy production, SnRK1 is activated to enhance defense, whereas TOR activity is suppressed. Conversely, under favorable, nutrient-rich conditions, TOR is activated to support growth and cell division, and SnRK1 is inhibited. The resulting trade-off between growth and defense may stem from both reciprocal regulation between SnRK1 and TOR, as well as their independent control of downstream targets. Red and blue components indicate negative and positive regulators, respectively, of the indicated kinase. Interactions confirmed experimentally are shown as solid

lines, and proposed interactions as dashed lines. SnRK1 (Snf1-related protein kinase 1), TOR (target of rapamycin), PP2Cs (type 2C protein phosphatases), SnAK (SnRK1 activating kinase), ROP2 (small GTPase Rho-related protein 2), SnRK2 (Snf1-related protein kinase 2), TPS-IIs (trehalose 6-phosphate synthase class II), FLZs (FCS-like Zinc Finger), X (unknown proteinaceous factor). Adapted from Margalha et al., 2019.

While the regulation of SnRK1 by T6P has been extensively studied, the extent to which SnRK1 influences T6P signaling remains less clear. Nonetheless, recent work using SnRK1α gain- and loss-of-function mutants suggests that SnRK1 may modulate the sucrose-dependent accumulation of T6P (Peixoto et al. 2021). Although the positive correlation between T6P and sucrose was maintained in these lines, SnRK1α1-OE plants accumulated disproportionately high T6P levels relative to sucrose, whereas *sesquia2* mutants with reduced SnRK1α activity showed lower T6P levels for the same sucrose concentration (Peixoto et al. 2021). In addition, several TPS-IIs are regulated by SnRK1 at both the transcriptional and post-translational levels (Glinski and Weckwerth 2005; Harthill et al. 2006; Baena-González et al. 2007; Cho et al. 2016; Nukarinen et al. 2016). Consistently, *TPS5* is induced by sugars and repressed by SnRK1, while TPS8-11 show the opposite pattern, being repressed by sugars and induced by SnRK1 under carbon starvation (Baena-González et al. 2007; Osuna et al. 2007; Usadel et al. 2008). Although further research is required, these findings highlight a potential feedback loop involving the reciprocal regulation of T6P signaling by SnRK1.

1.4. Thesis aims and scopes

This thesis reveals novel regulatory mechanisms of TPS-II proteins, identifying them as T6P-responsive regulators that modulate SnRK1 activity to align metabolism and growth with sucrose availability. One major goal of this work was to gain insight into the functional roles of non-catalytic TPS-II proteins, particularly TPS5-7, given their close phylogenic relationship and distinct transcriptional responsiveness to carbon compared to TPS8-11. A second aim was to investigate the interaction

between TPS-II proteins and SnRK1 by determining whether this interaction is T6P-dependent, how SnRK1 function is modified as a result, and the subsequent impact on plant growth and development.

This thesis is composed of four chapters (including this introductory **Chapter 1**), structured as follows:

Chapter 2: In this chapter, I explored the roles of TPS5, TPS6, and TPS7 in regulating plant growth, development, and metabolic traits influenced by T6P. I show that plants lacking TPS5/6/7 exhibit delayed flowering and stunted root growth that cannot be rescued by sugar supplementation or increased light intensity. These defects are further accompanied by marked metabolic disturbances, suggesting that TPS5/6/7 are essential for proper T6P signaling and the effective downstream utilization of sucrose to support growth.

Chapter 3: In this chapter, I investigated the functional relationship between TPS-II proteins and SnRK1. I demonstrate that the growth and developmental defects observed in the *tps5/6/7* mutant are largely SnRK1-dependent, as these defects can be nearly fully reverted by decreasing SnRK1 expression. Additionally, depletion of TPS5/6/7 leads to altered SnRK1 function, changes in its subcellular localization and modified responsiveness to energy stress. Furthermore, I show that T6P specifically enhances the physical interaction between TPS-II proteins and SnRK1, suggesting that TPS-II proteins may act as T6P sensors that facilitate the repression of SnRK1.

Chapter 4: In this chapter, I integrate the phenotypic, metabolic, and mechanistic findings from Chapters 2 and 3, providing a comprehensive discussion of results that establish TPS5/6/7 proteins as novel regulators of the SnRK1 kinase and key downstream effectors of T6P. I also propose new hypotheses and outline experimental approaches to advance research in this field and deepen our understanding of how the TPS-II–T6P–SnRK1 pathway coordinates carbon status with growth regulation in plants.

1.5. References

Ananieva EA, Gillaspy GE, Ely A, Burnette RN, and Erickson F Les. Interaction of the WD40 domain of a myoinositol polyphosphate 5-phosphatase with SnRK1 links inositol, sugar, and stress signaling. Plant Physiol. 2008:**148**(4):1868–82. https://doi.org/10.1104/pp.108.130575

Artins A and Caldana C. The metabolic homeostaTOR: The balance of holding on or letting grow. Curr Opin Plant Biol. 2022:**66**:102196. https://doi.org/10.1016/j.pbi.2022.102196

Artins A and Fernie AR. FCS-like zinc finger proteins maintain energy homeostasis during stresses. Trends Plant Sci. 2023:**28**(12):1347–1349. https://doi.org/10.1016/j.tplants.2023.09.004

Artins A, Martins MCM, Meyer C, Fernie AR, and Caldana C. Sensing and regulation of C and N metabolism – novel features and mechanisms of the TOR and SnRK1 signaling pathways. The Plant Journal. 2024:**118**(5):1268–1280. https://doi.org/10.1111/tpj.16684

Avidan O, Martins MCM, Feil R, Lohse M, Giorgi FM, Schlereth A, Lunn JE, and Stitt M. Direct and indirect responses of the Arabidopsis transcriptome to an induced increase in trehalose 6-phosphate. Plant Physiol. 2024:**196**(1):409–431. https://doi.org/10.1093/plphys/kiae196

Avidan O, Moraes TA, Mengin V, Feil R, Rolland F, Stitt M, and Lunn JE. In vivo protein kinase activity of SnRK1 fluctuates in Arabidopsis rosettes during light-dark cycles. Plant Physiol. 2023:**192**(1):387–408. https://doi.org/10.1093/plphys/kiad066

Avonce N, Mendoza-Vargas A, Morett E, and Iturriaga G. Insights on the evolution of trehalose biosynthesis. BMC Evol Biol. 2006:**6**(1):109. https://doi.org/10.1186/1471-2148-6-109

Baena-González E and Hanson J. Shaping plant development through the SnRK1–TOR metabolic regulators. Curr Opin Plant Biol. 2017. https://doi.org/10.1016/j.pbi.2016.12.004

Baena-González E and Lunn JE. SnRK1 and trehalose 6-phosphate – two ancient pathways converge to regulate plant metabolism and growth. Curr Opin Plant Biol. 2020. https://doi.org/10.1016/j.pbi.2020.01.010

Baena-González E, Rolland F, M. Thevelein J, and Sheen J. A central integrator of transcription networks in plant stress and energy signalling. Nature. 2007:**448**:938–942.

Baena-González E and Sheen J. Convergent energy and stress signaling. Trends Plant Sci. 2008:**13**(9):474–482. https://doi.org/10.1016/j.tplants.2008.06.006

Beczner F, Dancs G, Sós-Hegedűs A, Antal F, and Bánfalvi Z. Interaction between SNF1-related kinases and a cytosolic pyruvate kinase of potato. J Plant Physiol. 2010:**167**(13):1046–1051. https://doi.org/10.1016/j.jplph.2010.03.010

Belda-Palazón B, Adamo M, Valerio C, Ferreira LJ, Confraria A, Reis-Barata D, Rodrigues A, Meyer C, Rodriguez PL, and Baena-González E. A dual function of SnRK2 kinases in the regulation of SnRK1 and plant growth. Nat Plants. 2020:**6**(11):1345–1353. https://doi.org/10.1038/s41477-020-00778-w

Bhalerao RP, Salchert K, Bakó L, Okrész L, Szabados L, Muranaka T, Machida Y, Schell J, and Koncz C. Regulatory interaction of PRL1 WD protein with Arabidopsis SNF1-like protein kinases. Proc Natl Acad Sci U S A. 1999:**96**(9):5322–7. https://doi.org/10.1073/pnas.96.9.5322

Bitrián M, Roodbarkelari F, Horváth M, and Koncz C. BAC-recombineering for studying plant gene regulation: Developmental control and cellular localization of SnRK1 kinase subunits. Plant Journal. 2011. https://doi.org/10.1111/j.1365-313X.2010.04462.x

Blanford J, Zhai Z, Baer MD, Guo G, Liu H, Liu Q, Raugei S, and Shanklin J. Molecular mechanism of trehalose 6-phosphate inhibition of the plant metabolic sensor kinase SnRK1. Sci Adv. 2024:**10**(20). https://doi.org/10.1126/sciadv.adn0895

Bledsoe SW, Henry C, Griffiths CA, Paul MJ, Feil R, Lunn JE, Stitt M, and Lagrimini LM. The role of Tre6P and SnRK1 in maize early kernel development and events leading to stress-induced kernel abortion. BMC Plant Biol. 2017:**17**(1):74. https://doi.org/10.1186/s12870-017-1018-2

Broeckx T, Hulsmans S, and Rolland F. The plant energy sensor: evolutionary conservation and divergence of SnRK1 structure, regulation, and function. J Exp Bot. 2016:**67**(22):6215–6252. https://doi.org/10.1093/jxb/erw416

Bruns AN, Li S, Mohannath G, and Bisaro DM. Phosphorylation of Arabidopsis eIF4E and eIFiso4E by SnRK1 inhibits translation. FEBS J. 2019:**286**(19):3778–3796. https://doi.org/10.1111/febs.14935

Burkart GM and Brandizzi F. A Tour of TOR Complex Signaling in Plants. Trends Biochem Sci. 2021:**46**(5):417–428. https://doi.org/10.1016/j.tibs.2020.11.004

Bustos DM and Iglesias AA. Phosphorylated non-phosphorylating glyceraldehyde-3-phosphate dehydrogenase from heterotrophic cells of wheat interacts with 14-3-3 proteins. Plant Physiol. 2003:**133**(4):2081–8. https://doi.org/10.1104/pp.103.030981

Caldana C, Martins MCM, Mubeen U, and Urrea-Castellanos R. The magic "hammer" of TOR: the multiple faces of a single pathway in the metabolic regulation of plant growth and development. J Exp Bot. 2019:**70**(8):2217–2225. https://doi.org/10.1093/jxb/ery459

Carillo P, Feil R, Gibon Y, Satoh-Nagasawa N, Jackson D, Bläsing OE, Stitt M, and Lunn J. A fluorometric assay for trehalose in the picomole range. Plant Methods. 2013:**9**(1):21. https://doi.org/10.1186/1746-4811-9-21

Carvalho RF, Szakonyi D, Simpson CG, Barbosa ICR, Brown JWS, Baena-González E, and Duque P. The Arabidopsis SR45 Splicing Factor, a Negative Regulator of Sugar Signaling, Modulates SNF1-Related Protein Kinase 1 Stability. Plant Cell. 2016:**28**(8):1910–25. https://doi.org/10.1105/tpc.16.00301

Caspar T, Huber SC, and Somerville C. Alterations in Growth, Photosynthesis, and Respiration in a Starchless Mutant of Arabidopsis thaliana (L.) Deficient in Chloroplast Phosphoglucomutase Activity. Plant Physiol. 1985:**79**(1):11–7. https://doi.org/10.1104/pp.79.1.11

Chary SN, Hicks GR, Choi YG, Carter D, and Raikhel N V. Trehalose-6-Phosphate Synthase/Phosphatase Regulates Cell Shape and Plant Architecture in Arabidopsis. Plant Physiol. 2008:**146**(1):97–107. https://doi.org/10.1104/pp.107.107441

Chen L, Su Z-Z, Huang L, Xia F-N, Qi H, Xie L-J, Xiao S, and Chen Q-F. The AMP-Activated Protein Kinase KIN10 Is Involved in the Regulation of Autophagy in Arabidopsis. Front Plant Sci. 2017:**8**. https://doi.org/10.3389/fpls.2017.01201

Cho HY, Wen TN, Wang YT, and Shih MC. Quantitative phosphoproteomics of protein kinase SnRK1 regulated protein phosphorylation in Arabidopsis under submergence. J Exp Bot. 2016:**67**(9):2745–2760. https://doi.org/10.1093/jxb/erw107

Cho Y-H, Hong J-W, Kim E-C, and Yoo S-D. Regulatory Functions of SnRK1 in Stress-Responsive Gene Expression and in Plant Growth and Development. Plant Physiol. 2012:**158**(4):1955–1964. https://doi.org/10.1104/pp.111.189829

Claeys H, Vi SL, Xu X, Satoh-Nagasawa N, Eveland AL, Goldshmidt A, Feil R, Beggs GA, Sakai H, Brennan RG, et al. Control of meristem determinacy by trehalose 6-phosphate phosphatases is uncoupled from enzymatic activity. Nat Plants. 2019:**5**(4):352–357. https://doi.org/10.1038/s41477-019-0394-z

Coello P and Martínez-Barajas E. SnRK1 is differentially regulated in the cotyledon and embryo axe of bean (Phaseolus vulgaris L) seeds. Plant Physiology and Biochemistry. 2014. https://doi.org/10.1016/j.plaphy.2014.03.033

Cotelle V, Meek SE, Provan F, Milne FC, Morrice N, and MacKintosh C. 14-3-3s regulate global cleavage of their diverse binding partners in sugar-starved Arabidopsis cells. EMBO J. 2000:**19**(12):2869–76. https://doi.org/10.1093/emboj/19.12.2869

Crozet P, Margalha L, Butowt R, Fernandes N, Elias CA, Orosa B, Tomanov K, Teige M, Bachmair A, Sadanandom A, et al. SUMOylation represses SnRK1 signaling in Arabidopsis. Plant Journal. 2016. https://doi.org/10.1111/tpj.13096

Davies SP, Helps NR, Cohen PT, and Hardie DG. 5'-AMP inhibits dephosphorylation, as well as promoting phosphorylation, of the AMP-activated

protein kinase. Studies using bacterially expressed human protein phosphatase-2C alpha and native bovine protein phosphatase-2AC. FEBS Lett. 1995:**377**(3):421–5. https://doi.org/10.1016/0014-5793(95)01368-7

Debast S, Nunes-Nesi A, Hajirezaei MR, Hofmann J, Sonnewald U, Fernie AR, and Börnke F. Altering trehalose-6-phosphate content in transgenic potato tubers affects tuber growth and alters responsiveness to hormones during sprouting. Plant Physiol. 2011:**156**(4):1754–71. https://doi.org/10.1104/pp.111.179903

De Block M and Van Lijsebettens M. Energy efficiency and energy homeostasis as genetic and epigenetic components of plant performance and crop productivity. Curr Opin Plant Biol. 2011:**14**(3):275–282. https://doi.org/10.1016/j.pbi.2011.02.007

Delatte TL, Sedijani P, Kondou Y, Matsui M, de Jong GJ, Somsen GW, Wiese-Klinkenberg A, Primavesi LF, Paul MJ, and Schluepmann H. Growth Arrest by Trehalose-6-Phosphate: An Astonishing Case of Primary Metabolite Control over Growth by Way of the SnRK1 Signaling Pathway. Plant Physiol. 2011:**157**(1):160–174. https://doi.org/10.1104/pp.111.180422

Delorge I, Figueroa CM, Feil R, Lunn JE, and Van Dijck P. Trehalose-6-phosphate synthase 1 is not the only active TPS in Arabidopsis thaliana. Biochemical Journal. 2015:**466**(2):283–290. https://doi.org/10.1042/BJ20141322

Dijken AJH van, Schluepmann H, and Smeekens SCM. Arabidopsis Trehalose-6-Phosphate Synthase 1 Is Essential for Normal Vegetative Growth and Transition to Flowering. Plant Physiol. 2004:**135**(2):969–977. https://doi.org/10.1104/pp.104.039743

Dobrenel T, Mancera-Martínez E, Forzani C, Azzopardi M, Davanture M, Moreau M, Schepetilnikov M, Chicher J, Langella O, Zivy M, et al. The Arabidopsis TOR Kinase Specifically Regulates the Expression of Nuclear Genes Coding for Plastidic Ribosomal Proteins and the Phosphorylation of the Cytosolic Ribosomal Protein S6. Front Plant Sci. 2016:**7**. https://doi.org/10.3389/fpls.2016.01611

Dobrenel T, Marchive C, Azzopardi M, Clément G, Moreau M, Sormani R, Robaglia C, and Meyer C. Sugar metabolism and the plant target of rapamycin kinase: a sweet operaTOR? Front Plant Sci. 2013:**4**. https://doi.org/10.3389/fpls.2013.00093

dos Anjos L, Pandey PK, Moraes TA, Feil R, Lunn JE, and Stitt M. Feedback regulation by trehalose 6-phosphate slows down starch mobilization below the rate that would exhaust starch reserves at dawn in Arabidopsis leaves. Plant Direct. 2018. https://doi.org/10.1002/pld3.78

Dröge-Laser W and Weiste C. The C/S1 bZIP Network: A Regulatory Hub Orchestrating Plant Energy Homeostasis. Trends Plant Sci. 2018:**23**(5):422–433. https://doi.org/10.1016/j.tplants.2018.02.003

Eastmond PJ, Van Dijken AJH, Spielman M, Kerr A, Tissier AF, Dickinson HG, Jones JDG, Smeekens SC, and Graham IA. Trehalose-6-phosphate synthase 1, which catalyses the first step in trehalose synthesis, is essential for *Arabidopsis* embryo maturation. The Plant Journal. 2002:**29**(2):225–235. https://doi.org/10.1046/j.1365-313x.2002.01220.x

Emanuelle S, Hossain MI, Moller IE, Pedersen HL, Van De Meene AML, Doblin MS, Koay A, Oakhill JS, Scott JW, Willats WGT, et al. SnRK1 from Arabidopsis thaliana is an atypical AMPK. Plant Journal. 2015. https://doi.org/10.1111/tpj.12813

Estruch F, Treitel MA, Yang X, and Carlson M. N-terminal mutations modulate yeast SNF1 protein kinase function. Genetics. 1992:**132**(3):639–50. https://doi.org/10.1093/genetics/132.3.639

Feng L, Li X, Zheng X-A, Zheng Z, Liu Q-R, Liu C, Zhu Q-L, Shen W, Yang C, Li H, et al. SnRK1 and TOR: central regulators of autophagy in plant energy stress responses. aBIOTECH. 2025. https://doi.org/10.1007/s42994-025-00218-3

Fichtner F, Barbier FF, Annunziata MG, Feil R, Olas JJ, Mueller-Roeber B, Stitt M, Beveridge CA, and Lunn JE. Regulation of shoot branching in Arabidopsis by trehalose 6-phosphate. New Phytologist. 2021:**229**(4):2135–2151. https://doi.org/10.1111/nph.17006

Fichtner F, Barbier FF, Feil R, Watanabe M, Annunziata MG, Chabikwa TG, Höfgen R, Stitt M, Beveridge CA, and Lunn JE. Trehalose 6-phosphate is involved in triggering axillary bud outgrowth in garden pea (*Pisum sativum* L.). The Plant Journal. 2017:**92**(4):611–623. https://doi.org/10.1111/tpj.13705

Fichtner F and Lunn JE. The Role of Trehalose 6-Phosphate (Tre6P) in Plant Metabolism and Development. Annu Rev Plant Biol. 2021:**72**(1):737–760. https://doi.org/10.1146/annurev-arplant-050718-095929

Fichtner F, Olas JJ, Feil R, Watanabe M, Krause U, Hoefgen R, Stitt M, and Lunn JE. Functional Features of TREHALOSE-6-PHOSPHATE SYNTHASE1, an Essential Enzyme in Arabidopsis. Plant Cell. 2020:**32**(6):1949–1972. https://doi.org/10.1105/tpc.19.00837

Figueroa CM, Feil R, Ishihara H, Watanabe M, Kölling K, Krause U, Höhne M, Encke B, Plaxton WC, Zeeman SC, et al. Trehalose 6-phosphate coordinates organic and amino acid metabolism with carbon availability. Plant Journal. 2016. https://doi.org/10.1111/tpj.13114

Figueroa CM and Lunn JE. A Tale of Two Sugars: Trehalose 6-Phosphate and Sucrose. Plant Physiol. 2016. https://doi.org/10.1104/pp.16.00417

Fragoso S, Espindola L, Paez-Valencia J, Gamboa A, Camacho Y, Martinez-Barajas E, and Coello P. SnRK1 Isoforms AKIN10 and AKIN11 Are Differentially Regulated in Arabidopsis Plants under Phosphate Starvation. Plant Physiol. 2009:**149**(4):1906–1916. https://doi.org/10.1104/pp.108.133298

Gao X-Q, Liu CZ, Li DD, Zhao TT, Li F, Jia XN, Zhao X-Y, and Zhang XS. The Arabidopsis KINβγ Subunit of the SnRK1 Complex Regulates Pollen Hydration on the Stigma by Mediating the Level of Reactive Oxygen Species in Pollen. PLoS Genet. 2016:**12**(7):e1006228. https://doi.org/10.1371/journal.pgen.1006228

Geiger DR and Servaites JC. Diurnal Regulation of Photosynthetic Carbon Metabolism in C3 Plants. Annu Rev Plant Physiol Plant Mol Biol. 1994:**45**(1):235–256. https://doi.org/10.1146/annurev.pp.45.060194.001315

Geiger DR, Servaites JC, and Fuchs MA. Role of starch in carbon translocation and partitioning at the plant level. Functional Plant Biology. 2000:**27**(6):571. https://doi.org/10.1071/PP99128

Ghillebert R, Swinnen E, Wen J, Vandesteene L, Ramon M, Norga K, Rolland F, and Winderickx J. The AMPK/SNF1/SnRK1 fuel gauge and energy regulator: structure, function and regulation. FEBS J. 2011:**278**(21):3978–90. https://doi.org/10.1111/j.1742-4658.2011.08315.x

Gibon Y, Bläsing OE, Palacios-Rojas N, Pankovic D, Hendriks JHM, Fisahn J, Höhne M, Günther M, and Stitt M. Adjustment of diurnal starch turnover to short days: depletion of sugar during the night leads to a temporary inhibition of carbohydrate utilization, accumulation of sugars and post-translational activation of ADP-glucose pyrophosphorylase in the following light period. Plant J. 2004:**39**(6):847–62. https://doi.org/10.1111/j.1365-313X.2004.02173.x

Gissot L, Polge C, Bouly J-P, Lemaitre T, Kreis M, and Thomas M. AKINβ3, a plant specific SnRK1 protein, is lacking domains present in yeast and mammals non-catalytic β-subunits. Plant Mol Biol. 2004:**56**(5):747–759. https://doi.org/10.1007/s11103-004-5111-1

Gissot L, Polge C, Jossier M, Girin T, Bouly J-P, Kreis M, and Thomas M. AKINβγ contributes to SnRK1 heterotrimeric complexes and interacts with two proteins implicated in plant pathogen resistance through its KIS/GBD sequence. Plant Physiol. 2006:**142**(3):931–44. https://doi.org/10.1104/pp.106.087718

Glinski M and Weckwerth W. Differential multisite phosphorylation of the trehalose-6-phosphate synthase gene family in Arabidopsis thaliana: a mass spectrometry-based process for multiparallel peptide library phosphorylation analysis. Mol Cell Proteomics. 2005:**4**(10):1614–25. https://doi.org/10.1074/mcp.M500134-MCP200

Göbel M and Fichtner F. Functions of sucrose and trehalose 6-phosphate in controlling plant development. J Plant Physiol. 2023:**291**:154140. https://doi.org/10.1016/j.jplph.2023.154140

Gómez LD, Gilday A, Feil R, Lunn JE, and Graham IA. AtTPS1-mediated trehalose 6-phosphate synthesis is essential for embryogenic and vegetative growth and responsiveness to ABA in germinating seeds and stomatal guard cells. The Plant Journal. 2010:no-no. https://doi.org/10.1111/j.1365-313X.2010.04312.x

Griffiths CA, Sagar R, Geng Y, Primavesi LF, Patel MK, Passarelli MK, Gilmore IS, Steven RT, Bunch J, Paul MJ, et al. Chemical intervention in plant sugar signalling increases yield and resilience. Nature. 2016:**540**(7634):574–578. https://doi.org/10.1038/nature20591

Gururani MA, Venkatesh J, and Tran LSP. Regulation of Photosynthesis during Abiotic Stress-Induced Photoinhibition. Mol Plant. 2015:**8**(9):1304–20. https://doi.org/10.1016/j.molp.2015.05.005

Hanks SK and Hunter T. The eukaryotic protein kinase superfamily: kinase (catalytic) domain structure and classification. The FASEB Journal. 1995:**9**(8):576–596. https://doi.org/10.1096/fasebj.9.8.7768349

Hardie DG and Carling D. The AMP-activated protein kinase--fuel gauge of the mammalian cell? Eur J Biochem. 1997:**246**(2):259–73. https://doi.org/10.1111/j.1432-1033.1997.00259.x

Hardie DG, Carling D, and Carlson M. The AMP-activated/SNF1 protein kinase subfamily: metabolic sensors of the eukaryotic cell? Annu Rev Biochem. 1998:**67**:821–55. https://doi.org/10.1146/annurev.biochem.67.1.821

Hardie DG, Ross FA, and Hawley SA. AMPK: a nutrient and energy sensor that maintains energy homeostasis. Nat Rev Mol Cell Biol. 2012:**13**(4):251–62. https://doi.org/10.1038/nrm3311

Harthill JE, Meek SEM, Morrice N, Peggie MW, Borch J, Wong BHC, and MacKintosh C. Phosphorylation and 14-3-3 binding of Arabidopsis trehalose-phosphate synthase 5 in response to 2-deoxyglucose. Plant Journal. 2006:**47**(2):211–223. https://doi.org/10.1111/j.1365-313X.2006.02780.x

Hassan MU, Nawaz M, Shah AN, Raza A, Barbanti L, Skalicky M, Hashem M, Brestic M, Pandey S, Alamri S, et al. Trehalose: A Key Player in Plant Growth Regulation and Tolerance to Abiotic Stresses. J Plant Growth Regul. 2023:**42**(8):4935–4957. https://doi.org/10.1007/s00344-022-10851-7

Hatzfeld WD, Dancer J, and Stitt M. Fructose-2,6-bisphosphate, metabolites and “coarse” control of pyrophosphate: fructose-6-phosphate phosphotransferase during triose-phosphate cycling in heterotrophic cell-suspension cultures of Chenopodium rubrum. Planta. 1990:**180**(2):205–11. https://doi.org/10.1007/BF00193997

Hawley SA, Davison M, Woods A, Davies SP, Beri RK, Carling D, and Hardie DG. Characterization of the AMP-activated protein kinase kinase from rat liver and identification of threonine 172 as the major site at which it phosphorylates AMP-activated protein kinase. J Biol Chem. 1996:**271**(44):27879–87. https://doi.org/10.1074/jbc.271.44.27879

Hedbacker K, Townley R, and Carlson M. Cyclic AMP-dependent protein kinase regulates the subcellular localization of Snf1-Sip1 protein kinase. Mol Cell Biol. 2004:**24**(5):1836–43. https://doi.org/10.1128/MCB.24.5.1836-1843.2004

Henninger M, Pedrotti L, Krischke M, Draken J, Wildenhain T, Fekete A, Rolland F, Müller MJ, Fröschel C, Weiste C, et al. The evolutionarily conserved kinase SnRK1 orchestrates resource mobilization during Arabidopsis seedling establishment. Plant Cell. 2022:**34**(1):616–632. https://doi.org/10.1093/plcell/koab270

Henry C, Bledsoe SW, Griffiths CA, Kollman A, Paul MJ, Sakr S, and Lagrimini LM. Differential Role for Trehalose Metabolism in Salt-Stressed Maize. Plant Physiol. 2015:**169**(2):1072–89. https://doi.org/10.1104/pp.15.00729

Henry C, Bledsoe SW, Siekman A, Kollman A, Waters BM, Feil R, Stitt M, and Lagrimini LM. The trehalose pathway in maize: conservation and gene regulation in response to the diurnal cycle and extended darkness. J Exp Bot. 2014:**65**(20):5959–73. https://doi.org/10.1093/jxb/eru335

Herzig S and Shaw RJ. AMPK: guardian of metabolism and mitochondrial homeostasis. Nat Rev Mol Cell Biol. 2018:**19**(2):121–135. https://doi.org/10.1038/nrm.2017.95

Hey S, Mayerhofer H, Halford NG, and Dickinson JR. DNA sequences from Arabidopsis, which encode protein kinases and function as upstream regulators of Snf1 in yeast. J Biol Chem. 2007:**282**(14):10472–9. https://doi.org/10.1074/jbc.M611244200

Huang X, Zheng C, Liu F, Yang C, Zheng P, Lu X, Tian J, Chung T, Otegui MS, Xiao S, et al. Genetic Analyses of the Arabidopsis ATG1 Kinase Complex Reveal Both Kinase-Dependent and Independent Autophagic Routes during Fixed-Carbon Starvation. Plant Cell. 2019:**31**(12):2973–2995. https://doi.org/10.1105/tpc.19.00066

Huber SC, MacKintosh C, and Kaiser WM. Metabolic enzymes as targets for 14-3-3 proteins. Plant Mol Biol. 2002:**50**(6):1053–63. https://doi.org/10.1023/a:1021284002779

Huse M and Kuriyan J. The Conformational Plasticity of Protein Kinases. Cell. 2002:**109**(3):275–282. https://doi.org/10.1016/S0092-8674(02)00741-9

Ikeda Y, Koizumi N, Kusano T, and Sano H. Specific binding of a 14-3-3 protein to autophosphorylated WPK4, an SNF1-related wheat protein kinase, and to WPK4-phosphorylated nitrate reductase. J Biol Chem. 2000:**275**(41):31695–700. https://doi.org/10.1074/jbc.M004892200

Ishihara H, Alseekh S, Feil R, Perera P, George GM, Niedźwiecki P, Arrivault S, Zeeman SC, Fernie AR, Lunn JE, et al. Rising rates of starch degradation during daytime and trehalose 6-phosphate optimize carbon availability. Plant Physiol. 2022:**189**(4):1976–2000. https://doi.org/10.1093/plphys/kiac162

Jamsheer K M, Jindal S, Sharma M, Awasthi P, S S, Sharma M, Mannully CT, and Laxmi A. A negative feedback loop of TOR signaling balances growth and stress-response trade-offs in plants. Cell Rep. 2022:**39**(1):110631. https://doi.org/10.1016/j.celrep.2022.110631

Jamsheer K M, Kumar M, and Srivastava V. SNF1-related protein kinase 1: the many-faced signaling hub regulating developmental plasticity in plants. J Exp Bot. 2021:**72**(17):6042–6065. https://doi.org/10.1093/jxb/erab079

Jamsheer K M, Sharma M, Singh D, Mannully CT, Jindal S, Shukla BN, and Laxmi A. FCS-like zinc finger 6 and 10 repress SnRK 1 signalling in Arabidopsis. The Plant Journal. 2018a:**94**(2):232–245. https://doi.org/10.1111/tpj.13854

Jamsheer K M, Shukla BN, Jindal S, Gopan N, Mannully CT, and Laxmi A. The FCS-like zinc finger scaffold of the kinase SnRK1 is formed by the coordinated actions of the FLZ domain and intrinsically disordered regions. J Biol Chem. 2018b:**293**(34):13134–13150. https://doi.org/10.1074/jbc.RA118.002073

Jeong E-Y, Seo PJ, Woo JC, and Park C-M. AKIN10 delays flowering by inactivating IDD8 transcription factor through protein phosphorylation in Arabidopsis. BMC Plant Biol. 2015:**15**:110. https://doi.org/10.1186/s12870-015-0503-8

Jossier M, Bouly JP, Meimoun P, Arjmand A, Lessard P, Hawley S, Grahame Hardie D, and Thomas M. SnRK1 (SNF1-related kinase 1) has a central role in sugar and ABA signalling in Arabidopsis thaliana. Plant Journal. 2009:**59**(2):316–328. https://doi.org/10.1111/j.1365-313X.2009.03871.x

K MJ and Laxmi A. DUF581 Is Plant Specific FCS-Like Zinc Finger Involved in Protein-Protein Interaction. PLoS One. 2014:**9**(6):e99074. https://doi.org/10.1371/journal.pone.0099074

Kataya ARA, Elshobaky A, Heidari B, Dugassa N-F, Thelen JJ, and Lillo C. Multi-targeted trehalose-6-phosphate phosphatase I harbors a novel peroxisomal targeting signal 1 and is essential for flowering and development. Planta. 2020:**251**(5):98. https://doi.org/10.1007/s00425-020-03389-z

Kaul S, Koo H, Jenkins J, Rizzo M, Rooney, and et al. Analysis of the genome sequence of the flowering plant Arabidopsis thaliana. Nature. 2000:**408**(6814):796–815. https://doi.org/10.1038/35048692

Kim G-D, Cho Y-H, and Yoo S-D. Regulatory Functions of Cellular Energy Sensor SNF1-Related Kinase1 for Leaf Senescence Delay through ETHYLENE-INSENSITIVE3 Repression. Sci Rep. 2017:**7**(1):3193. https://doi.org/10.1038/s41598-017-03506-1

Kleinow T, Bhalerao R, Breuer F, Umeda M, Salchert K, and Koncz C. Functional identification of an Arabidopsis snf4 ortholog by screening for heterologous multicopy suppressors of snf4 deficiency in yeast. Plant J. 2000:**23**(1):115–22. https://doi.org/10.1046/j.1365-313x.2000.00809.x

Koncz C, deJong F, Villacorta N, Szakonyi D, and Koncz Z. The Spliceosome-Activating Complex: Molecular Mechanisms Underlying the Function of a Pleiotropic Regulator. Front Plant Sci. 2012:**3**. https://doi.org/10.3389/fpls.2012.00009

Kosar F, Akram NA, Sadiq M, Al-Qurainy F, and Ashraf M. Trehalose: A Key Organic Osmolyte Effectively Involved in Plant Abiotic Stress Tolerance. J Plant Growth Regul. 2019:**38**(2):606–618. https://doi.org/10.1007/s00344-018-9876-x

Krasensky J, Broyart C, Rabanal FA, and Jonak C. The redox-sensitive chloroplast trehalose-6-phosphate phosphatase AtTPPD regulates salt stress tolerance. Antioxid Redox Signal. 2014:**21**(9):1289–304. https://doi.org/10.1089/ars.2013.5693

Kulma A, Villadsen D, Campbell DG, Meek SEM, Harthill JE, Nielsen TH, and MacKintosh C. Phosphorylation and 14-3-3 binding of Arabidopsis 6-phosphofructo-2-kinase/fructose-2,6-bisphosphatase. Plant J. 2004:**37**(5):654–67. https://doi.org/10.1111/j.1365-313x.2003.01992.x

Lastdrager J, Hanson J, and Smeekens S. Sugar signals and the control of plant growth and development. J Exp Bot. 2014:**65**(3):799–807. https://doi.org/10.1093/jxb/ert474

Le DT, Nishiyama R, Watanabe Y, Mochida K, Yamaguchi-Shinozaki K, Shinozaki K, and Tran L-SP. Genome-wide survey and expression analysis of the plant-specific NAC transcription factor family in soybean during development and dehydration stress. DNA Res. 2011:**18**(4):263–76. https://doi.org/10.1093/dnares/dsr015

Lee J-H, Terzaghi W, Gusmaroli G, Charron J-BF, Yoon H-J, Chen H, He YJ, Xiong Y, and Deng XW. Characterization of Arabidopsis and rice DWD proteins and their roles as substrate receptors for CUL4-RING E3 ubiquitin ligases. Plant Cell. 2008:**20**(1):152–67. https://doi.org/10.1105/tpc.107.055418

Lee K-W, Chen P-W, Lu C-A, Chen S, Ho T-HD, and Yu S-M. Coordinated responses to oxygen and sugar deficiency allow rice seedlings to tolerate flooding. Sci Signal. 2009:**2**(91):ra61. https://doi.org/10.1126/scisignal.2000333

Leyman B, Van Dijck P, and Thevelein JM. An unexpected plethora of trehalose biosynthesis genes in Arabidopsis thaliana. Trends Plant Sci. 2001:**6**(11):510–513. https://doi.org/10.1016/S1360-1385(01)02125-2

Li C, Qi W, Liang Z, Yang X, Ma Z, and Song R. A SnRK1-ZmRFWD3-Opaque2 Signaling Axis Regulates Diurnal Nitrogen Accumulation in Maize Seeds. Plant Cell. 2020:**32**(9):2823–2841. https://doi.org/10.1105/tpc.20.00352

Li X, Cai W, Liu Y, Li H, Fu L, Liu Z, Xu L, Liu H, Xu T, and Xiong Y. Differential TOR activation and cell proliferation in Arabidopsis root and shoot apexes. Proc Natl Acad Sci U S A. 2017:**114**(10):2765–2770. https://doi.org/10.1073/pnas.1618782114

Liang J, Zhang S, Yu W, Wu X, Wang W, Peng F, and Xiao Y. *PpSnRK1α* overexpression alters the response to light and affects photosynthesis and carbon metabolism in tomato. Physiol Plant. 2021:**173**(4):1808–1823. https://doi.org/10.1111/ppl.13523

Lin C-R, Lee K-W, Chen C-Y, Hong Y-F, Chen J-L, Lu C-A, Chen K-T, Ho T-HD, and Yu S-M. SnRK1A-interacting negative regulators modulate the nutrient starvation signaling sensor SnRK1 in source-sink communication in cereal seedlings under abiotic stress. Plant Cell. 2014:**26**(2):808–27. https://doi.org/10.1105/tpc.113.121939

Lin Q, Gong J, Zhang Z, Meng Z, Wang J, Wang S, Sun J, Gu X, Jin Y, Wu T, et al. The Arabidopsis thaliana trehalose-6-phosphate phosphatase gene AtTPPI regulates primary root growth and lateral root elongation. Front Plant Sci. 2023a:**13**. https://doi.org/10.3389/fpls.2022.1088278

Lin Q, Wang J, Gong J, Zhang Z, Wang S, Sun J, Li Q, Gu X, Jiang J, and Qi S. The Arabidopsis thaliana trehalose-6-phosphate phosphatase gene AtTPPI improve chilling tolerance through accumulating soluble sugar and JA. Environ Exp Bot. 2023b:**205**:105117. https://doi.org/10.1016/j.envexpbot.2022.105117

Lin Q, Wang S, Dao Y, Wang J, and Wang K. Arabidopsis thaliana trehalose-6-phosphate phosphatase gene TPPI enhances drought tolerance by regulating stomatal apertures. J Exp Bot. 2020:**71**(14):4285–4297. https://doi.org/10.1093/jxb/eraa173

Lin Q, Yang J, Wang Q, Zhu H, Chen Z, Dao Y, and Wang K. Overexpression of the trehalose-6-phosphate phosphatase family gene AtTPPF improves the drought tolerance of Arabidopsis thaliana. BMC Plant Biol. 2019:**19**(1):381. https://doi.org/10.1186/s12870-019-1986-5

Lin S-C and Hardie DG. AMPK: Sensing Glucose as well as Cellular Energy Status. Cell Metab. 2018:**27**(2):299–313. https://doi.org/10.1016/j.cmet.2017.10.009

Lin SS, Manchester JK, and Gordon JI. Sip2, an N-myristoylated beta subunit of Snf1 kinase, regulates aging in Saccharomyces cerevisiae by affecting cellular histone kinase activity, recombination at rDNA loci, and silencing. J Biol Chem. 2003:**278**(15):13390–7. https://doi.org/10.1074/jbc.M212818200

Liu L and Li J. Communications Between the Endoplasmic Reticulum and Other Organelles During Abiotic Stress Response in Plants. Front Plant Sci. 2019:**10**:749. https://doi.org/10.3389/fpls.2019.00749

Liu X, Fu L, Qin P, Sun Y, Liu J, and Wang X. Overexpression of the wheat trehalose 6-phosphate synthase 11 gene enhances cold tolerance in Arabidopsis thaliana. Gene. 2019:**710**:210–217. https://doi.org/10.1016/j.gene.2019.06.006

Lopes FL, Formosa-Jordan P, Malivert A, Margalha L, Confraria A, Feil R, Lunn JE, Jönsson H, Landrein B, and Baena-González E. Sugar signaling modulates SHOOT MERISTEMLESS expression and meristem function in *Arabidopsis*. Proceedings of the National Academy of Sciences. 2024:**121**(37). https://doi.org/10.1073/pnas.2408699121

López-Paz C, Vilela B, Riera M, Pagès M, and Lumbreras V. Maize AKINβγ dimerizes through the KIS/CBM domain and assembles into SnRK1 complexes. FEBS Lett. 2009:**583**(12):1887–1894. https://doi.org/10.1016/j.febslet.2009.05.022

Lu Y, Gehan JP, and Sharkey TD. Daylength and circadian effects on starch degradation and maltose metabolism. Plant Physiol. 2005:**138**(4):2280–91. https://doi.org/10.1104/pp.105.061903

Lumbreras V, Alba MM, Kleinow T, Koncz C, and Pagès M. Domain fusion between SNF1-related kinase subunits during plant evolution. EMBO Rep. 2001:**2**(1):55–60. https://doi.org/10.1093/embo-reports/kve001

Lunn JE. Gene families and evolution of trehalose metabolism in plants. Functional Plant Biology. 2007:**34**(6):550. https://doi.org/10.1071/FP06315

Lunn JE. Sucrose Metabolism. In. Encyclopedia of Life Sciences. (Wiley), pp. 1–9. https://doi.org/10.1002/9780470015902.a0021259.pub2

Lunn JE, Delorge I, Figueroa CM, Van Dijck P, and Stitt M. Trehalose metabolism in plants. The Plant Journal. 2014:**79**(4):544–567. https://doi.org/10.1111/tpj.12509

Lunn JE, Feil R, Hendriks JHM, Gibon Y, Morcuende R, Osuna D, Scheible W-R, Carillo P, Hajirezaei M-R, and Stitt M. Sugar-induced increases in trehalose 6-phosphate are correlated with redox activation of ADPglucose pyrophosphorylase and higher rates of starch synthesis in *Arabidopsis thaliana*. Biochemical Journal. 2006:**397**(1):139–148. https://doi.org/10.1042/BJ20060083

Ma J, Hanssen M, Lundgren K, Hernández L, Delatte T, Ehlert A, Liu C-M, Schluepmann H, Dröge-Laser W, Moritz T, et al. The sucrose-regulated Arabidopsis transcription factor bZIP11 reprograms metabolism and regulates trehalose metabolism. New Phytol. 2011:**191**(3):733–745. https://doi.org/10.1111/j.1469-8137.2011.03735.x

Mahfouz MM, Kim S, Delauney AJ, and Verma DPS. Arabidopsis TARGET OF RAPAMYCIN interacts with RAPTOR, which regulates the activity of S6 kinase in response to osmotic stress signals. Plant Cell. 2006:**18**(2):477–90. https://doi.org/10.1105/tpc.105.035931

Mair A, Pedrotti L, Wurzinger B, Anrather D, Simeunovic A, Weiste C, Valerio C, Dietrich K, Kirchler T, Nägele T, et al. SnRK1-triggered switch of bZIP63 dimerization mediates the low-energy response in plants. Elife. 2015. https://doi.org/10.7554/eLife.05828

Margalha L, Confraria A, and Baena-González E. SnRK1 and TOR: modulating growth–defense trade-offs in plant stress responses. J Exp Bot. 2019:**70**(8):2261–2274. https://doi.org/10.1093/jxb/erz066

Martínez-Barajas E, Delatte T, Schluepmann H, de Jong GJ, Somsen GW, Nunes C, Primavesi LF, Coello P, Mitchell RAC, and Paul MJ. Wheat Grain Development

Is Characterized by Remarkable Trehalose 6-Phosphate Accumulation Pregrain Filling: Tissue Distribution and Relationship to SNF1-Related Protein Kinase1 Activity. Plant Physiol. 2011:**156**(1):373–381. https://doi.org/10.1104/pp.111.174524

Martins MCM, Hejazi M, Fettke J, Steup M, Feil R, Krause U, Arrivault S, Vosloh D, Figueroa CM, Ivakov A, et al. Feedback Inhibition of Starch Degradation in Arabidopsis Leaves Mediated by Trehalose 6-Phosphate. Plant Physiol. 2013:**163**(3):1142–1163. https://doi.org/10.1104/pp.113.226787

Mason MG, Ross JJ, Babst BA, Wienclaw BN, and Beveridge CA. Sugar demand, not auxin, is the initial regulator of apical dominance. Proc Natl Acad Sci U S A. 2014:**111**(16):6092–7. https://doi.org/10.1073/pnas.1322045111

Mayer F V, Heath R, Underwood E, Sanders MJ, Carmena D, McCartney RR, Leiper FC, Xiao B, Jing C, Walker PA, et al. ADP regulates SNF1, the Saccharomyces cerevisiae homolog of AMP-activated protein kinase. Cell Metab. 2011:**14**(5):707–14. https://doi.org/10.1016/j.cmet.2011.09.009

McMichael Jr RW, Bachmann M, and Huber SC. Spinach Leaf Sucrose-Phosphate Synthase and Nitrate Reductase Are Phosphorylated/Inactivated by Multiple Protein Kinases in Vitro. Plant Physiol. 1995:**108**(3):1077–1082. https://doi.org/10.1104/pp.108.3.1077

Meitzel T, Radchuk R, McAdam EL, Thormählen I, Feil R, Munz E, Hilo A, Geigenberger P, Ross JJ, Lunn JE, et al. Trehalose 6-phosphate promotes seed filling by activating auxin biosynthesis. New Phytologist. 2021:**229**(3):1553–1565. https://doi.org/10.1111/nph.16956

Moorhead G, Douglas P, Morrice N, Scarabel M, Aitken A, and MacKintosh C. Phosphorylated nitrate reductase from spinach leaves is inhibited by 14-3-3 proteins and activated by fusicoccin. Current Biology. 1996:**6**(9):1104–1113. https://doi.org/10.1016/S0960-9822(02)70677-5

Morales-Herrera S, Jourquin J, Coppé F, Lopez-Galvis L, De Smet T, Safi A, Njo M, Griffiths CA, Sidda JD, Mccullagh JSO, et al. Trehalose-6-phosphate signaling regulates lateral root formation in Arabidopsis thaliana. Proceedings of the National Academy of Sciences. 2023:**120**(40). https://doi.org/10.1073/pnas.2302996120

Muhammad I, Shalmani A, Ali M, Yang Q-H, Ahmad H, and Li FB. Mechanisms Regulating the Dynamics of Photosynthesis Under Abiotic Stresses. Front Plant Sci. 2020:**11**:615942. https://doi.org/10.3389/fpls.2020.615942

Nietzsche M, Landgraf R, Tohge T, and Börnke F. A protein–protein interaction network linking the energy-sensor kinase SnRK1 to multiple signaling pathways in Arabidopsis thaliana. Curr Plant Biol. 2016:**5**:36–44. https://doi.org/10.1016/j.cpb.2015.10.004

Nietzsche M, Schießl I, and Börnke F. The complex becomes more complex: protein-protein interactions of SnRK1 with DUF581 family proteins provide a

framework for cell- and stimulus type-specific SnRK1 signaling in plants. Front Plant Sci. 2014:**5**. https://doi.org/10.3389/fpls.2014.00054

Nuccio ML, Wu J, Mowers R, Zhou H-P, Meghji M, Primavesi LF, Paul MJ, Chen X, Gao Y, Haque E, et al. Expression of trehalose-6-phosphate phosphatase in maize ears improves yield in well-watered and drought conditions. Nat Biotechnol. 2015:**33**(8):862–9. https://doi.org/10.1038/nbt.3277

Nukarinen E, Ngele T, Pedrotti L, Wurzinger B, Mair A, Landgraf R, Börnke F, Hanson J, Teige M, Baena-Gonzalez E, et al. Quantitative phosphoproteomics reveals the role of the AMPK plant ortholog SnRK1 as a metabolic master regulator under energy deprivation. Sci Rep. 2016:**6**(August):1–19. https://doi.org/10.1038/srep31697

Nunes C, O'Hara LE, Primavesi LF, Delatte TL, Schluepmann H, Somsen GW, Silva AB, Fevereiro PS, Wingler A, and Paul MJ. The Trehalose 6-Phosphate/SnRK1 Signaling Pathway Primes Growth Recovery following Relief of Sink Limitation. Plant Physiol. 2013a:**162**(3):1720–1732. https://doi.org/10.1104/pp.113.220657

Nunes C, Primavesi LF, Patel MK, Martinez-Barajas E, Powers SJ, Sagar R, Fevereiro PS, Davis BG, and Paul MJ. Inhibition of SnRK1 by metabolites: Tissue-dependent effects and cooperative inhibition by glucose 1-phosphate in combination with trehalose 6-phosphate. Plant Physiology and Biochemistry. 2013b:**63**:89–98. https://doi.org/10.1016/j.plaphy.2012.11.011

Oakhill JS, Chen Z-P, Scott JW, Steel R, Castelli LA, Ling N, Macaulay SL, and Kemp BE. β-Subunit myristoylation is the gatekeeper for initiating metabolic stress sensing by AMP-activated protein kinase (AMPK). Proc Natl Acad Sci U S A. 2010:**107**(45):19237–41. https://doi.org/10.1073/pnas.1009705107

Oakhill JS, Steel R, Chen ZP, Scott JW, Ling N, Tam S, and Kemp BE. AMPK is a direct adenylate charge-regulated protein kinase. Science (1979). 2011. https://doi.org/10.1126/science.1200094

O'Brien M, Kaplan-Levy RN, Quon T, Sappl PG, and Smyth DR. PETAL LOSS, a trihelix transcription factor that represses growth in Arabidopsis thaliana, binds the energy-sensing SnRK1 kinase AKIN10. J Exp Bot. 2015:**66**(9):2475–2485. https://doi.org/10.1093/jxb/erv032

Osuna D, Usadel B, Morcuende R, Gibon Y, Bläsing OE, Höhne M, Günter M, Kamlage B, Trethewey R, Scheible W-R, et al. Temporal responses of transcripts, enzyme activities and metabolites after adding sucrose to carbon-deprived Arabidopsis seedlings. Plant J. 2007:**49**(3):463–91. https://doi.org/10.1111/j.1365-313X.2006.02979.x

Oszvald M, Primavesi LF, Griffiths CA, Cohn J, Basu SS, Nuccio ML, and Paul MJ. Trehalose 6-Phosphate Regulates Photosynthesis and Assimilate Partitioning in

Reproductive Tissue. Plant Physiol. 2018:**176**(4):2623–2638. https://doi.org/10.1104/pp.17.01673

Paul MJ, Jhurreea D, Zhang Y, Primavesi LF, Delatte T, Schluepmann H, and Wingler A. Up-regulation of biosynthetic processes associated with growth by trehalose 6-phosphate. Plant Signal Behav. 2010:**5**(4):386–392. https://doi.org/10.4161/psb.5.4.10792

Pedrotti L, Weiste C, Nägele T, Wolf E, Lorenzin F, Dietrich K, Mair A, Weckwerth W, Teige M, Baena-González E, et al. Snf1-RELATED KINASE1-Controlled C/S $_1$ -bZIP Signaling Activates Alternative Mitochondrial Metabolic Pathways to Ensure Plant Survival in Extended Darkness. Plant Cell. 2018:**30**(2):495–509. https://doi.org/10.1105/tpc.17.00414

Peixoto B, Moraes TA, Mengin V, Margalha L, Vicente R, Feil R, Höhne M, Sousa AGG, Lilue J, Stitt M, et al. Impact of the SnRK1 protein kinase on sucrose homeostasis and the transcriptome during the diel cycle. Plant Physiol. 2021:**187**(3):1357–1373. https://doi.org/10.1093/plphys/kiab350

Persyn F, Smagghe W, Eeckhout D, Mertens T, Smorscek T, De Winne N, Persiau G, Van De Slijke E, Crepin N, Gadeyne A, et al. A Nitrogen-specific Interactome Analysis Sheds Light on the Role of the SnRK1 and TOR Kinases in Plant Nitrogen Signaling. Molecular & Cellular Proteomics. 2024:**23**(10):100842. https://doi.org/10.1016/j.mcpro.2024.100842

Pfeiffer A, Janocha D, Dong Y, Medzihradszky A, Schöne S, Daum G, Suzaki T, Forner J, Langenecker T, Rempel E, et al. Integration of light and metabolic signals for stem cell activation at the shoot apical meristem. Elife. 2016:**5**. https://doi.org/10.7554/eLife.17023

Piattoni CV, Bustos DM, Guerrero SA, and Iglesias AÁ. Nonphosphorylating glyceraldehyde-3-phosphate dehydrogenase is phosphorylated in wheat endosperm at serine-404 by an SNF1-related protein kinase allosterically inhibited by ribose-5-phosphate. Plant Physiol. 2011:**156**(3):1337–50. https://doi.org/10.1104/pp.111.177261

Pierre M, Traverso JA, Boisson B, Domenichini S, Bouchez D, Giglione C, and Meinnel T. *N* -Myristoylation Regulates the SnRK1 Pathway in *Arabidopsis*. Plant Cell. 2007:**19**(9):2804–2821. https://doi.org/10.1105/tpc.107.051870

Plaxton WC. The Organization and Regulation of Plant Glycolysis. Annu Rev Plant Physiol Plant Mol Biol. 1996:**47**(1):185–214. https://doi.org/10.1146/annurev.arplant.47.1.185

Polge C, Jossier M, Crozet P, Gissot L, and Thomas M. β -Subunits of the SnRK1 Complexes Share a Common Ancestral Function Together with Expression and Function Specificities; Physical Interaction with Nitrate Reductase Specifically Occurs

via AKIN *β* 1-Subunit. Plant Physiol. 2008:**148**(3):1570–1582. https://doi.org/10.1104/pp.108.123026

Polge C and Thomas M. SNF1/AMPK/SnRK1 kinases, global regulators at the heart of energy control? Trends Plant Sci. 2007:**12**(1):20–28.

Ponnu J, Schlereth A, Zacharaki V, Działo MA, Abel C, Feil R, Schmid M, and Wahl V. The trehalose 6-phosphate pathway impacts vegetative phase change in *Arabidopsis thaliana*. The Plant Journal. 2020:**104**(3):768–780. https://doi.org/10.1111/tpj.14965

Radchuk R, Emery RJN, Weier D, Vigeolas H, Geigenberger P, Lunn JE, Feil R, Weschke W, and Weber H. Sucrose non-fermenting kinase 1 (SnRK1) coordinates metabolic and hormonal signals during pea cotyledon growth and differentiation. The Plant Journal. 2009:**61**(2):324–338. https://doi.org/10.1111/j.1365-313X.2009.04057.x

Ramon M, Dang TVT, Broeckx T, Hulsmans S, Crepin N, Sheen J, and Rolland F. Default Activation and Nuclear Translocation of the Plant Cellular Energy Sensor SnRK1 Regulate Metabolic Stress Responses and Development. Plant Cell. 2019:**31**(7):1614–1632. https://doi.org/10.1105/tpc.18.00500

Ramon M, Ruelens P, Li Y, Sheen J, Geuten K, and Rolland F. The hybrid four-CBS-domain KINβγ subunit functions as the canonical γ subunit of the plant energy sensor SnRK1. Plant J. 2013:**75**(1):11–25. https://doi.org/10.1111/tpj.12192

Ramon M, De Smet I, Vandesteene L, Naudts M, Leyman B, Van Dijck P, Rolland F, Beeckman T, and Thevelein JM. Extensive expression regulation and lack of heterologous enzymatic activity of the Class II trehalose metabolism proteins from *Arabidopsis thaliana*. Plant Cell Environ. 2009:**32**(8):1015–1032. https://doi.org/10.1111/j.1365-3040.2009.01985.x

Robertlee J, Kobayashi K, Suzuki M, and Muranaka T. AKIN10, a representative Arabidopsis SNF1-related protein kinase 1 (SnRK1), phosphorylates and downregulates plant HMG-CoA reductase. FEBS Lett. 2017:**591**(8):1159–1166. https://doi.org/10.1002/1873-3468.12618

Rodrigues A, Adamo M, Crozet P, Margalha L, Confraria A, Martinho C, Elias A, Rabissi A, Lumbreras V, Gonzalez-Guzman M, et al. ABI1 and PP2CA Phosphatases Are Negative Regulators of Snf1-Related Protein Kinase1 Signaling in Arabidopsis. Plant Cell. 2013. https://doi.org/10.1105/tpc.113.114066

Ruiz A, Xu X, and Carlson M. Ptc1 protein phosphatase 2C contributes to glucose regulation of SNF1/AMP-activated protein kinase (AMPK) in Saccharomyces cerevisiae. J Biol Chem. 2013:**288**(43):31052–8. https://doi.org/10.1074/jbc.M113.503763

Satoh-Nagasawa N, Nagasawa N, Malcomber S, Sakai H, and Jackson D. A trehalose metabolic enzyme controls inflorescence architecture in maize. Nature. 2006:**441**(7090):227–30. https://doi.org/10.1038/nature04725

Schepetilnikov M, Dimitrova M, Mancera-Martínez E, Geldreich A, Keller M, and Ryabova LA. TOR and S6K1 promote translation reinitiation of uORF-containing mRNAs via phosphorylation of eIF3h. EMBO J. 2013:**32**(8):1087–102. https://doi.org/10.1038/emboj.2013.61

Schepetilnikov M, Kobayashi K, Geldreich A, Caranta C, Robaglia C, Keller M, and Ryabova LA. Viral factor TAV recruits TOR/S6K1 signalling to activate reinitiation after long ORF translation. EMBO J. 2011:**30**(7):1343–56. https://doi.org/10.1038/emboj.2011.39

Schepetilnikov M, Makarian J, Srour O, Geldreich A, Yang Z, Chicher J, Hammann P, and Ryabova LA. GTPase ROP2 binds and promotes activation of target of rapamycin, TOR, in response to auxin. EMBO J. 2017:**36**(7):886–903. https://doi.org/10.15252/embj.201694816

Schluepmann H, Pellny T, van Dijken A, Smeekens S, and Paul M. Trehalose 6-phosphate is indispensable for carbohydrate utilization and growth in Arabidopsis thaliana. Proceedings of the National Academy of Sciences. 2003. https://doi.org/10.1073/pnas.1132018100

Schmid M, Davison TS, Henz SR, Pape UJ, Demar M, Vingron M, Schölkopf B, Weigel D, and Lohmann JU. A gene expression map of Arabidopsis thaliana development. Nat Genet. 2005:**37**(5):501–506. https://doi.org/10.1038/ng1543

Sheen J. Master Regulators in Plant Glucose Signaling Networks. J Plant Biol. 2014:**57**(2):67–79. https://doi.org/10.1007/s12374-014-0902-7

Shen W, Reyes MI, and Hanley-Bowdoin L. Arabidopsis Protein Kinases GRIK1 and GRIK2 Specifically Activate SnRK1 by Phosphorylating Its Activation Loop. Plant Physiol. 2009:**150**(2):996–1005. https://doi.org/10.1104/pp.108.132787

Shi L, Wu Y, and Sheen J. TOR signaling in plants: conservation and innovation. Development. 2018:**145**(13). https://doi.org/10.1242/dev.160887

Singh V, Louis J, Ayre BG, Reese JC, and Shah J. TREHALOSE PHOSPHATE SYNTHASE11-dependent trehalose metabolism promotes Arabidopsis thaliana defense against the phloem-feeding insect Myzus persicae. Plant Journal. 2011. https://doi.org/10.1111/j.1365-313X.2011.04583.x

Smith AM and Stitt M. Coordination of carbon supply and plant growth. Plant Cell Environ. 2007. https://doi.org/10.1111/j.1365-3040.2007.01708.x

Son S, Im JH, Ko J, Lee Y, Lee S, and Han K. SNF1 -related protein kinase 1 represses *Arabidopsis* growth through post-translational modification of E2Fa in

response to energy stress. New Phytologist. 2023:**237**(3):823–839. https://doi.org/10.1111/nph.18597

Steinberg GR and Kemp BE. AMPK in Health and Disease. Physiol Rev. 2009:**89**(3):1025–78. https://doi.org/10.1152/physrev.00011.2008

Stitt M. Fructose 2,6-Bisphosphate and Plant Carbohydrate Metabolism. Plant Physiol. 1987:**84**(2):201–204. https://doi.org/10.1104/pp.84.2.201

Stitt M. Fructose-2,6-Bisphosphate as a Regulatory Molecule in Plants. Annu Rev Plant Physiol Plant Mol Biol. 1990:**41**(1):153–185. https://doi.org/10.1146/annurev.pp.41.060190.001101

Stitt M. Pyrophosphate as an Energy Donor in the Cytosol of Plant Cells: an Enigmatic Alternative to ATP. Botanica Acta. 1998:**111**(3):167–175. https://doi.org/10.1111/j.1438-8677.1998.tb00692.x

Stitt M, Lunn J, and Usadel B. Arabidopsis and primary photosynthetic metabolism - more than the icing on the cake. Plant J. 2010:**61**(6):1067–91. https://doi.org/10.1111/j.1365-313X.2010.04142.x

Sugden C, Crawford RM, Halford NG, and Hardie DG. Regulation of spinach SNF1-related (SnRK1) kinases by protein kinases and phosphatases is associated with phosphorylation of the T loop and is regulated by 5'-AMP. Plant J. 1999a:**19**(4):433–9. https://doi.org/10.1046/j.1365-313x.1999.00532.x

Sugden C, Donaghy PG, Halford NG, and Hardie DG. Two SNF1-Related Protein Kinases from Spinach Leaf Phosphorylate and Inactivate 3-Hydroxy-3-Methylglutaryl-Coenzyme A Reductase, Nitrate Reductase, and Sucrose Phosphate Synthase in Vitro. Plant Physiol. 1999b:**120**(1):257–274. https://doi.org/10.1104/pp.120.1.257

Sulpice R, Flis A, Ivakov AA, Apelt F, Krohn N, Encke B, Abel C, Feil R, Lunn JE, and Stitt M. Arabidopsis Coordinates the Diurnal Regulation of Carbon Allocation and Growth across a Wide Range of Photoperiods. Mol Plant. 2014:**7**(1):137–155. https://doi.org/10.1093/mp/sst127

Suzuki N, Bajad S, Shuman J, Shulaev V, and Mittler R. The Transcriptional Co-activator MBF1c Is a Key Regulator of Thermotolerance in Arabidopsis thaliana. Journal of Biological Chemistry. 2008:**283**(14):9269–9275. https://doi.org/10.1074/jbc.M709187200

Tian L, Xie Z, Lu C, Hao X, Wu S, Huang Y, Li D, and Chen L. The trehalose-6-phosphate synthase TPS5 negatively regulates ABA signaling in Arabidopsis thaliana. Plant Cell Rep. 2019:**38**(8):869–882. https://doi.org/10.1007/s00299-019-02408-y

Toroser D, Plaut Z, and Huber SC. Regulation of a plant SNF1-related protein kinase by glucose-6-phosphate. Plant Physiol. 2000:**123**(1):403–12. https://doi.org/10.1104/pp.123.1.403

Tsai AYL and Gazzarrini S. AKIN10 and FUSCA3 interact to control lateral organ development and phase transitions in Arabidopsis. Plant Journal. 2012. https://doi.org/10.1111/j.1365-313X.2011.04832.x

Usadel B, Bläsing OE, Gibon Y, Retzlaff K, Höhne M, Günther M, and Stitt M. Global Transcript Levels Respond to Small Changes of the Carbon Status during Progressive Exhaustion of Carbohydrates in Arabidopsis Rosettes. Plant Physiol. 2008. https://doi.org/10.1104/pp.107.115592

van Dam TJP, Zwartkruis FJT, Bos JL, and Snel B. Evolution of the TOR pathway. J Mol Evol. 2011:**73**(3–4):209–20. https://doi.org/10.1007/s00239-011-9469-9

Vandesteene L, López-Galvis L, Vanneste K, Feil R, Maere S, Lammens W, Rolland F, Lunn JE, Avonce N, Beeckman T, et al. Expansive Evolution of the TREHALOSE-6-PHOSPHATE PHOSPHATASE Gene Family in Arabidopsis. Plant Physiol. 2012. https://doi.org/10.1104/pp.112.201400

Vandesteene L, Ramon M, Le Roy K, Van Dijck P, and Rolland F. A single active trehalose-6-P synthase (TPS) and a family of putative regulatory TPS-like proteins in arabidopsis. Mol Plant. 2010. https://doi.org/10.1093/mp/ssp114

Van Dijck P, Mascorro-Gallardo JO, De Bus M, Royackers K, Iturriaga G, and Thevelein JM. Truncation of Arabidopsis thaliana and Selaginella lepidophylla trehalose-6-phosphate synthase unlocks high catalytic activity and supports high trehalose levels on expression in yeast. Biochem J. 2002:**366**(Pt 1):63–71. https://doi.org/10.1042/BJ20020517

Van Houtte H, López-Galvis L, Vandesteene L, Beeckman T, and Van Dijck P. Redundant and non-redundant roles of the trehalose-6-phosphate phosphatases in leaf growth, root hair specification and energy-responses in Arabidopsis. Plant Signal Behav. 2013:**8**(3):e23209. https://doi.org/10.4161/psb.23209

Van Leene J, Eeckhout D, Gadeyne A, Matthijs C, Han C, De Winne N, Persiau G, Van De Slijke E, Persyn F, Mertens T, et al. Mapping of the plant SnRK1 kinase signalling network reveals a key regulatory role for the class II T6P synthase-like proteins. Nat Plants. 2022:**8**(11):1245–1261. https://doi.org/10.1038/s41477-022-01269-w

Vishal B, Krishnamurthy P, and Kumar PP. Arabidopsis class II TPS controls root development and confers salt stress tolerance through enhanced hydrophobic barrier deposition. Plant Cell Rep. 2024:**43**(5):115. https://doi.org/10.1007/s00299-024-03215-w

Vishal B, Krishnamurthy P, Ramamoorthy R, and Kumar PP. OsTPS8 controls yield-related traits and confers salt stress tolerance in rice by enhancing suberin deposition. New Phytol. 2019:**221**(3):1369–1386. https://doi.org/10.1111/nph.15464

Vogel G, Aeschbacher RA, Müller J, Boller T, and Wiemken A. Trehalose-6-phosphate phosphatases from Arabidopsis thaliana: identification by functional

complementation of the yeast tps2 mutant. Plant J. 1998:**13**(5):673–83. https://doi.org/10.1046/j.1365-313x.1998.00064.x

Vogel G, Fiehn O, Jean-Richard-dit-Bressel L, Boller T, Wiemken A, Aeschbacher RA, and Wingler A. Trehalose metabolism in Arabidopsis: occurrence of trehalose and molecular cloning and characterization of trehalose-6-phosphate synthase homologues. J Exp Bot. 2001:**52**(362):1817–1826. https://doi.org/10.1093/jexbot/52.362.1817

Wahl V, Ponnu J, Schlereth A, Arrivault S, Langenecker T, Franke A, Feil R, Lunn JE, Stitt M, and Schmid M. Regulation of Flowering by Trehalose-6-Phosphate Signaling in *Arabidopsis thaliana*. Science (1979). 2013:**339**(6120):704–707. https://doi.org/10.1126/science.1230406

Wang P, Zhao Y, Li Z, Hsu C-C, Liu X, Fu L, Hou Y-J, Du Y, Xie S, Zhang C, et al. Reciprocal Regulation of the TOR Kinase and ABA Receptor Balances Plant Growth and Stress Response. Mol Cell. 2018:**69**(1):100-112.e6. https://doi.org/10.1016/j.molcel.2017.12.002

Wang W, Lu Y, Li J, Zhang X, Hu F, Zhao Y, and Zhou D-X. SnRK1 stimulates the histone H3K27me3 demethylase JMJ705 to regulate a transcriptional switch to control energy homeostasis. Plant Cell. 2021:**33**(12):3721–3742. https://doi.org/10.1093/plcell/koab224

Wang X, Du Y, and Yu D. Trehalose phosphate synthase 5-dependent trehalose metabolism modulates basal defense responses in Arabidopsis thaliana. J Integr Plant Biol. 2019:**61**(4):509–527. https://doi.org/10.1111/jipb.12704

Wang Y, Wang L, Micallef BJ, Tetlow IJ, Mullen RT, Feil R, Lunn JE, and Emes MJ. AKINβ1, a subunit of SnRK1, regulates organic acid metabolism and acts as a global modulator of genes involved in carbon, lipid, and nitrogen metabolism. J Exp Bot. 2020:**71**(3):1010–1028. https://doi.org/10.1093/jxb/erz460

Warden SM, Richardson C, O'Donnell J, Stapleton D, Kemp BE, and Witters LA. Post-translational modifications of the beta-1 subunit of AMP-activated protein kinase affect enzyme activity and cellular localization. Biochem J. 2001:**354**(Pt 2):275–83. https://doi.org/10.1042/0264-6021:3540275

Williams SP, Rangarajan P, Donahue JL, Hess JE, and Gillaspy GE. Regulation of Sucrose non-Fermenting Related Kinase 1 genes in Arabidopsis thaliana. Front Plant Sci. 2014:**5**. https://doi.org/10.3389/fpls.2014.00324

Wilson WA, Hawley SA, and Hardie DG. Glucose repression/derepression in budding yeast: SNF1 protein kinase is activated by phosphorylation under derepressing conditions, and this correlates with a high AMP:ATP ratio. Curr Biol. 1996:**6**(11):1426–34. https://doi.org/10.1016/s0960-9822(96)00747-6

Wingler A, Delatte TL, O'Hara LE, Primavesi LF, Jhurreea D, Paul MJ, and Schluepmann H. Trehalose 6-Phosphate Is Required for the Onset of Leaf

Senescence Associated with High Carbon Availability. Plant Physiol. 2012:**158**(3):1241–1251. https://doi.org/10.1104/pp.111.191908

Xiong Y, McCormack M, Li L, Hall Q, Xiang C, and Sheen J. Glucose–TOR signalling reprograms the transcriptome and activates meristems. Nature. 2013:**496**(7444):181–186. https://doi.org/10.1038/nature12030

Yadav UP, Ivakov A, Feil R, Duan GY, Walther D, Giavalisco P, Piques M, Carillo P, Hubberten HM, Stitt M, et al. The sucrose-trehalose 6-phosphate (Tre6P) nexus: Specificity and mechanisms of sucrose signalling by. J Exp Bot. 2014. https://doi.org/10.1093/jxb/ert457

Yang C, Li X, Yang L, Chen S, Liao J, Li K, Zhou J, Shen W, Zhuang X, Bai M, et al. A positive feedback regulation of SnRK1 signaling by autophagy in plants. Mol Plant. 2023:**16**(7):1192–1211. https://doi.org/10.1016/j.molp.2023.07.001

Yuan P, Zhou G, Yu M, Hammond JP, Liu H, Hong D, Cai H, Ding G, Wang S, Xu F, et al. Trehalose-6-phosphate synthase 8 increases photosynthesis and seed yield in Brassica napus. Plant J. 2024:**118**(2):437–456. https://doi.org/10.1111/tpj.16617

Zacharaki V, Ponnu J, Crepin N, Langenecker T, Hagmann J, Skorzinski N, Musialak-Lange M, Wahl V, Rolland F, and Schmid M. Impaired KIN10 function restores developmental defects in the *Arabidopsis trehalose 6-phosphate synthase1 (tps1)* mutant. New Phytologist. 2022:**235**(1):220–233. https://doi.org/10.1111/nph.18104

Zang B, Li H, Li W, Deng XW, and Wang X. Analysis of trehalose-6-phosphate synthase (TPS) gene family suggests the formation of TPS complexes in rice. Plant Mol Biol. 2011:**76**(6):507–522. https://doi.org/10.1007/s11103-011-9781-1

Zhai Z, Keereetaweep J, Liu H, Feil R, Lunn JE, and Shanklin J. Trehalose 6-Phosphate Positively Regulates Fatty Acid Synthesis by Stabilizing WRINKLED1. Plant Cell. 2018:**30**(10):2616–2627. https://doi.org/10.1105/tpc.18.00521

Zhang Y, Primavesi LF, Jhurreea D, Andralojc PJ, Mitchell RAC, Powers SJ, Schluepmann H, Delatte T, Wingler A, and Paul MJ. Inhibition of SNF1-Related Protein Kinase1 Activity and Regulation of Metabolic Pathways by Trehalose-6-Phosphate. Plant Physiol. 2009:**149**(4):1860–1871. https://doi.org/10.1104/pp.108.133934

Zhang Z, Deng Y, Song X, and Miao M. Trehalose-6-phosphate and SNF1-related protein kinase 1 are involved in the first-fruit inhibition of cucumber. J Plant Physiol. 2015:**177**:110–120. https://doi.org/10.1016/j.jplph.2014.09.009

CHAPTER 2

TPS5/6/7 are essential for T6P-dependent coordination of sucrose metabolism with growth and development in *Arabidopsis thaliana*.

Author contributions: Diana Reis-Barata, John E. Lunn, Mark Stitt and Elena Baena-González conceived the research plan and designed the experiments. Diana Reis-Barata and Vinay Shukla (measurements of oxygen consumption rates) performed the experiments. Leonor Margalha assisted with RPS6 immunoblots. Regina Feil assisted with metabolite profiling. Camila Caldana assisted with metabolite profiling and metabolite data analyses. Stephanie Arrivault assisted with protein measurements. Andrzej Koczut and Umesh Prasad Yadav generated *tps* mutants. Diana Reis-Barata and Elena Baena-González analyzed, interpreted data, and wrote the manuscript. John E. Lunn and Mark Stitt interpreted data and edited the manuscript.

2.1. Abstract

The ability to sense and respond to carbon resources determines adaptation and survival in all organisms. In plants, sucrose stimulates growth and developmental progression via the signaling sugar trehalose 6-phosphate (T6P), which reflects sucrose availability. Although Class II trehalose 6-phosphate synthase (TPS) proteins share structural homology with catalytically active Class I TPS enzymes, they lack enzymatic activity, leaving their functional significance in the T6P pathway unresolved. Here, we show that Arabidopsis Class II TPS proteins TPS5/6/7 are indispensable for T6P-mediated coordination of carbon availability with growth and development. The combinatorial knockout of TPS5/6/7 results in delayed flowering and severe growth defects, particularly in roots. This is accompanied by a metabolic signature that is suggestive of T6P insensitivity and impaired sucrose utilization, characterized by hyperaccumulation of T6P and sucrose alongside depleted amino acid pools, root-specific dysregulation of phosphoenolpyruvate carboxylase (PEPC), and aberrantly high oxygen consumption rates. Together, these findings support a model where TPS5/6/7 serve as critical components of the T6P signaling network, potentially as T6P sensors.

2.2. Introduction

Plants meticulously coordinate growth and development with carbon availability to ensure metabolic balance across tissues. Among these carbon resources, sucrose is indispensable in most species, serving both as a primary product of photosynthesis and the dominant form of transported carbon from autotrophic source tissues to heterotrophic sink organs (Lunn 2016). Given this central role, precise sucrose monitoring and allocation are critical for plant survival, enabling dynamic partitioning of carbon and energy between growth, storage, and stress responses in changing environments (Smith and Stitt 2007).

Trehalose 6-phosphate (T6P), is a key sugar-signaling molecule, functioning both as a sucrose-specific signal and a negative feedback regulator of sucrose levels (Yadav et al., 2014; Figueroa & Lunn, 2016). As a signal, T6P levels fluctuate in parallel with sucrose, acting as a proxy for carbon availability to regulate metabolism (Figueroa et al. 2016; Fichtner and Lunn 2021) as well as to influence growth and developmental decisions that require substantial sucrose investment (Fichtner and Lunn 2021), including flowering (Wahl et al., 2013; Fichtner et al., 2020, 2021; Gramma et al., 2024), shoot branching (Fichtner et al. 2017, 2021), and root architecture (Morales-Herrera et al. 2023). As T6P levels rise, sucrose homeostasis is maintained by restricting further sucrose synthesis in source tissues while promoting its consumption in sink organs. In source leaves, high T6P during the day deflects the flux of newly fixed carbon from sucrose towards the synthesis of organic and amino acids, via post-translational activation of phosphoenolpyruvate carboxylase (PEPC) and nitrate reductase (NR) (Figueroa et al. 2016). At night, high T6P restricts starch mobilization (Martins et al., 2013; dos Anjos et al., 2018; Ishihara et al., 2022). In sink tissues, high T6P stimulates sucrose import by altering the expression of sucrolytic enzymes and SWEET transporters (Bledsoe et al., 2017; Oszvald et al., 2018; Fichtner et al., 2021) and enhances the accumulation of storage reserves (Zhai et al. 2018; Meitzel et al. 2021). T6P promotes sucrose consumption and growth, in part by antagonizing the activity of Sucrose Non Fermenting1-related protein kinase 1 (SnRK1) (Zhang et al. 2009; Nunes et al. 2013; Zhai et al. 2018; Avidan et al. 2024; Blanford et al. 2024), a highly conserved, energy-sensing protein kinase complex (composed of α, β, and βγ subunits) that plays critical roles in plant stress responses and growth regulation (Jamsheer K et al. 2021).

T6P is synthesized by T6P synthase (TPS) through condensation of UDP-glucose (UDPG) and glucose 6-phosphate (G6P), followed by dephosphorylation to trehalose mediated by T6P phosphatase (TPP) (Cabib & Leloir, 1958; Avonce et al., 2006). The *Arabidopsis thaliana* genome encodes eleven TPS isoforms subdivided into two clades: Class I (TPS1-4, hereafter termed TPS-I) and Class II (TPS5-11, hereafter termed TPS-II). Phylogenetically, TPS-II proteins further segregate into two distinct subclades, with TPS5-7 clustering separately from TPS8-10, and TPS11

possibly grouping with the latter (Lunn 2007). This phylogenetic division broadly parallels expression patterns under carbon starvation, with *TPS8-11* being strongly induced and *TPS5-7* largely unresponsive (Usadel et al. 2008; Cookson et al. 2016).

Among TPS-I members, TPS1 serves as the primary catalytic enzyme, with TPS2/4 displaying only residual activity (Vandesteene et al., 2010; Delorge et al., 2015). The essential role of TPS1 is underscored by the embryo lethality of *tps1* null mutants and the pleiotropic developmental defects of hypomorphic alleles, including dwarfism, delayed flowering, and aberrant cell wall morphology (Eastmond et al. 2002; Dijken et al. 2004; Gómez et al. 2006, 2010; Wahl et al. 2013; Fichtner et al. 2020). TPS-II proteins share the conserved domain structure of TPS-I isoforms, with N-terminal TPS-like and C-terminal TPP-like domains (Lunn 2007). However, TPS-II proteins lack catalytic activity (Vogel et al., 2001; Ramon et al., 2009; Vandesteene et al., 2010; Delorge et al., 2015) and appear to have evolved instead regulatory or signaling roles (Lunn et al. 2014; Van Leene et al. 2022). Notably, the rice TPS1 and TPS-II proteins were shown to physically interact in yeast two-hybrid and bimolecular fluorescence complementation assays (Zang et al. 2011), raising the possibility of functional cooperation between the clades.

Despite limited understanding of their functions, TPS-II proteins are widely distributed across plant tissues (Mergner et al. 2020), and exhibit tight transcriptional regulation, with distinct tissue-specific expression patterns and responsiveness to hormonal, carbon (Ramon et al. 2009), and nitrogen signals (Persyn et al. 2024), as demonstrated by promoter activity and transcript analyses. Recent studies revealed that TPS-II proteins physically interact with all SnRK1 subunits (α, β, and βγ) and inhibit SnRK1 activity *in vitro* and in transient protoplast assays (Van Leene et al. 2022), positioning them as potential integral regulatory components of the SnRK1 complex. Additionally, TPS-II proteins are themselves transcriptionally and post-translationally regulated by SnRK1 (Harthill et al., 2006; Cho et al., 2016; Nukarinen et al., 2016); however, the functional relevance of this regulation remains unresolved. Genetic evidence also implicates TPS-II proteins in various physiological processes: TPS5 in ABA signaling and thermotolerance (Tian et al., 2019; Suzuki et al., 2008)

TPS6 in cell shape (Chary et al. 2008) TPS9 in root development and salt stress tolerance (Vishal et al. 2024), and TPS11 in cold adaptation and aphid defense (Singh et al. 2011; Liu et al. 2019). However, whether these roles arise from TPS-II proteins acting downstream of T6P or through T6P-independent mechanisms remains unclear. Moreover, potential functional redundancy within this multi-gene family further complicates efforts to pinpoint their precise roles.

Here, we employ a combinatorial knockout approach, alongside genetic, biochemical, and plant phenotyping analyses, to investigate the function of TPS-II on plant growth and development. Plants lacking TPS5/6/7 exhibit delayed flowering, impaired root growth and severe metabolic imbalances. Our results suggest that these defects stem from disrupted T6P signaling and impaired sucrose utilization. This disruption leads to aberrantly high levels of T6P and soluble sugars, reduced amino acid pools, elevated oxygen consumption rates, and defective posttranslational activation of PEPC. Altogether, our findings suggest that TPS5/6/7 act as nodal regulators, integrating T6P signaling with metabolism, development and growth.

2.3. Results

2.3.1. Lack of TPS5/6/7 causes delayed flowering.

In sink tissues, T6P has been hypothesized to act as an indicator of the plant's carbon status, influencing growth and developmental transitions accordingly. In line with this, in various studies, T6P has been associated with the control of flowering (Wahl et al., 2013; Fichtner et al., 2020, 2021). To investigate the function of TPS-II proteins in this process, we explored the flowering-related phenotypes of loss-of-function mutants of these genes. We focused on *TPS5* and *TPS7* for two reasons. First, preliminary findings from our lab suggested a possible connection between TPS7 and flowering (Koczut et al., unpublished observations). Secondly, a recent proteome-wide interactome screen in Arabidopsis revealed an interaction between the flowering

time regulator FVE and TPS5 and TPS7 (Van Leene et al. 2022). Considering the partially overlapping pattern of *TPS6* promoter activity with that of *TPS5* and *TPS7* in Arabidopsis floral organs (Ramon et al. 2009) and their close phylogenetic relationship (Lunn 2007), we also included *TPS6* in this analysis. Col-0, *tps5*, *tps6* and *tps7* mutant plants were grown in soil under long-day conditions. Flowering time was determined by counting the number of days to flower ("chronological age") and the number of rosette leaves when the floral bud was first visible ("developmental age").

As shown in Figure 2.1A and C, *tps7* mutant plants displayed a significant late flowering phenotype, flowering on average two days later than Col-0 and producing approximately three more rosette leaves before flowering. To investigate whether the flowering phenotype of the *tps7* mutant was indeed dependent on TPS7, we generated *TPS7* complementation lines expressing mCherry-tagged TPS7 under the control of the *TPS7* endogenous promoter and terminator. To mitigate the potential influence of tag positioning on protein functionality, mCherry was placed either at the C- or N-terminus. In total, we isolated three independent lines for each construct. The lines with the mCherry tag at the C-terminus successfully rescued the late flowering phenotype of the *tps7* mutant (Figure 2.1A). In some cases, such as lines *C#7.10* and *C#6.3* which accumulated higher levels of TPS7 (Figure 2.1B; Supplementary Figure 2.1), the resulting plants flowered even earlier than Col-0 – on average, 2.8 and 1.4 days before, with 3.8 and 2.5 fewer leaves, respectively (Figure 2.1.A, all changes significant). In contrast, the lines with the mCherry tag at the N-terminus reverted only partly the flowering time of the *tps7* mutant, displaying an intermediate flowering phenotype between Col-0 and *tps7* (Figure 2.1A). Notably, Western blot analysis revealed a double band for N-terminally tagged TPS7, with an upper band at the predicted molecular weight (~125 kDa) and a smaller one (Figure 2.1B; Supplementary Figure 2.1), suggesting protein instability or alternative translation initiation that may explain its partial complementation capacity. Hence, for all subsequent assays, we used the C-terminally tagged version of TPS7 due to its complete complementation of the flowering phenotype.

Unlike *tps7*, *tps5* and *tps6* mutants exhibited no flowering phenotype (Koczut et al., unpublished observations). To account for potential compensatory functions of these proteins in flowering, we also examined double *tps5/7* and triple *tps5/6/7* mutants. The flowering time of these mutants was further delayed, increasing with the progressive accumulation of mutations (Supplementary Figure 2.2; Figure 2.1C). Specifically, the *tps5/6/7* mutant displayed the most pronounced phenotype, with a flowering delay of seven days and an average increase of four rosette leaves at flowering compared to Col-0 (Figure 2.1C). Furthermore, *tps5/6/7* plants grown in soil showed a reduced rosette diameter compared to Col-0, both at flowering and during earlier growth stages (Figure 2.1C; Supplementary Figure 2.3).

Overall, these findings implicate TPS5/6/7 proteins in the transition to flowering, and hint at a potential functional overlap between individual TPSs in the control of this process.

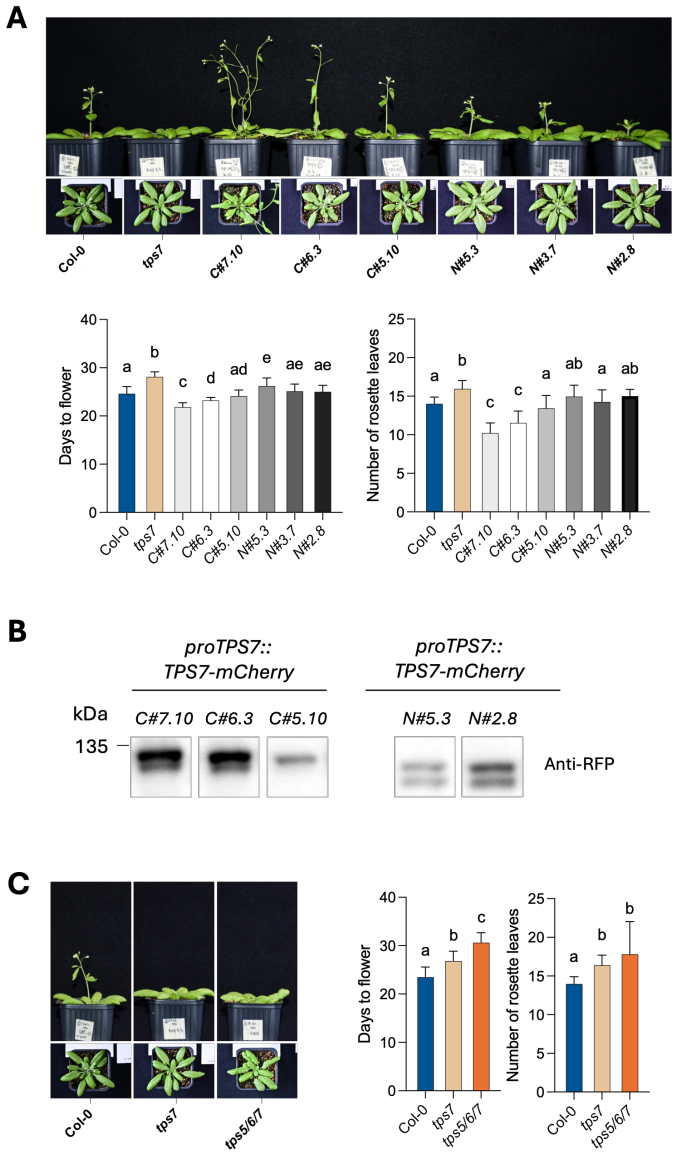

Figure 2.1. Lack of TPS5/6/7 causes delayed flowering.
Up (**A**) and left (**C**), representative images of 33-d old (**A**) Col-0, *tps7*, *tps7/proTPS7::TPS7-mCherry* (*C#7.10*, *C#6.3* and *C#5.10*) and *tps7/proTPS7::mCherry-TPS7* (*N#2.8*, *N#3.7* and *N#5.3*), and (**C**) Col-0, *tps7* and *tps5/6/7* plants grown on soil under long-day conditions (16 h light, 110 µmol m^{-2} s^{-1}, 22 °C / 8 h dark, 18 °C). Bottom (**A**) and right (**C**), quantification of flowering time based on days to flower and number of rosette leaves when the floral bud was first visible. Number of independent experiments and plants per genotype: (**A**) *n=2*, 19 plants; (**C**) *n=3*, 29 plants. Bars represent the mean of independent experiments (error bars, SD). Different letters indicate statistically significant differences between genotypes (one-way ANOVA with Tukey HSD test). **B,** Protein blot analysis of TPS7 levels in the indicated *tps7* complementation lines. The image shown is a cropped representation of the original uncut blot provided in Supplementary Figure 2.1.

2.3.2. Lack of TPS5/6/7 impairs root growth.

T6P has also been associated with the regulation of root growth (Fichtner et al. 2020; Morales-Herrera et al. 2023). Additionally, GUS reporter assays and proteomic analyses performed in Arabidopsis have revealed the activity of *TPS5/6/7* promoters and the expression of the corresponding proteins in root tissues, indicating a potential role in root development (Ramon et al., 2009; Mergner et al., 2020). Thus, to explore whether the function of TPS5/6/7 proteins is specific to flowering or extends to other sink tissues such as roots, we compared root growth in Col-0, single and higher degree *tps* mutants. To minimize the potential impact of germination asynchrony and root growth heterogeneity, which was particularly pronounced in the *tps5/6/7* mutant (Supplementary Figure 2.4), seedlings were grown vertically on 0.5× MS medium plates for 7 d and seedlings with comparable root sizes were thereafter transferred to new plates and grown for an additional 7 days. Primary root growth was measured as the length of root developed post-transfer. Whilst both *tps5* and *tps7* mutants exhibited a slight reduction in primary root length compared to Col-0, with the latter being statistically significant, *tps6* displayed no evident phenotype (Figure 2.2.A). Consistent with the effect seen in flowering, *TPS7* complementation lines *C#5.10* and *C#6.3* exhibited primary root lengths similar to Col-0, effectively reversing the root growth defect of the *tps7* mutant (Figure 2.2.B). The reduction in growth was more pronounced in higher-order mutants and increased in severity with the progressive accumulation of *tps* mutations, with *tps5/7* and *tps5/6/7* roots reaching only 67% and 59% of Col-0 length, respectively (Figure 2.2C-D).

In summary, our results demonstrate that TPS5/6/7 proteins play an important role in the regulation of flowering time and root development. Given that the shoot apical meristem (SAM) plays a major role in the floral transition (Barton 2010) and that the SAM and the root are both sink organs, this may suggest a more general role of TPS5/6/7 proteins in sink tissues.

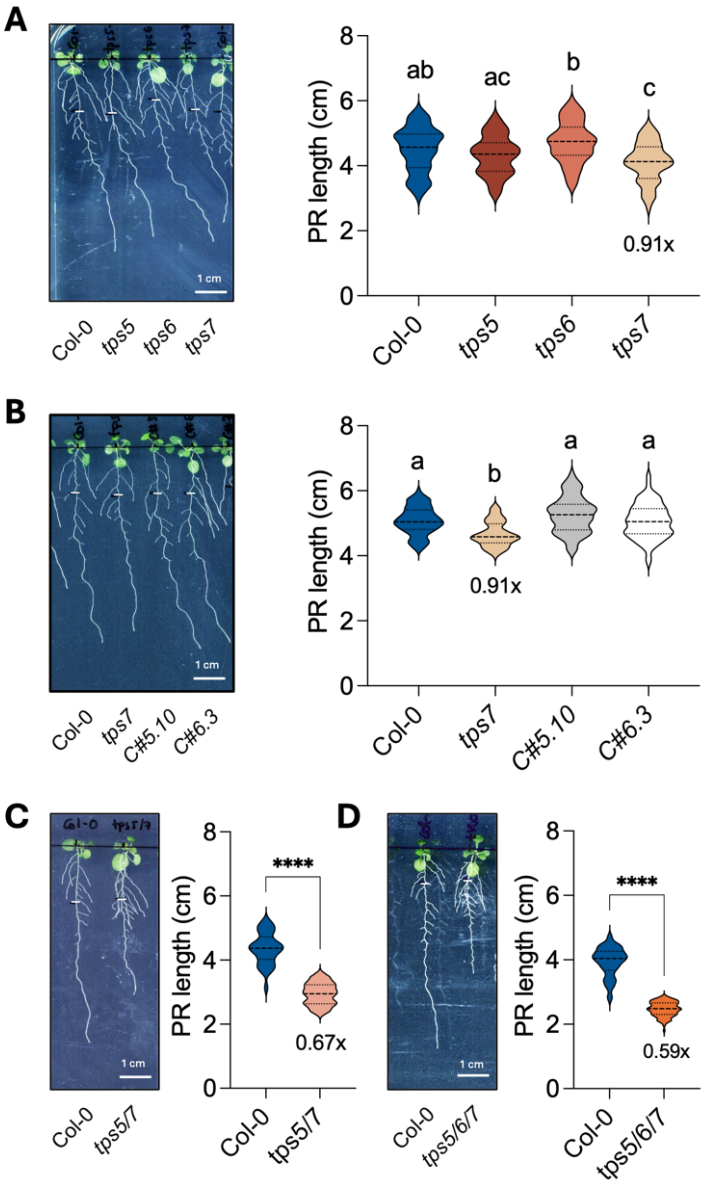

Figure 2.2. Lack of TPS5/6/7 impairs root growth.
Left (**A-D**), representative images of 14-d old (**A**) Col-0, *tps5*, *tps6* and *tps7*, (**B**) Col-0, *tps7* and *tps7/proTPS7::TPS7-mCherry* (*C#5.10* and *C#6.3*), (**C**) Col-0 and *tps5/7*, and (**D**) Col-0 and *tps5/6/7* seedlings grown vertically on 0.5× MS medium for 7 d, transferred to fresh 0.5× MS plates, and grown for an additional 7 d. White marks indicate the position of the root tip at transfer. Scale bar 1 cm. Right (**A-D**), quantification of the increase in primary root (PR) length, measured from the white mark to the root tip. Number of independent experiments and seedlings per genotype: (**A**) *n=3*, 48-64 seedlings; (**B**) *n=3*, 58-67 seedlings; (**C**) *n=2*, 34 seedlings; (**D**) *n=6*, 79-100 seedlings. The upper and lower horizontal lines represent the first and third quartiles, respectively. The middle horizontal dashed line indicates the median. Different letters (**A**,**B**) or asterisks (**C**,**D**) indicate statistically significant differences between genotypes ($p < 0.05$, one-way ANOVA with Tukey HSD test in **A**, and **B**; $p < 0.05$, two-tailed unpaired t-test in **C** and **D**). 0.67x and 0.59x indicate PR length relative to that in Col-0 (=1)

2.3.3. TPS5/6/7 promote root growth in response to sugar availability.

To investigate further TPS5/6/7 function, we focused on root growth, due to the easier manipulation of the nutrient status in plate-grown seedlings and the easier harvestability of roots as compared to the SAM.

Given the involvement of T6P metabolism in carbon allocation (see Introduction), we reasoned that the stunted root phenotype of the *tps5/6/7* mutant could result from disrupted sugar provision from source leaves to roots. To test this, Col-0 and *tps5/6/7* seedlings were grown vertically on 0.5× MS medium plates supplemented or not with 1% sucrose. The experimental setup and primary root length quantifications were as in 2.3.2. As expected, in Col-0 seedlings, sucrose treatment induced a significant increase in primary root length, with roots growing 1.22-fold longer than in mock conditions. However, the primary root length of the *tps5/6/7* mutant remained unaffected by sucrose (Figure 2.3A). This led to a much more pronounced difference in root growth in sucrose-containing medium, where *tps5/6/7* roots reached only 49% of the length observed in Col-0 (Figure 2.3A), compared to 61% on control plates (Figure 2.3A; see also Figure 2.2D).

Sucrose catabolism in heterotrophic tissues provides crucial substrates for primary metabolism, including glucose and fructose, which support cellular maintenance and growth. We therefore next investigated whether the growth defects of the *tps5/6/7* mutant could be rescued by supplementing the breakdown products of sucrose. As expected, the addition of glucose and fructose promoted primary root growth in Col-0; however, these sugars had no effect in the *tps5/6/7* mutant (Supplementary Figure 2.5). Altogether, our results show that TPS5/6/7 proteins are required to promote root growth in response to sugar availability and that they play at least a partially redundant function in this process.

Sucrose and glucose were shown to reactivate the quiescent root apical meristem (RAM), essential for root growth, in a Target of Rapamycin (TOR)-dependent manner (Xiong et al. 2013). Moreover, sucrose activates TOR in seedlings (Forzani et al. 2019; Ingargiola et al. 2023; Pereyra et al. 2023). Hence, a defective activation of

the TOR signaling pathway could provide a plausible explanation for the inability of the *tps5/6/7* mutant to utilize exogenous sugars for growth. Since the depletion of TPS5/6/7 primarily affects root growth, we aimed to determine whether potential differences in TOR activation were specific to this organ or also extended to aerial tissues. To investigate this, we monitored the status of TOR signaling in Col-0 and *tps5/6/7* seedlings using the phosphorylation of ribosomal protein 6 (phosphoS240-RPS6, hereafter referred as pRPS6) as a well-established readout (Dobrenel et al. 2016). Seedlings were grown with or without 1% sucrose for 14 d, and roots and shoots were harvested separately at the end of the night (EN), when growth rates are known to increase significantly both in roots (Yazdanbakhsh et al. 2011) and shoots (Nozue et al. 2007).

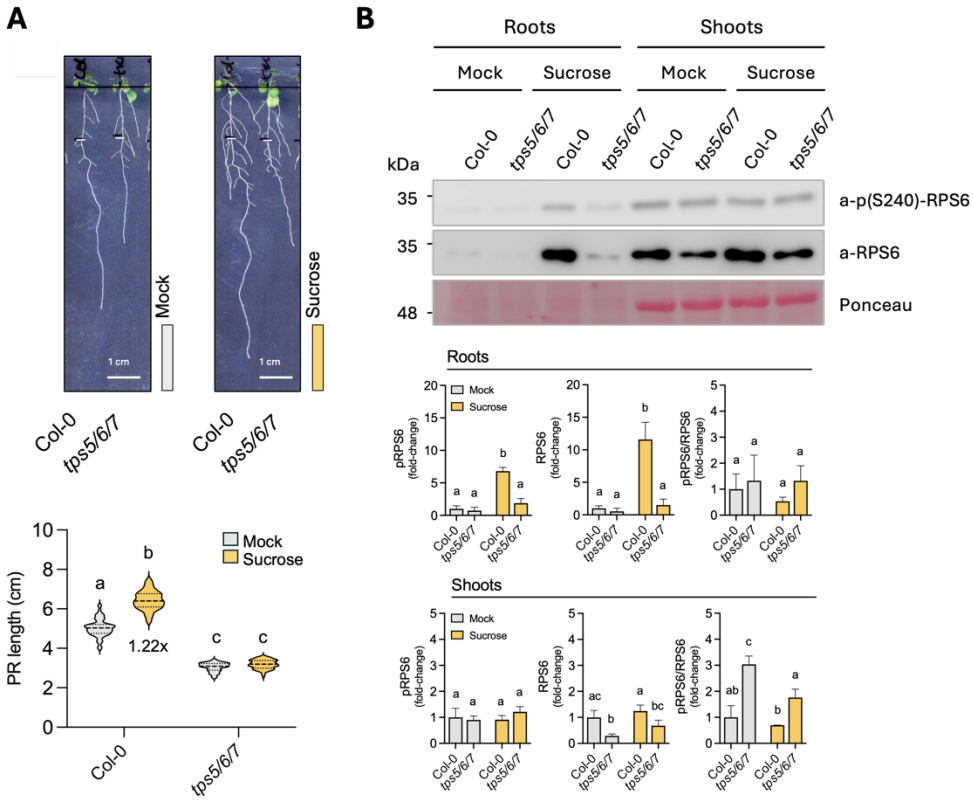

Figure 2.3. TPS5/6/7 promote root growth in response to sugar availability.
(**A**) Up, representative images of 14-d old Col-0 and *tps5/6/7* seedlings grown vertically on 0.5× MS medium for 7 d, transferred to 0.5× MS medium supplemented (right) or not (left) with 30 mM sucrose and grown for an additional 7 d. White marks indicate the position of the root tip at transfer. Scale bar 1 cm. Bottom, quantification of primary root (PR) length, measured from the white mark to the root tip (*n*=3, 76-85 seedlings per genotype per condition). The upper and lower horizontal lines represent the first and

third quartiles, respectively. The middle horizontal dashed line indicates the median. Different letters indicate statistically significant differences genotype and condition combinations ($p < 0.05$, one-way ANOVA with Tukey HSD test). (**B**) Up, representative immunoblots of p(S240)-RPS6 (top) and total RPS6 (bottom) from 14-d old Col-0 and *tps5/6/7* seedlings (roots and shoots). Seedlings were grown vertically on 0.5× MS medium 7 d, transferred to 0.5× MS medium supplemented or not with 1% sucrose, and grown for an additional 7 d. Samples were harvested at the end of the night. Three independent experiments were performed with similar results (Supplementary Figure 2.6). Bottom, quantification of pRPS6, RPS6 and relative pRPS6 (pRPS6/RPS6) in roots and shoots. Values were normalized to the Col-0 mock condition and expressed as fold- change. Bars show the mean of 3 independent experiments (error bars, SD). Different letters indicate statistically significant differences between genotype and condition combinations ($p < 0.05$, one-way ANOVA with Tukey HSD test).

In both Col-0 and *tps5/6/7* **shoots**, sucrose had a negligible effect on pRPS6 levels but induced a slight, non-significant increase in RPS6 (Figure 2.3B; Supplementary Figure 2.6). Nevertheless, RPS6 levels were consistently lower in the *tps5/6/7* mutant, reaching only 29% and 55% of the levels observed in Col-0 under mock and sucrose conditions, respectively. These differences in total RPS6, rather than an actual increase in pRPS6, led to unexpectedly higher relative RPS6 phosphorylation levels in the mutant, an effect that was stronger in mock conditions than in sucrose (Figure 2.3B; Supplementary Figure 2.6). In contrast to shoots, sucrose had a prominent impact on **roots**. In Col-0, sucrose caused a significant increase in total RPS6 (11.6-fold) and pRPS6 (6.8-fold) compared to the mock conditions. This led to a slight, non-significant decrease in relative RPS6 phosphorylation (pRPS6/total RPS6). Strikingly, *tps5/6/7* mutant roots showed nearly complete insensitivity to sucrose supplementation, with only subtle, non-significant increases in RPS6 and pRPS6 abundance that did not alter the relative RPS6 phosphorylation levels (Figure 2.3B; Supplementary Figure 2.6).

Overall, our results highlight a stark contrast in sucrose responsiveness between Col-0 and the *tps5/6/7* mutant. RPS6 protein abundance and its response to sucrose are impaired in *tps5/6/7* shoots and roots, with roots being more severely affected.

2.3.4. Lack of TPS5/6/7 causes aberrantly high sucrose, T6P and T6P:sucrose ratios.

To investigate the cause for the impaired growth of the *tps5/6/7* mutant and its lack of response to sugar, we first performed metabolite analyses. To avoid sugar carry-over from the medium, we tested whether growing seedlings in mock plates under two contrasting light intensities (Control light, 110 µmol m^{-2} s^{-1}; High Light, 200 µmol m^{-2} s^{-1}) could reproduce the differences in primary root growth observed between genotypes in the absence or presence of exogenous sugars. Growth under high light intensity led to a significant increase (1.17-fold) in primary root length in Col-0 but had no effect in the *tps5/6/7* mutant, whose root length was only 61% of that in Col-0 in control light and 51% of that in Col-0 in high light (Figure 2.4A), hence recapitulating, albeit to a milder extent, the effect of sugar supplementation (Figure 2.3A). We then grew seedlings under control and high light and harvested samples at the end of the night. To minimize masking potential tissue-specific responses, we collected shoots, roots, and root tips (<0.5 cm) separately and analyzed metabolites related to carbon and nitrogen primary metabolism by LC-MS/MS.

In Col-0, sucrose levels were lowest in root tips whilst T6P levels were highest in this tissue (Figure 2.4B). This resulted in higher T6P:sucrose ratios in root tips (Table 2.1) than in the rest of the tissues, consistent with the higher T6P:sucrose ratios reported in actively growing sinks (Lunn et al. 2014). Under control light, sucrose levels were similar in Col-0 and *tps5/6/7* but T6P levels were significantly higher in the mutant across all tissues (Figure 2.4B). Under high light, sucrose levels were higher in all *tps5/6/7* tissues (Figure 2.4B) and this was accompanied by a higher accumulation of the intermediate of sucrose synthesis, sucrose 6-phosphate (S6P) (Supplementary Figure 2.7). Under high light the differences between genotypes were dramatically larger for T6P, mounting up to 41-fold in roots (Figure 2.4B). This resulted in significantly higher T6P:sucrose ratios in the *tps5/6/7* mutant across all tissues and light conditions (Table 2.1). In all Col-0 tissues, both sucrose and T6P levels were in a similar range in the control and high light samples, as expected from the tight coupling between the two sugars (*ns*, Student t-test). However, this was not the case

in the mutant where sucrose and T6P were significantly higher in the high light than the low light samples across all tissues (p< 0.05, Student t-test).

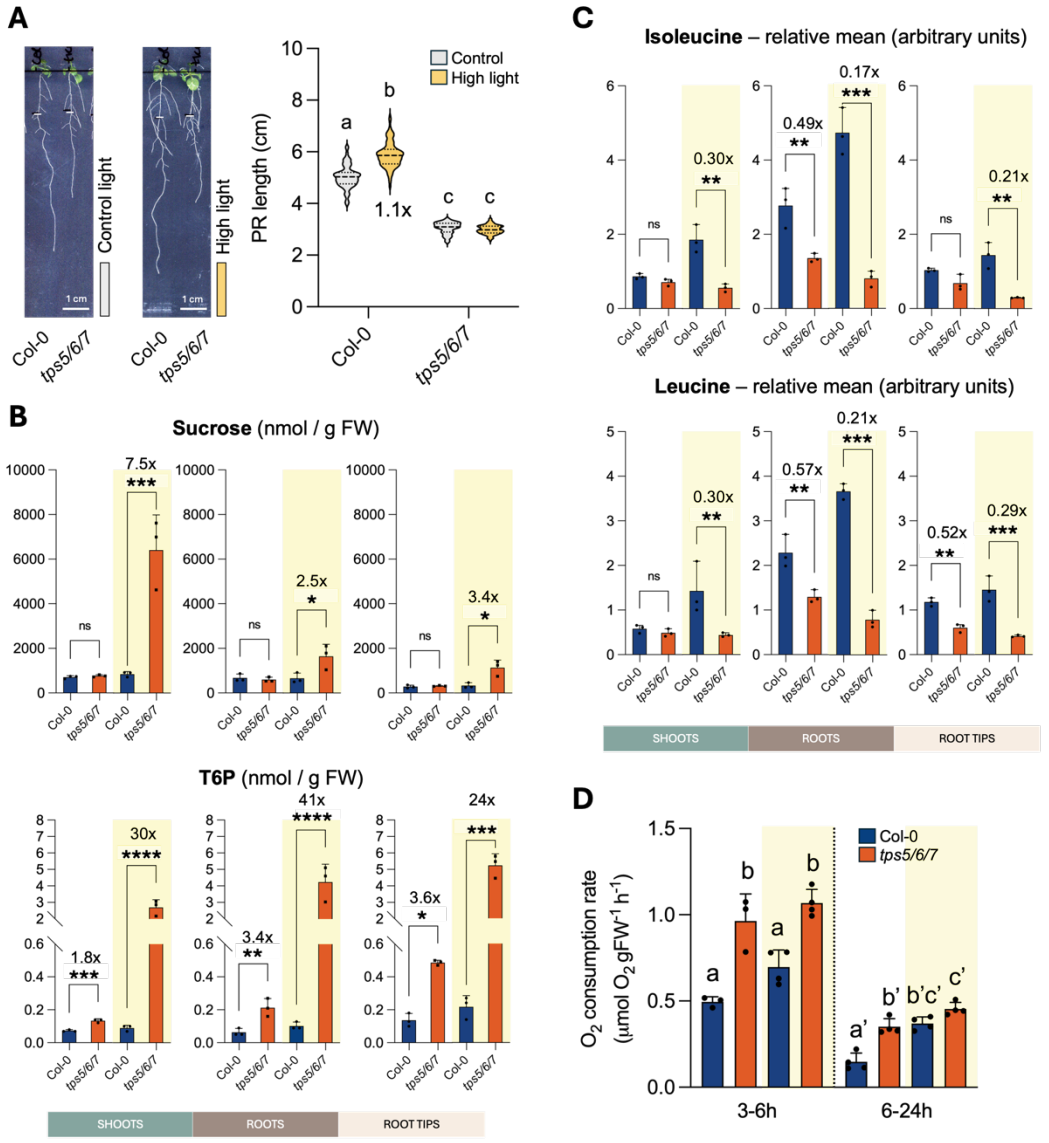

Figure 2.4. Lack of TPS5/6/7 causes a metabolic syndrome suggestive of altered T6P signaling. (**A**) Left and middle, representative images of 14-d old Col-0 and *tps5/6/7* seedlings grown vertically on 0.5× MS medium under control light conditions (110 µmol m^{-2} s^{-1}) for 7 d, transferred to fresh 0.5× MS plates and grown for an additional 7 d under control light (CL; left) or high light conditions (HL; 200 µmol m^{-2} s^{-1}; right). Scale bar 1 cm. Right, quantification of PR length, measured from the white mark to the root tip (n=3 independent experiments, 76-82 seedlings per genotype per condition). The upper and lower horizontal lines represent the first and third quartiles, respectively. The middle horizontal dashed line indicates the median. Different letters indicate statistically significant differences between genotype and condition (p < 0.05, one-way ANOVA with Tukey HSD test). (**B-C**), Levels of sucrose and T6P (**B**), and Isoleucine and Leucine (**C**) in the indicated tissues of 14d-old Col-0 and *tps5/6/7* seedlings grown as in

(A) under contrasting light intensities (CL, white; HL, yellow) and harvested at the end of the night. Graphs show the mean of 3 independent experiments (each consisting of 200-250 seedlings per genotype per condition, error bars, SD). Asterisks indicate statistically significant differences between genotypes within each tissue and condition ($p < 0.05$, two-tailed unpaired t-test). (**D**) Oxygen consumption rates (µmol O_2 g^{-1} FW h^{-1}) of 10d-old Col-0 and *tps5/6/7* seedlings upon transfer to fresh 0.5× MS medium with (yellow) or without sucrose (white). Shown are rates in the 3-6h and 6-24h time windows. Bars show the mean of 4 independent experiments (error bars, SD). Different letters indicate statistically significant differences between genotype and condition ($p < 0.05$, one-way ANOVA with Tukey HSD test).

Table 2.1. Impact of TPS5/6/7 on T6P:sucrose ratios.
T6P:sucrose ratios are means ± SD and were calculated using the T6P and sucrose values represented in Figure 2.4B. p-values refer to statistically significant differences between Col-0 and *tps5/6/7* for each growth condition (as described in Figure 2.4A) within the different tissues (two-tailed unpaired t-test)

Tissue	Genotype	Growth conditions	T6P:suc	*p*-value
Shoots	Col-0	Control light	0.105 ± 0.01	0.0015
	tps5/6/7		0.169 ± 0.01	
	Col-0	High light	0.101 ± 0.01	0.0001
	tps5/6/7		0.428 ± 0.04	
Roots	Col-0	Control light	0.095 ± 0.00	0.0005
	tps5/6/7		0.350 ± 0.04	
	Col-0	High light	0.156 ± 0.02	<0.0001
	tps5/6/7		2.643 ± 0.25	
Root tips	Col-0	Control light	0.463 ± 0.03	<0.0001
	tps5/6/7		1.540 ± 0.07	
	Col-0	High light	0.656 ± 0.16	0.0024
	tps5/6/7		4.793 ± 1.03	

The *tps5/6/7* mutant had also higher levels of the sucrose degradation products, glucose and fructose (Supplementary Figure 2.7), consistent with the inability of these sugars to rescue the growth defects of the mutant (Supplementary Figure 2.5). Under control light, glucose and fructose were moderately elevated in *tps5/6/7* root tissues, but the differences were markedly exacerbated under high light (Supplementary Figure 2.7), being highest for glucose in shoots and root tips and for fructose in shoots. Aberrantly high levels were also observed for the degradation product of T6P, trehalose, whose pattern followed closely that of T6P (Supplementary

Figure 2.7). These increases were particularly pronounced under high light in all tissues.

Collectively, our results reveal substantially altered sucrose and T6P metabolism in the *tps5/6/7* mutant, leading to dramatically increased T6P:sucrose ratios, particularly under high light conditions. This, together with the elevated levels of sucrose and T6P breakdown products and the inability of the *tps5/6/7* mutant to promote root growth, suggests a potential disruption in T6P signaling and sugar utilization.

2.3.5. Lack of TPS5/6/7 causes a metabolic syndrome suggestive of altered T6P signaling.

Previous studies in Arabidopsis have reported that an inducible rise in T6P leads to major metabolic changes, including increased accumulation of organic and amino acids (Figueroa et al., 2016; Ishihara et al., 2022; Avidan et al., 2024). Consequently, we investigated whether the elevated T6P levels observed in the *tps5/6/7* mutant elicited similar metabolic alterations in our EN samples.

Despite the substantial accumulation of T6P and sugars in the mutant, most central metabolites remained similar between Col-0 and *tps5/6/7* (Supplementary Figure 2.8A; see Supplementary Table 2.1 for the numeric values). Within glycolysis, significant differences were only observed for fructose 1,6-bisphosphate (Fru1,6BP) and pyruvate which were at higher levels in *tps5/6/7* roots under high light (2.3- and 1.7-fold higher, respectively) and for glucose 6-phosphate (G6P) and phosphoenolpyruvate (PEP), whose levels were lower in *tps5/6/7* shoots under control light (81% and 53% of Col-0 levels, respectively). For TCA cycle intermediates the differences were moderate and varied between the different tissues. In shoot samples, the *tps5/6/7* mutant had significantly higher levels of most organic acids than Col-0 under high light (Supplementary Figure 2.8A, see Supplementary Table 2.1A for the numeric values). A similar trend was observed in roots, though only citrate showed a

statistically significant increase in the mutant (1.7-fold higher under high light). In root tips, on the other hand, organic acid levels were mostly lower in the mutant, with significant decreases occurring for malate, oxoglutarate (2-OG), and fumarate under control light and for malate and aconitate under high light.

To gain further insight into the metabolic alterations of the *tps5/6/7* mutant, we used GC-MS/MS to measure the relative levels of amino acids. Most amino acids were at lower levels in the mutant tissues, especially under high light (Supplementary Figure 2.8A), with particularly pronounced decreases for Lys and branched-chain amino acids (BCAAs, Leu, Iso and Val) (Figure 2.4C; Supplementary Figure 2.8B). In control conditions, the levels of Leu and Iso in *tps5/6/7* roots were roughly half of those in Col-0. Under high light, these differences were strongly accentuated, becoming evident in all tissues (ranging from 30% to 17% of Col-0 levels; Figure 2.4C) and affecting also Val and Lys (Supplementary Figure 2.8B). In contrast, three amino acids exhibited significant changes in the opposite direction under high light, with Pro being significantly elevated in shoots and root tips, and Ala and Gln in roots in *tps5/6/7* compared to Col-0 (Supplementary Fig. 2.8A). Despite these changes in free amino acids, total protein levels appeared similar between Col-0 and *tps5/6/7* across all tissues and conditions (Supplementary Figure 2.9).

The degradation of sugars and amino acids generates TCA cycle intermediates that can be used for ATP production in mitochondrial respiration (O'Leary et al. 2019). We therefore next wondered whether the accumulation of sugars in the *tps5/6/7* mutant and its reduced growth could be related to altered respiration. To this end, we measured oxygen consumption rates in 10-d old seedlings supplemented or not with 1% sucrose. Measurements were taken upon transferring seedlings to an air-tight oxygen electrode chamber at ZT4, as well as 3h, 6h and 24h after the transfer. Oxygen consumption rates were calculated for the time windows of 3-6 h and 6-24 h (indicated as 6 h and 24 h in Figure 2.4D, respectively). In the 3-6h interval, the rate of oxygen consumption was significantly higher in *tps5/6/7* seedlings (Figure 2.4D). This was true both in the absence and presence of exogenous sucrose (1.94-fold and 1.53-fold, respectively), suggesting that the differences are not solely

due to the higher endogenous sugar levels of the mutant. In the 6-24h interval, rates were overall lower (>50%) than in the 3-6h interval, possibly reflecting the lower metabolic demands of plants under prolonged darkness. In the absence of sucrose, rates were significantly higher in *tps5/6/7* seedlings (2.38-fold) but in the presence of sucrose the rates were similar in both genotypes. Indeed, sucrose had a stimulatory effect on oxygen consumption in Col-0 (1.4-fold at 6 h and 2.5-fold at 24 h) that was clearly weaker in *tps5/6/7* (1.1-fold at 6 h and 1.3-fold at 24 h), with this difference reaching significance in the 6-24h interval (p=0.03, Student t-test).

Altogether, the metabolic profile of the *tps5/6/7* mutant does not align with what would be expected from its elevated sucrose and T6P levels, suggesting that lack of TPS-II proteins causes T6P insensitivity and impaired sucrose utilization.

2.3.6. Lack of TPS5/6/7 enhances NR activity in leaves but reduces stimulatory phosphorylation of PEPC in roots.

The metabolic response to high T6P typically involves a shift in carbon redistribution, achieved in part through post-translational modifications of enzymes such as NR and PEPC (Figueroa et al., 2016). We therefore next examined whether the observed metabolic defects of the *tps5/6/7* mutant correlated with changes in post-translational activation of these key enzymes.

NR catalyzes the first step in nitrogen assimilation, thereby providing a source of reduced nitrogen for biosynthetic processes (Xu et al. 2012). To examine the activation status of NR, Col-0 and *tps5/6/7* rosettes of Arabidopsis plants grown in soil under equinoctial conditions were harvested at four time points over a 24 h period: ZT0 (end of the night; EN), ZT6 (middle of the day; MD), ZT12 (end of the day; ED), and ZT18 (middle of the night; MN). The choice of rosettes and growth conditions was based on two factors: First, these plants were routinely grown in our lab in chambers set to a 12 h light/12 h dark photoperiod, providing readily available material for analysis. Second, the same material and conditions were used in the work by Figueroa

et al. (2016), offering a relevant comparative framework for studying the effects of T6P on NR activation. NR activity is post-translationally regulated through inhibitory phosphorylation, which is reversed under activating conditions (Kaiser and Huber 2001). To assess both the total enzymatic capacity and the physiologically active NR pool, we measured maximal activity (V*max*) in Mg^{2+}-free assay buffer, which captures all NR protein regardless of phosphorylation state. We also measured NR selective activity (V*sel*) by adding Mg^{2+} to the buffer. These conditions specifically reveal the non-phosphorylated (active) NR fraction by allowing Mg^{2+}-dependent binding of an inhibitory 14-3-3 protein to phosphorylated NR. This dual approach enabled us to distinguish changes in total NR abundance from alterations in its activation state. Whereas the maximal catalytic activity of NR (V*max*) was comparable between both lines across the different time points, the selective activity (V*sel*) was higher in the *tps5/6/7* mutant, specifically at MD (1.39-fold and significant; Figure 2.5A). This resulted in a significant 9% higher NR activation in the mutant compared to Col-0, consistent with the peak stimulatory effect of T6P on NR at the middle of the day reported by Figueroa et al. (2016). At MN and EN, NR activation was also slightly higher in the mutant, although the differences did not reach statistical significance (Figure 2.5A). Overall, the increase in NR activation observed after elevating T6P is also evident in the *tps5/6/7* mutant, although the effect is relatively modest.

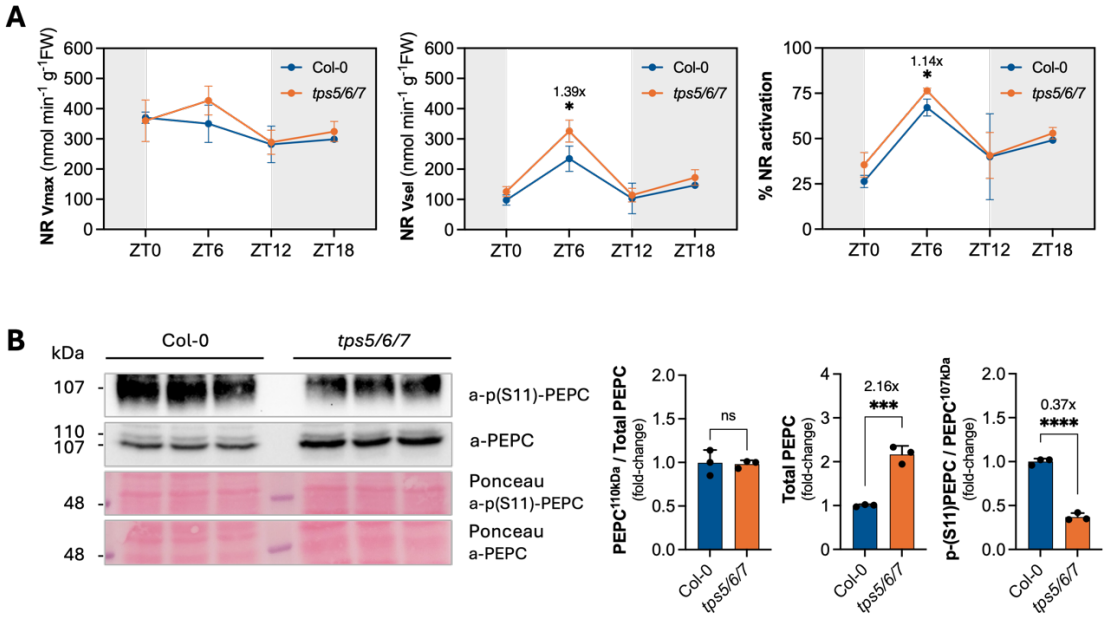

Figure 2.5. NR activation and PEPC phosphorylation are altered in the *tps5/6/7* mutant. (**A**), NR maximal activity (*Vmax*), NR selective activity (*Vsel*), and % NR activation in 25d-old Col-0 and *tps5/6/7* rosettes grown on soil under equinoctial conditions (12 h light, 110 µmol m^{-2} s^{-1}, 22 °C / 12 h dark, 18 °C). Samples were harvested at ZT0 (end of the night), ZT6 (middle of the day), ZT12 (end of the day), and ZT18 (middle of the night). White and shaded areas indicate light and dark periods, respectively. Data represent the mean of 3 independent experiments (4 rosettes per genotype per time point; error bars, SD). Asterisks denote statistically significant differences between genotypes at each time point ($p < 0.05$, two-tailed unpaired t-test). (**B**), Left, immunoblot of p(S11)-PEPC (phosphorylated form) and total PEPC, showing mono-ubiquitinated (110 kDa) and non-ubiquitinated (107 kDa) forms, in roots of 14d-old Col-0 and *tps5/6/7* seedlings grown under long day conditions (16 h light, 110 µmol m^{-2} s^{-1}, 22 °C / 8 h dark, 18 °C) and harvested at the end of the night. Right, quantification of monoubiquitinated ($PEPC^{110kDa}$/Total PEPC), total and phosphorylated PEPC [p(S11)PEPC/$PEPC^{107kDa}$]. Values were normalized to Col-0 and expressed as fold-change. Bars show the mean of 3 independent experiments (error bars, SD). Asterisks indicate significant differences between genotypes ($p < 0.05$, two-tailed unpaired t-test).

PEPC catalyzes the conversion of PEP into oxaloacetate (OAA), which can then be reduced to malate and fumarate, supporting the anaplerotic replenishment of the TCA cycle (Plaxton and Podestá 2006) as well as providing precursors for amino acid synthesis. Various mechanisms, including protein phosphorylation and mono-ubiquitination, regulate PEPC activity, activating or deactivating the enzyme, respectively, by modulating its sensitivity to allosteric inhibition by malate (Hartwell et al., 1999; O'Leary et al., 2011b). Notably, an inducible rise in T6P was shown to post-translationally activate PEPC, increasing PEPC phosphorylation while decreasing its mono-ubiquitination (Figueroa et al. 2016). Given that the T6P hyperaccumulation of

the *tps5/6/7* mutant was highest in roots, we used this tissue to compare the levels of total, phosphorylated and mono-ubiquitinated PEPC between Col-0 and *tps5/6/7*. To this end, we used immunoblotting with an anti-PEPC antibody that recognizes two distinct polypeptides: a 107 kDa non-ubiquitinated plant-type PEPC and the corresponding 110 kDa mono-ubiquitinated form (O'Leary et al., 2011a). Additionally, we used an anti-pSer11 antibody which specifically targets the activated phospho-Ser11 form of plant-type PEPC (Gregory et al. 2009).

Surprisingly, whilst similar mono-ubiquitinated PEPC amounts were observed between genotypes, *tps5/6/7* roots showed 2.2-fold higher total PEPC levels and phospho-PEPC levels reduced to 37% of those in Col-0 (Figure 2.5B). These findings are contrary to expectations for a mutant with elevated T6P levels, as higher T6P would typically promote PEPC phosphorylation and activation (Figueroa et al. 2016). Instead, the observed decrease in the phosphorylated form and increase in total PEPC levels likely suggests a disruption in the regulatory mechanisms linking T6P to PEPC activity.

Altogether, these results suggest that T6P signaling is likely more disrupted in roots than in shoots in the *tps5/6/7* mutant. While NR activation in aerial tissues aligns, to a certain extent, with the expected effects of high T6P (see section 4.3 of the General discussion), the unexpected PEPC regulation in roots points to tissue-specific differences in T6P signaling that could underlie the more pronounced growth impairment observed in the mutant's roots. However, an alternative explanation is that NR activation in shoots may be maintained through additional regulatory inputs that compensate for impaired T6P signaling, whereas PEPC regulation in roots may be more directly affected. To distinguish between these possibilities, it would be necessary to examine PEPC post-translational regulation in shoot tissues under comparable conditions. This would help clarify whether the contrasting regulatory patterns observed reflect tissue-specific differences in responsiveness to T6P or differences in the robustness of enzyme regulation.

2.4. Discussion

Here, we identify TPS5/6/7 proteins as signaling components of the T6P pathway. The *tps5/6/7* mutant displays growth and developmental defects, along with a metabolic signature indicative of disrupted T6P signaling, supporting a critical role for these proteins in proper T6P signal transduction.

2.4.1. T6P requires TPS5/6/7 to promote flowering.

According to the sucrose-T6P nexus model, T6P signals sucrose availability and regulates sucrose levels homeostatically, controlling sucrose synthesis in source leaves and facilitating its consumption in actively growing sink tissues, thereby affecting developmental decisions, such as flowering (Yadav et al., 2014; Figueroa & Lunn, 2016; Göbel & Fichtner, 2023). Flowering time is regulated by multiple interconnected pathways that integrate environmental inputs and endogenous signals. Genetic studies have shown that both AtTPS1 and T6P regulate key floral integrators within these pathways (Wahl et al., 2013; Fichtner et al., 2020, 2021; Gramma et al., 2024). In long-day conditions, flowering is triggered by FLOWERING LOCUS T (FT) expression in the leaf vasculature and its subsequent movement (as florigen) to the SAM (Turck et al. 2008). This expression, along with that of its upstream regulator *CONSTANS* (*CO*) and close homologue *TWIN SISTER OF FT* (*TSF*), has been shown to depend on the T6P-synthesizing activity of AtTPS1 (Wahl et al., 2013; Fichtner et al., 2021). Additionally, the T6P pathway promotes flowering at the SAM independently of photoperiodic signals by interacting with the miR156-SQUAMOSA PROMOTER BINDING PROTEIN-LIKE (SPL) module (Wahl et al. 2013). However, no studies to date have implicated TPS-II proteins in the regulation of flowering.

In our study, Arabidopsis plants lacking TPS7 exhibited a late-flowering phenotype under long-day conditions. This phenotype was more pronounced in the double (*tps5/7*) and most extreme in the triple (*tps5/6/7*) mutant (Figure 2.1A,C; Supplementary Figure 2.2). The underlying mechanisms for these phenotypes remain to be explored, but both direct and indirect roles of TPS5/6/7 in the regulation of

flowering time should be considered. Support for a direct role comes from recent research showing that TPS5 and TPS7 interact with the flowering time regulator FVE (Van Leene et al. 2022). This further supports a functional overlap between these proteins that is consistent with the stronger flowering delay of the *tps5/6/7* mutant compared to *tps7* (Figure 2.1C; Supplementary Figure 2.2).

On the other hand, TPS5/6/7 may indirectly affect flowering via T6P signaling. Higher and lower T6P levels are associated with early and late flowering, respectively. This was shown in Arabidopsis plants overexpressing an *E. coli* TPS (OtsA) or TPP (OtsB) either ubiquitously (Schluepmann et al. 2003), in the SAM (Wahl et al. 2013), or in the vasculature (Fichtner et al. 2021). In particular, OtsA overexpression in the vasculature led to a local increase in T6P levels along with upregulation of SWEET transporter genes in source leaves and rosette cores, potentially accelerating flowering by enhancing sucrose delivery to the SAM (Fichtner et al. 2021). Moreover, a similar link between T6P and SWEET gene expression was observed in the reproductive tissues of transgenic maize plants (Oszvald et al. 2018). Intriguingly, the *tps5/6/7* mutant flowered later than Col-0, despite having higher T6P levels, including in the shoots (Figure 2.4B), suggesting that this phenotype may result from disrupted T6P signaling.

The delayed flowering in *tps5/6/7* is reminiscent of reports of *tps1-1* mutant plants complemented with truncated (*AtTPS1[ΔNΔC]* or *AtTPS1[ΔC]*) or mutated (*AtTPS1[A119W]*) forms of *AtTPS1*, which also exhibited late or absent flowering despite elevated T6P levels (Fichtner et al. 2020). Also in this study, a disruption in T6P signaling was proposed as the underlying cause of the flowering phenotype. Noteworthy, the Fichtner study reported a correlation between the severity of the phenotypes and the accumulation of two unknown T6P-isomeric disaccharide-monophosphates, which elute just before and just after S6P, and that were hypothesized to interfere with signaling possibly through competitive binding to T6P-interacting proteins (Fichtner et al. 2020). The delayed flowering phenotype of the *tps5/6/7* mutant could potentially be explained by an increased accumulation of these T6P-like compounds. However, their levels in the shoots of the *tps5/6/7* mutant were

only marginally higher compared to Col-0 under CL conditions (similar to those used in the flowering assay; Supplementary Figure 2.10; Supplementary Table 2.1), suggesting that any disruption in T6P signaling in the *tps5/6/7* mutant likely arises from a different cause.

Notably, most of the active site residues within the C-terminal phosphatase-like domain of TPS-II proteins are highly conserved (Lunn 2007), possibly allowing for T6P binding. This prompts the hypothesis that TPS5/6/7 function as T6P sensors. If so, their absence could lead to a misinterpretation of T6P levels and, consequently, disrupt T6P-mediated processes that regulate flowering.

Importantly, the metabolic signature of the *tps5/6/7* mutant provides further compelling evidence that compromised T6P perception may indeed underlie its flowering delay and growth defects, as discussed below. First, compromised T6P sensing would impair sucrose utilization, creating a vicious cycle of sucrose accumulation and T6P overproduction that disrupts the T6P-sucrose feedback loop that in wild-type plants coordinates production and consumption of sucrose. This is consistent with our T6P and sucrose measurements (Figure 2.4B), with the paradoxically elevated T6P:sucrose ratios and growth impairment in the *tps5/6/7* mutant (Table 2.1 and Figure 2.4A, respectively) and with the inability of sugars to rescue these growth defects (Figures 2.3A, 2.4A and Supplementary Figure 2.5). Second, compromised T6P perception would also affect the levels of biosynthetic building blocks, such as organic and amino acids, required for sustained growth. Notably, this also aligns with the broad depletion of amino acids observed in the mutant (Figure2.4 C and Supplementary Figure2.8; discussed in detail in Section 2.4.3). In addition, the increase of sucrose was accompanied by an even larger relative increase in T6P. This might indicate that not only sucrose and central metabolism is perturbed, but that the unknown regulatory loops that lead to an increase in T6P levels when sucrose rises are amplified in *tps5/6/7*.

Together, these findings suggest that TPS5/6/7 promote flowering, at least in part, by ensuring proper T6P perception and downstream metabolic responses.

2.4.2. T6P requires TPS5/6/7 to promote root growth.

Growing evidence supports a role for T6P as a key regulator of root architecture (Schluepmann et al., 2003; Dijken et al., 2004; Fichtner et al., 2020; Göbel & Fichtner, 2023; Morales-Herrera et al., 2023). Consistent with this, and in addition to the flowering phenotypes, we observed a decrease in primary root length in the *tps7* mutant, but not in *tps5* or *tps6* mutants, with progressively more severe phenotypes in higher-order *tps5/7* and *tps5/6/7* mutants (Figure 2.2A-D). TPS5/6/7 proteins accumulate to varying degrees in root tissues, with TPS7 being the most abundant, particularly in root tips (Mergner et al., 2020; Supplementary Figure 2.11). This likely explains the differences in phenotype severity and suggests a dominant role for TPS7 in regulating root growth, with TPS5 and TPS6 playing minor roles that become apparent only in the absence of TPS7. Notably, the similarities between the root and flowering phenotypes point to a broader role for these proteins in regulating sink-related processes, possibly through similar mechanisms operating in both the SAM and the root apical meristem (RAM).

Interestingly, shorter root phenotypes have also been reported for plants with disrupted AtTPS1 activity, domain structure, or subcellular localization (Dijken et al. 2004; Fichtner et al. 2020). For example, the short-root phenotype of the *tps1-1* null mutant is fully complemented by TPS1 but not by OtsA or TPS1 variants carrying a strong nuclear signal or lacking the N-terminal domain. This indicates that the correct distribution of TPS1 between the nucleus and cytosol is essential for normal root growth, and suggests that the function of TPS1 may extend beyond T6P synthesis (Fichtner et al. 2020). Given that the role of TPS1 in root development cannot be explained solely by its enzymatic activity, one possibility is that it may operate, at least in part, via interactions with TPS-II proteins. Indeed, physical interactions between rice TPS-I and TPS-II proteins have been reported in yeast two-hybrid and bimolecular fluorescence complementation assays (Zang et al. 2011), suggesting that similar interactions may also occur in Arabidopsis. If so, TPS5/6/7 proteins could modulate TPS1 activity, subcellular localization, or interactions with other proteins, thereby

influencing root growth. Two studies lend support to this interpretation. On one hand, a GFP-TPS1 protein fusion was shown to localize in the root vasculature, particularly in companion cells and sieve elements of the phloem (Fichtner et al. 2020). On the other hand, the TPS5/6/7 promoters were shown to be active in the same phloem tissues (Ramon et al. 2009), altogether suggesting a functional interaction between TPS1 and TPS5/6/7 proteins.

2.4.3. TPS5/6/7 are essential for T6P-mediated metabolic responses.

Previous studies in Arabidopsis rosettes have shown that an inducible rise in T6P redirects fixed carbon away from sucrose synthesis towards the production of organic and amino acids (Figueroa et al., 2016; Avidan et al., 2024), in part via the post-translational regulation of PEPC and NR (Figueroa et al. 2016). In line with this, enhanced carbon fixation due to HL acclimation (Ma et al. 2014) led to increased accumulation of organic and amino acids in Col-0 shoots but also in roots (Figure 2.4C; Supplementary Table 2.1). This suggests that the effects of T6P on C/N metabolism may extend beyond leaves to other tissues, as observed also in buds of decapitated plants (Fichtner et al. 2017). In contrast, despite the high T6P levels, the *tps5/6/7* mutant exhibited root tip-specific deficits in malate, 2-OG, and fumarate, along with a decrease in most amino acids in shoots, roots and the root tip (Supplementary Figure 2.8A; Supplementary Table 2.1), and reduced PEPC phosphorylation in roots (Figure 2.5B).

Such an imbalance, especially the marked depletion of amino acids, may arise from a combination of mechanisms, including (1) impaired nitrogen assimilation or *de novo* amino acid biosynthesis, (2) increased amino acid incorporation into proteins, (3) decreased protein turnover, and (4) enhanced amino acid catabolism. The first possibility seems less plausible, as NR activity and levels of Glu and Gln were either comparable between genotypes or slightly elevated in the *tps5/6/7* mutant (Figure 2.5A, Supplementary Figure 2.8A). Additionally, the mutant accumulated certain amino acids (e.g. proline and alanine) to higher levels (Supplementary Figure 2.8A),

indicating that nitrogen assimilation and amino acid biosynthetic pathways remain functional. Nevertheless, the sustained synthesis of amino acids requires continuous 2-OG supply, a demand met through both cyclic TCA flux and anaplerotic pathways, including PEPC-mediated conversion of PEP to OAA (Sweetlove et al. 2010; Zhang and Fernie 2023). Given that PEPC phosphorylation is impaired in the mutant's roots and 2-OG levels are reduced in root tips, we cannot exclude some degree of constraint on GS/GOGAT-dependent nitrogen assimilation. Alternatively, amino acid depletion could arise from altered dynamics in protein synthesis and degradation. However, total protein content did not differ significantly between genotypes (Supplementary Figure 2.9). Yet, the mutant exhibited lower RPS6 levels in shoots as well as in roots under sucrose-supplemented conditions, along with increased PEPC levels in the roots. This suggests a distinct reprogramming of protein composition in the *tps5/6/7* mutant. Such changes could increase the demand for specific amino acids during protein synthesis, potentially explaining the selective depletion of certain amino acids despite unchanged total protein levels. In any case, based on our observations, the most compelling explanation is that T6P insensitivity in the mutant reconfigures metabolism to promote the use of BCAAs and Lys as alternative substrates for ATP production. This is supported by several lines of evidence. First, the ratio of ATP synthesis to oxygen consumption is lower when amino acids are respired instead of glucose (Leverve et al. 2007). Second, the oxygen consumption rates of the mutant were >1.5-fold higher than in Col-0 both in the absence and presence of exogenous sucrose (3-6h interval). Furthermore, the positive effect of sucrose on respiration rates was significantly lower in the mutant than in Col-0 (6-24h interval). Third, the difference in amino acid levels between Col-0 and the *tps5/6/7* mutant was most prominent under high light conditions (Figure 2.4C; Supplementary Figure 2.8B), where Col-0 exhibited increased growth (Figure 2.4A).

2.4.4. TPS5/6/7 coordinate growth responses to sugar availability.

Under laboratory conditions, exogenous sugar supplementation and exposure to high light intensities have been shown to enhance primary root elongation in wild-

type plants (Freixes et al. 2002). However, neither sucrose supplementation, a mix of glucose and fructose, nor higher light intensities were able to rescue the stunted root growth in the *tps5/6/7* mutant. This unresponsiveness to carbon sources, further aligns with fundamental defects in sugar signaling and/or utilization.

Such a disruption in sugar signaling and utilization could reflect the malfunction of key pathways that regulate growth in response to carbon availability. Central to this regulation are two evolutionarily conserved protein kinase complexes with antagonistic roles: TOR, which promotes growth under carbon-sufficient conditions, and SnRK1, which suppresses growth during carbon starvation (Baena-González and Hanson 2017). While T6P is postulated to promote growth and development by inhibiting SnRK1 activity (Zhang et al. 2009; Zhai et al. 2018; Blanford et al. 2024) and TPS-II proteins have been identified as negative regulators of SnRK1 (Van Leene et al. 2022), recent research has further shown that the positive effect of T6P on lateral root density requires the TOR kinase (Morales-Herrera et al. 2023). Therefore, two non-mutually exclusive hypotheses could explain the counterintuitive behavior of the *tps5/6/7* mutant whose primary root growth is impaired, despite elevated T6P levels: (i) in the absence of TPS5/6/7, SnRK1 becomes aberrantly active, thereby hindering growth (refer to chapter 3 for more details); (ii) the absence of TPS5/6/7 may disrupt T6P signalling, thereby compromising carbon sensing, which in turn leads to defective TOR activation and impaired growth.

In roots, RAM activation and growth are stimulated by sugars in a TOR-dependent manner (Xiong et al., 2013; Pereyra et al., 2023). Consistent with this, sucrose supplementation increased RPS6 phosphorylation in Col-0 roots (Figure 2.3B), which aligns with the enhanced root growth and suggests increased TOR activity under this condition. However, this was accompanied by an unexpected and even more pronounced increase in total RPS6 levels, which resulted in similar relative RPS6 phosphorylation levels in mock and sugar conditions (Figure 2.3B). This was contrary to expectations, given that the activation of TOR was shown to increase RPS6 phosphorylation without altering RPS6 protein levels (Dobrenel et al., 2016; Forzani et al., 2019; Riegler et al., 2021; Pereyra et al., 2023). Our results likely reflect

differences in experimental conditions compared to previous studies, rather than indicating unchanged TOR activity between treatments. For example, most studies employed shorter-term treatments that likely captured rapid RPS6 phosphorylation dynamics but did not allow sufficient time for changes in total RPS6 levels to become apparent. Additionally, such measurements were often conducted on whole seedlings (Dobrenel et al. 2016; Pereyra et al. 2023), potentially diluting the root-specific RPS6 response, as evidenced by our observation of minimal differences in total RPS6 levels in Col-0 shoots between control and sucrose conditions. In any case, sucrose had little effect on RPS6 phosphorylation and total RPS6 levels in *tps5/6/7* roots (Figure 2.3B), underscoring a fundamentally altered and subdued response to sugars compared to Col-0, potentially reflecting differences in TOR activation between the genotypes. In contrast to roots, sucrose-induced changes in the phosphorylation and overall accumulation of RPS6 were much less pronounced in the shoots of both genotypes (Figure 2.3B). Yet, total RPS6 remained consistently lower in the *tps5/6/7* mutant than Col-0, both in the absence and presence of added sugar.

While our focus was on RPS6 phosphorylation as a read out of TOR activity as a key regulator of root growth, total RPS6 accumulation *per se* plays a significant role in regulating global translation and transcription, as well as growth (Creff et al., 2010; Ren et al., 2013; Dasgupta et al., 2024). It is therefore possible that the *tps5/6/7* growth defects are at least partly due to the reduced accumulation of RPS6. Our results further suggest an unforeseen role for TPS5/6/7 in regulating RPS6 expression and/or stability. It remains to be determined whether the observed decrease in RPS6 reflects a broader response involving the downregulation of other ribosomal proteins and components of the ribosome biogenesis machinery in *tps5/6/7*. Interestingly, a recent study suggested a connection between T6P and ribosomal proteins. An induced accumulation of T6P levels in Arabidopsis led to widespread changes in transcripts related to ribosome biogenesis and ribosomal proteins, including the induction of RPS6 (Avidan et al. 2024). It is therefore possible that changes in ribosome biogenesis occur as an indirect consequence of disrupted T6P signaling in the *tps5/6/7* mutant, though whether this is linked to TOR signaling remains an open question for future investigation. In addition, T6P has been shown to suppress

autophagy in Arabidopsis (Soto-Burgos and Bassham 2017). Thus, TPS5/6/7 may also help maintain RPS6 protein stability through this regulatory pathway. In the *tps5/6/7* mutant, disrupted T6P signaling could lead to autophagy de-repression, resulting in increased RPS6 degradation and compensatory amino acid mobilization through protein catabolism. However, increased autophagy would typically be expected to raise free amino acid levels, which is inconsistent with the amino acid depletion observed in the mutant. This suggests that if autophagy is indeed elevated, it may be accompanied by a disproportionate increase in amino acid catabolism or metabolic rerouting, such that amino acid turnover exceeds their release from protein degradation.

In summary, our findings position TPS5/6/7 as essential mediators of T6P signaling, linking carbon availability with metabolism and growth regulation. Their absence uncouples T6P levels from growth, implicating them in signal perception, transduction, or both. Future research should address whether these proteins function as T6P sensors, binding T6P directly as their conserved domains suggest, or are downstream effectors of the T6P sensor. Future research will address their mode of action, which may involve, amongst others, the modulation of TPS1 activity through physical interaction, or the regulation of SnRK1. Resolving these mechanisms could unlock new strategies for crop improvement, building on existing successes in T6P pathway engineering (Paul et al. 2018).

2.5. Materials and Methods

A list of all primers and antibodies used in this study is provided in Supplementary Table 2.2.

2.5.1. Plant material and growth conditions.

All *Arabidopsis thaliana* plants used in this study are in the Columbia (Col-0) background. The *tps5* T-DNA insertion mutant (SALK_144791, *tps5-1*) was previously described (Tian et al. 2019). The *tps6* (GK-362A03) and *tps7* (GK_341E02) mutants were identified from the publicly available collection of *Arabidopsis thaliana* T-DNA insertion lines (http://signal.salk.edu/cgi-bin/tdnaexpress). Homozygosity of the *tps* mutations was confirmed by genomic PCR (Supplementary Figure 2.12), using LP, RP and T-DNA LB primers (LBb1.3 and o8409 for SALK and GABI-Kat lines, respectively). The loss of full-length transcripts was verified by RT-PCR (Supplementary Figure 2.12). The *tps5/7* and *tps5/6/7* mutants were obtained by crossing *tps5-1* with *tps7* (GK_341E02) and subsequently with *tps6* (GK-362A03) for the triple mutant. F1 seeds were grown and allowed to self-fertilize to produce the F2 generation. Homozygosity of individual plants from a segregating F2 population was confirmed by PCR using gene-specific and T-DNA primers.

Seeds were surface sterilized for 1 min in 70% (v/v) ethanol followed by 10 min in 20% (v/v) bleach by gentle rocking and then washed at least 5 times with sterile water. Sterilized seeds were stratified in the dark at 4 °C for 2-3 days. Unless otherwise specified, plants were grown under long-day conditions (16 h light, 110 µmol m^{-2} s^{-1}, 22 °C / 8 h dark, 18 °C, control light) on 0.5× MS medium (0.05% MES and 0.8% phytoagar).

2.5.2. Molecular cloning and Arabidopsis transformation.

For generating the *pTPS7::TPS7-mCherry* and *pTPS7::mCherry-TPS7* complementation lines, relevant DNA fragments were amplified by PCR using Phusion™ High-Fidelity DNA Polymerase and primers containing appropriate overhangs. Fragments were thereafter assembled into the final vector using the Gibson Assembly® method (Gibson et al. 2009, 2010). The full-length *TPS7* gene (AT1G06410, 2738 bp), a 2000 bp region upstream of the *TPS7* start codon (promoter), and a downstream terminator sequence (833 bp) were separately amplified from Arabidopsis Col-0 genomic DNA. The mCherry sequence (708 bp) was

amplified from a construct for expressing a Golgi-mCherry marker (Nelson et al. 2007). A 5039 bp segment of the pCB302 (Xiang et al. 1999) binary vector sequence, excluding the C-terminal GFP tag region, was amplified for the construct backbone. Purified PCR products were incubated at 50 °C for 1 h with the NEBuilder® Hifi DNA assembly master mix, following the manufacturer's instructions. The resulting constructs were introduced into *E. coli* (TOP10) cells, and correct assembly was validated by colony PCR and sequencing. Verified constructs were introduced into *Agrobacterium tumefaciens* GV3101, and *tps7* plants were transformed by the floral dip method (Clough and Bent 1998). BASTA®-resistant transformants were selected based on their segregation ratio (T2) and homozygosity (T3). To assess differences in signal intensity of TPS7-mCherry fusion proteins, 50 µg protein samples from homozygous *proTPS7::TPS7-mCherry* and *proTPS7::mCherry-TPS7* plants were prepared as described in Sections 2.5.4. and 2.5.8. The samples were resolved on an 8% acrylamide SDS-PAGE gel, wet-transferred to PVDF membranes (80 V, 90 min at 4 °C), and subjected to immunodetection using an anti-RFP antibody.

2.5.3. Phenotyping assays.

To assess flowering, plants were grown in a 1:3 vermiculite:soil (Bord Na Mona Pot Plant Substrate Plus+ Irish Peat Moss) mixture under long-day conditions. Flowering time was determined by counting the number of days to flower (when floral buds became visible in the center of the rosette) and the number of rosette leaves when plants reached a stem height of approximately 1 cm.

For root growth assays, seedlings were grown vertically for 7 days on 0.5× MS medium under control light conditions. Seedlings with comparable root sizes were then transferred to fresh 0.5× MS plates with or without 30 mM sucrose or to plates supplemented with 30 mM fructose and 30 mM glucose. These plates were either maintained under the same light conditions or shifted to high light (16 h light, 200 µmol m^{-2} s^{-1}, 22 °C / 8 h dark, 18 °C). The position of the root tip was marked immediately after transfer and seedlings were grown on the fresh plates for an additional 7 days

before scanning. Post-transfer root growth was measured as primary root length from scanned plates. Root tracing and measurements were performed using the NeuronJ plugin in ImageJ.

2.5.4. RPSP6^{240} phosphorylation assays.

Col-0 and *tps5/6/7* seedlings were grown vertically for 7 days on 0.5× MS medium, then transferred to fresh 0.5× MS plates with or without 1% sucrose for an additional 7 days. Shoots and roots of the 14d-old seedlings were harvested separately at the end of the night, flash frozen and reduced to a fine powder in liquid nitrogen. Proteins were extracted with extraction buffer [1.5 mL buffer/ g fresh weight; 50 mM Tris-HCl pH 7.5, 150 mM NaCl, 1 mM EDTA, 0.05% (v/v) Triton-X100, 0.002% (v/v) phosphatase inhibitor cocktail #2 (Sigma P572G), 0.002% (v/v) phosphatase inhibitor cocktail #3 (Sigma P0044) and cOmplete™ protease inhibitor cocktail (Roche; 1 tablet/ 10 mL)] on ice. After clearing samples by centrifugation (21130 *g* at 4 °C, 15 min), the supernatants were recovered, and total protein was quantified using the Bradford protein assay. Samples were denatured in 4x Laemmli solubilization buffer and boiled at 95 °C for 5 minutes. Equal amounts of protein per sample (20 µg) were resolved on a 10% acrylamide SDS-PAGE gel, wet-transferred to PVDF membranes (80 V, 90 min at 4 °C), and immunodetected using antiphospho-RPS6^{240} and anti-RPS6 (Dobrenel et al. 2016) antibodies. Protein band intensities were determined in ImageJ (version 2.1.0), and fold-change values for pRPS6, RPS6 and pRPS6/RPS6 ratios were analyzed with GraphPad Prism (version 10.3.1).

2.5.5. Metabolite extraction and measurement.

For metabolite analyses, Col-0 and *tps5/6/7* seedlings were grown vertically for 7 days on 0.5× MS medium under control light conditions. Seedlings with comparable root sizes were then transferred to fresh 0.5× MS plates, where they grew on calibrated Nitex mesh (pore size 30 µm) under control or high light conditions (16

h light, 200 µmol m^{-2} s^{-1}, 22 °C / 8 h dark, 18 °C) for an additional 7 days. 14d-old shoots, roots (excluding the apical region) and root apices (~0.5 cm) were harvested separately at the end of the night (EN), flash frozen and reduced to a fine powder in liquid nitrogen. For LC-MS/MS- and GC-MS-based quantifications, approximately 18 mg of finely ground plant material was quenched in a 3:7 (v/v) chloroform:methanol mixture at liquid nitrogen temperature and warmed to -20 °C for 2 h. The chloroform organic phase was subsequently extracted twice with ice-cold ultra-pure water. Both water phases were combined and dried to a powder in a centrifugal vacuum dryer at 20 °C. Pellets were resuspended in 350 µL of ultra-pure water and filtered through a Multiscreen Ultracel-10 (Millipore) membrane to eliminate high molecular weight components. Dilutions of 1:10 were used to quantify T6P, other phosphorylated intermediates and organic acids via high-performance anion-exchange chromatography coupled to tandem mass spectrometry, as described in (Lunn et al. 2006) with modifications (Figueroa et al. 2016). Soluble sugars and sugar alcohols were quantified by high-performance hydrophilic interaction liquid chromatography (HILIC) on a 150 x 2.1 mm Luna Omega Sugar column (3 µm, 100Å; Phenomenex Inc.; Aschaffenburg, Germany; www.phenomenex.com) column fitted with a SUGAR 4 x 2.0 mm Security Guard Cartridge (Phenomenex), coupled to a QTrap 5500 triple quadrupole mass spectrometer (AB Sciex, Foster City, USA; sciex.com). The column was maintained at 25°C and equilibrated with eluent A (90% acetonitrile, 5% isopropanol, 5% water, by volume) before injection of samples (1 µl). Samples were spiked with ^{13}C-labelled internal standards for correction of ion suppression and other matrix effects. Sugars were eluted (flow rate 0.25 ml min^{-1}) by mixing eluent A and eluent B (5% acetonitrile, 25% isopropanol, 70% water, by volume) with the following gradient:: 0 – 2.5 min [10 % B]; 2.5 – 25 min [10 – 30 % B]; 25 – 30.5 min [30 % B]; 30.5 – 31 min [30 – 10 % B]; 31 – 40 min [10 % B]. Sugars were quantified by tandem mass spectrometry in multiple reaction mode (MRM) using the settings and stable-isotope-labelled internal standards (SIL-IS) summarized in Supplementary Tables 2.3 and 2.4.

Total protein amounts were extracted from the left-over pellets of the chloroform:methanol extraction (Hendriks et al. 2003). Pellets were dried at room

temperature, resuspended in 400µl NaOH, shaken vigorously, heated at 120°C for 30 min, cooled down at room temperature and centrifuged at 21,000 g for 10 min at room temperature. Total protein amounts were determined with the Bradford method, using bovine serum albumin as standard.

Amino acids and other polar metabolites were measured by drying 200 µL of the organic phase and derivatizing it according to (Roessner et al. 2001). 1 µL of the derivatized sample was analyzed on a Combi-PAL autosampler (Agilent Technologies) coupled with an Agilent 7890 GC and Leco Pegasus 2 TOF-MS (LECO, St. Joseph, MI, USA) (Lisec et al. 2006) . Chromatograms were exported to R software via Leco CHROMA TOF (v. 3.25) for peak detection, retention time alignment, and library matching using R/TARGETSEARCH (Cuadros-Inostroza et al. 2009). Metabolites were quantified based on the peak intensity of a selective mass and normalized to FW and total ion count. Final values were normalized by the median intensity of the metabolite across all samples.

2.5.6. Measurements of oxygen consumption rates.

Oxygen consumption in Arabidopsis seedlings was measured using Screw Cap Septum Vials (37.5 mL). Ten-day-old seedlings, grown on vertical 0.5× MS plates, were transferred into vials partially filled with 20 mL of 0.5× MS medium, with or without 1% sucrose, and solidified with 0.8% agar. Each vial contained approximately 15–20 seedlings. Incubation and measurements were carried out at 22 °C in darkness (with green light) to prevent photosynthesis and resulting oxygen production. Seedlings were transferred at ZT4. Once the transfer was completed, vials were quickly closed and T0 oxygen measurements were initiated. Each measurement lasted 25 seconds per sample. Oxygen concentration in the air space was monitored at three time points (3, 6 and 24 hours) using a needle-type oxygen sensor (Unisense), which was inserted through the septum to measure the oxygen concentration. The decrease in oxygen levels between 3 and 6h and between 6 and 24h was used as a proxy for respiration rate in the corresponding time interval. Following the measurements, the fresh weight

of the seedlings and the headspace volume of each vial were recorded for normalization to express respiration rates as µmol O_2 consumed /g FW /hour.

2.5.7. Nitrate reductase (NR) activity assays.

Rosettes of Col-0 and *tps5/6/7* plants grown for 25d in soil under an equinoctial photoperiod (12 h light, 110 µmol m^{-2} s^{-1}, 22 °C / 12 h dark, 18 °C) were harvested at ZT0 (end of the night), ZT6 (middle of the day), ZT12 (end of the day), and ZT18 (middle of the night), flash frozen, and ground to a fine powder in liquid nitrogen. Soluble enzymes were extracted using extraction buffer [1 mL buffer/ 20 mg fresh weight; 50 mM Hepes-KOH pH 7.5, 10 mM $MgCl_2$, 1 mM EDTA, 1 mM EGTA, 1 mM benzamidine, 1 mM ε-aminocaproic acid, 0.25% (w/v) BSA, 20 µM leupeptin, 0.5 mM DTT, 1 mM PMSF, 1% (v/v) Triton X-100, 20% (v/v) glycerol] and PVPP on ice and cleared by centrifugation (14000 *g* at 4 °C, 5 min). Nitrite standards ranging from 0 to 2 mM were prepared in extraction buffer. NR activity was assayed in 96-well plates by incubating the extracts and standards at 25 °C with assay buffer [50 mM Hepes-KOH pH 7.5, 2 mM EDTA, 20 mM KNO_3, 0.05% (v/v) Triton X-100, 10 µM Na_2MoO_4, 20 µM FAD, 0.5 mM DTT, 20 µM leupeptin and 0 (maximal activity) or 10 mM (selective activity) Mg-acetate] and NADH to a final concentration of 0.5 mM (to start the reaction). The reactions were stopped after 20 and 40 min by adding 20 µL of 600 mM Zn-acetate. Subsequently, 20 µL of 0.5 mM PMS were added, and plates were incubated for 15 min at room temperature, after which 50 µL of 1% (w/v) sulfanilamide in 5% (v/v) H_3PO_4 and 50 µL of 0.02% (w/v) NNEDA were added. The optical density (OD) was measured at 540 nm after 5 minutes.

2.5.8. PEPC^{S11} phosphorylation assays.

The roots of 14d-old Col-0 and *tps5/6/7* seedlings were harvested at EN, flash frozen and reduced to a fine powder in liquid nitrogen. Proteins were extracted with extraction buffer [1.5 mL buffer/ g fresh weight; 50 mM Tris-HCl pH 8.0, 150 mM NaCl,

1 mM EDTA, 1% (v/v) Triton X-100, 3 mM DTT, 50 µM MG-132, 0.002% (v/v) phosphatase inhibitor cocktail #2 (Sigma P572G), 0.002% (v/v) phosphatase inhibitor cocktail #3 (Sigma P0044) and cOmplete™ protease inhibitor cocktail (Roche; 1 tablet/ 10 mL)] on ice. After clearing samples by centrifugation (21130 *g* at 4 °C, 15 min), the supernatants were recovered, and total protein was quantified using the Bradford protein assay. Samples were denatured in 4x Laemmli solubilization buffer and boiled at 95 °C for 5 minutes. Equal amounts of protein per sample (50 µg) were resolved on an 8% acrylamide SDS-PAGE gel, wet-transferred to PVDF membranes (80 V, 90 min at 4 °C), and immunodetected using a polyclonal rabbit anti-RcPPC3 antibody (Gregory et al. 2009) to detect non-ubiquitinated (p107) and mono-ubiquitinated (p110) plant-type PEPC polypeptides(O'Leary et al., 2011a) or a polyclonal rabbit antibody against a phospho-Ser11 containing peptide (Gregory et al. 2009) in the presence of 10 µg/ mL of the corresponding dephosphopeptide to detect phosphorylated plant-type $PEPC^{107kDa}$ subunits. Protein band intensities were determined in ImageJ (version 2.1.0), and fold-change values for Total PEPC, $PEPC^{110kDa}$/Total PEPC and p-(S11)PEPC/$PEPC^{107kDa}$ were analyzed with GraphPad Prism (version 10.3.1).

2.5.9. RNA extraction, cDNA synthesis and RT-PCR.

Total RNA was extracted from 14d-old Col-0, *tps6-1,* and *tps7-1* seedlings grown vertically on 0.5× MS medium under long-day conditions (16 h light, 110 µmol m^{-2} s^{-1}, 22 °C / 8 h dark, 18 °C). Seedlings were harvested at the end of the night, and RNA extraction was performed using the Nucleospin RNA plants purification kit (Macherey-Nagel) according to the manufacturer's instructions. DNase-treated RNA (1 µg) was reverse transcribed in a total reaction volume of 10 µL using OligoDT and Super Script III Reverse Transcriptase. The resulting cDNA was then diluted to a final volume of 80 µL and used for RT-PCR amplification of *TPS6*, *TPS7*, and *ACTIN*. RT-PCR was performed with an annealing temperature of 55 °C for 30 cycles (*TPS6* and *TPS7*) or 26 cycles (*ACTIN*). PCR products were separated on a 1.2% (w/v) agarose gel by electrophoresis at 100 V for 30 minutes.

Acknowledgements

We thank the IGC Plant Facility (Vera Nunes) for excellent plant management. This work was supported by Fundação para a Ciência e a Tecnologia grants UIDB/04551/2020 (DOI 10.54499/UIDB/04551/2020**)**, UIDP/04551/2020 (DOI 10.54499/UIDP/04551/2020, GREEN-IT-Bioresources for Sustainability), LA/P/0087/2020 (LS4FUTURE Associated Laboratory), PTDC/BIA-FBT/4942/2020, PD/BD/150239/2019, and by the Max Planck Society.

2.6. References

dos Anjos L, Pandey PK, Moraes TA, Feil R, Lunn JE, and Stitt M. Feedback regulation by trehalose 6-phosphate slows down starch mobilization below the rate that would exhaust starch reserves at dawn in Arabidopsis leaves. Plant Direct. 2018. https://doi.org/10.1002/pld3.78

Avidan O, Martins MCM, Feil R, Lohse M, Giorgi FM, Schlereth A, Lunn JE, and Stitt M. Direct and indirect responses of the Arabidopsis transcriptome to an induced increase in trehalose 6-phosphate. Plant Physiol. 2024:**196**(1):409–431. https://doi.org/10.1093/plphys/kiae196

Avonce N, Mendoza-Vargas A, Morett E, and Iturriaga G. Insights on the evolution of trehalose biosynthesis. BMC Evol Biol. 2006:**6**(1):109. https://doi.org/10.1186/1471-2148-6-109

Baena-González E and Hanson J. Shaping plant development through the SnRK1–TOR metabolic regulators. Curr Opin Plant Biol. 2017. https://doi.org/10.1016/j.pbi.2016.12.004

Barton MK. Twenty years on: The inner workings of the shoot apical meristem, a developmental dynamo. Dev Biol. 2010:**341**(1):95–113. https://doi.org/10.1016/j.ydbio.2009.11.029

Blanford J, Zhai Z, Baer MD, Guo G, Liu H, Liu Q, Raugei S, and Shanklin J. Molecular mechanism of trehalose 6-phosphate inhibition of the plant metabolic sensor kinase SnRK1. Sci Adv. 2024:**10**(20). https://doi.org/10.1126/sciadv.adn0895

Bledsoe SW, Henry C, Griffiths CA, Paul MJ, Feil R, Lunn JE, Stitt M, and Lagrimini LM. The role of Tre6P and SnRK1 in maize early kernel development and events leading to stress-induced kernel abortion. BMC Plant Biol. 2017:**17**(1):74. https://doi.org/10.1186/s12870-017-1018-2

Cabib E and Leloir LF. The biosynthesis of trehalose phosphate. American Society for Biochemistry and Molecular Biology. 1958.

Chary SN, Hicks GR, Choi YG, Carter D, and Raikhel N V. Trehalose-6-Phosphate Synthase/Phosphatase Regulates Cell Shape and Plant Architecture in Arabidopsis. Plant Physiol. 2008:**146**(1):97–107. https://doi.org/10.1104/pp.107.107441

Cho HY, Wen TN, Wang YT, and Shih MC. Quantitative phosphoproteomics of protein kinase SnRK1 regulated protein phosphorylation in Arabidopsis under submergence. J Exp Bot. 2016:**67**(9):2745–2760. https://doi.org/10.1093/jxb/erw107

Clough SJ and Bent AF. **Floral dip: a simplified method for *Agrobacterium* - mediated transformation of *Arabidopsis thaliana***. The Plant Journal. 1998:**16**(6):735–743. https://doi.org/10.1046/j.1365-313x.1998.00343.x

Cookson SJ, Yadav UP, Klie S, Morcuende R, Usadel B, Lunn JE, and Stitt M. Temporal kinetics of the transcriptional response to carbon depletion and sucrose readdition in *Arabidopsis* seedlings. Plant Cell Environ. 2016:**39**(4):768–786. https://doi.org/10.1111/pce.12642

Creff A, Sormani R, and Desnos T. The two Arabidopsis RPS6 genes, encoding for cytoplasmic ribosomal proteins S6, are functionally equivalent. Plant Mol Biol. 2010:**73**(4–5):533–546. https://doi.org/10.1007/s11103-010-9639-y

Cuadros-Inostroza Á, Caldana C, Redestig H, Kusano M, Lisec J, Peña-Cortés H, Willmitzer L, and Hannah MA. TargetSearch - a Bioconductor package for the efficient preprocessing of GC-MS metabolite profiling data. BMC Bioinformatics. 2009:**10**. https://doi.org/10.1186/1471-2105-10-428

Dasgupta A, Urquidi Camacho RA, Enganti R, Cho SK, Tucker LL, Torreverde JS, Abraham PE, and von Arnim AG. A phosphorylation-deficient ribosomal protein eS6 is largely functional in *Arabidopsis thaliana*, rescuing mutant defects from global translation and gene expression to photosynthesis and growth. Plant Direct. 2024:**8**(1). https://doi.org/10.1002/pld3.566

Delorge I, Figueroa CM, Feil R, Lunn JE, and Van Dijck P. Trehalose-6-phosphate synthase 1 is not the only active TPS in Arabidopsis thaliana. Biochemical Journal. 2015. https://doi.org/10.1042/bj20141322

Dijken AJH van, Schluepmann H, and Smeekens SCM. Arabidopsis Trehalose-6-Phosphate Synthase 1 Is Essential for Normal Vegetative Growth and Transition to Flowering. Plant Physiol. 2004:**135**(2):969–977. https://doi.org/10.1104/pp.104.039743

Dobrenel T, Mancera-Martínez E, Forzani C, Azzopardi M, Davanture M, Moreau M, Schepetilnikov M, Chicher J, Langella O, Zivy M, et al. The Arabidopsis TOR Kinase Specifically Regulates the Expression of Nuclear Genes Coding for Plastidic Ribosomal Proteins and the Phosphorylation of the Cytosolic Ribosomal Protein S6. Front Plant Sci. 2016:**7**. https://doi.org/10.3389/fpls.2016.01611

Eastmond PJ, Van Dijken AJH, Spielman M, Kerr A, Tissier AF, Dickinson HG, Jones JDG, Smeekens SC, and Graham IA. Trehalose-6-phosphate synthase 1, which catalyses the first step in trehalose synthesis, is essential for *Arabidopsis* embryo maturation. The Plant Journal. 2002:**29**(2):225–235. https://doi.org/10.1046/j.1365-313x.2002.01220.x

Fichtner F, Barbier FF, Annunziata MG, Feil R, Olas JJ, Mueller-Roeber B, Stitt M, Beveridge CA, and Lunn JE. Regulation of shoot branching in arabidopsis by trehalose 6-phosphate. New Phytologist. 2021:**229**(4):2135–2151. https://doi.org/10.1111/nph.17006

Fichtner F, Barbier FF, Feil R, Watanabe M, Annunziata MG, Chabikwa TG, Höfgen R, Stitt M, Beveridge CA, and Lunn JE. Trehalose 6-phosphate is involved in triggering axillary bud outgrowth in garden pea (*Pisum sativum* L.). The Plant Journal. 2017:**92**(4):611–623. https://doi.org/10.1111/tpj.13705

Fichtner F and Lunn JE. The Role of Trehalose 6-Phosphate (Tre6P) in Plant Metabolism and Development. Annu Rev Plant Biol. 2021:**72**(1):737–760. https://doi.org/10.1146/annurev-arplant-050718-095929

Fichtner F, Olas JJ, Feil R, Watanabe M, Krause U, Hoefgen R, Stitt M, and Lunn JE. Functional Features of TREHALOSE-6-PHOSPHATE SYNTHASE1, an Essential Enzyme in Arabidopsis. Plant Cell. 2020:**32**(6):1949–1972. https://doi.org/10.1105/tpc.19.00837

Figueroa CM, Feil R, Ishihara H, Watanabe M, Kölling K, Krause U, Höhne M, Encke B, Plaxton WC, Zeeman SC, et al. Trehalose 6–phosphate coordinates organic and amino acid metabolism with carbon availability. The Plant Journal. 2016:**85**(3):410–423. https://doi.org/10.1111/tpj.13114

Figueroa CM and Lunn JE. A Tale of Two Sugars: Trehalose 6-Phosphate and Sucrose. Plant Physiol. 2016:**172**(1):7–27. https://doi.org/10.1104/pp.16.00417

Forzani C, Duarte GT, Van Leene J, Clément G, Huguet S, Paysant-Le-Roux C, Mercier R, De Jaeger G, Leprince A-S, and Meyer C. Mutations of the AtYAK1 Kinase Suppress TOR Deficiency in Arabidopsis. Cell Rep. 2019:**27**(12):3696-3708.e5. https://doi.org/10.1016/j.celrep.2019.05.074

Freixes S, Thibaud M, Tardieu F, and Muller B. Root elongation and branching is related to local hexose concentration in *Arabidopsis thaliana* seedlings. Plant Cell Environ. 2002:**25**(10):1357–1366. https://doi.org/10.1046/j.1365-3040.2002.00912.x

Gibson DG, Smith HO, Hutchison CA, Venter JC, and Merryman C. Chemical synthesis of the mouse mitochondrial genome. Nat Methods. 2010:**7**(11):901–903. https://doi.org/10.1038/nmeth.1515

Gibson DG, Young L, Chuang R-Y, Venter JC, Hutchison CA, and Smith HO. Enzymatic assembly of DNA molecules up to several hundred kilobases. Nat Methods. 2009:**6**(5):343–345. https://doi.org/10.1038/nmeth.1318

Göbel M and Fichtner F. Functions of sucrose and trehalose 6-phosphate in controlling plant development. J Plant Physiol. 2023:**291**:154140. https://doi.org/10.1016/j.jplph.2023.154140

Gómez LD, Baud S, Gilday A, Li Y, and Graham IA. Delayed embryo development in the *ARABIDOPSIS TREHALOSE-6-PHOSPHATE SYNTHASE 1* mutant is associated with altered cell wall structure, decreased cell division and starch accumulation. The Plant Journal. 2006:**46**(1):69–84. https://doi.org/10.1111/j.1365-313X.2006.02662.x

Gómez LD, Gilday A, Feil R, Lunn JE, and Graham IA. AtTPS1-mediated trehalose 6-phosphate synthesis is essential for embryogenic and vegetative growth and responsiveness to ABA in germinating seeds and stomatal guard cells. The Plant Journal. 2010:no-no. https://doi.org/10.1111/j.1365-313X.2010.04312.x

Gramma V, Olas JJ, Zacharaki V, Ponnu J, Musialak-Lange M, and Wahl V. Carbon and nitrogen signaling regulate *FLOWERING LOCUS C* and impact flowering time in Arabidopsis. Plant Physiol. 2024:**197**(1). https://doi.org/10.1093/plphys/kiae594

Gregory AL, Hurley BA, Tran HT, Valentine AJ, She Y-M, Knowles VL, and Plaxton WC. *In vivo* regulatory phosphorylation of the phosphoenolpyruvate carboxylase AtPPC1 in phosphate-starved *Arabidopsis thaliana*. Biochemical Journal. 2009:**420**(1):57–65. https://doi.org/10.1042/BJ20082397

Harthill JE, Meek SEM, Morrice N, Peggie MW, Borch J, Wong BHC, and MacKintosh C. Phosphorylation and 14-3-3 binding of Arabidopsis trehalose-phosphate synthase 5 in response to 2-deoxyglucose. Plant Journal. 2006:**47**(2):211–223. https://doi.org/10.1111/j.1365-313X.2006.02780.x

Hartwell J, Gill A, Nimmo GA, Wilkins MB, Jenkins GI, and Nimmo HG. Phosphoenolpyruvate carboxylase kinase is a novel protein kinase regulated at the level of expression. The Plant Journal. 1999:**20**(3):333–342. https://doi.org/10.1046/j.1365-313X.1999.00609.x

Hendriks JHM, Kolbe A, Gibon Y, Stitt M, and Geigenberger P. ADP-Glucose Pyrophosphorylase Is Activated by Posttranslational Redox-Modification in Response to Light and to Sugars in Leaves of Arabidopsis and Other Plant Species. Plant Physiol. 2003:**133**(2):838–849. https://doi.org/10.1104/pp.103.024513

Ingargiola C, Jéhanno I, Forzani C, Marmagne A, Broutin J, Clément G, Leprince A-S, and Meyer C. The Arabidopsis Target of Rapamycin kinase regulates ammonium assimilation and glutamine metabolism. Plant Physiol. 2023:**192**(4):2943–2957. https://doi.org/10.1093/plphys/kiad216

Ishihara H, Alseekh S, Feil R, Perera P, George GM, Niedźwiecki P, Arrivault S, Zeeman SC, Fernie AR, Lunn JE, et al. Rising rates of starch degradation during daytime and trehalose 6-phosphate optimize carbon availability. Plant Physiol. 2022:**189**(4):1976–2000. https://doi.org/10.1093/plphys/kiac162

Jamsheer K M, Kumar M, and Srivastava V. SNF1-related protein kinase 1: the many-faced signaling hub regulating developmental plasticity in plants. J Exp Bot. 2021:**72**(17):6042–6065. https://doi.org/10.1093/jxb/erab079

Kaiser WM and Huber SC. Post-translational regulation of nitrate reductase: mechanism, physiological relevance and environmental triggers. J Exp Bot. 2001:**52**(363):1981–1989. https://doi.org/10.1093/jexbot/52.363.1981

Leverve X, Batandier C, and Fontaine E. Choosing the right substrate. Novartis Found Symp. 2007:**280**:108–21; discussion 121-7, 160–4.

Lisec J, Schauer N, Kopka J, Willmitzer L, and Fernie AR. Gas chromatography mass spectrometry-based metabolite profiling in plants. Nat Protoc. 2006:**1**(1). https://doi.org/10.1038/nprot.2006.59

Liu X, Fu L, Qin P, Sun Y, Liu J, and Wang X. Overexpression of the wheat trehalose 6-phosphate synthase 11 gene enhances cold tolerance in Arabidopsis thaliana. Gene. 2019:**710**:210–217. https://doi.org/10.1016/j.gene.2019.06.006

Lunn JE. Gene families and evolution of trehalose metabolism in plants. Functional Plant Biology. 2007:**34**(6):550. https://doi.org/10.1071/FP06315

Lunn JE. Sucrose Metabolism. In. Encyclopedia of Life Sciences. (Wiley), pp. 1–9. https://doi.org/10.1002/9780470015902.a0021259.pub2

Lunn JE, Delorge I, Figueroa CM, Van Dijck P, and Stitt M. Trehalose metabolism in plants. The Plant Journal. 2014:**79**(4):544–567. https://doi.org/10.1111/tpj.12509

Lunn JE, Feil R, Hendriks JHM, Gibon Y, Morcuende R, Osuna D, Scheible WR, Carillo P, Hajirezaei MR, and Stitt M. Sugar-induced increases in trehalose 6-phosphate are correlated with redox activation of ADPglucose pyrophosphorylase and higher rates of starch synthesis in Arabidopsis thaliana. Biochemical Journal. 2006:**397**(1):139–148. https://doi.org/10.1042/BJ20060083

Ma F, Jazmin LJ, Young JD, and Allen DK. Isotopically nonstationary ^{13}C flux analysis of changes in *Arabidopsis thaliana* leaf metabolism due to high light acclimation. Proceedings of the National Academy of Sciences. 2014:**111**(47):16967–16972. https://doi.org/10.1073/pnas.1319485111

Martins MCM, Hejazi M, Fettke J, Steup M, Feil R, Krause U, Arrivault S, Vosloh D, Figueroa CM, Ivakov A, et al. Feedback Inhibition of Starch Degradation in Arabidopsis Leaves Mediated by Trehalose 6-Phosphate. Plant Physiol. 2013. https://doi.org/10.1104/pp.113.226787

Meitzel T, Radchuk R, McAdam EL, Thormählen I, Feil R, Munz E, Hilo A, Geigenberger P, Ross JJ, Lunn JE, et al. Trehalose 6-phosphate promotes seed filling by activating auxin biosynthesis. New Phytologist. 2021:**229**(3):1553–1565. https://doi.org/10.1111/nph.16956

Mergner J, Frejno M, List M, Papacek M, Chen X, Chaudhary A, Samaras P, Richter S, Shikata H, Messerer M, et al. Mass-spectrometry-based draft of the Arabidopsis proteome. Nature. 2020:**579**(7799):409–414. https://doi.org/10.1038/s41586-020-2094-2

Morales-Herrera S, Jourquin J, Coppé F, Lopez-Galvis L, De Smet T, Safi A, Njo M, Griffiths CA, Sidda JD, Mccullagh JSO, et al. Trehalose-6-phosphate signaling regulates lateral root formation in Arabidopsis thaliana. Proceedings of the National Academy of Sciences. 2023:**120**(40). https://doi.org/10.1073/pnas.2302996120

Nelson BK, Cai X, and Nebenführ A. A multicolored set of *in vivo* organelle markers for co-localization studies in Arabidopsis and other plants. The Plant Journal. 2007:**51**(6):1126–1136. https://doi.org/10.1111/j.1365-313X.2007.03212.x

Nozue K, Covington MF, Duek PD, Lorrain S, Fankhauser C, Harmer SL, and Maloof JN. Rhythmic growth explained by coincidence between internal and external cues. Nature. 2007:**448**(7151):358–361. https://doi.org/10.1038/nature05946

Nukarinen E, Ngele T, Pedrotti L, Wurzinger B, Mair A, Landgraf R, Börnke F, Hanson J, Teige M, Baena-Gonzalez E, et al. Quantitative phosphoproteomics reveals the role of the AMPK plant ortholog SnRK1 as a metabolic master regulator under energy deprivation. Sci Rep. 2016:**6**(August):1–19. https://doi.org/10.1038/srep31697

Nunes C, Primavesi LF, Patel MK, Martinez-Barajas E, Powers SJ, Sagar R, Fevereiro PS, Davis BG, and Paul MJ. Inhibition of SnRK1 by metabolites: Tissue-dependent effects and cooperative inhibition by glucose 1-phosphate in combination with trehalose 6-phosphate. Plant Physiology and Biochemistry. 2013:**63**:89–98. https://doi.org/10.1016/j.plaphy.2012.11.011

O'Leary B, Fedosejevs ET, Hill AT, Bettridge J, Park J, Rao SK, Leach CA, and Plaxton WC. Tissue-specific expression and post-translational modifications of plant- and bacterial-type phosphoenolpyruvate carboxylase isozymes of the castor oil plant, Ricinus communis L. J Exp Bot. 2011a:**62**(15):5485–5495. https://doi.org/10.1093/jxb/err225

O'Leary B, Park J, and Plaxton WC. The remarkable diversity of plant PEPC (phosphoenolpyruvate carboxylase): recent insights into the physiological functions

and post-translational controls of non-photosynthetic PEPCs. Biochemical Journal. 2011b:**436**(1):15–34. https://doi.org/10.1042/BJ20110078

O'Leary BM, Asao S, Millar AH, and Atkin OK. Core principles which explain variation in respiration across biological scales. New Phytologist. 2019:**222**(2):670–686. https://doi.org/10.1111/nph.15576

Oszvald M, Primavesi LF, Griffiths CA, Cohn J, Basu SS, Nuccio ML, and Paul MJ. Trehalose 6-Phosphate Regulates Photosynthesis and Assimilate Partitioning in Reproductive Tissue. Plant Physiol. 2018:**176**(4):2623–2638. https://doi.org/10.1104/pp.17.01673

Paul MJ, Gonzalez-Uriarte A, Griffiths CA, and Hassani-Pak K. The Role of Trehalose 6-Phosphate in Crop Yield and Resilience. Plant Physiol. 2018:**177**(1):12–23. https://doi.org/10.1104/pp.17.01634

Pereyra C, Parola R, Lando AP, Rodriguez M, and Martínez-Noël GMA. High Sugar Concentration Inhibits TOR Signaling Pathway in Arabidopsis thaliana. J Plant Growth Regul. 2023:**42**(7):4309–4323. https://doi.org/10.1007/s00344-022-10894-w

Persyn F, Smagghe W, Eeckhout D, Mertens T, Smorscek T, De Winne N, Persiau G, Van De Slijke E, Crepin N, Gadeyne A, et al. A Nitrogen-specific Interactome Analysis Sheds Light on the Role of the SnRK1 and TOR Kinases in Plant Nitrogen Signaling. Molecular & Cellular Proteomics. 2024:**23**(10):100842. https://doi.org/10.1016/j.mcpro.2024.100842

Plaxton WC and Podestá FE. The Functional Organization and Control of Plant Respiration. CRC Crit Rev Plant Sci. 2006:**25**(2):159–198. https://doi.org/10.1080/07352680600563876

Ramon M, De Smet I, Vandesteene L, Naudts M, Leyman B, Van Dijck P, Rolland F, Beeckman T, and Thevelein JM. Extensive expression regulation and lack of heterologous enzymatic activity of the Class II trehalose metabolism proteins from *Arabidopsis thaliana*. Plant Cell Environ. 2009:**32**(8):1015–1032. https://doi.org/10.1111/j.1365-3040.2009.01985.x

Ren M, Venglat P, Qiu S, Feng L, Cao Y, Wang E, Xiang D, Wang J, Alexander D, Chalivendra S, et al. Target of Rapamycin Signaling Regulates Metabolism, Growth, and Life Span in *Arabidopsis*. Plant Cell. 2013:**24**(12):4850–4874. https://doi.org/10.1105/tpc.112.107144

Riegler S, Servi L, Scarpin MR, Godoy Herz MA, Kubaczka MG, Venhuizen P, Meyer C, Brunkard JO, Kalyna M, Barta A, et al. Light regulates alternative splicing outcomes via the TOR kinase pathway. Cell Rep. 2021:**36**(10):109676. https://doi.org/10.1016/j.celrep.2021.109676

Roessner U, Luedemann A, Brust D, Fiehn O, Linke T, Willmitzer L, and Fernie AR. Metabolic profiling allows comprehensive phenotyping of genetically or

environmentally modified plant systems. Plant Cell. 2001:**13**(1). https://doi.org/10.1105/tpc.13.1.11

Schluepmann H, Pellny T, van Dijken A, Smeekens S, and Paul M. Trehalose 6-phosphate is indispensable for carbohydrate utilization and growth in Arabidopsis thaliana. Proceedings of the National Academy of Sciences. 2003. https://doi.org/10.1073/pnas.1132018100

Singh V, Louis J, Ayre BG, Reese JC, and Shah J. TREHALOSE PHOSPHATE SYNTHASE11-dependent trehalose metabolism promotes Arabidopsis thaliana defense against the phloem-feeding insect Myzus persicae. Plant Journal. 2011. https://doi.org/10.1111/j.1365-313X.2011.04583.x

Smith AM and Stitt M. Coordination of carbon supply and plant growth. Plant Cell Environ. 2007. https://doi.org/10.1111/j.1365-3040.2007.01708.x

Soto-Burgos J and Bassham DC. SnRK1 activates autophagy via the TOR signaling pathway in Arabidopsis thaliana. PLoS One. 2017:**12**(8):e0182591. https://doi.org/10.1371/journal.pone.0182591

Suzuki N, Bajad S, Shuman J, Shulaev V, and Mittler R. The Transcriptional Co-activator MBF1c Is a Key Regulator of Thermotolerance in Arabidopsis thaliana. Journal of Biological Chemistry. 2008:**283**(14):9269–9275. https://doi.org/10.1074/jbc.M709187200

Sweetlove LJ, Beard KFM, Nunes-Nesi A, Fernie AR, and Ratcliffe RG. Not just a circle: flux modes in the plant TCA cycle. Trends Plant Sci. 2010:**15**(8):462–470. https://doi.org/10.1016/j.tplants.2010.05.006

Tian L, Xie Z, Lu C, Hao X, Wu S, Huang Y, Li D, and Chen L. The trehalose-6-phosphate synthase TPS5 negatively regulates ABA signaling in Arabidopsis thaliana. Plant Cell Rep. 2019:**38**(8):869–882. https://doi.org/10.1007/s00299-019-02408-y

Turck F, Fornara F, and Coupland G. Regulation and Identity of Florigen: FLOWERING LOCUS T Moves Center Stage. Annu Rev Plant Biol. 2008:**59**(1):573–594. https://doi.org/10.1146/annurev.arplant.59.032607.092755

Usadel B, Bläsing OE, Gibon Y, Retzlaff K, Höhne M, Günther M, and Stitt M. Global Transcript Levels Respond to Small Changes of the Carbon Status during Progressive Exhaustion of Carbohydrates in Arabidopsis Rosettes. Plant Physiol. 2008. https://doi.org/10.1104/pp.107.115592

Vandesteene L, Ramon M, Le Roy K, Van Dijck P, and Rolland F. A single active trehalose-6-P synthase (TPS) and a family of putative regulatory TPS-like proteins in arabidopsis. Mol Plant. 2010. https://doi.org/10.1093/mp/ssp114

Van Leene J, Eeckhout D, Gadeyne A, Matthijs C, Han C, De Winne N, Persiau G, Van De Slijke E, Persyn F, Mertens T, et al. Mapping of the plant SnRK1 kinase signalling network reveals a key regulatory role for the class II T6P synthase-like

proteins. Nat Plants. 2022:**8**(11):1245–1261. https://doi.org/10.1038/s41477-022-01269-w

Vishal B, Krishnamurthy P, and Kumar PP. Arabidopsis class II TPS controls root development and confers salt stress tolerance through enhanced hydrophobic barrier deposition. Plant Cell Rep. 2024:**43**(5):115. https://doi.org/10.1007/s00299-024-03215-w

Vogel G, Fiehn O, Jean-Richard-dit-Bressel L, Boller T, Wiemken A, Aeschbacher RA, and Wingler A. Trehalose metabolism in Arabidopsis: occurrence of trehalose and molecular cloning and characterization of trehalose-6-phosphate synthase homologues. J Exp Bot. 2001:**52**(362):1817–1826. https://doi.org/10.1093/jexbot/52.362.1817

Wahl V, Ponnu J, Schlereth A, Arrivault S, Langenecker T, Franke A, Feil R, Lunn JE, Stitt M, and Schmid M. Regulation of Flowering by Trehalose-6-Phosphate Signaling in *Arabidopsis thaliana*. Science (1979). 2013:**339**(6120):704–707. https://doi.org/10.1126/science.1230406

Xiang C, Han P, Lutziger I, Wang K, and Oliver DJ. A mini binary vector series for plant transformation. Plant Mol Biol. 1999:**40**(4):711–717. https://doi.org/10.1023/A:1006201910593

Xiong Y, McCormack M, Li L, Hall Q, Xiang C, and Sheen J. Glucose–TOR signalling reprograms the transcriptome and activates meristems. Nature. 2013:**496**(7444):181–186. https://doi.org/10.1038/nature12030

Xu G, Fan X, and Miller AJ. Plant Nitrogen Assimilation and Use Efficiency. Annu Rev Plant Biol. 2012:**63**(1):153–182. https://doi.org/10.1146/annurev-arplant-042811-105532

Yadav UP, Ivakov A, Feil R, Duan GY, Walther D, Giavalisco P, Piques M, Carillo P, Hubberten HM, Stitt M, et al. The sucrose-trehalose 6-phosphate (Tre6P) nexus: Specificity and mechanisms of sucrose signalling by. J Exp Bot. 2014. https://doi.org/10.1093/jxb/ert457

Yazdanbakhsh N, Sulpice R, Graf A, Stitt M, and Fisahn J. Circadian control of root elongation and C partitioning in *Arabidopsis thaliana*. Plant Cell Environ. 2011:**34**(6):877–894. https://doi.org/10.1111/j.1365-3040.2011.02286.x

Zang B, Li H, Li W, Deng XW, and Wang X. Analysis of trehalose-6-phosphate synthase (TPS) gene family suggests the formation of TPS complexes in rice. Plant Mol Biol. 2011:**76**(6):507–522. https://doi.org/10.1007/s11103-011-9781-1

Zhai Z, Keereetaweep J, Liu H, Feil R, Lunn JE, and Shanklin J. Trehalose 6-Phosphate Positively Regulates Fatty Acid Synthesis by Stabilizing WRINKLED1. Plant Cell. 2018:**30**(10):2616–2627. https://doi.org/10.1105/tpc.18.00521

Zhang Y and Fernie AR. The Role of TCA Cycle Enzymes in Plants. Adv Biol. 2023:**7**(8). https://doi.org/10.1002/adbi.202200238

Zhang Y, Primavesi LF, Jhurreea D, Andralojc PJ, Mitchell RAC, Powers SJ, Schluepmann H, Delatte T, Wingler A, and Paul MJ. Inhibition of SNF1-Related Protein Kinase1 Activity and Regulation of Metabolic Pathways by Trehalose-6-Phosphate. Plant Physiol. 2009:**149**(4):1860–1871. https://doi.org/10.1104/pp.108.133934

2.7. Supplementary Information

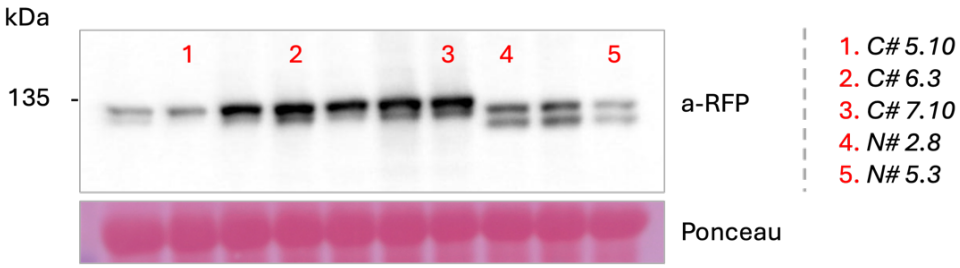

Supplementary Figure 2.1. TPS7 levels in *proTPS7::TPS7-mCherry* and *proTPS7::mCherry-TPS7* plants.
Original immunoblot of TPS7 levels in the *proTPS7::TPS7-mCherry* (C#5.10, C#6.3, and C#7.10) and *proTPS7::mCherry-TPS7* (N#2.8 and N#5.3) complementation lines. An anti-RFP antibody was used to detect TPS7-mCherry fusion proteins. The cropped version of this blot is presented in the main text (Figure 2.1B) for clarity.

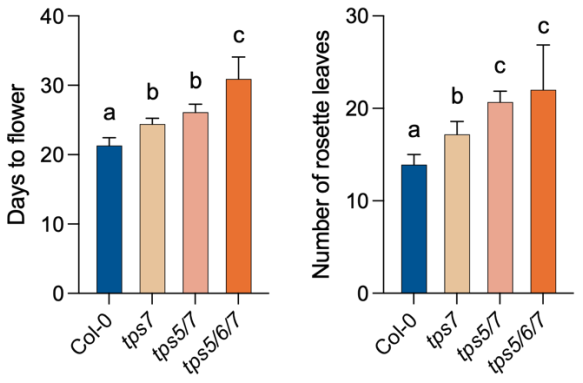

Supplementary Figure 2.2. Flowering phenotypes of *tps* mutants.
Quantification of flowering time in Col-0, *tps7*, *tps5/7* and *tps5/6/7* plants grown on soil under long-day conditions (16 h light, 110 µmol m^{-2} s^{-1}, 22 °C / 8 h dark, 18 °C), measured as days to flower and number of rosette leaves when the floral bud was first visible. Bars show the mean of 1 independent experiment (10 plants per genotype; error bars, SD). Different letters indicate statistically significant differences between genotypes (one-way ANOVA with Tukey HSD test).

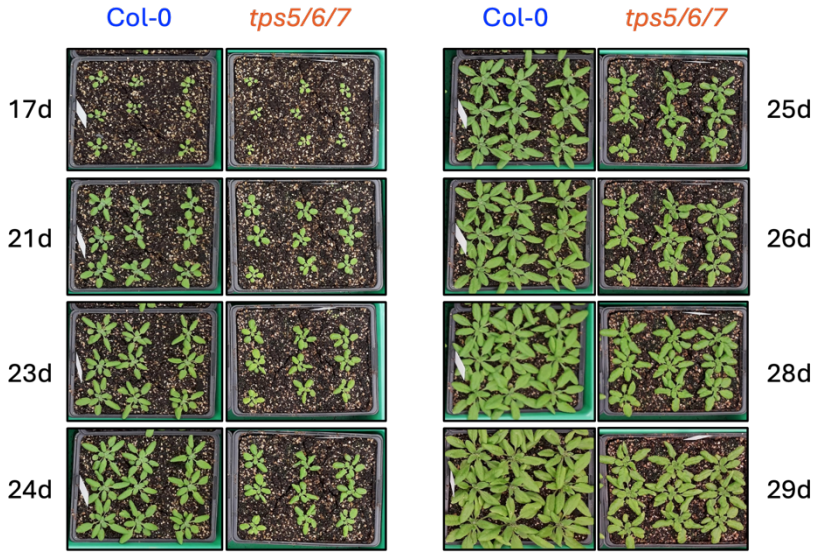

Supplementary Figure 2.3. Rosette phenotype of Col-0 and *tps5/6/7* plants.
Representative images of rosettes from Col-0 (left) and *tps5/6/7* (right) plants grown on soil under long-day conditions (16 h light, 110 µmol m^{-2} s^{-1}, 22 °C / 8 h dark, 18 °C). Images were captured over 12 days, from day 17 to day 29 after sowing.

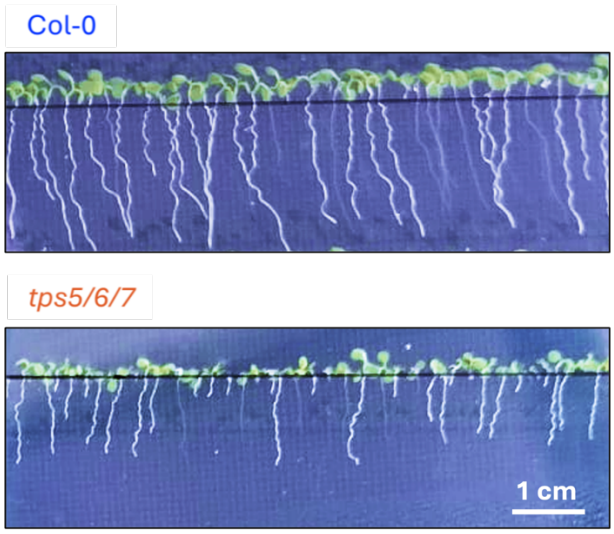

Supplementary Figure 2.4. Root growth variability in Col-0 and *tps5/6/7* seedlings.
Representative images of 7-d old Col-0 and *tps5/6/7* seedlings grown vertically on 0.5× MS medium under long-day conditions (16 h light, 110 µmol m^{-2} s^{-1}, 22 °C / 8 h dark, 18 °C), prior to transfer for root growth assays. Scale bar 1 cm.

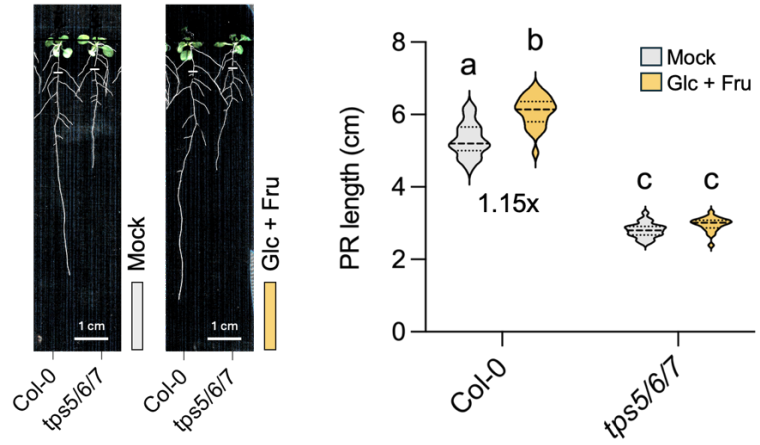

Supplementary Figure 2.5. Impact of glucose and fructose on *tps5/6/7* root growth.
Left, representative images of 14d-old Col-0 and *tps5/6/7* seedlings grown vertically on 0.5× MS medium for 7 d, transferred to 0.5× MS medium supplemented (right) or not (left) with 30 mM Glucose + 30 mM fructose and grown for an additional 7 d. White marks indicate root length at transfer. Scale bar 1 cm. Right, quantification of PR length, measured from the white mark to the root tip (n=1 independent experiment, 22-24 seedlings per genotype per condition). Upper and lower violin box lines represent the first and third quartiles, respectively. Horizontal lines mark the median. Different letters indicate statistically significant differences between genotype and condition combinations ($p < 0.05$, one-way ANOVA with Tukey HSD test).

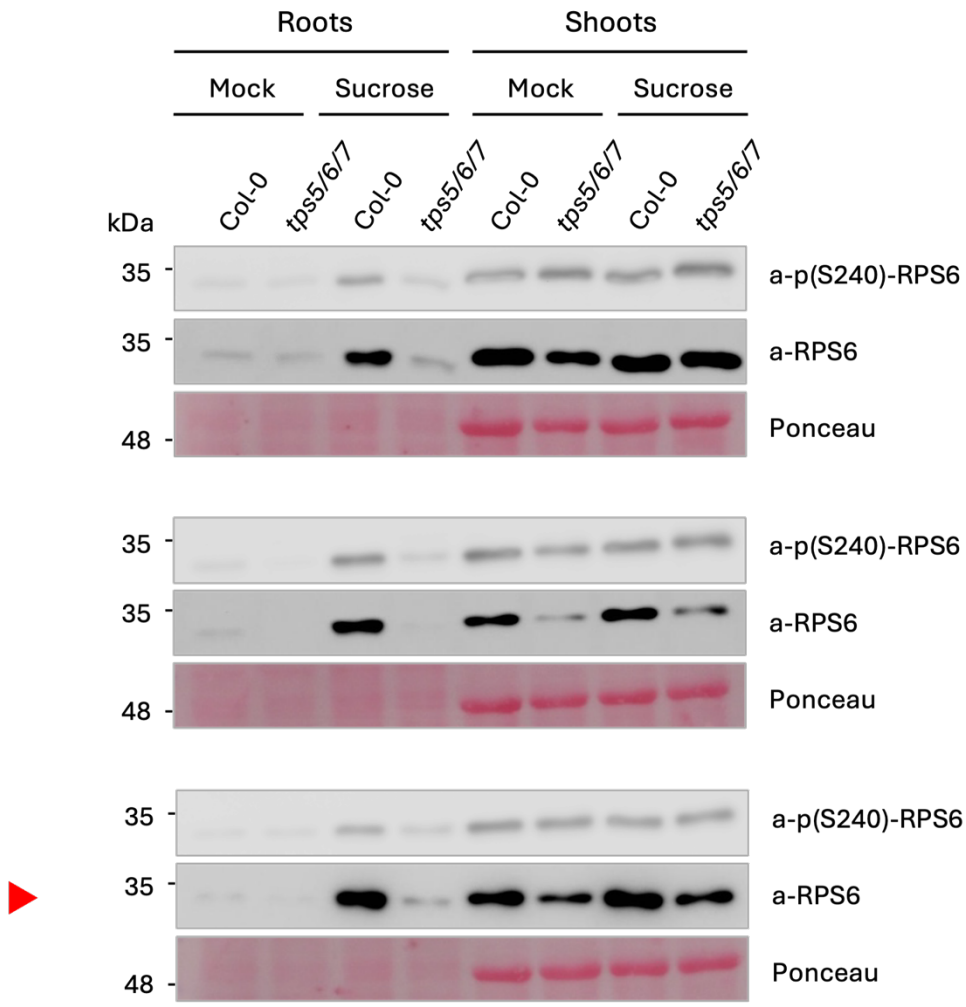

Supplementary Figure 2.6. Impact of TPS5/6/7 depletion on RPS6 and pRPS6 levels.
Immunoblots of p(S240)-RPS6 and total RPS6 from 14-d old Col-0 and *tps5/6/7* seedlings (roots and shoots) grown vertically on 0.5× MS medium for 7 d, transferred to 0.5× MS medium supplemented or not with 1% sucrose, and grown for an additional 7 d. Samples were harvested at the end of the night. Shown are results from three independent experiments to demonstrate reproducibility. The arrow indicates the image used as a representative result in the main text (Figure 2.3B).

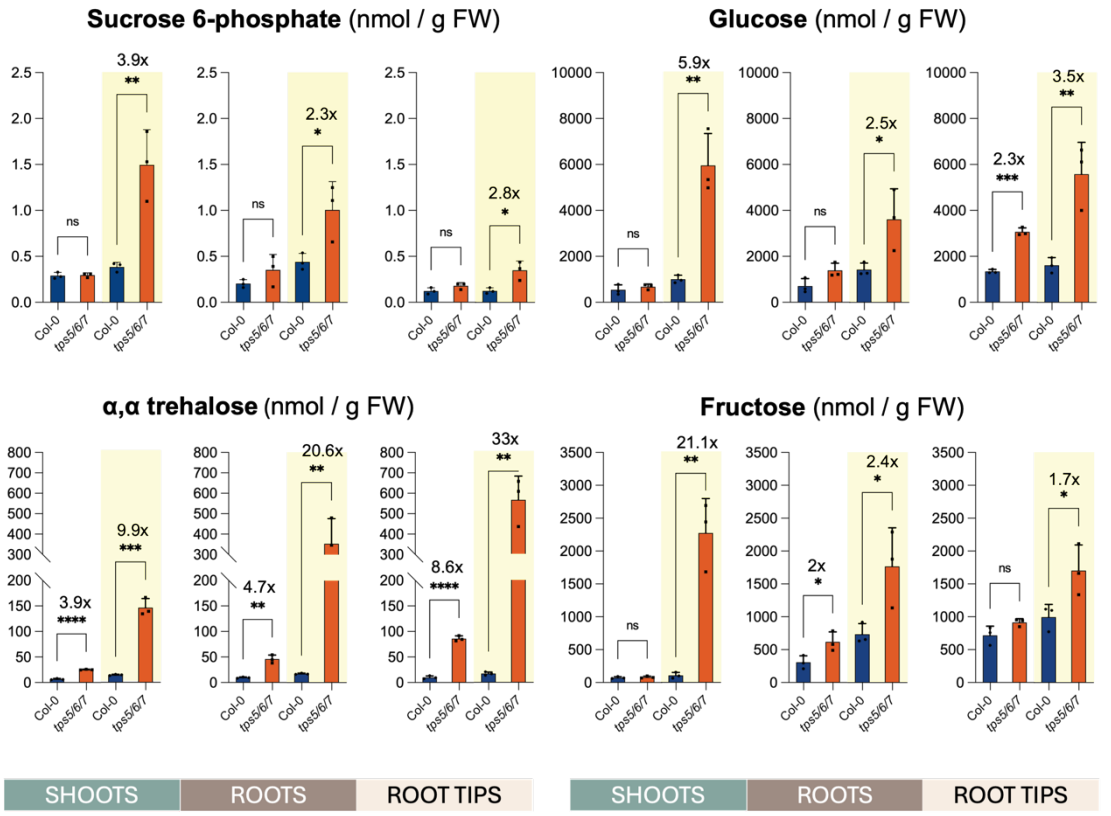

Supplementary Figure 2.7. Impact of TPS5/6/7 depletion on sugars related to sucrose and trehalose metabolism.
Levels of S6P, glucose, fructose, and α,α trehalose in the indicated tissues of 14d-old Col-0 and *tps5/6/7* seedlings. Seedlings were grown vertically on 0.5× MS medium under control light conditions (110 µmol m^{-2} s^{-1}) for 7 d, transferred to fresh 0.5× MS plates and grown for an additional 7 d under control light (CL; left) or high light conditions (HL; 200 µmol m^{-2} s^{-1}; right). Samples were harvested at the end of the night. Graphs show the mean of 3 independent experiments (each consisting of 200-250 seedlings per genotype per condition, error bars, SD). Asterisks indicate statistically significant differences between genotypes within each tissue and condition ($p < 0.05$, two-tailed unpaired t-test).

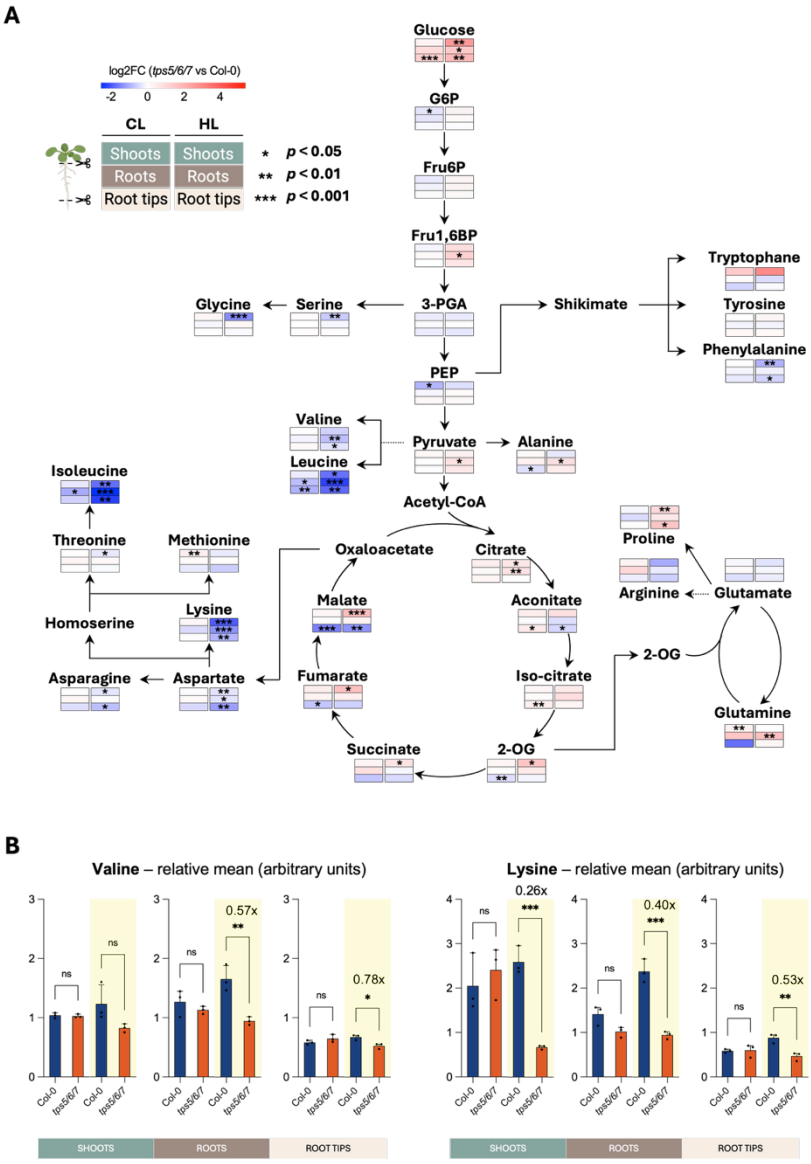

Supplementary Figure 2.8. Impact of TPS5/6/7 depletion on primary metabolism.
(**A**) Ratios of primary metabolites in the indicated tissues of 14d-old Col-0 and *tps5/6/7* seedlings. Seedlings were grown vertically on 0.5× MS medium under control light conditions (110 µmol m^{-2} s^{-1}) for 7 d, transferred to fresh 0.5× MS plates and grown for an additional 7 d under control light (CL; left) or high light conditions (HL; 200 µmol m^{-2} s^{-1}; right). Samples were harvested at the end of the night. Colors indicate the log2 ratios of the mean values (*tps5/6/7* vs. Col-0; n=3). Asterisks indicate statistically significant changes in metabolite levels between genotypes within each tissue and light condition (*p < 0.05, **p < 0.01, ***p < 0.001; two-tailed unpaired t-test). (**B**) Levels of Lysine and Valine in the indicated tissues of 14d-old Col-0 and *tps5/6/7* seedlings grown as in (**A**) under contrasting light intensities (CL, white; HL, yellow). Graphs show the mean of 3 independent experiments (each consisting of 200-250 seedlings per genotype per condition, error bars, SD). Asterisks indicate statistically significant differences between genotypes within each tissue and condition (p < 0.05, two-tailed unpaired t-test).

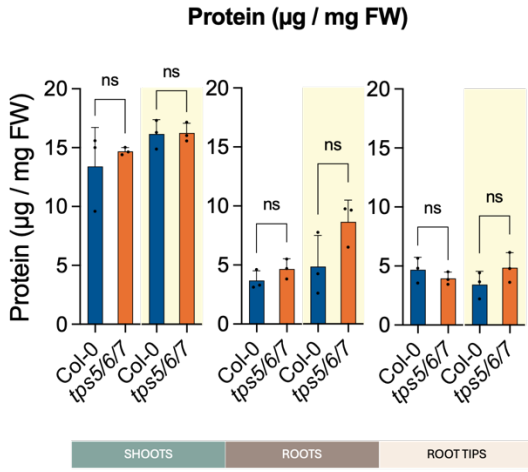

Supplementary Figure 2.9. Impact of TPS5/6/7 depletion on protein levels.
Total protein levels in the indicated tissues of 14d-old Col-0 and *tps5/6/7* seedlings. Seedlings were grown vertically on 0.5× MS medium under control light conditions (110 µmol m^{-2} s^{-1}) for 7 d, transferred to fresh 0.5× MS plates and grown for an additional 7 d under control light (CL; left) or high light conditions (HL; 200 µmol m^{-2} s^{-1}; right). Samples were harvested at the end of the night. Graphs show the mean of 3 independent experiments (each consisting of 200-250 seedlings per genotype per condition, error bars, SD). Asterisks indicate statistically significant differences between genotypes within each tissue and condition ($p < 0.05$, two-tailed unpaired t-test).

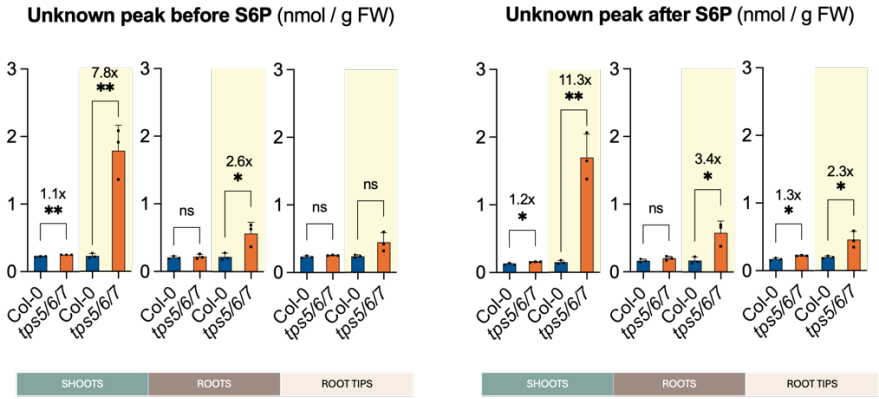

Supplementary Figure 2.10. Impact of TPS5/6/7 depletion on disaccharide-monophosphates isomeric with T6P.
Levels of two unidentified disaccharide-monophosphates isomeric with T6P in the indicated tissues of 14d-old Col-0 and *tps5/6/7* seedlings. Seedlings were grown vertically on 0.5× MS medium under control light conditions (110 µmol m^{-2} s^{-1}) for 7 d, transferred to fresh 0.5× MS plates and grown for an additional 7 d under control light (CL; left) or high light conditions (HL; 200 µmol m^{-2} s^{-1}; right). Samples were harvested at the end of the night. Graphs show the mean of 3 independent experiments (each consisting of 200-250 seedlings per genotype per condition, error bars, SD). Asterisks indicate statistically significant differences between genotypes within each tissue and condition ($p < 0.05$, two-tailed unpaired t-test).

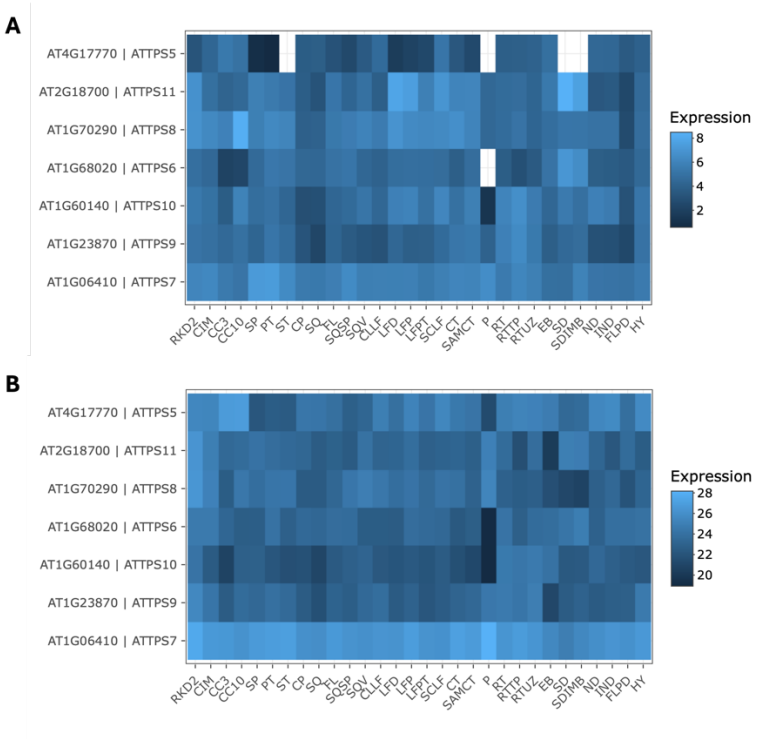

Supplementary Figure 2.11. Expression atlas of class II TPS in Arabidopsis.
Relative transcript (**A**) and protein (**B**) abundance in different tissues based on data from Mergner et al. (2020) and visualized with ATHENA proteomics; https://athena.proteomics.wzw.tum.de/master_arabidopsisshiny/). *RKD2*, egg-cell like callus; *CIM*, callus; *CC3*, root cell culture early; *CC10*, root cell culture late; *SP*, sepal (flower stage 15); *PT*, petal (flower stage 15); *ST*, stamen (flower stage 15); *CP*, carpel (flower stage 15); *SQ*, silique (stage 3); *FL*, flower (stage 15); *SQSP*, silique septum; *SQV*, silique valves; *CLLF*, 1st cauline leaf; *LFD*, rosette leaf 7, distal part; *LFP*, rosette leaf 7, proximal part; *LFPT*, rosette leaf 7, petiole; *SCLF*, senescent leaf; *CT*, cotyledons; *SAMCT*, shoot apical meristem, cotyledons and first leaves; *P*, pollen; *RT*, root; *RTP*, root tip; *RTUZ*, root upper zone; *EB*, seed (embryo stage 10); *SD*, seed (mature, dry); SDIMB, seed (mature, imbibed); *ND*, stem, 1st node; *IND*, stem, 2nd internode; *FLPD*, flower pedicle (flower stage 15); *HY*, hypocotyl.

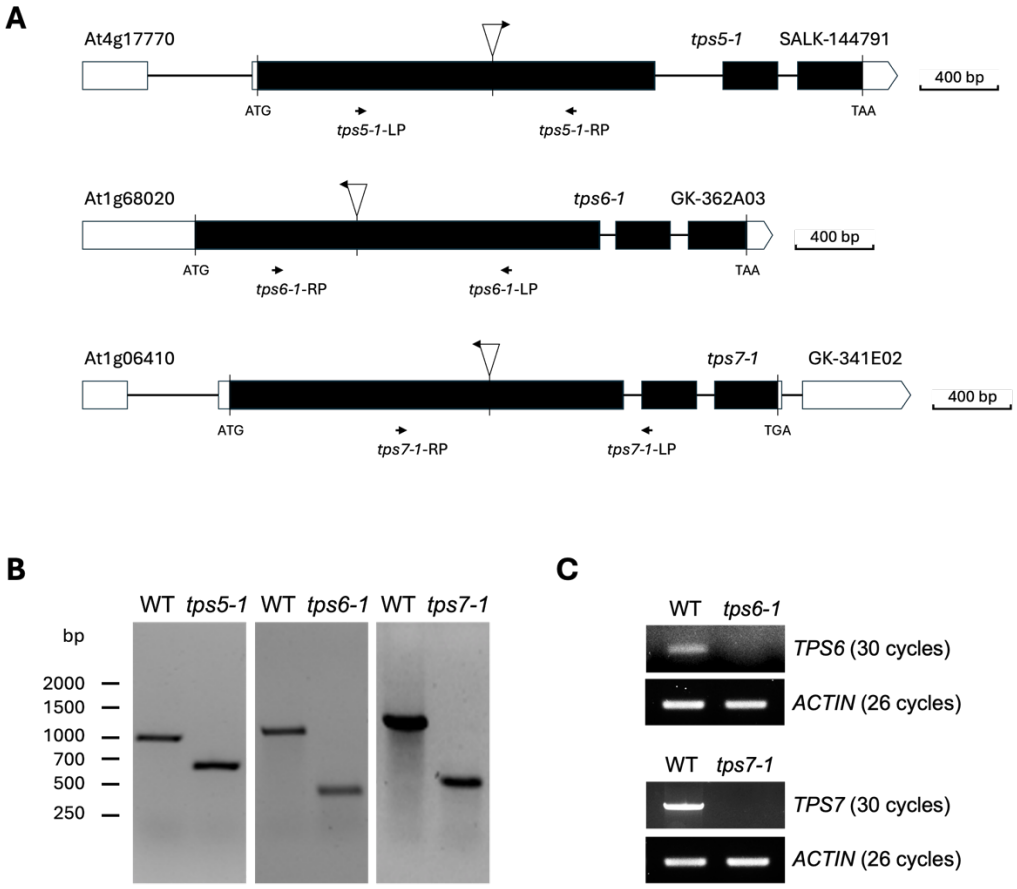

Supplementary Figure 2.12. Analysis of *tps* mutants.
(**A**) Schematic representation of the insertion sites of the *tps5*, *tps6*, and *tps7* T-DNA mutants used in this study. The ATG start codon and TAA/TGA stop codons are indicated. Exons are shown as black boxes, introns as black lines, and T-DNA insertion sites as triangles above the corresponding gene diagrams. Scale bar: 400 bp. (**B**) Confirmation of tps mutant identities by genotyping using T-DNA left border and gene-specific primers (LP and RP, indicated in **A**). (**C**) RT-PCR analyses of the *TPS6* (left panel) and *TPS7* (right panel) transcripts in *tps6-1* and *tps7-1* mutants, respectively. Amplification of ACTIN mRNA was used as a control. The *tps5-1* mutant was previously described (Tian et al., 2019).

Supplementary Table 2.1. Tissue-specific metabolite levels in 14d-old Col-0 and *tps5/6/7* seedlings.

Seedlings were grown vertically for 7 days on 0.5× MS medium under control light (110 µmol m^{-2} s^{-1}), then transferred to fresh plates and grown for 7 additional days under either control light or high light (HL; 200 µmol m^{-2} s^{-1}). Metabolites were profiled separately in shoots, roots, and root tips harvested at end of night. Biological replicate values are shown for each metabolite, with corresponding average values and standard deviations. Data shown as: sugar phosphates/organic acids (nmol/g FW; Table S2.1A), soluble sugars (nmol/g FW; Table S2.1B), and amino acids (relative means; Table S2.1C).

Supplementary Table 2.1A Sugar phosphates and organic acids

Light intensity	genotype	tissue	replicate	Tre6P			Unknow peak before Suc6P			Suc6P			Unknow peak after Suc6P			ADPGlc		
				nmol / g FW	average	stdev	nmol / g FW	average	stdev	nmol / g FW	average	stdev	nmol / g FW	average	stdev	nmol / g FW	average	stdev
Control light	**Col-0**	Shoots	1	0,07	0,07	0,01	0,23	0,23	0,01	0,28	0,29	0,03	0,12	0,13	0,01	0,016	0,017	0,003
			2	0,07			0,23			0,26			0,12			0,020		
			3	0,08			0,22			0,33			0,14			0,016		
Control light	**tps5/6/7**	Shoots	1	0,14	0,13	0,01	0,25	0,25	0,00	0,31	0,30	0,02	0,16	0,15	0,00	0,013	0,017	0,005
			2	0,12			0,25			0,27			0,16			0,023		
			3	0,14			0,25			0,31			0,15			0,014		
High light	**Col-0**	Shoots	1	0,07	0,09	0,02	0,20	0,23	0,03	0,33	0,39	0,05	0,13	0,15	0,02	0,027	0,025	0,002
			2	0,10			0,22			0,42			0,14			0,024		
			3	0,10			0,27			0,41			0,18			0,024		
High light	**tps5/6/7**	Shoots	1	2,87	2,71	0,46	1,91	1,78	0,38	1,53	1,49	0,38	1,65	1,70	0,35	0,044	0,059	0,024
			2	2,19			1,36			1,10			1,38			0,047		
			3	3,07			2,08			1,86			2,07			0,086		
Control light	**Col-0**	Roots	1	0,05	0,06	0,02	0,19	0,21	0,02	0,20	0,20	0,04	0,14	0,16	0,03	0,022	0,024	0,002
			2	0,05			0,20			0,16			0,16			0,024		
			3	0,09			0,23			0,25			0,19			0,026		
Control light	**tps5/6/7**	Roots	1	0,16	0,21	0,05	0,19	0,22	0,04	0,17	0,35	0,17	0,17	0,20	0,03	0,022	0,020	0,004
			2	0,21			0,21			0,50			0,20			0,016		
			3	0,27			0,26			0,39			0,23			0,023		
High light	**Col-0**	Roots	1	0,09	0,10	0,02	0,20	0,22	0,05	0,43	0,45	0,09	0,15	0,17	0,05	0,017	0,022	0,010
			2	0,09			0,18			0,36			0,13			0,016		
			3	0,13			0,28			0,54			0,23			0,034		
High light	**tps5/6/7**	Roots	1	4,63	4,26	1,09	0,63	0,56	0,17	1,25	1,01	0,31	0,66	0,58	0,17	0,022	0,039	0,026
			2	3,04			0,37			0,66			0,38			0,028		
			3	5,12			0,69			1,11			0,70			0,069		
Control light	**Col-0**	Root tips	1	0,10	0,13	0,04	0,22	0,23	0,02	0,09	0,12	0,03	0,15	0,17	0,02	0,013	0,019	0,006
			2	0,13			0,25			0,12			0,17			0,020		
			3	0,18			0,23			0,16			0,19			0,024		
Control light	**tps5/6/7**	Root tips	1	0,49	0,48	0,02	0,25	0,26	0,01	0,14	0,18	0,04	0,22	0,22	0,01	0,015	0,025	0,012
			2	0,47			0,25			0,20			0,22			0,023		
			3	0,50			0,26			0,20			0,23			0,038		
High light	**Col-0**	Root tips	1	0,14	0,21	0,06	0,22	0,24	0,02	0,10	0,13	0,03	0,18	0,20	0,02	0,015	0,019	0,006
			2	0,24			0,24			0,12			0,20			0,017		
			3	0,27			0,26			0,16			0,22			0,026		
High light	**tps5/6/7**	Root tips	1	5,44	5,22	0,70	0,60	0,45	0,14	0,44	0,35	0,10	0,59	0,46	0,12	0,033	0,024	0,012
			2	4,44			0,32			0,24			0,35			0,011		
			3	5,77			0,42			0,37			0,44			0,028		

Supplementary Table 2.1A Sugar phosphates and organic acids

Light intensity	genotype	tissue	replicate	Gal1P			G1,6BP			UDPGal			Glc1P			Gly3P		
				nmol / g FW	average	stdev	nmol / g FW	average	stdev	nmol / g FW	average	stdev	nmol / g FW	average	stdev	nmol / g FW	average	stdev
Control light	**Col-0**	Shoots	1	2,5	2,7	0,2	1,4	1,6	0,3	18	20	2	14	15	1	23	24	2
			2	2,6			1,4			20			15			23		
			3	2,9			1,9			22			17			27		
Control light	**tps5/6/7**	Shoots	1	2,2	2,4	0,3	1,6	1,4	0,3	19	18	1	12	12	1	23	21	1
			2	2,3			1,1			18			11			22		
			3	2,7			1,5			18			12			20		
High light	**Col-0**	Shoots	1	2,7	2,9	0,4	1,2	1,4	0,3	17	19	2	10	12	2	19	21	3
			2	2,6			1,4			18			11			21		
			3	3,3			1,7			22			14			24		
High light	**tps5/6/7**	Shoots	1	2,8	2,9	0,3	1,8	1,4	0,4	18	20	3	12	12	2	18	17	1
			2	2,6			1,3			19			10			17		
			3	3,2			1,1			23			14			17		
Control light	**Col-0**	Roots	1	1,3	1,6	0,3	0,7	0,8	0,2	14	15	2	11	11	2	18	20	6
			2	1,5			0,6			14			10			16		
			3	2,0			1,0			18			13			28		
Control light	**tps5/6/7**	Roots	1	1,4	1,7	0,3	0,7	0,9	0,2	13	16	2	8	9	1	19	23	5
			2	1,7			1,1			15			9			22		
			3	1,9			0,9			18			10			29		
High light	**Col-0**	Roots	1	2,3	2,5	0,5	0,8	1,0	0,1	18	20	3	11	12	3	21	22	4
			2	2,1			1,0			18			10			19		
			3	3,0			1,1			24			15			27		
High light	**tps5/6/7**	Roots	1	2,7	2,5	0,6	1,4	1,3	0,3	28	25	5	14	12	3	24	25	6
			2	1,9			1,0			20			8			19		
			3	2,9			1,6			27			14			31		
Control light	**Col-0**	Root tips	1	1,7	2,3	0,5	1,1	1,3	0,2	14	19	5	9	12	2	16	21	6
			2	2,4			1,5			20			12			19		
			3	2,7			1,4			23			13			28		
Control light	**tps5/6/7**	Root tips	1	2,1	2,0	0,1	1,5	1,3	0,2	18	17	1	10	10	1	26	24	4
			2	2,0			1,2			18			11			26		
			3	1,8			1,0			16			9			20		
High light	**Col-0**	Root tips	1	2,3	2,7	0,5	1,3	1,6	0,3	19	21	3	11	13	3	17	20	5
			2	2,5			1,7			20			12			17		
			3	3,2			1,7			24			16			25		
High light	**tps5/6/7**	Root tips	1	2,8	2,2	0,5	1,7	1,4	0,2	26	22	4	12	10	2	26	23	4
			2	1,8			1,4			17			8			18		
			3	2,2			1,2			22			10			24		

Supplementary Table 2.1A Sugar phosphates and organic acids

Light intensity	genotype	tissue	replicate	PEP			Fru6P			Man6P			Fru1,6BP			UDPGlc		
				nmol / g FW	average	stdev	nmol / g FW	average	stdev	nmol / g FW	average	stdev	nmol / g FW	average	stdev	nmol / g FW	average	stdev
Control light	**Col-0**	Shoots	1	11,7	11,8	0,7	45	50	6	37	39	2	0,8	0,8	0,1	56	59	3
			2	12,6			48			39			0,6			58		
			3	11,2			56			42			0,9			62		
Control light	**tps5/6/7**	Shoots	1	5,0	6,2	1,7	39	41	3	28	30	2	0,6	0,7	0,2	50	52	2
			2	7,5			40			32			0,6			51		
			3	N/A			45			32			0,9			54		
High light	**Col-0**	Shoots	1	3,3	6,5	3,1	37	43	7	27	29	3	0,4	0,5	0,1	53	56	4
			2	6,6			41			27			0,4			54		
			3	9,5			50			32			0,6			60		
High light	**tps5/6/7**	Shoots	1	7,9	4,8	3,4	51	50	5	22	23	2	1,3	0,9	0,4	62	65	9
			2	5,3			44			21			0,7			58		
			3	1,3			54			25			0,6			76		
Control light	**Col-0**	Roots	1	2,2	2,5	0,9	31	35	6	15	18	3	1,7	1,6	0,1	42	45	8
			2	3,5			32			18			1,6			39		
			3	1,6			42			21			1,6			54		
Control light	**tps5/6/7**	Roots	1	1,8	2,2	0,4	28	32	3	12	14	2	1,8	1,8	0,2	38	44	6
			2	2,6			33			15			1,6			45		
			3	2,3			34			16			2,1			50		
High light	**Col-0**	Roots	1	0,8	1,5	0,8	40	42	7	19	20	4	1,0	1,5	0,4	61	66	7
			2	1,4			36			18			1,5			63		
			3	2,4			50			24			1,9			74		
High light	**tps5/6/7**	Roots	1	1,2	1,6	0,6	57	49	10	15	13	2	3,3	3,4	0,4	82	71	16
			2	2,3			38			11			3,0			54		
			3	1,5			53			14			3,8			78		
Control light	**Col-0**	Root tips	1	1,2	1,2	0,1	25	29	4	12	15	2	1,6	1,7	0,2	55	67	10
			2	1,3			33			16			1,8			73		
			3	1,1			29			16			1,5			73		
Control light	**tps5/6/7**	Root tips	1	1,8	1,4	0,4	33	30	4	14	14	1	1,9	1,6	0,3	56	51	5
			2	1,2			31			14			1,6			52		
			3	1,1			25			13			1,4			45		
High light	**Col-0**	Root tips	1	1,1	1,5	0,3	30	38	8	15	16	3	1,2	1,8	0,5	72	84	10
			2	1,7			38			15			2,0			88		
			3	1,7			45			20			2,2			91		
High light	**tps5/6/7**	Root tips	1	1,4	1,7	0,6	52	40	10	14	12	2	3,5	2,9	0,6	75	63	11
			2	2,3			35			10			2,7			55		
			3	1,3			34			11			2,4			58		

Supplementary Table 2.1A Sugar phosphates and organic acids

Light intensity	genotype	tissue	replicate	shikimate			Iso-Citrate			Aconitate			Glc6P			2-OG		
				nmol / g FW	average	stdev	nmol / g FW	average	stdev	nmol / g FW	average	stdev	nmol / g FW	average	stdev	nmol / g FW	average	stdev
Control light	**Col-0**	Shoots	1	9	10	2	4,7	5,1	0,4	N/A	2,5	0,2	131	136	8	5	5	1
			2	8			5,4			2,7			131			5		
			3	12			5,2			2,4			145			4		
Control light	**tps5/6/7**	Shoots	1	13	12	1	7,5	6,0	1,3	4,2	3,5	0,8	104	110	10	8	6	3
			2	11			5,2			2,7			104			7		
			3	12			5,4			3,7			122			2		
High light	**Col-0**	Shoots	1	7	9	2	10,6	10,8	0,3	6,8	6,8	0,2	103	113	17	9	7	2
			2	10			10,7			7,0			103			8		
			3	9			11,2			6,7			132			5		
High light	**tps5/6/7**	Shoots	1	18	20	4	16,2	15,8	3,5	15,1	11,8	3,0	131	127	14	22	21	5
			2	17			12,1			11,0			112			15		
			3	24			19,1			9,4			139			25		
Control light	**Col-0**	Roots	1	4	5	2	2,4	3,1	0,7	1,1	1,3	0,3	95	103	11	12	14	3
			2	5			3,1			1,2			98			13		
			3	8			3,9			1,7			115			17		
Control light	**tps5/6/7**	Roots	1	5	6	1	2,9	3,4	0,6	1,0	1,3	0,3	72	84	10	10	14	4
			2	6			3,1			1,3			89			15		
			3	7			4,1			1,5			90			18		
High light	**Col-0**	Roots	1	6	6	1	3,7	3,8	0,6	2,6	2,7	0,3	96	109	20	21	21	2
			2	5			3,2			2,4			99			19		
			3	7			4,4			2,9			131			24		
High light	**tps5/6/7**	Roots	1	10	10	2	7,5	7,0	2,2	1,3	2,0	0,6	140	124	30	27	32	11
			2	8			4,6			2,1			89			24		
			3	13			8,8			2,5			142			44		
Control light	**Col-0**	Root tips	1	17	18	8	1,8	2,0	0,2	0,6	0,8	0,1	72	88	15	27	27	2
			2	27			2,0			0,9			99			25		
			3	11			2,2			0,8			95			29		
Control light	**tps5/6/7**	Root tips	1	10	10	0	2,8	2,7	0,1	1,1	1,1	0,1	91	84	7	21	20	2
			2	9			2,7			1,2			83			21		
			3	9			2,6			1,1			77			19		
High light	**Col-0**	Root tips	1	11	11	1	3,7	4,3	1,1	2,3	2,2	0,2	80	105	24	29	36	7
			2	10			3,6			2,1			109			35		
			3	11			5,5			2,0			127			43		
High light	**tps5/6/7**	Root tips	1	12	12	3	6,4	5,2	1,2	1,8	1,5	0,3	128	103	22	37	33	4
			2	10			4,0			1,4			94			30		
			3	15			5,1			1,3			88			31		

Supplementary Table 2.1A Sugar phosphates and organic acids

Light intensity	genotype	tissue	replicate	pyruvate			succinate			3-PGA			glycerate			citrate		
				nmol / g FW	average	stdev	nmol / g FW	average	stdev	nmol / g FW	average	stdev	nmol / g FW	average	stdev	nmol / g FW	average	stdev
Control light	**Col-0**	Shoots	1	7	7	1	143	160	21	137	147	13	80	92	32	248	273	22
			2	7			184			144			68			288		
			3	6			153			161			129			283		
Control light	**tps5/6/7**	Shoots	1	7	8	1	207	195	32	100	125	29	92	79	12	449	373	70
			2	7			158			118			80			359		
			3	9			219			156			67			311		
High light	**Col-0**	Shoots	1	11	12	4	250	212	36	100	129	32	112	124	10	573	589	55
			2	17			209			125			130			650		
			3	9			178			162			128			543		
High light	**tps5/6/7**	Shoots	1	13	16	3	341	349	74	135	108	28	171	154	16	1032	913	154
			2	16			279			109			149			738		
			3	19			426			79			140			968		
Control light	**Col-0**	Roots	1	12	14	2	102	89	53	32	33	3	208	210	32	139	199	62
			2	15			31			32			179			196		
			3	16			134			37			244			263		
Control light	**tps5/6/7**	Roots	1	13	15	2	125	159	80	27	32	5	235	252	19	190	220	42
			2	15			101			34			272			203		
			3	16			250			35			249			268		
High light	**Col-0**	Roots	1	21	20	3	194	190	27	25	31	7	662	634	37	266	270	8
			2	17			162			30			592			279		
			3	23			216			39			648			265		
High light	**tps5/6/7**	Roots	1	36	34	6	170	176	26	34	33	4	605	490	111	474	447	55
			2	28			153			29			482			384		
			3	40			205			36			384			484		
Control light	**Col-0**	Root tips	1	8	8	0	104	178	81	25	28	3	845	616	234	126	147	24
			2	7			165			31			625			173		
			3	8			264			27			378			141		
Control light	**tps5/6/7**	Root tips	1	9	8	1	149	108	44	28	23	4	349	349	2	169	179	20
			2	8			112			22			351			202		
			3	6			62			20			348			166		
High light	**Col-0**	Root tips	1	10	11	1	256	303	41	23	31	9	816	704	103	285	341	88
			2	12			323			29			615			295		
			3	12			329			41			680			443		
High light	**tps5/6/7**	Root tips	1	24	18	6	308	218	78	27	25	2	498	351	157	419	352	60
			2	15			163			24			370			304		
			3	14			184			24			186			334		

Supplementary Table 2.1A Sugar phosphates and organic acids

Light intensity	genotype	tissue	replicate	malate			fumarate		
				nmol / g FW	average	stdev	nmol / g FW	average	stdev
Control light	**Col-0**	Shoots	1	275	306	64	435	390	70
			2	264			310		
			3	380			424		
Control light	**tps5/6/7**	Shoots	1	407	362	39	727	532	169
			2	338			428		
			3	341			441		
High light	**Col-0**	Shoots	1	362	414	73	476	597	269
			2	498			905		
			3	382			411		
High light	**tps5/6/7**	Shoots	1	1402	1351	196	2094	1778	274
			2	1135			1606		
			3	1516			1636		
Control light	**Col-0**	Roots	1	257	312	109	4	8	5
			2	241			5		
			3	438			14		
Control light	**tps5/6/7**	Roots	1	256	319	62	7	10	3
			2	321			11		
			3	380			11		
High light	**Col-0**	Roots	1	508	551	82	18	20	4
			2	499			17		
			3	645			24		
High light	**tps5/6/7**	Roots	1	614	699	111	26	27	7
			2	660			20		
			3	825			34		
Control light	**Col-0**	Root tips	1	999	1119	109	16	19	2
			2	1145			19		
			3	1212			21		
Control light	**tps5/6/7**	Root tips	1	397	391	49	11	11	1
			2	436			13		
			3	340			10		
High light	**Col-0**	Root tips	1	1278	1464	210	23	29	6
			2	1420			28		
			3	1692			35		
High light	**tps5/6/7**	Root tips	1	740	591	174	22	19	4
			2	634			21		
			3	400			15		

Supplementary Table 2.1B Soluble sugars

Light intensity	genotype	tissue	replicate	α,α trehalose			sucrose			glucose			fructose		
				nmol / g FW	average	stdev	nmol / g FW	average	stdev	nmol / g FW	average	stdev	nmol / g FW	average	stdev
Control light	**Col-0**	Shoots	1	5,4	6,5	1,4	633	706	64	354	542	222	69	75	14
			2	8,0			749			485			64		
			3	6,1			737			788			91		
Control light	**tps5/6/7**	Shoots	1	24,4	25,2	0,9	820	770	49	737	680	117	100	83	15
			2	26,2			722			758			79		
			3	25,1			767			545			71		
High light	**Col-0**	Shoots	1	14,9	14,6	1,2	718	854	117	1188	1001	171	65	107	47
			2	15,7			929			963			158		
			3	13,3			914			852			99		
High light	**tps5/6/7**	Shoots	1	139,2	146,4	17,0	7004	6423	1580	5327	5946	1389	2689	2269	525
			2	134,2			4634			4974			1681		
			3	165,9			7630			7537			2438		
Control light	**Col-0**	Roots	1	8,7	9,8	1,3	576	673	176	587	711	327	298	308	101
			2	9,5			566			465			212		
			3	11,2			876			1082			413		
Control light	**tps5/6/7**	Roots	1	38,3	45,9	8,2	535	600	108	1188	1386	316	490	618	151
			2	44,7			541			1220			580		
			3	54,6			725			1750			785		
High light	**Col-0**	Roots	1	16,8	17,2	1,4	558	662	232	1249	1430	291	634	738	161
			2	16,1			500			1274			656		
			3	18,8			927			1765			924		
High light	**tps5/6/7**	Roots	1	346,6	354,4	122,9	1796	1647	546	3699	3624	1330	1882	1771	586
			2	235,6			1042			2258			1138		
			3	481,0			2104			4916			2293		
Control light	**Col-0**	Root tips	1	7,4	10,1	3,0	225	283	70	1289	1345	88	565	719	139
			2	9,5			264			1299			760		
			3	13,3			362			1447			833		
Control light	**tps5/6/7**	Root tips	1	81,7	86,1	5,2	300	315	20	3271	3072	174	849	913	56
			2	84,8			308			2951			941		
			3	91,9			338			2993			951		
High light	**Col-0**	Root tips	1	16,7	17,1	3,2	254	336	120	1284	1615	335	776	999	194
			2	14,1			279			1606			1102		
			3	20,5			474			1953			1119		
High light	**tps5/6/7**	Root tips	1	605,0	564,2	115,2	1409	1137	344	6636	5587	1391	2117	1706	391
			2	434,2			751			4009			1338		
			3	653,6			1252			6116			1663		

Supplementary Table 2.1B Soluble sugars

Light intensity	genotype	tissue	replicate	rhamnose			maltose			maltotriose			iso-erythritol			arabinose		
				nmol / g FW	average	stdev	nmol / g FW	average	stdev	nmol / g FW	average	stdev	nmol / g FW	average	stdev	nmol / g FW	average	stdev
Control light	**Col-0**	Shoots	1	11,1	11,4	0,5	24,0	26,5	4,2	6,3	5,3	0,9	6,4	6,6	0,5	6,1	6,4	0,4
			2	11,1			24,1			4,7			6,2			N/A		
			3	12,0			31,4			4,8			7,2			6,7		
Control light	**tps5/6/7**	Shoots	1	9,3	9,8	0,6	31,6	29,3	3,7	5,1	4,5	0,5	5,6	6,2	0,6	6,3	6,0	0,3
			2	10,4			25,1			4,3			6,2			5,8		
			3	9,7			31,4			4,1			6,7			6,0		
High light	**Col-0**	Shoots	1	10,1	10,6	0,4	25,1	30,9	5,4	5,3	4,9	0,3	6,5	6,7	0,7	8,0	7,0	1,1
			2	10,8			35,7			4,9			6,1			7,0		
			3	10,9			32,0			4,6			7,4			5,9		
High light	**tps5/6/7**	Shoots	1	10,5	10,9	0,3	67,1	76,3	23,3	9,8	8,8	1,5	10,1	11,5	1,2	7,5	8,0	0,6
			2	11,1			59,1			7,1			12,4			8,6		
			3	11,0			102,8			9,5			12,0			7,8		
Control light	**Col-0**	Roots	1	7,6	7,9	0,7	3,8	3,9	0,1	3,6	3,2	0,4	8,8	8,1	0,8	6,9	7,5	0,6
			2	8,7			3,9			3,2			7,2			7,7		
			3	7,5			3,9			2,8			8,4			7,9		
Control light	**tps5/6/7**	Roots	1	7,9	8,4	0,6	4,7	4,2	0,6	4,0	3,4	0,6	8,8	7,7	1,4	6,0	7,1	1,2
			2	9,0			3,6			3,0			6,1			6,9		
			3	8,2			4,3			3,1			8,2			8,4		
High light	**Col-0**	Roots	1	8,3	8,5	0,3	4,5	10,1	10,2	4,6	11,0	12,2	8,4	7,3	1,1	9,7	9,2	0,4
			2	8,7			21,9			25,0			6,2			9,0		
			3	8,7			4,0			3,3			7,4			8,9		
High light	**tps5/6/7**	Roots	1	7,8	8,2	0,4	5,2	5,2	0,6	3,7	3,3	0,3	8,3	8,4	1,5	9,0	9,6	0,6
			2	8,0			4,7			3,3			7,0			10,0		
			3	8,6			5,9			3,0			9,9			9,8		
Control light	**Col-0**	Root tips	1	7,9	7,6	0,4	4,9	4,6	0,3	5,1	3,7	1,2	5,2	5,1	0,6	8,6	8,7	1,3
			2	7,1			4,4			3,0			4,5			7,5		
			3	7,8			4,6			3,2			5,7			10,1		
Control light	**tps5/6/7**	Root tips	1	8,4	8,5	0,2	4,8	4,7	0,1	3,8	3,4	0,3	6,7	6,6	0,3	11,2	10,1	1,0
			2	8,3			4,8			3,2			6,2			9,5		
			3	8,6			4,6			3,4			6,8			9,5		
High light	**Col-0**	Root tips	1	9,0	7,9	1,0	5,1	4,9	0,2	4,1	3,5	0,5	5,9	5,5	0,7	8,6	9,6	1,7
			2	7,0			4,7			3,3			4,7			8,7		
			3	7,7			4,8			3,2			5,9			11,6		
High light	**tps5/6/7**	Root tips	1	7,9	8,7	0,8	6,1	5,5	0,6	6,3	4,5	1,5	10,8	9,8	1,7	14,6	14,7	2,8
			2	8,7			5,0			3,9			7,8			11,9		
			3	9,4			5,4			3,4			10,9			17,5		

Supplementary Table 2.1B Soluble sugars

Light intensity	genotype	tissue	replicate	arabitol			sorbitol			myo-inositol			raffinose			1-kestose		
				nmol / g FW	average	stdev	nmol / g FW	average	stdev	nmol / g FW	average	stdev	nmol / g FW	average	stdev	nmol / g FW	average	stdev
Control light	**Col-0**	Shoots	1	4,0	3,7	0,3	3,0	5,8	5,3	162	201	34	11,4	11,6	1,7	1,6	1,6	0,0
			2	3,5			2,6			222			9,9			1,6		
			3	3,6			12,0			218			13,4			1,6		
Control light	**tps5/6/7**	Shoots	1	3,4	3,5	0,1	2,5	7,3	6,2	190	194	7	6,5	6,6	0,2	1,5	1,6	0,2
			2	3,6			5,2			202			6,4			1,8		
			3	3,6			14,3			190			6,9			1,6		
High light	**Col-0**	Shoots	1	3,9	3,9	0,2	3,2	7,2	5,9	169	173	12	5,2	5,5	0,7	1,7	1,8	0,4
			2	3,7			4,5			187			6,3			1,6		
			3	4,0			13,9			164			4,9			2,2		
High light	**tps5/6/7**	Shoots	1	4,2	4,0	0,1	7,4	13,5	7,7	265	282	28	19,3	16,6	2,5	8,9	9,1	1,3
			2	4,0			11,0			266			14,5			8,0		
			3	3,9			22,2			315			16,0			10,5		
Control light	**Col-0**	Roots	1	3,5	3,6	0,1	2,5	5,2	4,8	218	248	73	21,6	30,8	10,8	1,6	1,7	0,1
			2	3,7			2,4			195			28,2			1,7		
			3	3,7			10,7			331			42,6			1,9		
Control light	**tps5/6/7**	Roots	1	3,8	3,9	0,2	3,7	7,6	8,2	353	308	76	14,6	18,9	6,8	1,8	1,8	0,1
			2	3,7			2,0			220			15,3			1,7		
			3	4,1			17,0			351			26,8			1,9		
High light	**Col-0**	Roots	1	4,0	3,8	0,2	5,3	7,2	4,5	335	370	72	10,5	12,6	3,9	1,7	1,7	0,1
			2	3,9			3,9			323			10,1			1,6		
			3	3,6			12,3			453			17,1			1,8		
High light	**tps5/6/7**	Roots	1	4,0	3,9	0,2	4,8	8,8	7,3	503	444	139	31,4	35,5	20,0	2,9	2,5	0,5
			2	3,7			4,3			285			18,0			1,9		
			3	4,1			17,2			543			57,2			2,6		
Control light	**Col-0**	Root tips	1	3,7	3,9	0,4	2,7	6,4	6,1	338	464	153	2,7	2,8	0,6	1,3	1,5	0,2
			2	4,4			3,0			421			2,3			1,5		
			3	3,6			13,4			635			3,6			1,7		
Control light	**tps5/6/7**	Root tips	1	3,9	3,6	0,2	4,2	13,4	8,0	515	475	44	2,7	2,6	0,2	2,0	1,8	0,1
			2	3,5			18,6			428			2,5			1,8		
			3	3,5			17,5			483			2,8			1,8		
High light	**Col-0**	Root tips	1	4,0	3,6	0,3	5,7	14,1	7,8	361	399	69	2,4	2,3	0,3	1,5	1,4	0,1
			2	3,3			15,2			358			1,9			1,3		
			3	3,5			21,3			478			2,5			1,5		
High light	**tps5/6/7**	Root tips	1	4,1	4,1	0,0	5,4	10,1	4,6	669	594	159	3,2	3,5	1,1	3,1	2,5	0,5
			2	4,1			10,4			411			2,6			2,2		
			3	4,1			14,6			701			4,7			2,3		

Supplementary Table 2.1C Amino acids

Light intensity	genotype	tissue	replicate	isoleucine			leucine			valine			alanine			b-alanine		
				relative mean	average	stdev	relative mean	average	stdev	relative mean	average	stdev	relative mean	average	stdev	relative mean	average	stdev
Control light	**Col-0**	Shoots	1	0,848	0,865	0,071	0,481	0,584	0,092	1,042	1,039	0,046	1,116	1,202	0,140	0,353	0,478	0,110
			2	0,943			0,657			1,084			1,363			0,522		
			3	0,805			0,615			0,991			1,127			0,560		
Control light	**tps5/6/7**	Shoots	1	0,788	0,713	0,096	0,582	0,491	0,084	1,009	1,029	0,031	1,262	1,327	0,118	0,337	0,368	0,028
			2	0,745			0,474			1,064			1,462			0,393		
			3	0,605			0,416			1,013			1,256			0,372		
High light	**Col-0**	Shoots	1	2,271	1,861	0,378	2,091	1,425	0,584	1,599	1,231	0,321	1,261	1,096	0,143	0,730	0,654	0,109
			2	1,785			1,183			1,084			1,010			0,529		
			3	1,526			1,001			1,010			1,016			0,704		
High light	**tps5/6/7**	Shoots	1	0,566	0,559	0,107	0,433	0,441	0,044	0,828	0,824	0,070	0,959	0,929	0,028	0,275	0,441	0,216
			2	0,663			0,488			0,751			0,903			0,363		
			3	0,449			0,401			0,891			0,924			0,686		
Control light	**Col-0**	Roots	1	2,933	2,778	0,552	1,990	2,288	0,367	1,346	1,268	0,228	0,512	0,443	0,069	0,858	1,163	0,419
			2	3,236			2,698			1,447			0,442			0,991		
			3	2,166			2,177			1,011			0,375			1,641		
Control light	**tps5/6/7**	Roots	1	1,330	1,362	0,117	1,190	1,298	0,140	1,063	1,130	0,066	0,620	0,575	0,050	0,678	0,995	0,300
			2	1,491			1,457			1,194			0,583			1,032		
			3	1,264			1,248			1,134			0,521			1,275		
High light	**Col-0**	Roots	1	5,400	4,723	0,633	3,821	3,657	0,175	1,912	1,662	0,227	0,786	0,711	0,066	1,094	1,354	0,526
			2	4,623			3,678			1,607			0,682			1,009		
			3	4,146			3,472			1,468			0,665			1,960		
High light	**tps5/6/7**	Roots	1	0,853	0,810	0,218	0,730	0,785	0,193	1,022	0,951	0,069	1,358	1,139	0,206	1,405	1,761	1,057
			2	1,003			0,999			0,946			0,950			0,927		
			3	0,574			0,625			0,885			1,110			2,950		
Control light	**Col-0**	Root tips	1	1,020	1,034	0,046	1,086	1,181	0,094	0,549	0,583	0,035	0,921	1,007	0,097	0,784	1,636	1,068
			2	1,085			1,183			0,583			1,112			1,289		
			3	0,997			1,275			0,618			0,990			2,833		
Control light	**tps5/6/7**	Root tips	1	0,928	0,687	0,213	0,494	0,606	0,098	0,719	0,649	0,064	0,834	0,788	0,087	0,803	1,179	0,328
			2	0,608			0,676			0,636			0,843			1,330		
			3	0,525			0,647			0,592			0,687			1,405		
High light	**Col-0**	Root tips	1	1,780	1,441	0,349	1,764	1,454	0,289	0,701	0,678	0,045	1,322	1,372	0,070	1,235	1,805	0,857
			2	1,083			1,191			0,626			1,451			1,389		
			3	1,462			1,407			0,706			1,342			2,791		
High light	**tps5/6/7**	Root tips	1	0,288	0,296	0,011	0,397	0,416	0,023	0,558	0,531	0,046	2,467	1,979	0,440	1,285	1,830	1,173
			2	0,309			0,409			0,477			1,857			1,028		
			3	0,292			0,442			0,557			1,612			3,177		

Supplementary Table 2.1C Amino acids

Light intensity	genotype	tissue	replicate	asparagine			aspartate			methionine			threonine			lysine		
				relative mean	average	stdev	relative mean	average	stdev	relative mean	average	stdev	relative mean	average	stdev	relative mean	average	stdev
Control light	**Col-0**	Shoots	1	2,215	2,183	0,111	2,308	2,327	0,079	0,917	0,957	0,035	0,596	0,649	0,047	1,593	2,049	0,650
			2	2,273			2,414			0,976			0,686			2,793		
			3	2,059			2,259			0,978			0,666			1,761		
Control light	**tps5/6/7**	Shoots	1	2,313	2,128	0,188	2,330	2,238	0,104	1,210	1,294	0,074	0,698	0,675	0,054	1,731	2,409	0,597
			2	2,134			2,259			1,349			0,713			2,639		
			3	1,937			2,125			1,323			0,613			2,858		
High light	**Col-0**	Shoots	1	2,197	2,054	0,148	2,272	2,173	0,087	1,167	1,057	0,190	1,078	1,128	0,080	2,972	2,605	0,320
			2	2,063			2,138			0,837			1,086			2,379		
			3	1,902			2,108			1,166			1,221			2,464		
High light	**tps5/6/7**	Shoots	1	1,729	1,638	0,186	1,739	1,702	0,119	0,799	0,876	0,126	0,894	0,923	0,036	0,622	0,677	0,048
			2	1,761			1,799			0,808			0,963			0,706		
			3	1,423			1,569			1,022			0,913			0,703		
Control light	**Col-0**	Roots	1	0,835	0,884	0,065	0,824	0,898	0,078	0,800	0,964	0,142	0,900	1,042	0,128	1,522	1,412	0,226
			2	0,958			0,980			1,053			1,076			1,563		
			3	0,859			0,891			1,039			1,150			1,152		
Control light	**tps5/6/7**	Roots	1	0,853	1,037	0,160	0,856	1,010	0,156	0,745	1,050	0,264	1,109	1,277	0,146	0,887	1,020	0,119
			2	1,113			1,169			1,195			1,350			1,116		
			3	1,145			1,006			1,209			1,372			1,057		
High light	**Col-0**	Roots	1	1,063	1,043	0,026	1,080	1,084	0,027	1,407	1,457	0,322	1,633	1,626	0,144	2,669	2,388	0,262
			2	1,013			1,060			1,163			1,479			2,346		
			3	1,052			1,113			1,802			1,767			2,149		
High light	**tps5/6/7**	Roots	1	0,929	1,011	0,126	0,955	0,852	0,105	1,460	1,514	0,160	2,012	1,837	0,157	1,023	0,952	0,086
			2	0,947			0,858			1,387			1,707			0,977		
			3	1,156			0,745			1,694			1,792			0,857		
Control light	**Col-0**	Root tips	1	0,726	0,794	0,170	0,721	0,806	0,175	0,472	0,704	0,204	0,679	0,755	0,067	0,542	0,586	0,042
			2	0,987			1,008			0,780			0,807			0,624		
			3	0,668			0,689			0,858			0,778			0,592		
Control light	**tps5/6/7**	Root tips	1	0,651	0,586	0,077	0,631	0,580	0,075	0,491	0,569	0,068	0,734	0,779	0,065	0,703	0,601	0,146
			2	0,607			0,614			0,615			0,853			0,667		
			3	0,501			0,494			0,601			0,751			0,434		
High light	**Col-0**	Root tips	1	0,797	0,878	0,072	0,793	0,909	0,104	0,930	1,145	0,297	1,042	1,091	0,195	0,946	0,888	0,106
			2	0,904			0,941			1,022			0,926			0,766		
			3	0,935			0,994			1,484			1,306			0,953		
High light	**tps5/6/7**	Root tips	1	0,458	0,502	0,104	0,454	0,399	0,083	0,721	0,740	0,151	1,037	1,020	0,171	0,520	0,472	0,095
			2	0,427			0,438			0,600			0,841			0,363		
			3	0,621			0,304			0,900			1,181			0,533		

Supplementary Table 2.1C Amino acids

Light intensity	genotype	tissue	replicate	serine			glycine			tryptophan			phenylalanine			tyrosine		
				relative mean	average	stdev	relative mean	average	stdev	relative mean	average	stdev	relative mean	average	stdev	relative mean	average	stdev
Control light	**Col-0**	Shoots	1	0,747	0,849	0,105	0,504	0,462	0,065	N/A	1,119	0,340	1,416	1,940	0,492	0,520	0,641	0,105
			2	0,843			0,387			0,879			2,015			0,693		
			3	0,957			0,495			1,360			2,391			0,710		
Control light	**tps5/6/7**	Shoots	1	0,971	0,910	0,116	0,562	0,540	0,043	0,580	2,834	3,546	1,365	1,957	0,545	0,614	0,626	0,011
			2	0,983			0,568			1,000			2,070			0,634		
			3	0,777			0,491			6,921			2,437			0,632		
High light	**Col-0**	Shoots	1	1,688	1,591	0,089	5,541	6,725	1,096	1,047	1,057	0,162	3,532	3,175	0,310	0,524	0,514	0,055
			2	1,511			7,702			1,224			2,977			0,563		
			3	1,574			6,933			0,900			3,014			0,456		
High light	**tps5/6/7**	Shoots	1	1,089	1,006	0,118	2,579	2,603	0,189	0,320	8,206	7,039	1,447	1,642	0,294	0,574	0,606	0,037
			2	1,059			2,803			10,442			1,500			0,597		
			3	0,871			2,428			13,854			1,980			0,647		
Control light	**Col-0**	Roots	1	0,693	0,730	0,035	0,857	0,714	0,128	N/A	1,065	#DIV/0!	0,766	0,914	0,134	1,137	1,185	0,161
			2	0,736			0,612			N/A			1,025			1,055		
			3	0,762			0,671			1,065			0,952			1,365		
Control light	**tps5/6/7**	Roots	1	0,748	0,719	0,026	0,794	0,647	0,130	N/A	1,123	0,240	0,656	0,825	0,155	1,225	1,080	0,155
			2	0,701			0,545			1,293			0,861			0,917		
			3	0,708			0,603			0,953			0,959			1,097		
High light	**Col-0**	Roots	1	1,172	1,116	0,049	0,915	0,909	0,079	0,405	0,762	0,457	1,222	1,317	0,174	1,010	1,029	0,051
			2	1,096			0,985			0,604			1,211			0,990		
			3	1,081			0,827			1,277			1,518			1,087		
High light	**tps5/6/7**	Roots	1	1,175	1,025	0,133	1,231	1,055	0,160	0,266	0,557	0,324	1,208	1,156	0,161	0,942	0,919	0,071
			2	0,979			0,919			0,907			0,975			0,839		
			3	0,922			1,015			0,497			1,285			0,975		
Control light	**Col-0**	Root tips	1	0,930	0,990	0,052	1,529	1,357	0,159	N/A	1,312	0,353	0,592	0,752	0,139	1,235	1,331	0,188
			2	1,017			1,214			1,562			0,852			1,212		
			3	1,023			1,328			1,062			0,811			1,548		
Control light	**tps5/6/7**	Root tips	1	1,271	1,044	0,197	2,180	1,343	0,725	1,402	0,900	0,454	0,713	0,611	0,091	1,544	1,539	0,076
			2	0,940			0,919			0,519			0,538			1,460		
			3	0,922			0,930			0,779			0,583			1,612		
High light	**Col-0**	Root tips	1	1,275	1,203	0,086	1,531	1,403	0,111	N/A	0,885	0,714	0,630	0,722	0,107	0,949	1,007	0,051
			2	1,107			1,345			0,380			0,697			1,036		
			3	1,226			1,334			1,390			0,840			1,037		
High light	**tps5/6/7**	Root tips	1	1,383	1,260	0,111	1,507	1,316	0,186	1,074	0,844	0,325	0,489	0,492	0,092	1,133	1,151	0,097
			2	1,230			1,134			N/A			0,401			1,064		
			3	1,168			1,308			0,614			0,585			1,255		

Supplementary Table 2.1C Amino acids

Light intensity	genotype	tissue	replicate	glutamine			glutamate			proline			arginine			putrescine		
				relative mean	average	stdev	relative mean	average	stdev	relative mean	average	stdev	relative mean	average	stdev	relative mean	average	stdev
Control light	**Col-0**	Shoots	1	1,424	1,441	0,020	1,901	1,769	0,147	1,669	1,909	0,219	18,492	23,569	8,132	3,135	3,556	0,527
			2	1,434			1,796			1,961			19,267			3,385		
			3	1,463			1,610			2,098			32,949			4,148		
Control light	**tps5/6/7**	Shoots	1	1,896	1,864	0,154	1,801	1,630	0,182	1,982	1,764	0,189	25,429	29,942	4,744	3,575	5,176	2,469
			2	2,000			1,649			1,652			29,510			3,934		
			3	1,698			1,439			1,658			34,887			8,020		
High light	**Col-0**	Shoots	1	1,070	1,194	0,138	1,627	1,429	0,182	2,122	2,684	0,533	11,225	9,799	3,028	2,657	2,704	0,535
			2	1,342			1,391			3,180			6,321			2,194		
			3	1,170			1,269			2,751			11,850			3,261		
High light	**tps5/6/7**	Shoots	1	1,416	1,215	0,174	1,230	1,108	0,166	5,628	5,375	0,220	3,130	4,803	1,658	1,623	2,710	0,981
			2	1,111			1,176			5,274			6,445			2,976		
			3	1,119			0,919			5,223			4,835			3,530		
Control light	**Col-0**	Roots	1	0,021	0,209	0,274	0,855	0,948	0,111	0,706	0,951	0,216	0,256	0,393	0,132	1,518	1,239	0,300
			2	0,082			1,070			1,035			0,403			0,922		
			3	0,524			0,919			1,113			0,520			1,278		
Control light	**tps5/6/7**	Roots	1	0,172	0,580	0,415	1,000	1,049	0,109	0,695	0,685	0,065	0,481	0,780	0,305	1,326	1,585	0,406
			2	0,567			1,174			0,616			0,768			1,377		
			3	1,003			0,972			0,745			1,091			2,053		
High light	**Col-0**	Roots	1	0,494	0,523	0,123	1,104	1,005	0,099	0,912	0,901	0,070	1,498	1,247	0,296	0,922	0,781	0,151
			2	0,417			1,006			0,826			1,323			0,622		
			3	0,658			0,906			0,965			0,921			0,799		
High light	**tps5/6/7**	Roots	1	1,914	1,619	0,281	1,083	0,924	0,181	1,346	1,386	0,530	0,877	1,036	0,343	0,871	0,897	0,169
			2	1,354			0,963			0,877			0,800			0,742		
			3	1,588			0,727			1,935			1,429			1,078		
Control light	**Col-0**	Root tips	1	0,338	0,424	0,103	0,770	0,860	0,123	0,412	0,544	0,137	0,314	0,544	0,203	0,222	0,308	0,128
			2	0,539			1,000			0,535			0,617			0,246		
			3	0,397			0,810			0,685			0,701			0,456		
Control light	**tps5/6/7**	Root tips	1	0,033	0,126	0,091	0,619	0,647	0,087	0,587	0,545	0,051	0,301	0,464	0,188	0,208	0,292	0,083
			2	0,130			0,744			0,560			0,420			0,293		
			3	0,214			0,576			0,489			0,670			0,375		
High light	**Col-0**	Root tips	1	0,690	0,874	0,179	0,818	0,899	0,098	0,486	0,554	0,177	0,869	1,057	0,179	0,209	0,227	0,042
			2	0,885			1,008			0,422			1,224			0,196		
			3	1,047			0,870			0,755			1,079			0,275		
High light	**tps5/6/7**	Root tips	1	1,330	1,027	0,289	0,937	0,763	0,166	1,572	1,498	0,526	0,713	0,704	0,144	0,212	0,282	0,152
			2	0,754			0,748			0,939			0,556			0,178		
			3	0,997			0,606			1,983			0,844			0,456		

Supplementary Table 2.1C Amino acids

Light intensity	genotype	tissue	replicate	ornithine			spermidine			agmatine			citrulline			tyramine		
				relative mean	average	stdev	relative mean	average	stdev	relative mean	average	stdev	relative mean	average	stdev	relative mean	average	stdev
Control light	**Col-0**	Shoots	1	8,146	9,786	1,512	0,936	1,138	0,178	3,051	2,663	0,439	1,106	1,160	0,049	4,299	5,744	1,295
			2	10,088			1,270			2,187			1,200			6,801		
			3	11,124			1,207			2,750			1,176			6,132		
Control light	**tps5/6/7**	Shoots	1	10,935	13,646	2,562	1,035	1,381	0,704	2,398	4,010	2,543	1,049	1,164	0,100	4,069	4,608	0,470
			2	16,025			0,917			2,689			1,216			4,825		
			3	13,979			2,192			6,942			1,226			4,931		
High light	**Col-0**	Shoots	1	6,281	5,606	1,171	1,207	1,368	0,153	1,661	1,837	0,608	0,925	0,973	0,049	5,819	6,088	0,657
			2	4,254			1,387			1,336			0,972			5,608		
			3	6,283			1,510			2,514			1,023			6,836		
High light	**tps5/6/7**	Shoots	1	3,263	4,053	0,685	0,956	1,319	0,330	1,099	1,999	0,818	0,927	0,939	0,011	4,190	4,706	1,051
			2	4,459			1,399			2,202			0,942			4,012		
			3	4,438			1,601			2,696			0,948			5,915		
Control light	**Col-0**	Roots	1	0,498	0,500	0,066	0,426	0,646	0,283	1,079	0,859	0,232	0,285	0,491	0,236	0,509	0,703	0,326
			2	0,436			0,546			0,616			0,441			0,520		
			3	0,567			0,965			0,881			0,749			1,079		
Control light	**tps5/6/7**	Roots	1	0,618	0,697	0,068	0,482	0,827	0,343	1,010	1,322	0,375	0,565	0,931	0,317	0,259	0,682	0,368
			2	0,730			0,831			1,218			1,116			0,931		
			3	0,742			1,168			1,738			1,112			0,856		
High light	**Col-0**	Roots	1	0,767	0,744	0,025	0,508	0,563	0,109	0,485	0,466	0,058	0,786	0,850	0,061	1,000	1,358	0,619
			2	0,718			0,492			0,401			0,855			1,001		
			3	0,748			0,689			0,512			0,908			2,073		
High light	**tps5/6/7**	Roots	1	0,964	0,968	0,068	0,689	0,754	0,340	1,201	1,080	0,109	0,977	1,058	0,085	1,427	1,475	0,521
			2	0,903			0,451			1,049			1,146			0,979		
			3	1,038			1,121			0,990			1,052			2,019		
Control light	**Col-0**	Root tips	1	0,611	0,800	0,174	0,379	0,917	0,549	0,264	0,322	0,051	0,732	0,825	0,084	N/A	0,427	0,151
			2	0,838			0,896			0,356			0,850			0,534		
			3	0,952			1,476			0,346			0,894			0,321		
Control light	**tps5/6/7**	Root tips	1	3,367	1,847	1,316	1,318	1,571	0,224	0,204	0,294	0,078	0,976	1,059	0,080	0,583	0,624	0,081
			2	1,069			1,653			0,337			1,065			0,573		
			3	1,107			1,743			0,340			1,136			0,717		
High light	**Col-0**	Root tips	1	0,707	0,840	0,125	0,737	0,879	0,200	0,413	0,498	0,099	0,851	1,009	0,140	0,215	0,421	0,186
			2	0,956			0,793			0,475			1,054			0,473		
			3	0,856			1,108			0,607			1,121			0,575		
High light	**tps5/6/7**	Root tips	1	0,992	1,017	0,031	1,104	1,203	0,381	0,650	0,573	0,088	1,105	1,205	0,087	0,395	0,399	0,164
			2	1,008			0,882			0,477			1,254			0,238		
			3	1,052			1,624			0,593			1,256			0,565		

Supplementary Table 2.1C Amino acids

Light intensity	genotype	tissue	replicate	5-oxoproline			glycerate			glycerol			glycerol 3-P			dehydroascorbate		
				relative mean	average	stdev	relative mean	average	stdev	relative mean	average	stdev	relative mean	average	stdev	relative mean	average	stdev
Control light	**Col-0**	Shoots	1	1,279	1,177	0,089	0,178	0,193	0,066	1,264	1,045	0,191	0,987	1,284	0,310	1,699	2,165	0,680
			2	1,143			0,137			0,917			1,260			2,946		
			3	1,110			0,265			0,953			1,606			1,850		
Control light	**tps5/6/7**	Shoots	1	1,096	1,088	0,010	0,210	0,146	0,063	1,000	0,839	0,140	1,027	1,026	0,060	1,842	2,540	0,616
			2	1,091			0,142			0,761			0,965			2,772		
			3	1,076			0,085			0,755			1,085			3,006		
High light	**Col-0**	Shoots	1	1,070	1,021	0,057	0,268	0,277	0,024	0,732	0,863	0,136	0,714	0,909	0,286	3,131	2,753	0,330
			2	0,959			0,305			0,853			0,776			2,521		
			3	1,035			0,259			1,003			1,237			2,608		
High light	**tps5/6/7**	Shoots	1	0,760	0,767	0,029	0,322	0,304	0,043	0,633	0,635	0,077	0,563	0,547	0,048	3,838	4,032	0,576
			2	0,799			0,254			0,713			0,492			3,578		
			3	0,743			0,335			0,560			0,585			4,680		
Control light	**Col-0**	Roots	1	1,036	1,040	0,034	1,118	1,037	0,208	2,001	1,821	0,259	0,900	1,281	0,466	0,554	0,636	0,181
			2	1,076			0,801			1,938			1,141			0,511		
			3	1,009			1,193			1,524			1,800			0,843		
Control light	**tps5/6/7**	Roots	1	1,224	1,108	0,105	0,977	0,974	0,014	1,440	1,109	0,290	0,959	1,161	0,249	0,140	0,656	0,451
			2	1,020			0,986			0,991			1,086			0,976		
			3	1,080			0,958			0,896			1,439			0,851		
High light	**Col-0**	Roots	1	0,979	0,985	0,018	2,332	2,133	0,278	1,065	1,110	0,088	0,659	0,836	0,294	1,149	1,507	0,585
			2	0,970			2,251			1,211			0,675			1,191		
			3	1,005			1,815			1,054			1,175			2,183		
High light	**tps5/6/7**	Roots	1	0,812	0,871	0,085	1,548	1,206	0,341	0,583	0,684	0,121	0,995	0,966	0,360	1,433	1,477	0,476
			2	0,968			1,204			0,818			0,592			1,024		
			3	0,831			0,867			0,649			1,310			1,974		
Control light	**Col-0**	Root tips	1	0,926	0,959	0,069	2,832	2,282	0,611	1,565	1,331	0,221	0,593	1,100	0,551	0,083	0,350	0,290
			2	1,038			2,391			1,124			1,021			0,658		
			3	0,912			1,624			1,303			1,687			0,308		
Control light	**tps5/6/7**	Root tips	1	0,961	0,819	0,124	1,529	1,506	0,129	1,258	1,182	0,073	1,005	1,175	0,148	0,682	0,739	0,095
			2	0,763			1,622			1,113			1,276			0,686		
			3	0,733			1,367			1,174			1,243			0,849		
High light	**Col-0**	Root tips	1	1,140	1,047	0,081	2,423	2,130	0,254	1,245	1,066	0,156	0,628	0,801	0,256	0,296	0,524	0,199
			2	1,000			1,998			1,000			0,681			0,620		
			3	1,000			1,970			0,954			1,095			0,658		
High light	**tps5/6/7**	Root tips	1	0,871	0,936	0,064	1,090	0,898	0,270	0,672	0,845	0,169	0,688	0,766	0,287	0,445	0,454	0,169
			2	0,999			1,014			1,010			0,525			0,289		
			3	0,939			0,589			0,852			1,084			0,627		

Supplementary Table 2.1C Amino acids

Light intensity	genotype	tissue	replicate	gluconate			benzoate			orthophosphate			nonanoate			nicotinate		
				relative mean	average	stdev	relative mean	average	stdev	relative mean	average	stdev	relative mean	average	stdev	relative mean	average	stdev
Control light	**Col-0**	Shoots	1	0,441	0,552	0,099	0,324	0,323	0,005	1,324	1,110	0,187	0,646	0,680	0,033	0,370	0,381	0,022
			2	0,584			0,318			1,031			0,711			0,367		
			3	0,631			0,328			0,976			0,683			0,406		
Control light	**tps5/6/7**	Shoots	1	0,505	0,573	0,059	0,358	0,311	0,041	0,976	0,860	0,101	0,736	0,700	0,063	0,327	0,294	0,034
			2	0,598			0,280			0,792			0,737			0,297		
			3	0,616			0,296			0,811			0,627			0,259		
High light	**Col-0**	Shoots	1	0,954	1,021	0,060	0,376	0,482	0,144	0,908	0,817	0,079	1,082	1,144	0,105	0,334	0,290	0,044
			2	1,069			0,423			0,766			1,086			0,245		
			3	1,040			0,646			0,777			1,266			0,290		
High light	**tps5/6/7**	Shoots	1	1,331	1,494	0,176	0,331	0,355	0,025	0,562	0,570	0,072	0,890	0,929	0,037	0,224	0,225	0,040
			2	1,472			0,353			0,645			0,964			0,186		
			3	1,681			0,381			0,502			0,932			0,266		
Control light	**Col-0**	Roots	1	0,847	1,091	0,287	1,053	1,041	0,230	2,218	1,871	0,493	0,957	1,090	0,120	2,983	3,396	0,358
			2	1,018			0,805			2,088			1,120			3,595		
			3	1,407			1,264			1,306			1,191			3,611		
Control light	**tps5/6/7**	Roots	1	0,796	1,095	0,282	0,981	0,988	0,011	1,618	1,284	0,317	1,136	1,284	0,129	2,625	2,671	0,303
			2	1,133			0,983			1,249			1,345			2,394		
			3	1,356			1,001			0,986			1,372			2,995		
High light	**Col-0**	Roots	1	1,007	1,125	0,223	1,993	1,971	0,061	1,203	1,090	0,236	1,613	1,629	0,169	1,707	1,707	0,202
			2	0,987			2,019			1,249			1,468			1,505		
			3	1,382			1,902			0,819			1,805			1,910		
High light	**tps5/6/7**	Roots	1	1,754	1,581	0,287	1,297	1,166	0,152	0,583	0,692	0,153	1,977	1,839	0,154	2,068	1,665	0,397
			2	1,250			1,200			0,867			1,673			1,274		
			3	1,740			0,999			0,624			1,868			1,652		
Control light	**Col-0**	Root tips	1	0,499	0,739	0,293	2,255	2,024	0,281	1,819	1,358	0,399	0,726	0,785	0,053	0,721	0,993	0,240
			2	0,651			2,106			1,121			0,828			1,089		
			3	1,066			1,712			1,135			0,801			1,170		
Control light	**tps5/6/7**	Root tips	1	0,649	0,846	0,190	1,370	1,468	0,120	1,439	1,349	0,084	0,768	0,802	0,052	1,454	1,457	0,052
			2	1,029			1,601			1,272			0,862			1,510		
			3	0,859			1,433			1,337			0,777			1,406		
High light	**Col-0**	Root tips	1	0,454	0,668	0,286	2,045	1,939	0,126	1,244	1,006	0,242	1,088	1,117	0,206	0,825	0,885	0,090
			2	0,558			1,800			1,014			0,928			0,842		
			3	0,993			1,972			0,760			1,336			0,989		
High light	**tps5/6/7**	Root tips	1	1,316	1,162	0,221	0,986	0,894	0,207	0,740	0,844	0,163	1,036	1,028	0,181	1,000	0,875	0,216
			2	0,909			1,040			1,031			0,844			0,626		
			3	1,261			0,657			0,760			1,205			1,000		

Supplementary Table 2.1C Amino acids

Light intensity	genotype	tissue	replicate	4-aminobutanoate			3-indoleacetonitrile			adenine			uracil			cellobiose		
				relative mean	average	stdev	relative mean	average	stdev	relative mean	average	stdev	relative mean	average	stdev	relative mean	average	stdev
Control light	**Col-0**	Shoots	1	0,270	0,334	0,055	1,021	1,134	0,109	0,492	0,616	0,125	0,637	0,879	0,211	0,283	0,254	0,122
			2	0,367			1,238			0,613			1,023			0,358		
			3	0,364			1,143			0,743			0,977			0,120		
Control light	**tps5/6/7**	Shoots	1	0,335	0,305	0,055	1,002	0,952	0,085	0,836	0,798	0,138	0,717	0,781	0,066	0,394	0,274	0,126
			2	0,339			0,853			0,914			0,849			0,284		
			3	0,241			0,999			0,645			0,778			0,142		
High light	**Col-0**	Shoots	1	0,311	0,289	0,032	1,264	1,364	0,102	1,124	0,921	0,177	1,201	1,198	0,062	0,336	0,239	0,084
			2	0,303			1,359			0,798			1,134			0,202		
			3	0,253			1,469			0,843			1,257			0,181		
High light	**tps5/6/7**	Shoots	1	0,271	0,326	0,052	0,930	0,870	0,071	0,665	1,252	0,701	0,597	0,618	0,079	0,469	0,692	0,196
			2	0,374			0,890			1,063			0,705			0,837		
			3	0,334			0,791			2,029			0,552			0,769		
Control light	**Col-0**	Roots	1	1,862	1,760	0,106	0,528	0,711	0,239	1,245	1,938	1,141	0,728	1,209	0,419	2,631	2,376	0,672
			2	1,767			0,623			1,314			1,408			2,883		
			3	1,650			0,981			3,254			1,491			1,614		
Control light	**tps5/6/7**	Roots	1	2,295	2,295	0,127	0,594	0,868	0,260	1,005	1,804	0,756	0,932	1,020	0,084	2,627	2,532	0,164
			2	2,168			0,899			1,898			1,026			2,626		
			3	2,423			1,111			2,508			1,101			2,343		
High light	**Col-0**	Roots	1	1,434	1,356	0,074	0,544	0,606	0,166	2,463	2,436	0,405	1,023	1,099	0,119	1,465	1,254	0,202
			2	1,346			0,480			2,019			1,038			1,063		
			3	1,288			0,794			2,828			1,236			1,234		
High light	**tps5/6/7**	Roots	1	2,258	2,223	0,090	0,676	0,767	0,328	2,896	2,750	1,200	0,654	0,787	0,142	3,010	2,007	0,885
			2	2,289			0,494			1,483			0,771			1,679		
			3	2,120			1,131			3,871			0,936			1,333		
Control light	**Col-0**	Root tips	1	0,870	1,005	0,122	0,443	0,987	0,537	0,460	0,703	0,269	0,532	1,132	0,526	0,580	0,689	0,215
			2	1,035			1,001			0,657			1,351			0,937		
			3	1,109			1,517			0,993			1,512			0,549		
Control light	**tps5/6/7**	Root tips	1	1,160	1,839	0,646	1,512	1,669	0,157	0,735	1,205	0,427	0,765	1,187	0,366	2,537	2,527	0,298
			2	2,445			1,669			1,569			1,416			2,820		
			3	1,914			1,825			1,310			1,380			2,225		
High light	**Col-0**	Root tips	1	0,756	0,716	0,035	0,792	0,900	0,168	0,526	0,635	0,154	0,883	1,031	0,133	0,521	0,596	0,136
			2	0,693			0,815			0,567			1,067			0,514		
			3	0,698			1,094			0,812			1,143			0,753		
High light	**tps5/6/7**	Root tips	1	1,257	1,034	0,197	1,162	1,245	0,293	0,995	0,896	0,310	0,704	0,854	0,226	2,262	1,682	0,521
			2	0,881			1,002			0,549			0,744			1,532		
			3	0,965			1,570			1,145			1,114			1,252		

Supplementary Table 2.1C Amino acids										
Light intensity	genotype	tissue	replicate	galactinol			2-hydroxypyridine			
				relative	mean	average	stdev	relative	mean	average	stdev
Control light	**Col-0**	Shoots	1	0,635	0,981	0,303	1,179	1,144	0,187
			2	1,195			1,310		
			3	1,113			0,942		
Control light	**tps5/6/7**	Shoots	1	0,739	0,920	0,159	1,021	1,397	0,338
			2	0,982			1,494		
			3	1,039			1,676		
High light	**Col-0**	Shoots	1	1,018	1,213	0,228	1,392	1,374	0,117
			2	1,158			1,249		
			3	1,464			1,480		
High light	**tps5/6/7**	Shoots	1	0,934	1,122	0,199	1,353	1,392	0,246
			2	1,101			1,167		
			3	1,330			1,655		
Control light	**Col-0**	Roots	1	0,859	1,076	0,226	0,971	1,074	0,089
			2	1,060			1,121		
			3	1,310			1,130		
Control light	**tps5/6/7**	Roots	1	0,572	0,890	0,295	0,553	0,865	0,273
			2	0,943			1,060		
			3	1,154			0,982		
High light	**Col-0**	Roots	1	0,688	0,821	0,212	1,060	1,154	0,215
			2	0,709			1,001		
			3	1,065			1,400		
High light	**tps5/6/7**	Roots	1	0,811	0,818	0,123	0,753	0,859	0,097
			2	0,698			0,880		
			3	0,943			0,944		
Control light	**Col-0**	Root tips	1	0,636	0,994	0,326	0,360	0,670	0,269
			2	1,072			0,835		
			3	1,273			0,817		
Control light	**tps5/6/7**	Root tips	1	1,048	1,397	0,319	0,766	0,983	0,210
			2	1,469			0,999		
			3	1,673			1,185		
High light	**Col-0**	Root tips	1	0,644	0,898	0,259	0,488	0,668	0,171
			2	0,888			0,687		
			3	1,162			0,829		
High light	**tps5/6/7**	Root tips	1	0,799	0,797	0,148	0,472	0,579	0,137
			2	0,648			0,531		
			3	0,945			0,734		

Supplementary Table 2.2. Primers, Plant lines and Antibodies.

List of all primers, plant lines and antibodies used in this study.

Supplementary Table 2.2. Primers, Plant lines and antibodies			
Genotyping primers	**Name**	**Sequence (5' => 3')**	
tps5-1 (SALK-144791)	*tps5-1*-LP	TGATCGTTCTTTATGGCAAGC	
	tps5-1-RP	GCATTTGCTTCTCTGCTTCTG	
tps6-1 (GK-362A03)	*tps6-1*-LP	TGCATCAGCTACTGCATCAAC	
	tps6-1-RP	AGTGTGTGCCTACGTTTTTGC	
tps7-1 (GK-341E02)	*tps7-1*-LP	TTCACTGCCTGACCACCTAAG	
	tps7-1-RP	GCTGGAGTATTACGGGAGGAC	
T-DNA primer SALK	LBb1.3	ATTTTGCCGATTTCGGAAC	
T-DNA primer GABI-Kat	o8409 (GABI LB)	ATATTGACCATCATACTCATTGC	
T-DNA primer WISC	T-DNA-Wis	AACGTCCGCAATGTGTTATTAAGTTGTC	
RT-PCR primers	**Name**	**Sequence (5' => 3')**	
TPS6	tps6-RT-PCRFw	TTCTGAGGCTAAGGAAGGCAGTAG	
	tps6-RT-PCRRev	GCTCGGCAATTTGCTTCCAAGAAC	
TPS7	tps7-RT-PCRFw	ATGATTTCTAGGTCGTACACG	
	tps7-RT-PCRRev	TCAAAGGGCTTCATCAAGTTC	
ACTIN7	ACT_Q_F	GGAACTGGAATGGTGAAGGCTG	
	ACT_Q_R	CGATTGGATACTTCAGAGTGAGGA	
Cloning primers	**Name**	**Sequence (5' => 3')**	**Description**
proTPS7::gTPS7-mCherry	pCB302_C_N_Fw	AAAAGAATCAGGGCTGCAGGAATTCCCG	Cloning to pCB302 vector
	pCB302_C_N_Rev	GAATAAATATGGGGGATCCACTAGTTCTAGAG	
	ProTPS7_C_N_Fw	TGGATCCCCCATATTTATTCACATATAGGTACAATTTTAAAAATC	
	ProTPS7+gTPS7_C_Rev	CCTTGCTCACAAGGGCTTCATCAAGTTC	
	mCherry_C_Fw	TGAAGCCCTTGTGAGCAAGGGCGAGGAG	
	mCherry_C_Rev	TGGTTCCAAATTACTTGTACAGCTCGTCCATG	
	TermTPS7_C_Fw	GTACAAGTAATTTGGAACCAGATCTTTTG	
	TermTPS7_C_N_Rev	CCTGCAGCCCTGATTCTTTTTTTGTTTTTTACTTTG	

Supplementary Table 2.2. Primers, Plant lines and antibodies

Plant line	Line ID	Reference
tps5-1	SALK_144791	Tian et al., 2019 Plant Cell Reports
tps6-1	GK-362A03	This study
tps7-1	GK-341E02	This study
tps5/7	SALK_144791/GK-341E02	This study
tps5/6/7	SALK_144791/GK-362A03/GK-341E02	This study
TPS7-mCherry	*proTPS7::gTPS7-mCherry*	This study
mCherry-TPS7	*proTPS7::mCherry-gTPS7*	This study

Supplementary Table 2.2. Primers, Plant lines and antibodies

Antibody - short name	Antibody - full description	Source	Company	Product number		Dilution	Dilution buffer
Anti-RFP	RFP Mouse IgG2c Monoclonal Antibody	Commercial	Chromotek	[6G6]	Mouse monoclonal	1:1000	1% (w/v) non-fat dry milk in 1X TBS
Anti-p(S240)-RPS6	Anti Phospho-RPS6 (S240)	Custom-made	Proteogenix	CA-15P #1	Rabbit polyclonal	1:4000	1% (w/v) non-fat dry milk in 1X TBS
Anti-RPS6	Anti Ribosomal Protein S6 (C-8)	Commercial	Santa Cruz Biotechnology, Inc.	sc-74459	Mouse monoclonal	1:1000	1% (w/v) non-fat dry milk in 1X TBS
Anti-p(S11)-PEPC	Anti Phospho-PEPC (S11) (LEKLApSIDAQLR) IgG	Custom-made		Gregory et al., 2009	Rabbit polyclonal	1:1000	1% (w/v) non-fat dry milk in 1X TBS
Anti-PEPC	Anti RcPPC3 IgG	Custom-made		Gregory et al., 2009	Rabbit polyclonal	1:1000	1% (w/v) non-fat dry milk in 1X TBS
Anti-rabbit	Peroxidase Affinipure goat anti-rabbit IgG	Commercial	Jackson Immuno Research	111035144	Goat polyclonal	1:10000	1% (w/v) non-fat dry milk in 1X TBS
Anti-mouse	Peroxidase Affinipure goat anti-mouse IgG	Commercial	Jackson Immuno Research	115035146	Goat polyclonal	1:10000	1% (w/v) non-fat dry milk in 1X TBS

Supplementary Table 2.3. Multiple reaction mode settings for HILIC-MS/MS analysis of sugars and sugar alcohols

RT, retention time; Q1, first quadrupole; Q3, third quadrupole, DP, declustering potential; EP, excitation potential; CP, collision potential; CXP, cell exit potential

Supplemental Table 2.3. Multiple reaction mode settings for HILIC-MS/MS analysis of sugars and sugar alcohols

Compound	RT	Q1	Q3	DP	EP	CP	CXP
	min	*m/z*	*m/z*	*V*	*V*	*eV*	*V*
glyceraldehyde1	2,5	89	43	-25	-10	-14	-7
glyceraldehyde2	2,5	89	45	-25	-10	-14	-7
glyceraldehyde3	2,5	89	41	-25	-10	-32	-19
glycerol1	3,75	91	59	-35	-10	-13	-5
glycerol2	3,75	91	45	-35	-10	-14	-7
glycerol3	3,75	91	71	-35	-10	-10	-7
xylulose1	4,21	149	89	-15	-10	-9	-9
xylulose2	4,21	149	59	-15	-10	-21	-6
xylulose3	4,21	149	71	-15	-10	-19	-6
ribulose1	4,36	149,02	89	-15	-10	-9	-9
ribulose2	4,36	149,02	59	-15	-10	-21	-6
ribulose3	4,36	149,02	71	-15	-10	-19	-6
rhamnose1	4,44	163,01	59	-25	-10	-16	-7
rhamnose2	4,44	163,01	103	-25	-10	-10	-9
rhamnose3	4,44	163,01	89	-25	-10	-10	-5
ribose1	4,5	149,04	89	-15	-10	-9	-9
ribose2	4,5	149,04	59	-15	-10	-21	-6
ribose3	4,5	149,04	71	-15	-10	-19	-6
iso-erythritol1	4,78	121	71	-40	-10	-20	-9
iso-erythritol2	4,78	121	89	-40	-10	-12	-5
iso-erythritol3	4,78	121	101	-40	-10	-11	-7
xylose1	5,26	149,01	59	-41	-10	-18	-7
xylose2	5,26	149,01	89	-41	-10	-8	-11
xylose3	5,26	149,01	71	-41	-10	-14	-7
fucose1	5,75	163	59	-45	-10	-18	-5
fucose2	5,75	163	89	-45	-10	-10	-9
fucose3	5,75	163	71	-45	-10	-18	-7
ribitol1	6,15	151,05	89	-35	-10	-15	-11
ribitol2	6,15	151,05	101	-35	-10	-16	-9
ribitol3	6,15	151,05	59	-35	-10	-22	-5
arabinose1	6,2	149,03	59	-41	-10	-18	-7
arabinose2	6,2	149,03	89	-41	-10	-8	-11
arabinose3	6,2	149,03	71	-41	-10	-14	-7
talose	6,21	179,07	59	-25	-10	-18	-6
xylitol1	6,58	151	89	-45	-10	-16	-9
xylitol3	6,58	151	59	-45	-10	-22	-7
xylitol2	6,58	151	71	-45	-10	-21	-7
allose	6,6	179,06	89	-25	-10	-22	-9
arabitol1	6,61	151,25	89	-45	-10	-16	-9
arabitol2	6,61	151,25	71	-45	-10	-21	-7
arabitol3	6,61	151,25	59	-45	-10	-22	-7
fructose1	7,41	179	88,9	-21	-10	-11	-9
fructose2	7,41	179	58,9	-21	-10	-22	-9
fructose3	7,41	179	119,1	-21	-10	-11,5	-11
[$^{13}C_6$]fructose*	7,41	185	92	-21	-10	-11	-9
altrose	7,64	179,05	59	-25	-10	-18	-6
mannose1	8,29	179,01	89	-40	-10	-14	-9
mannose2	8,29	179,01	59	-40	-10	-21	-5
mannose3	8,29	179,01	119	-40	-10	-10	-11
glucose1	8,67	179,02	88,9	-21	-10	-11	-9
glucose2	8,67	179,02	58,9	-21	-10	-55	-11
glucose3	8,67	179,02	119,1	-21	-10	-11,5	-9
[$^{13}C_6$]glucose*	8,67	185,02	92	-21	-10	-11	-9
sorbitol1	8,76	181	89	-74	-10	-19	-6
sorbitol2	8,76	181	59	-74	-10	-29	-9
sorbitol3	8,76	181	101	-74	-10	-20	-6
[$^{13}C_6$]sorbitol*	8,76	187	105	-74	-10	-20	-6
galactose1	9,34	179,03	89	-25	-10	-13	-9
galactose2	9,34	179,03	59	-25	-10	-18	-5
galactose3	9,34	179,03	71	-25	-10	-18,5	-7

Supplemental Table 2.3. Multiple reaction mode settings for HILIC-MS/MS analysis of sugars and sugar alcohols

Compound	RT	Q1	Q3	DP	EP	CP	CXP
	min	*m/z*	*m/z*	*V*	*V*	*eV*	*V*
mannitol1	8,76	181,05	59	-55	-10	-27	-7
mannitol2	8,76	181,05	89	-55	-10	-19	-6
mannitol3	8,76	181,05	101	-55	-10	-20	-9
galactitol1	9,19	181,1	101	-93	-10	-21	-16
galactitol2	9,19	181,1	71	-93	-10	-26	-11
galactitol3	9,19	181,1	119	-93	-10	-17	-13
sucrose1	12,25	341	161	-40	-10	-12	-15
sucrose2	12,25	341	97	-40	-10	-27	-9
sucrose3	12,25	341	79	-40	-10	-70	-7
[*fructosyl*-$^{13}C_6$]sucrose*	12,25	347	179	-60	-10	-11	-13
laminaribiose1	13,13	341,01	113	-51	-10	-22	-10
laminaribiose2	13,13	341,01	161	-51	-10	-10	-14
laminaribiose3	13,13	341,01	179	-51	-10	-11	-13
palatinose	13,46	341,02	179	-51	-10	-11	-13
turanose	13,55	341,03	179	-51	-10	-11	-13
myo-inositol1	13,71	179,04	87	-45	-10	-21	-11
myo-inositol2	13,71	179,04	71	-45	-10	-30	-6
myo-inositol3	13,71	179,04	99	-45	-10	-23	-13
cellobiose1	13,93	341,05	161	-65	-10	-10,5	-13
cellobiose2	13,93	341,05	101	-65	-10	-22,5	-14
cellobiose4	13,93	341,05	73	-65	-10	-35	-11
maltose1	13,99	341,04	161	-40	-10	-12	-15
maltose2	13,99	341,04	97	-40	-10	-27	-9
maltose3	13,99	341,04	79	-40	-10	-70	-7
[$^{13}C_{12}$]maltose*	13,99	353,04	167	-40	-10	-12	-15
maltitol1	14,18	343	59	-70	-10	-45	-7
maltitol2	14,18	343	89	-70	-10	-26	-7
maltitol3	14,18	343	119	-70	-10	-24	-9
αβ-trehalose1	14,3	341,06	59	-110	-10	-57	-7
αβ-trehalose2	14,3	341,06	89	-110	-10	-25,5	-10
αβ-trehalose3	14,3	341,06	119	-110	-10	-24	-11
[$^{13}C_{12}$]αβ-trehalose*	14,3	353,06	185	-110	-10	-11	-13
αα-trehalose1	14,99	341,07	59	-110	-10	-57	-7
αα-trehalose2	14,99	341,07	89	-110	-10	-25,5	-10
αα-trehalose3	14,99	341,07	119	-110	-10	-24	-11
[$^{13}C_{12}$]αα-trehalose*	14,99	353,07	185	-110	-10	-11	-13
lactulose1	15,15	341,1	161	-70	-10	-12	-15
lactulose2	15,15	341,1	101	-70	-10	-24	-9
lactulose3	15,15	341,1	59	-70	-10	-38	-5
lactose	15,52	341,08	161	-40	-10	-12	-15
melibiose1	16,55	341,09	179	-60	-10	-11	-13
melibiose2	16,55	341,09	59	-60	-10	-52	-9
melibiose3	16,55	341,09	101	-60	-10	-22,5	-14
kestose1	17,36	503,1	59	-35	-10	-85	-8
kestose3	17,36	503,1	179	-35	-10	-27	-13
kestose4	17,36	503,1	71	-35	-10	-76	-9
maltotriose1	18,3	503,2	161	-58	-10	-20	-17
maltotriose2	18,3	503,2	341,1	-58	-10	-13	-19
maltotriose3	18,3	503,2	101	-58	-10	-36	-12
raffinose1	18,6	503,15	179	-25	-10	-28	-17
raffinose2	18,6	503,15	59	-25	-10	-78	-7
raffinose3	18,6	503,15	221	-25	-10	-37	-17
galactinol1	19,61	341,15	179	-75	-10	-20	-14
galactinol2	19,61	341,15	59	-75	-10	-52	-9
galactinol4	19,61	341,15	119	-75	-10	-23	-11
stachyose1	23,8	665,1	383,2	-50	-10	-36	-19
stachyose2	23,8	665,1	179	-50	-10	-42	-11
stachyose3	23,8	665,1	59	-50	-10	-100	-9

*stable-isotope labelled internal standard (SIL-IS)

Supplementary Table 2.4. Stable-isotope labelled internal standards (SIL-IS) used to correct for ion suppression and other matrix effects during HILIC-MS/MS

Supplemental Table 2.4. Stable-isotope labelled internal standards (SIL-IS) used to correct for ion suppression and other matrix effects during HILIC-MS/MS analysis of sugars and sugar alcohols

Metabolite	SIL-IS	Also used to normalize
arabinose	[$^{13}C_5$]arabinose	iso-erythritol, arabitol
arabitol	n.a.	
fructose	[$^{13}C_6$]fructose	rhamnose
galactinol	n.a.	
galactose	[$^{13}C_6$]galactose	
glucose	[$^{13}C_6$]glucose	
iso-erythritol	n.a.	
1-kestose	n.a.	
laminaribiose	n.a.	
maltose	[$^{13}C_6$]maltose	melibiose, maltotriose,
maltotriose	n.a.	
mannitol	n.a.	
melibiose	n.a.	
myo-inositol	[$^{2}H_6$]myo-inositol	
raffnose	n.a.	
rhamnose	n.a.	
sorbitol	[$^{13}C_6$]sorbitol	mannitol
stachyose	n.a.	
sucrose	[*Fru*-$^{13}C_6$]sucrose	
αα-trehalose	[$^{13}C_{12}$]a,a-trehalose	ββ-trehalose, 1-kestose, raffinose, galactinol, stachyose
αβ-trehalose	[$^{13}C_{12}$]a,b-trehalose	

n.a. - not available

CHAPTER 3

TPS5/6/7 proteins coordinate plant growth and development with sugar availability via the SnRK1 kinase.

Author contributions: Diana Reis-Barata, John E. Lunn, Mark Stitt and Elena Baena-González conceived the research plan and designed the experiments. Diana Reis-Barata, Bruno Peixoto (TPS7-mCherry microscopy), Borja Belda-Palazon (SnRK1α1 microscopy) and Farnusch Kaschani (LC-MS/MS analysis) performed the experiments. Ana Confraria and Leonor Margalha assisted with p-ACC and p-SnRK1α1 immunoblots. Filipa Lopes assisted with root phenotyping. Diana Reis-Barata and Elena Baena-González analyzed, interpreted data, and wrote the manuscript. John E. Lunn and Mark Stitt interpreted data and edited the manuscript.

3.1. Abstract

Plants dynamically adjust growth and development to the energy status through integrated sugar signaling pathways. The signaling molecule trehalose 6-phosphate (T6P) serves as a central regulator of this process, mirroring cellular sucrose availability and fine-tuning metabolic and developmental responses accordingly. T6P acts at least partly by inhibiting the protein kinase SUCROSE NON-FERMENTING 1 (SNF1)-RELATED KINASE 1 (SnRK1) but the underlying mechanisms are poorly understood. Here, we identify a group of catalytically inactive T6P synthase (TPS) proteins, TPS5/6/7, as essential factors for coupling the T6P signal to SnRK1 activity. In *Arabidopsis thaliana*, lack of TPS5/6/7 causes severe root growth defects and delayed flowering. This is accompanied by a metabolic signature that is suggestive of T6P insensitivity and impaired sucrose utilization. Using a combination of genetics, SnRK1 activity assays, and imaging, we demonstrate that the growth and developmental defects of the *tps5/6/7* mutant are SnRK1-dependent, with SnRK1 becoming malfunctional when TPS5/6/7 are depleted. Co-immunoprecipitation assays further show that T6P promotes the interaction of TPS proteins with SnRK1 in a highly specific and dose-dependent manner. Our results support a model where T6P-bound TPS proteins sequester SnRK1 in repressor complexes that sensitize SnRK1 to energy signals. TPS proteins may therefore act as T6P sensors, modulating SnRK1 activity to adjust plant metabolism and growth to sucrose availability.

3.2. Introduction

Carbon resources sustain life by providing energy and the building blocks for biomass. The ability to sense and respond to these resources determines adaptation and survival and therefore all species have evolved efficient sensing mechanisms suited to their needs and environments (Chantranupong et al. 2015). In plants, one

such mechanism involves the sugar signal trehalose 6-phosphate (T6P), which acts as a key indicator of sucrose availability and plays a central role in coordinating carbon metabolism with growth and developmental demands (Baena-González and Lunn 2020; Fichtner and Lunn 2021).

In plants, T6P is synthesized from UDP-glucose (UDPG) and glucose 6-phosphate (G6P) by trehalose 6-phosphate synthase (TPS) and is then converted to trehalose by trehalose 6-phosphate phosphatase (TPP) (Cabib and Leloir 1958; Avonce et al. 2006). In addition to the enzymatically active class I TPS isoforms (primarily TPS1 and TPS2/4 showing residual activity) (Vandesteene et al. 2010; Delorge et al. 2015), Arabidopsis thaliana encodes a family of non-catalytic class II TPS proteins (TPS5-11, hereafter TPS-II) (Vogel et al. 2001; Ramon et al. 2009; Vandesteene et al. 2010; Delorge et al. 2015), which are suggested to play signaling functions instead (Lunn et al. 2014; Van Leene et al. 2022).

One way T6P exerts its regulatory effects is by inhibiting the protein kinase SUCROSE-NON-FERMENTING-1-RELATED KINASE 1 (SnRK1) (Zhang et al. 2009; Paul et al. 2020), a conserved key regulator of metabolism and energy homeostasis during stress but also during normal growth and development (Baena-González et al. 2007; Broeckx et al. 2016; Peixoto et al. 2021; Peixoto and Baena-González 2022). SnRK1 is activated under carbon starvation (Baena-González et al. 2007; Mair et al. 2015; Pedrotti et al. 2018; Ramon et al. 2019) and conversely inhibited by T6P and other sugar phosphates when carbon levels are high (Zhang et al. 2009; Nunes et al. 2013; Zhai et al. 2018; Avidan et al. 2024; Blanford et al. 2024). Through this regulation, T6P-mediated inhibition of SnRK1 promotes biosynthetic pathways and growth, whereas under low T6P conditions, SnRK1 is released from inhibition and downregulates growth-related processes via the coordinated control of metabolism and gene expression (Baena-González and Lunn 2020).

However, the precise molecular mechanisms linking T6P perception to SnRK1 regulation remain poorly understood. SnRK1 is a heterotrimeric protein complex composed of an α catalytic subunit and regulatory β and βγ subunits (Crozet et al.

2014). T6P was shown to bind to SnRK1α in vitro, precluding its phosphorylation and activation by its upstream kinase (Zhai et al. 2018; Blanford et al. 2024); however, the physiological relevance of this binding remains to be evaluated in planta. Additionally, T6P has been shown to inhibit SnRK1 indirectly via an as-yet unidentified proteinaceous factor present in actively growing tissues (Zhang et al. 2009). This role could potentially be fulfilled by TPS-II proteins, as they physically interact with all SnRK1 subunits (α, β, and βγ), inhibit SnRK1 activity in vitro and in transient protoplast assays (Van Leene et al. 2022), and retain key residues for T6P binding in their phosphatase-like domain (Lunn 2007). Indeed, our previous work showed that loss of TPS5/6/7 leads to delayed flowering, impaired root growth, and a complex metabolic profile, suggestive of restricted sucrose utilization, despite elevated levels of T6P (Chapter 2). These findings suggest that TPS5/6/7 proteins are required for proper T6P signaling, possibly by mediating the repression of SnRK1 activity. However, whether the physiological defects observed in the *tps5/6/7* mutant stem from altered SnRK1 regulation, and how TPS-II proteins influence SnRK1 function, remain open questions.

To tackle this, we investigated the relationship between TPS5/6/7 and SnRK1 in Arabidopsis, focusing on genetic interactions, subcellular localization, and protein-protein interactions in the context of T6P signaling. Our findings reveal that TPS-II proteins are not only critical for repressing basal SnRK1 activity to support growth but also modulate SnRK1 responsiveness to energy stress. Moreover, we show that T6P enhances the physical interaction between TPS-II proteins and SnRK1 in a highly specific manner, suggesting that TPS-II proteins may act as T6P sensors that facilitate SnRK1 inhibition.

3.3. Results

3.3.1. Loss of SnRK1 suppresses the *tps5/6/7* mutant developmental and growth defects.

In our previous work, we demonstrated that *tps7* single mutants and combinatorial *tps5/7* and *tps5/6/7* mutants exhibit delayed flowering and reduced root growth, with phenotypic severity increasing in higher-order mutants (Chapter 2). Notably, SnRK1 has been implicated in the regulation of both flowering time (Tsai and Gazzarrini 2012; Jeong et al. 2015; Zacharaki et al. 2022) and root development (Weiste et al. 2017; Belda-Palazón et al. 2020, 2022; Muralidhara et al. 2021). To investigate whether these phenotypes were related to SnRK1 function, we first examined the flowering phenotypes of *tps7* plants crossed to loss- and gain-of-function mutants of SnRK1α1 (*snrk1α1* and *35S::SnRK1α1*, *aka. SnRK1α1-OE*, respectively), and of *tps5/7* plants crossed to *snrk1α1*. These lines, together with the corresponding parental lines, were grown in soil under long-day conditions. Flowering time was determined by counting the number of days to flower and the number of rosette leaves when the floral bud was first visible. Importantly, we focused on SnRK1α1 for the flowering assessment based on findings from Zacharaki et al. (2022). Their study showed that loss-of-function mutations in *SnRK1α1*, but not *SnRK1α2*, rescued both embryogenesis and flowering in *tps1-2* mutants, indicating a role specific to SnRK1α1 in T6P-mediated developmental transitions.

Depletion of SnRK1α1 rescued the delayed flowering phenotype of *tps7* plants, while overexpression further aggravated it (Figure 3.1A). *tps7/SnRK1α1-OE* plants flowered on average five days later than Col-0 and two days later than *tps7* mutants, producing six more rosette leaves than Col-0 and four more than *tps7*. The *SnRK1α1-OE* behaved similarly to Col-0, with only minor, non-significant delays in flowering (one day) and a slight increase in rosette leaf number (one extra leaf), whereas *snrk1α1* plants flowered at the same time as Col-0 but produced significantly fewer rosette leaves (a reduction of almost two leaves). Consistent with the *tps7* results, the *snrk1α1* mutation completely reverted the delayed flowering phenotype of *tps5/7* mutants, restoring both flowering time and rosette leaf number to Col-0 levels (Figure 3.1B). These results indicate that the developmental defects observed in *tps7* and *tps5/7* mutants are SnRK1α1-dependent.

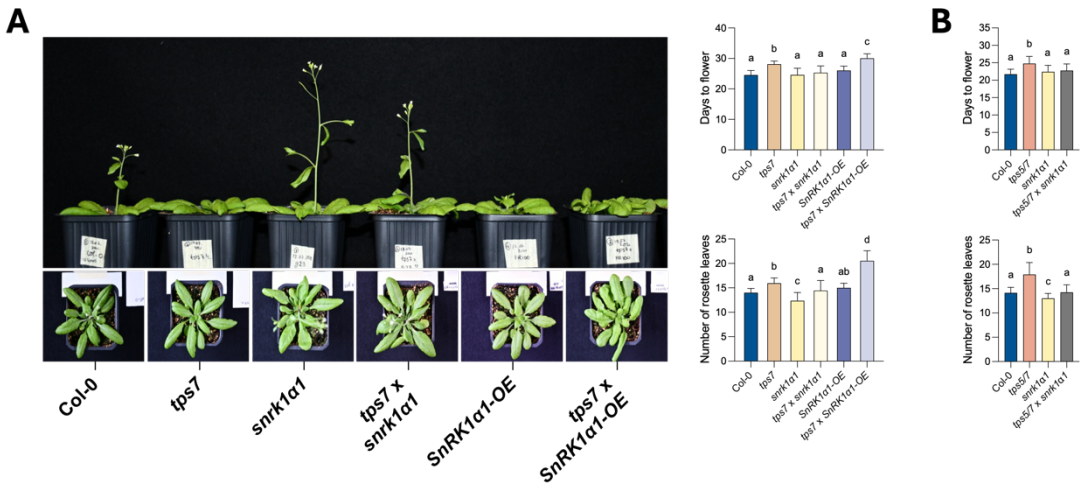

Figure 3.1. Depletion of SnRK1α1 rescues flowering delays in *tps7* and *tps5/7* mutants.
(**A**) *Left*, representative images of 33-d old Col-0, *tps7*, *snrk1α1* and *tps7 x snrk1α1*, *SnRK1α1-OE* and *tps7 x SnRK1α1-OE* plants grown on soil under long-day conditions (16 h light, 110 µmol m^{-2} s^{-1}, 22 °C / 8 h dark, 18 °C). *Right*, quantification of flowering time based on days to flower and number of rosette leaves when the floral bud was first visible. (**B**) Quantification of flowering time of Col-0, *tps5/7*, *snrk1α1* and *tps5/7 x snrk1α1* plants grown under the same conditions and based on the same metrics as in (A). Number of independent experiments and plants per genotype: (**A**) *n*=2, 19 plants; (**C**) *n*=3, 28-30 plants. Bars represent the mean of independent experiments (error bars, SD). Different letters indicate statistically significant differences between genotypes (one-way ANOVA with Tukey HSD test).

Given the SnRK1-dependent basis of the flowering defects of *tps7* and *tps5/7* mutants, we next sought to determine whether SnRK1 function similarly contributed to the primary root growth defects observed in *tps5/6/7* plants. We therefore crossed *tps5/6/7* plants to a partial loss-of-function mutant of the SnRK1α catalytic subunit, which is encoded by two genes (*SnRK1α1* and *SnRK1α2*) in Arabidopsis. From the cross with the SnRK1 *snrk1α1*$^{-/-}$*/snrk1α2*$^{-/+}$–mutant (hereafter "*sesquiα*" mutant), we retrieved *tps5/6/7/snrk1α1* and *tps5/6/7/sesquiα* progeny. In parallel, we crossed *tps5/6/7* plants to *SnRK1α1-OE* to assess the impact of enhanced SnRK1 activity in the *tps5/6/7* background. These lines, together with the corresponding parental lines, were used in primary root phenotyping assays. Following the same protocol as in Chapter 2, seedlings were grown vertically on 0.5× MS medium for 7 days before transferring size-matched individuals to fresh plates for an additional 7-day growth period to ensure comparability and minimize variability. Primary root growth was then measured as the length of root developed post-transfer. The depletion of SnRK1α

function markedly alleviated the primary root growth defects of the *tps5/6/7* mutant, with the *snrk1α1* and *sesquia* mutations restoring the *tps5/6/7* root growth defects from 48% to 72% and 92% of the Col-0 levels, respectively (Figure 3.2). Notably, this rescue was already evident at the 7-day pre-growth stage, with *tps5/6/7/sesquia* seedlings displaying root lengths comparable to Col-0, unlike the severely stunted roots of *tps5/6/7* mutants (Supplementary Figure 3.1). Conversely, SnRK1α1 overexpression further exacerbated the *tps5/6/7* root impairment, with *tps5/6/7/SnRK1α1-OE* roots reaching only 41% of Col-0 length compared to 48% in *tps5/6/7* alone (Supplementary Figure 3.2). Notably, *SnRK1α1-OE* plants alone also exhibited a mild but significant reduction in root growth, with roots reaching 90% of Col-0 length. This demonstrates that the root growth defects of *tps5/6/7* mutants, similar to their delayed flowering phenotypes, are largely SnRK1-dependent and suggests TPS5/6/7 are negative regulators of SnRK1 function.

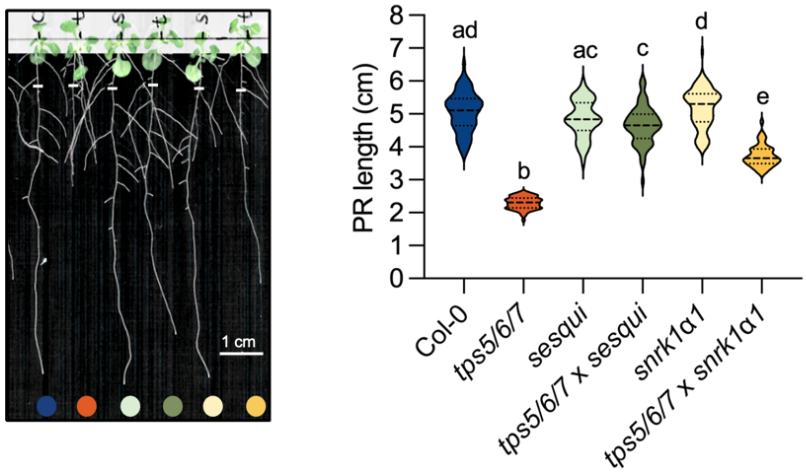

Figure 3.2. Depletion of SnRK1α restores *tps5/6/7* root growth defects.
Left, representative images of 14-d old Col-0, *tps5/6/7*, *sesqui*, *tps5/6/7 x sesqui*, *snrk1α1* and *tps5/6/7 x snrk1α1* seedlings grown vertically on 0.5× MS medium for 7 d and transferred to fresh 0.5× MS plates for 7 d. Scale bar 1 cm. *Right*, quantification of PR length, measured from the white mark to the root tip (*n*=3; 54-92 seedlings per genotype). The upper and lower horizontal lines represent the first and third quartiles, respectively. The middle horizontal dashed line indicates the median. Different letters indicate statistically significant differences between genotypes ($p < 0.05$, one-way ANOVA with Tukey HSD test).

3.3.2. Lack of TPS proteins alters SnRK1 function.

To investigate which aspects of SnRK1 activity are altered in the absence of TPS5/6/7, we first compared total SnRK1α1 levels and SnRK1α T-loop phosphorylation, which is essential for SnRK1 activity (Baena-González et al. 2007; Shen et al. 2009). This revealed no differences between Col-0 and the mutant (Supplementary Figure 3.3A). We next compared the subcellular localization of SnRK1α1 in Col-0 and *tps5/6/7* seedlings, given that SnRK1 function is largely determined by its subcellular localization (Ramon et al. 2019; Gutierrez-Beltran and Crespo 2022). To this end, we crossed the *tps5/6/7* mutant with a line expressing SnRK1α1-GFP under the *SnRK1α1* upstream and downstream regulatory regions (Crozet et al. 2016) and imaged roots of the fully homozygous progeny at the end of the night by confocal laser scanning microscopy (CLSM). The total mean fluorescence was similar in the two genotypes (Fig. 3.3A, upper panel), confirming the immunoblot analyses (Supplementary Figure 3.3A). As previously reported (Ramon et al. 2019; Belda-Palazón et al. 2020, 2022), in Col-0 roots, SnRK1α1 was present in the cytoplasm and was strongly enriched in the nucleus. In the *tps5/6/7* mutant, however, the nucleus-to-cytosolic ratio was 30% lower than in Col-0 (Fig. 3.3A, lower panel), pointing to a redistribution of SnRK1α1 from the nucleus to the cytosol. To compare SnRK1α1 localization to that of TPS7, we next imaged our *TPS7-mCherry* complementation line *C#6.3* (Figure 2.2B) under the same conditions as SnRK1α1-GFP. This revealed a fully extranuclear localization for TPS7 (Supplementary Figure 3.7).

To assess the possible functional consequences of altered SnRK1α1 localization, we crossed the *tps5/6/7* mutant with a reporter line expressing a peptide from rat acetyl-CoA carboxylase (ACC) that is specifically phosphorylated by SnRK1 (Muralidhara et al. 2021; Sanagi et al. 2021). The reporter protein is localized to the nucleus by virtue of a Nuclear Localization Signal (NLS) and therefore its relative phosphorylation serves as readout for SnRK1 nuclear activity (Muralidhara et al. 2021). We subjected *NLS-ACC* and *tps5/6/7/NLS-ACC* seedlings to an “energy stress” treatment (4h of sudden darkness from ZT4-ZT6) that triggers nuclear SnRK1

signalling (Margalha et al. 2023). The treatment increased NLS-ACC phosphorylation in whole seedlings of both lines, indicating the induction of SnRK1 nuclear activity (Figure 3.3B). However, the phosphorylation of the reporter under energy stress conditions was significantly lower in the *tps5/6/7* mutant (31% reduction compared to Col-0). To further assess the functional impact of altered SnRK1α1 localization in the *tps5/6/7* mutant, we compared the expression of a subset of well-established downstream targets of SnRK1 nuclear activity (*DIN1*, *DIN6*, *PYL5* and *BGAL4*; Baena-González et al. 2007) between Col-0 and *tps5/6/7* seedlings following 5 h of sudden darkness (from ZT3-ZT8). While the expression of the four tested SnRK1 target genes was induced by the treatment in whole seedlings of both genotypes, this induction appeared slightly reduced in the *tps5/6/7* mutant, although the differences relative to Col-0 did not reach statistical significance (Supplementary Figure 3.3B). This suggests that SnRK1 nuclear activity is weaker in *tps5/6/7* seedlings, consistent with the reduced nuclear localization of SnRK1α1 in the mutant (Figure 3.3A).

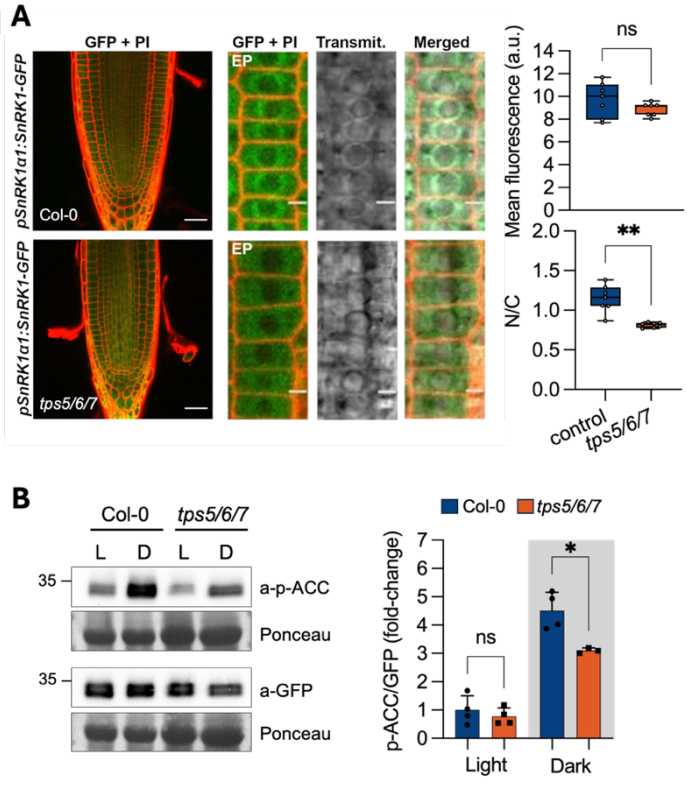

Figure 3.3. Lack of TPS proteins alters SnRK1α1 function.

(**A**) Analyses of SnRK1α1 subcellular localization by CLSM in root apical meristems of 8d-old *SnRK1α1-GFP* and *tps5/6/7 SnRK1α1-GFP* seedlings stained with propidium iodide (PI). *Left*, representative images of SnRK1α1 localization in the root apex. *Right*, quantification of mean cellular fluorescence (up) and nucleus-to-cytosol ratio (N/C) ratio (down) of SnRK1α1-GFP in the indicated genotypes (n=7 root tips, each consisting of the average of 5 meristematic cells). Lower and upper box boundaries represent the first and third quantiles, respectively, horizontal lines mark the median and whiskers mark the highest and lowest values. *P* values denote statistically significant differences (unpaired t-test with Welch's correction). EP, epidermis; a.u., arbitrary units. Scale bars, 30 μm or 5 μm for photographs of the whole root apex or epidermal cells (EP), respectively. (**B**) *Left*, representative immunoblots showing in vivo phosphorylation of a nuclear rat ACC-GFP-HA reporter protein in 14d-old Col-0 and *tps5/6/7* seedlings, either maintained in the light (L) or transferred to darkness (D) at ZT2 for 4 h and harvested at ZT6. GFP immunodetection was used for normalization. *Right*, quantification of SnRK1α1 nuclear activity, presented as the p-ACC/GFP ratio. Bars show the mean of 4 independent experiments (error bars, SD). Asterisks indicate significant differences between genotypes (**p*<0.05, ***p*<0.01, ****p*<0.001; two-tailed unpaired t-test).

3.3.3. T6P enhances the interaction of TPS proteins with SnRK1.

TPS proteins have a phosphatase-like domain that retains key residues for T6P binding (Lunn 2007). Given their physical interaction with SnRK1 (Van Leene et al. 2022), the apparent insensitivity of the *tps5/6/7* mutant to T6P (Chapter 2), the observation that the mutant's phenotypes are largely SnRK1-dependent (Figures 3.1 and 3.2; Supplementary Figures 3.1 and 3.2), and the inhibition of SnRK1 by T6P (Zhang et al. 2009; Nunes et al. 2013; Zhai et al. 2018; see also Baena-González and Lunn 2020), we next wondered whether the interaction of TPS proteins with SnRK1 is affected by T6P. To this end, we performed co-immunoprecipitation experiments making use of our *TPS7-mCherry* complementation lines (Figure 2.2B). We grew *TPS7-mCherry* (C#6.3) seedlings in mock plates, immunoprecipitated TPS7 from whole seedling extracts in the absence or presence of T6P and assessed the interaction with endogenous SnRK1α1 by immunoblotting (see experimental set-up in Supplementary Figure 3.4A). The presence of T6P increased in a clear dose-dependent manner the interaction between TPS7 and SnRK1α1 (Figure 3.4A). To further assess the specificity of this effect, we next performed similar experiments in the presence of other sugars linked to T6P metabolism (sucrose, UDPG, G6P and Trehalose) or previously shown to inhibit SnRK1 [G6P and G1P; (Nunes et al. 2013)]. However, the interaction between SnRK1 and TPS7 was not affected by any of the other tested sugars, indicating that the effect of T6P is highly specific (Figure 3.4B). To further confirm the effect of T6P in the TPS7-SnRK1 interaction we performed

reciprocal co-immunoprecipitation analyses using a SnRK1α1-GFP complementation line (Crozet et al. 2016) followed by tandem mass spectrometry (MS/MS) analyses of the SnRK1α1-GFP protein interactors (see experimental set-up in Supplementary Figure 3.4B). The presence of T6P led to a significantly increased interaction of SnRK1α1-GFP with TPS7, but also with all other TPS-II proteins except TPS5, corroborating the results obtained with the *TPS7-mCherry* line and revealing a possible more general effect of T6P in regulating the interaction of SnRK1 with the whole TPS-II protein family (Figure 3.4C).

To validate these proteomic observations, we sought to perform similar experiments for TPS5 (as a representative protein of the same subclade as TPS7) and TPS10 (as a representative protein of the other TPS-II protein subclade; Lunn 2007). To this end, we transformed *tps5* and *tps10* T-DNA insertional mutants (Supplementary Figure 3.5) with constructs for expressing, respectively, TPS5-mCherry and TPS10-mTurquoise under the control of their endogenous regulatory regions. This resulted in three independent complementation lines per construct, from which we selected those with the highest expression levels and minimal degradation products (Supplementary Figure 3.6, line C#24.5 for TPS5 and C#2.7 for TPS10) for the co-immunoprecipitation experiments. In the case of TPS10, we found a significant T6P-dependent enhancement of SnRK1α1 binding (2.7-fold with 1 mM T6P; Figure 3.4D), albeit the extent to which T6P promoted the SnRK1α1-TPS10 interaction was markedly weaker than that observed for TPS7 (13.9-fold; Figure 3.4B). Intriguingly, in the case of TPS5, T6P had only minimal, non-significant changes in the interaction with SnRK1 (Figure 3.4D), consistent with the results of the SnRK1α1-GFP immunoprecipitation and MS/MS experiment (Figure 3.4C).

Altogether, our results show that T6P enhances the TPS-SnRK1 interaction, suggesting that TPS-II proteins may serve as T6P sensors that repress SnRK1 activity.

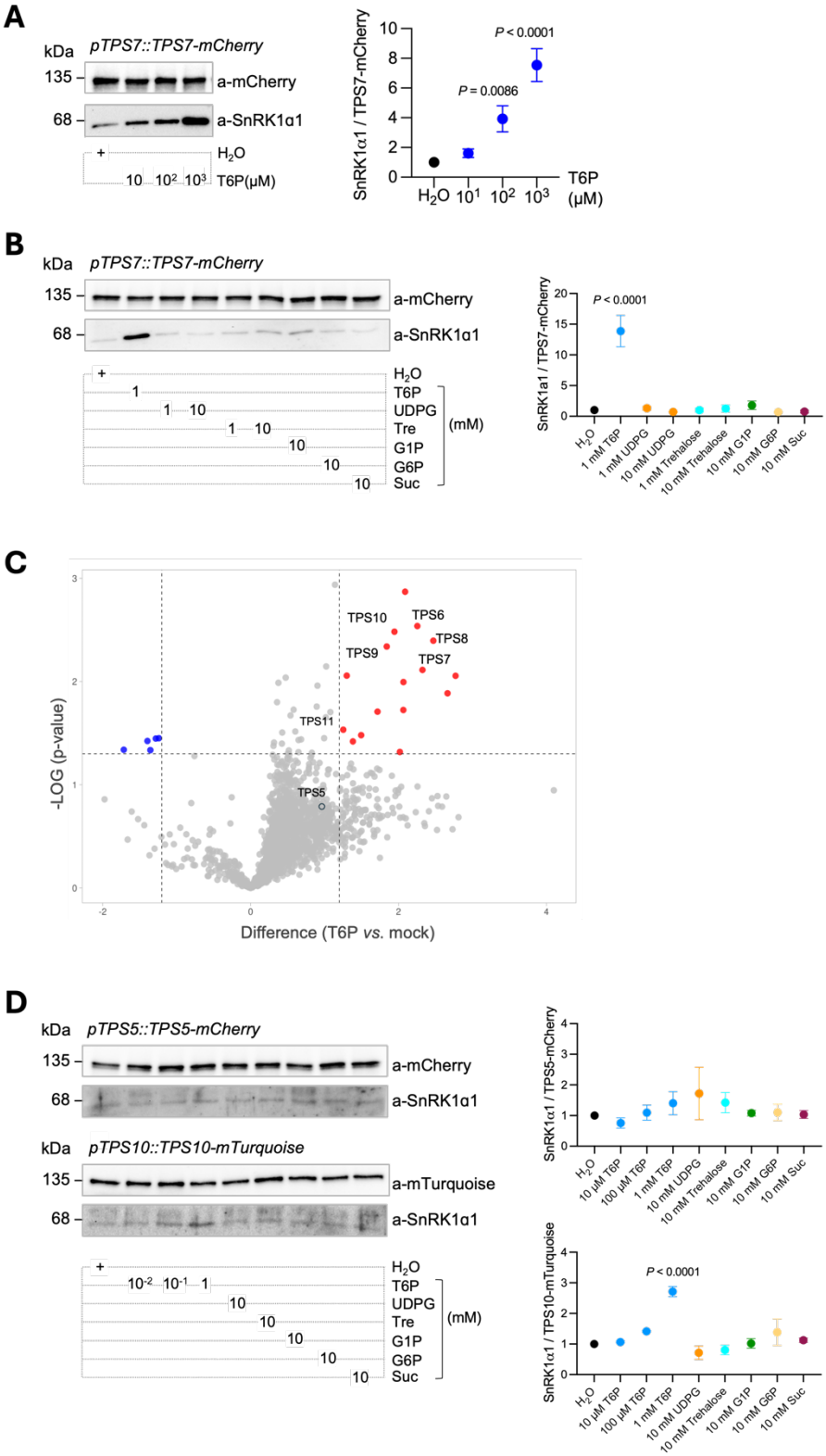
A
kDa
pTPS7::TPS7-mCherry
135
a-mCherry
68
a-SnRK1α1
+
H2O
10 10² 10³ T6P(μM)
SnRK1α1 / TPS7-mCherry
P < 0.0001
P = 0.0086
H2O 10¹ 10² 10³ T6P (μM)
B
kDa
pTPS7::TPS7-mCherry
135
a-mCherry
68
a-SnRK1α1
H2O
T6P
UDPG
Tre
G1P
G6P
Suc
(mM)
SnRK1α1 / TPS7-mCherry
P < 0.0001
H2O
1 mM T6P
1 mM UDPG
10 mM UDPG
1 mM Trehalose
10 mM Trehalose
10 mM G1P
10 mM G6P
10 mM Suc
C
-LOG (p-value)
Difference (T6P vs. mock)
TPS10
TPS6
TPS8
TPS9
TPS7
TPS11
TPS5
D
kDa
pTPS5::TPS5-mCherry
135
a-mCherry
68
a-SnRK1α1
kDa
pTPS10::TPS10-mTurquoise
135
a-mTurquoise
68
a-SnRK1α1
H2O
T6P
UDPG
Tre
G1P
G6P
Suc
(mM)
SnRK1α1 / TPS5-mCherry
H2O
10 μM T6P
100 μM T6P
1 mM T6P
10 mM UDPG
10 mM Trehalose
10 mM G1P
10 mM G6P
10 mM Suc
SnRK1α1 / TPS10-mTurquoise
P < 0.0001

Figure 3.4. T6P enhances TPS-SnRK1α1 interactions.
(**A**,**B**) *Left*, representative western blots (WB) of immunoprecipitated TPS7-mCherry (top) and co-immunoprecipitated SnRK1α1 (bottom) in the presence of the indicated concentrations of T6P (**A**) and/or other sugars (**B**) (experimental set-up in Supplementary Figure 3.4A). *Right*, relative quantification of SnRK1α1 amounts co-immunoprecipitated with TPS7-mCherry in the indicated conditions. (**C**) Volcano plot showing changes in SnRK1α1 interactors in the presence of T6P as per the experimental setup in Supplementary Figure 3.4B. The x-axis represents the Difference (LFQ T6P - LFQ mock), and the y-axis indicates the -log10(P-value). Points represent individual interactors, with the ones significantly changed highlighted in blue (depleted) or red (enriched). (**D**) *Left*, representative WBs of immunoprecipitated TPS5-mCherry or TPS10-mTurquoise from their respective complementation lines. Co-immunoprecipitations were carried out in the presence of the indicated concentrations of T6P or other sugars, using a similar experimental approach to that in (A,B), with minor variations in sugar concentrations. Co-immunoprecipitated SnRK1α1 is shown below each corresponding IP. *Right*, relative quantification of SnRK1α1 amounts co-immunoprecipitated with TPS5-mCherry (**D**), or TPS10-mTurquoise (**D**) in the indicated conditions. (**A**,**B**,**D**) Graphs show the mean of 3 independent experiments (error bars, SEM). *P* values denote statistically significant differences between control and treated samples (one-way ANOVA with Dunnet's test).

3.4. Discussion

In plants, T6P is crucial for coordinating growth with carbon availability (Schluepmann et al. 2003; Baena-González and Lunn 2020; Fichtner and Lunn 2021). Particularly in actively growing sink organs, T6P is believed to stimulate sucrose utilization for growth, in part by inhibiting the SnRK1 kinase (Zhang et al. 2009; Nunes et al. 2013). However, the molecular basis of T6P perception and subsequent SnRK1 inhibition remains poorly understood. Our previous results demonstrated that depletion of TPS-II proteins – including TPS7 alone, or the combined loss of TPS5/7 and TPS5/6/7 – delays flowering and impairs root growth. Notably, the *tps5/6/7* mutant exhibited the most severe phenotypes, which correlated with metabolic changes, consistent with defective T6P sensing and potentially with persistent SnRK1 activation (Chapter 2). Here, we show that TPS5/6/7 proteins act as T6P-responsive modulators that link T6P signaling to SnRK1 activity.

A T6P sensory role for TPS-II proteins is supported by two lines of evidence. First, the active site residues critical for T6P binding appear conserved in the TPP-like domain of TPS-II proteins (Lunn 2007). Second, the interaction of TPS-II proteins with SnRK1α1 is enhanced in a T6P-dependent manner (Figure 3.4). We, therefore, postulate that TPS-II proteins act as T6P sensors and that upon T6P binding, they become competent to interact with SnRK1. However, it is also possible that T6P binds

to other proteins, including SnRK1. Indeed, T6P was shown to bind to the SnRK1α1 subunit, preventing its interaction with the SnRK1 activating kinase (SnAK) and, thereby, SnRK1 T-loop phosphorylation and activity (Zhai et al. 2018; Blanford et al. 2024). It is, therefore, possible that T6P binding to SnRK1 may also determine its interaction with TPS-II proteins.

Regardless of which protein binds T6P, our results demonstrate that TPS-II proteins are crucial for proper SnRK1 function, altering both its basal and stress-induced activities (Figure 3.5). On one hand, the flowering delay of *tps7* and *tps5/7* along with the marked growth defects of *tps5/6/7* are rescued by SnRK1α depletion (Figures 3.1 and 3.2; Supplementary Figure 3.1). Conversely, SnRK1α1 overexpression exacerbates these phenotypes, specifically further delaying the flowering of *tps7* and further impairing the root growth of *tps5/6/7* (Figure 3.1A; Supplementary Figure 3.2). This indicates that TPS-II proteins promote growth and development by inhibiting SnRK1 and that, without TPS-II proteins, SnRK1 becomes aberrantly active under normal conditions. Support for this comes from genetic evidence (Figures 3.1 and 3.2; Supplementary Figures 3.1 and 3.2) but also from the T6P:suc ratios of the *tps5/6/7* mutant. The T6P:suc ratios of *tps5/6/7* shoots (0.169, 1.6-fold higher than in Col-0, Table 2.1) are remarkably similar to those reported for rosettes of SnRK1α1 overexpressors at the end of the night [0.170, 1.4-fold higher than in Col-0, (Peixoto et al. 2021)], and clearly different from those of rosettes overexpressing an *E. coli* TPS (otsA) [2.831, 21-fold higher than in Col-0, (Yadav et al. 2014)]. On the other hand, the activation of SnRK1 nuclear functions by energy stress appears attenuated in the *tps5/6/7* mutant (Figure 3.3B; Supplementary Figure 3.3.B) suggesting that, without TPS-II proteins, SnRK1 is less sensitive to energy signals. We envision two possible scenarios to explain this.

Lower activation of SnRK1 by energy stress in the *tps5/6/7* mutant could be a direct consequence of TPS-II depletion. TPS-II proteins may sequester a pool of SnRK1 in repressor complexes that respond to energy signals (Figure 3.5). In the absence of TPS5/6/7, this SnRK1 pool would be aberrantly active, yet partly insensitive to further activation by energy stress, as it lacks the proteins that associate

SnRK1 to the energy signal. This would be reminiscent of how SnRK2 proteins regulate SnRK1 in response to abscisic acid (ABA) (Belda-Palazón et al. 2020, 2022). ABA-responsive SnRK2 kinases (SnRK2.2, SnRK2.3, and SnRK2.6) form, together with type 2C protein phosphatases (PP2Cs), complexes that inhibit SnRK1 under favorable conditions but allow its activation in response to ABA. Consequently, *snrk2.2/snrk2.3* seedlings show aberrant repression of root growth under normal conditions, and this is fully reverted by the *snrk1α1* mutation. Meanwhile, the activation of SnRK1 by ABA is defective in the *snrk2.2/snrk2.3* mutant, as it lacks the proteins that link SnRK1 to this signal. However, contrary to SnRK2s (Belda-Palazón et al. 2020, 2022), we could not detect TPS7-mCherry in the nucleus at EN (Supplementary Figure 3.7). This suggests that TPS-II proteins form non-nuclear SnRK1 repressor complexes, consistent with the observation that transient co-expression of TPS-II proteins with SnRK1 decreases its nuclear localization and activity (Van Leene et al. 2022). It is therefore difficult to explain how the lack of TPS5/6/7 alone could reduce SnRK1 nuclear localization (Figure 3.3A), as well as NLS-ACC phosphorylation – non-significantly in the light and significantly following a dark treatment (Figure 3.3B).

A second scenario is that defective activation by energy stress might be an indirect consequence of TPS-II depletion. Aberrantly high T6P levels could interfere with T-loop phosphorylation by the SnAK kinase (Zhai et al. 2018; Blanford et al. 2024). However, the levels of T-loop phosphorylation were not significantly different between Col-0 and *tps5/6/7* seedlings (Supplementary Figure 3.3A), arguing against this possibility. It is also important to consider that if the TPS-II–SnRK1α1 interaction is T6P-dependent, then in Col-0 plants this interaction likely occurs primarily in the light, when T6P levels are high, but not after a dark treatment when T6P is very low. Therefore, differences observed between Col-0 and *tps5/6/7* mutants under dark are unlikely to result from loss of T6P-mediated inhibition of SnRK1 by TPS5/6/7. This suggests that the effect of TPS-II depletion on SnRK1 activity in the dark may involve other mechanisms independent of T6P regulation. For example, the high levels of soluble sugars in the mutant could indirectly dampen SnRK1 activation through mechanisms unrelated to T6P/TPS that remain to be elucidated. Sugars might interfere with the initial activation of SnRK1 by energy stress, its nuclear import,

downstream signaling events, or a combination of these. In the context of downstream signaling, sucrose has been shown to repress the translation of SnRK1-regulated S1 bZIP transcription factors via the sucrose-induced repression of translation (SIRT) pathway (Wiese et al. 2004; Rahmani et al. 2009). Hence, this mechanism could indirectly reduce the nuclear output of SnRK1 in the *tps5/6/7* mutant by limiting the availability of its downstream effectors. Distinguishing between a direct and an indirect effect of TPS-II proteins on SnRK1 activation by energy stress would require uncoupling elevated T6P and soluble sugars from TPS5/6/7 depletion in the future.

Importantly, differences in SnRK1α1 localization have been shown to directly impact root growth under non-stress conditions. Nuclear enrichment through fusion of SnRK1 to a Nuclear Localization Signal (NLS) promoted root elongation. Conversely, nuclear exclusion through fusion of SnRK1 to a membrane-anchoring myristoylation motif (βMYR) inhibited root growth (Ramon et al. 2019). Therefore, the reduced SnRK1α1 nuclear localization in the *tps5/6/7* mutant (Figure 3.3A), phenocopying the *SnRK1α1-βMYR* line, albeit less severely, further supports that the growth defects in the mutant likely arise from a combination of SnRK1 mislocalization and altered signaling output.

Despite these disruptions, the *tps5/6/7* mutant retains some capacity for growth, suggesting that additional factors contribute to SnRK1 regulation. Indeed, our data show that SnRK1 interacts with all TPS-II proteins, with T6P enhancing these interactions to varying degrees (Figure 3.4). This supports previous findings that the entire TPS-II family participates in SnRK1 regulation (Van Leene et al. 2022) and further suggests a competitive mechanism for context-specific SnRK1 modulation. Notably, TPS5 showed minimal T6P-dependent enhancement of SnRK1 binding, in contrast to the marked response observed for TPS7 and, to a lesser extent, TPS10 (Figure 3.4). This could reflect one of two possibilities. First, TPS5 may intrinsically lack T6P responsiveness, indicating distinct biochemical properties compared to other TPS-II isoforms. Alternatively, these co-immunoprecipitation assays were conducted on whole-seedling extracts, where spatial resolution is lost. In such homogenized samples, TPS5-SnRK1 interactions may be masked by higher-affinity isoforms like

TPS7, which could outcompete TPS5 for SnRK1 binding in a T6P-dependent manner. In vivo, however, TPS-II isoforms exhibit differential expression across tissues and cell types (Ramon et al. 2009; Mergner et al. 2020), and TPS5 may predominate in specific cellular contexts where TPS7 is less abundant, allowing a T6P-responsive interaction that remains undetectable in bulk assays. To test whether the observed TPS5 insensitivity reflects experimental limitations rather than true biochemical indifference, TPS5-mCherry could be expressed in the *tps5/6/7* background, where competing isoforms are absent. A T6P-dependent interaction in this context would indicate that TPS5 responsiveness is normally masked by competition with higher-affinity isoforms in Col-0 plants. Such competitive dynamics could enable functional compensation when specific isoforms are absent, as likely occurs in the *tps5/6/7* mutant, with TPS8-11 potentially compensating for the loss of TPS5-7. Nevertheless, the extent to which other TPS-II proteins contribute to SnRK1 regulation and growth requires further investigation.

In summary, our findings uncover a crucial role for TPS5/6/7 as mediators of T6P signaling, fine-tuning SnRK1 activity to balance metabolism and growth. Further studies are needed to fully elucidate the roles of TPS-II proteins across different tissues and environmental conditions, as well as their interactions with other components of the T6P-SnRK1 regulatory network. Given their conservation across plant species, such insights will not only deepen our understanding of plant energy sensing but also inform strategies to optimize crop performance under increasingly challenging environments.

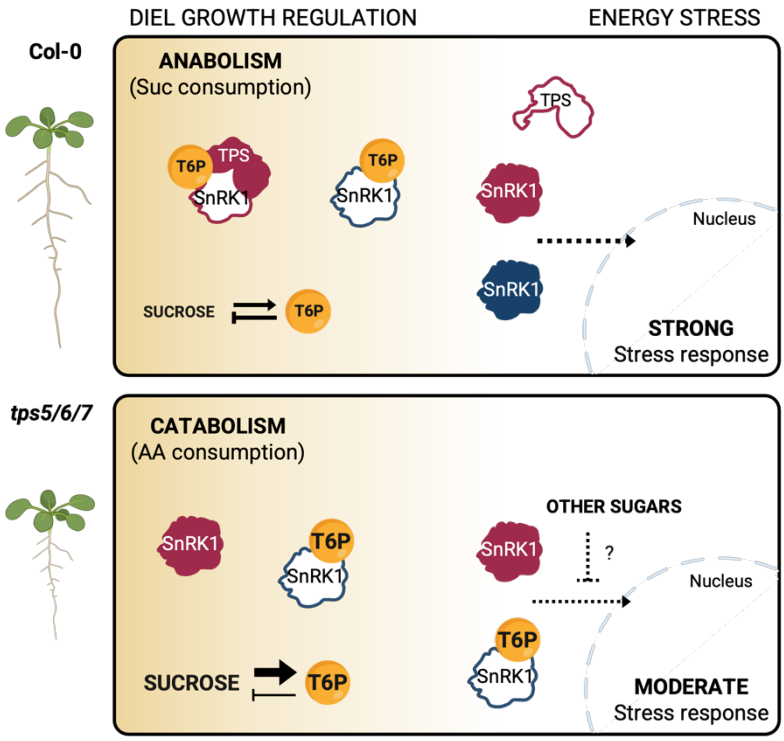

Figure 3.5. TPS-II proteins coordinate plant growth with sugar availability via the SnRK1 kinase – model.
Up left, in wild-type plants (Col-0) growing under favorable conditions, high T6P enhances the TPS-SnRK1 interaction, leading to inhibition of a non-nuclear SnRK1 pool. Other (non-nuclear) pools of SnRK1 may be directly inhibited by T6P or other signals/factors. Low SnRK1 activity promotes sucrose consumption through anabolic processes, supporting growth and maintaining sucrose homeostasis. *Up right*, in response to stress, sucrose and T6P levels decrease, causing the dissociation of TPS-SnRK1 complexes and possibly the activation of other SnRK1 pools. This leads to high SnRK1 activity in the nucleus and strong activation of stress responses. *Bottom left*, the inability to perceive T6P disrupts sucrose homeostasis. In the absence of TPS5/6/7, a pool of non-nuclear SnRK1 is aberrantly active, promoting catabolic processes and growth repression despite high sucrose and T6P levels. The inhibition of other (non-nuclear) pools of SnRK1 by T6P or other signals/factors is normal. *Bottom right*, under stress, nuclear SnRK1 activity is weaker in the *tps5/6/7* mutant leading to mildly compromised stress responses. This is possibly caused by the overaccumulation of T6P and other sugars when TPS5/6/7 are depleted. White filling: inactive proteins, red or blue filling: active proteins. Created with Biorender.com.

3.5. Materials and Methods

A list of all primers and antibodies used in this study is provided in the Supplementary Table 3.1.

3.5.1. Plant material and growth conditions

All *Arabidopsis thaliana* plants used in this study are in the Columbia (Col-0) background. The *tps10* T-DNA insertion mutant (SALK_110873) was identified from the publicly available collection of *Arabidopsis thaliana* T-DNA insertion lines (http://signal.salk.edu/cgi-bin/tdnaexpress). Homozygosity of the *tps10* mutation was confirmed by genomic PCR, using LP, RP and T-DNA LB primers (Supplementary Figure 3.5C) and loss of full-length transcript was verified by RT-PCR (Yadav et al., unpublished observations). The *snrk1α1-3* (Mair et al. 2015), *sesquiα2-2* (*snrk1α1-3*$^{-/-}$ *snrk1α2-2*$^{+/-}$; referred as *sesqui*; Belda-Palazón et al. 2020), *pro35S::NLS-ratACC-GFP-2xHA* (referred as *NLS-ACC*; Muralidhara et al. 2021), *SnRK1α1-OE* (Jossier et al. 2009), *proSnRK1α1::SnRK1α1-GFP* (Crozet et al. 2016) and *tps5-1* (Tian et al. 2019) have been previously described. The *tps7*, *tps5/7*, *tps5/6/7* and *proTPS7::TPS7-mCherry* C#6.3 lines were generated as described in Chapter 2. The *proTPS5::TPS5-mCherry* and *proTPS10::TPS10-mTurquoise* complementation lines were generated as described in Section 3.5.2. Combinatorial *tps5/6/7/snrk1α1-3*, *tps5/6/7/sesqui*, *tps5/6/7/NLS-ACC*, *tps5/6/7/SnRK1α1-OE* and *tps5/6/7/proSnRK1α1::SnRK1α1-GFP* mutants were obtained by crossing the *tps5/6/7* mutant with *snrk1α1-3*, *sesquiα2-2*, *pro35S:NLS-ratACC-GFP-2xHA*, *SnRK1α1-OE* or *proSnRK1α1::SnRK1α1-GFP*, respectively. The *tps5/7/snrk1α1-3* was obtained by crossing the *tps5/7* mutant with *snrk1α1-3*. The *tps7/snrk1α1-3* and *tps7/SnRK1α1-OE* mutants were obtained by crossing the *tps7* mutant with *snrk1α1-3* or *SnRK1α1-OE*, respectively.

Seeds were surface sterilized for 1 min in 70% (v/v) ethanol followed by 10 min in 20% (v/v) bleach under gentle rocking and then washed at least 5 times with sterile water. Sterilized seeds were stratified in the dark at 4°C for 2-3 days. Unless otherwise specified, plants were grown under long-day conditions (16 h light, 110 µmol m^{-2} s^{-1}, 22 °C / 8 h dark, 18 °C) on 0.5× MS medium (0.05% MES and 0.8% phytoagar).

3.5.2. Molecular cloning and Arabidopsis transformation

To generate C-terminally tagged *proTPS5::TPS5-mCherry* and *proTPS10::TPS10-mTurquoise* complementation lines, relevant DNA fragments were amplified by PCR using Phusion™ High-Fidelity DNA Polymerase and primers containing appropriate overhangs. Fragments were thereafter assembled into the final vector using the Gibson Assembly® method (Gibson et al. 2009, 2010). The full-length *TPS5* (AT4G17770, 3027 bp) and *TPS10* (AT1G60140, 2825 bp) genes, a 2000 bp region upstream of the *TPS5* and *TPS10* start codons (promoter), and downstream terminator sequences (1000 bp) were separately amplified from Arabidopsis Col-0 genomic DNA. The mCherry sequence (708 bp) was amplified from a construct for expressing a Golgi-mCherry marker (Nelson et al. 2007). The mTurquoise (717 bp) sequence was amplified from the p2R3a-Tq2CFP-OcsT plasmid (Addgene clone 71268). A 5039 bp segment of the pCB302 binary vector (Xiang et al. 1999) sequence was amplified for the construct backbone. Purified PCR products were incubated at 50 °C for 1 h with the NEBuilder® Hifi DNA assembly master mix, following the manufacturer's instructions. The resulting constructs were introduced into *E. coli* (TOP10) cells, and correct assembly was validated by colony PCR and sequencing. Verified constructs were introduced into *Agrobacterium tumefaciens* GV3101 and *tps5* (SALK_144791) and *tps10* (SALK_110873) mutant plants were transformed with *pTPS5::TPS5-mCherry* and *pTPS10::TPS10-mTurquoise*, respectively, by the floral dip method (Clough and Bent 1998). BASTA®-resistant transformants were selected based on their segregation ratio (T2) and homozygosity (T3). To assess differences in signal intensity of TPS5-mCherry and TPS10-mTurquoise fusion proteins (Supplementary Figure 3.6), 50 µg protein samples from homozygous *proTPS5::TPS5-mCherry* and *proTPS10::TPS10-mTurquoise* plants, respectively, were prepared and immunoblotted as described in Section 3.5.5. Membranes were probed with anti-RFP (TPS5) and anti-GFP (TPS10) antibodies.

3.5.3. Phenotyping assays

To assess flowering, plants were grown in a 1:3 vermiculite:soil (Bord Na Mona Pot Plant Substrate Plus+ Irish Peat Moss) mixture under long-day conditions.

Flowering time was determined by counting the number of days to flower (when floral buds became visible in the center of the rosette) and the number of rosette leaves when plants reached a stem height of approximately 1 cm.

For root growth assays, seedlings were grown vertically for 7 days on 0.5× MS medium under long-day conditions (16 h light, 110 µmol m^{-2} s^{-1}, 22 °C / 8 h dark, 18 °C). Seedlings with comparable root sizes were then transferred to fresh 0.5× MS plates and maintained under the same light conditions. The position of the root tip was marked immediately after transfer and seedlings were grown on the fresh plates for an additional 7 days before scanning. Post-transfer root growth was measured as primary root length from scanned plates. Root tracing and measurements were performed using the NeuronJ plugin (Meijering et al. 2004) in ImageJ. In assays involving segregating *sesqui* and *tps5/6/7/sesqui* lines, seedlings were harvested after scanning the plates, and their identity was determined by PCR.

3.5.4. Subcellular localization analyses by confocal microscopy

The localization of SnRK1α1 was investigated in roots of SnRK1α1-GFP and *tps5/6/7*;SnRK1α1-GFP seedlings grown vertically on 0.5× MS plates under long-day conditions (16 h light, 110 µmol m^{-2} s^{-1}, 22°C / 8 h dark, 18 °C) for 8 days. On day 8, one hour before the onset of the lights, roots were stained for 2 min with an aqueous solution of propidium iodide (PI; 10 µg/mL) and images were acquired on a Zeiss AxioObserver 780, using a 40× water immersion objective. For the visualization of GFP, pinholes were adjusted to 1 Airy Unit (488 nm/500-530 nm). For quantitative analysis of GFP, the 488 nm laser power was set to 3.0% transmission, and the master gain was set to 800. For the visualization of cell walls, pinholes were also adjusted to 1 Airy Unit (561 nm/600-660 nm). Post-acquisition image processing was performed using ImageJ (http://rsb.info.gov/ij/).

The nuclear/cytoplasmic localization of SnRK1α1 was assessed using CLSM and ImageJ software, calculating the N/C ratio (N/C = Mean Nuclear Fluorescence

Intensity / Mean Cytoplasmic Fluorescence Intensity, with Mean Fluorescence Intensity being the ratio between the total fluorescence intensity measured and the number of pixels measured) (Kelley and Paschal 2019). The area of the nucleus was determined by analyzing the bright field acquired through the transmitted light mode whilst the area of the cytoplasm was selected using the PI signal as a reference.

The localization of TPS7 was investigated at the end of the night in roots of *TPS7-mCherry* seedlings (line C#6.3), grown vertically on 0.5× MS plates under long-day conditions (16 h light, 110 µmol m^{-2} s^{-1}, 22°C / 8 h dark, 18°C) for 8 days. On day 8, one hour before the onset of dawn, roots were mounted in water. Images were acquired using a Leica Stellaris 8 system, using a 63x water immersion objective. For the visualization of mCherry, a white light laser was used at 85% power and 8% intensity to excite the fluorophore at 581 nm. Red fluorescent signal was detected on the 587 – 700 nm range, with a hybrid HyD S detector operating in analogue mode at 600 Hz. Pinholes were kept at 1 airy units (AU), and the final image was acquired by averaging 6x over each line and accumulating signal 2x over the entire frame. Gray value histograms were adjusted, and scale bars were added to the images in Leica's software Las X Office v. 1.4.7.28982, prior to being exported.

3.5.5. Protein extraction, quantification and immunoblotting

Proteins were extracted on ice with extraction buffer [1.5 mL buffer/ g fresh weight; 50 mM Tris-HCl pH 8.0, 150 mM NaCl, 1 mM EDTA, 1% (v/v) Triton X-100, 3 mM DTT, 50 µM MG-132, 0.002% (v/v) phosphatase inhibitor cocktail #2 (Sigma P572G), 0.002% (v/v) phosphatase inhibitor cocktail #3 (Sigma P0044) and cOmplete™ protease inhibitor cocktail (Roche; 1 tablet/10mL)]. Homogenates were cleared by centrifugation at 21130 *g* for 15 min at 4 °C. Protein concentration in the resulting supernatants was quantified using the Bradford assay (for assays in Sections 3.5.2, 3.5.6 and 3.5.7).

Proteins were denatured in Laemmli buffer, loaded onto 8% (Sections 3.5.2, 3.5.7 and 3.5.9) or 10% (Section 3.5.6) acrylamide gels and resolved by SDS-PAGE. Separated proteins were transferred to PVDF membranes (wet transfer at 4 °C, 80 V, 90 min), using transfer buffer (192 mM glycine, 25 mM Tris, 0.1% SDS, 20% ethanol) and a Bio-Rad wet blotting transfer system. Membranes were blocked for 1 h (5% w/v non-fat dry milk in 1X TBS, 0.05% Tween®) and probed with primary antibodies under gentle rocking overnight at 4 °C, followed by incubation with secondary antibodies at RT for 1 h. Chemiluminescent detection was performed using ECL Prime Western Blotting Detection Reagent (Amersham, RPN2232) or SuperSignal West Femto Maximum Sensitivity Substrate (Thermo Scientific).

3.5.6. *In planta* SnRK1 activity assay

Arabidopsis *NLS-ACC* and *tps5/6/7/NLS-ACC* seedlings were grown vertically for 7 days on 0.5× MS medium. Seedlings with comparable root sizes were then transferred to fresh 0.5× MS plates and grown for an additional 7 days. On day 14, seedlings were either kept in the light or shifted to darkness at ZT2 for 4 hours. Seedlings of both groups were harvested at ZT6, flash-frozen and reduced to a fine powder in liquid nitrogen. Proteins were extracted from whole seedlings and immunoblotted as described in Section 3.5.5. Membranes were probed with anti-P(S79)-ACC or anti-GFP. Protein band intensities were determined in ImageJ (version 2.1.0), and p-ACC/GFP ratios were analyzed with GraphPad Prism (version 10.3.1).

3.5.7. SnRK1 T-loop phosphorylation assay

Arabidopsis Col-0 and *tps5/6/7* seedlings were grown vertically for 7 days on 0.5× MS medium. Seedlings with comparable root sizes were then transferred to fresh 0.5× MS plates and grown for an additional 7 days. On day 14, seedlings were either kept in the light or shifted to darkness at ZT2 for 4 hours. Seedlings of both groups were harvested at ZT6, flash-frozen and reduced to a fine powder in liquid nitrogen.

Proteins were extracted and immunoblotted as described in Section 3.5.5. Membranes were probed with anti-P(T172)-AMPKα or anti-SnRK1α1. Protein band intensities were determined in ImageJ (version 2.1.0), and p-SnRK1α1/SnRK1α1 ratios were analyzed with GraphPad Prism (version 10.3.1).

3.5.8. RNA extraction and qRT-PCR

Total RNA was extracted from approximately 25 mg of finely ground tissue, using the Nucleospin RNA plants purification kit (Macherey-Nagel) following the manufacturers' instructions. DNase-treated RNA (1 µg) was reverse transcribed, and cDNA was synthesized using OligoDT and Super Script III Reverse Transcriptase (Life Technologies) in a total reaction volume of 10 µL, then diluted to a final volume of 80 µL. Quantitative real-time RT-PCR (qPCR) reactions were prepared in a total volume of 10 µL containing 1 µL of cDNA, 5 µL of iTaq™ Universal SYBR® Green Supermix (BioRad) and 0.8 µL of each gene-specific 5 µM primer. Reactions were run in a QuantStudio™ 7 platform (Applied Biosystems®), and relative quantification was performed using the $2^{-\Delta\Delta Ct}$ method (Livak and Schmittgen 2001). Expression values of SnRK1-induced genes were normalized to the geometric mean of Ct values obtained for the following housekeeping genes: *UBQ10* and *UBC21*.

3.5.9. Coimmunoprecipitation experiments

For assessing the interaction of TPS7 with SnRK1α1, 14d-old *proTPS7::TPS7-mCherry* seedlings (line C #6.3) grown vertically on 0.5× MS medium were harvested at the end of the night, flash frozen and reduced to a fine powder in liquid nitrogen. Proteins were extracted as described in Section 3.5.5. The resulting cleared protein extract was divided into 250 µL aliquots, to which 10 µL of one of the following was added to achieve the indicated concentrations in a final volume of 500µL: H_2O, T6P (10 µM, 100 µM or 1 mM), UDPG (1 mM or 10 mM), trehalose (1 mM or 10 mM), G1P (10 mM), G6P (10 mM) or sucrose (10 mM). Volumes were then adjusted to 500 µL

by adding 240 µL of dilution buffer [50 mM Tris-HCl pH 8.0, 150 mM NaCl, 1 mM EDTA, 3 mM DTT, 0.002% (v/v) phosphatase inhibitor cocktail #2 (Sigma P572G), 0.002% (v/v) phosphatase inhibitor cocktail #3 (Sigma P0044) and cOmplete™ protease inhibitor cocktail (Roche; 1 tablet/10mL)]. mCherry-tagged TPS7 was immunoprecipitated using ChromoTek RFP-Trap® Magnetic Agarose beads. Immunoprecipitated TPS7-mCherry was eluted in 50 µL of 2x Laemmli buffer by boiling for 5 min at 95 °C, and coimmunoprecipitated proteins were analyzed by western blotting using anti-RFP and anti-SnRK1α1 antibodies. Protein band intensities were determined in ImageJ (version 2.1.0), and SnRK1α1/TPS7-mCherry ratios were analyzed with GraphPad Prism (version 10.3.1).

For TPS5 and TPS10 interactions with SnRK1α1, we used *proTPS5::TPS5-mCherry* (C# *24.5*) and *proTPS10::TPS10-mTurquoise* (C# *2.7*) seedlings to perform similar experiments as for TPS7. TPS5-mCherry was immunoprecipitated with ChromoTek RFP-Trap® Magnetic Agarose beads and detected with anti-RFP. TPS10-mTurquoise was immunoprecipitated with GFP-Trap® Magnetic Agarose beads (ChromoTek) and detected with anti-GFP.

To explore the effect of T6P on the SnRK1α1 interactome, 14d-old *proSnRK1α1::SnRK1α1-GFP* seedlings grown vertically on 0.5× MS medium were harvested at the end of the night, flash frozen and reduced to a fine powder in liquid nitrogen. Cleared protein extracts were prepared as described above, split into 300 µL aliquots, and mixed with either H_2O or 1 mM T6P along 190 µL of dilution buffer to reach a final reaction volume of 500 µL. GFP-tagged SnRK1α1 was immunoprecipitated using ChromoTek GFP-Trap® Magnetic Agarose beads.

3.5.10. Sample preparation for LC-MS/MS

Samples for proteomic analysis were prepared using the single-pot, solid-phase-enhanced sample-preparation (SP3) strategy (Hughes et al. 2019). All buffers and solutions were prepared with mass spectrometry (MS)-grade water (Avantor,

Radnor, PA, USA). Proteins from SnRK1α1-GFP pull down experiments were eluted twice in 50 µL of 2X elution buffer [2% (w/v) SDS, 20 mM TCEP, 80 mM chloracetamide, 100 mM HEPES pH 8.0] by heating each time for 5 min at 90 °C and clearing by centrifugation. The eluates were combined (100 µL in total) in a fresh tube, flash-frozen in liquid nitrogen, and stored at -80 °C. For LC-MS/MS analyses, eluted proteins were transferred to a 96-well plate. Then, 3 µL of a 50 µg μL^{-1} 1:1 mixture of hydrophilic (#45152105050250) and hydrophobic (#65152105050250) carboxylate modified Sera-Mag™ SpeedBeads (Cytiva, Marlborough, MA, USA) that were washed twice with MS-grade water were added to the samples. Afterwards, the samples were mixed shortly (1 min, 1000 rpm, RT) and collected by short centrifugation (10 sec, 200 *g*, RT). Protein binding was induced by the addition of an equal volume of pure ethanol (24 °C, 10 min, 1000 rpm), the beads were collected by a brief centrifugation step (10 sec, 200 *g*, RT) and the plate was placed on a magnetic stand. Beads were allowed to bind for at least 5 min before the supernatant was removed. The beads were then taken up in 180 µL 80% ethanol and transferred to a fresh multiwell plate. Subsequently the beads were washed four times with 180 µL 80% (v/v) ethanol prior to the addition of 100 µL digestion enzyme mix (0.6 µg of trypsin (V5111; Promega, Madison, WI, USA) and 0.6 µg LysC (125-05061; FUJIFILM Wako Pure Chemical, Osaka, Japan) in 25 mM ammonium bicarbonate). Samples were incubated at 37 °C for 19 h while shaking (1300 rpm). Next day, the samples were briefly centrifuged (10 sec, 200 ×*g*, RT) and placed on a magnet for 5 min. The clear solution containing the tryptic peptides was transferred to a fresh multiwell plate. The beads were taken up in 47 µL 25 mM ABC and incubated while shaking (RT, 10 min, 1000 rpm). The plate was then placed once more on a magnetic stand and after 5 min the cleared supernatant was again collected and combined with the recovered first peptide mix. This was followed by the addition of formic acid (FA; 2% final concentration) to the samples (trypsin inactivation).

3.5.11. Sample clean-up for LC-MS/MS

Peptides were desalted on home-made C18 StageTips (Rappsilber et al. 2007) containing two layers of an octadecyl silica membrane (CDS Analytical, Oxford, PA, USA). All centrifugation steps were carried out at room temperature. The StageTips were first activated and equilibrated by passing 50 µL of methanol (600 *g*, 2 min), 80% (v/v) acetonitrile (ACN) with 0.5% (v/v) FA (600 *g*, 2 min) and 0.5% (v/v) FA (600 *g*, 2 min) over the tips. Next, the acidified tryptic digests were passed over the tips (800 *g*, 3 min). The immobilized peptides were then washed with 50 µL and 25 µL 0.5% (v/v) FA (800 *g*, 3 min). Bound peptides were eluted from the StageTips by application of two rounds of 25 µL 80% (v/v) ACN with 0.5% (v/v) FA (800 *g*, 2 min). After elution from the StageTips, the peptide samples were dried using a vacuum concentrator (Eppendorf, Hamburg, Germany) and the peptides were dissolved in 15 µl 0.1% (v/v) FA prior to analysis by MS.

3.5.12. LC-MS/MS Analysis

LC-MS/MS analysis of peptide samples were performed on an Orbitrap Fusion Lumos mass spectrometer (Thermo Scientific, Waltham, MA, USA) coupled to an Easy nLC 1200 ultra high-performance liquid chromatography (UHPLC) system (Thermo Scientific, Waltham, MA, USA) that were operated in the one-column mode. The analytical column was a fused silica capillary (inner diameter 75 µm, outer diameter 360 µm, length 28 cm; CoAnn Technologies, Richland, WA, USA) with an integrated sintered frit packed in-house with Kinetex 1.7 µm XB-C18 core shell material (Phenomenex, Aschaffenburg, Germany). The analytical column was encased by a PRSO-V2 column oven (Sonation, Biberach, Germany) and attached to a nanospray flex ion source (Thermo Scientific, Waltham, MA, USA). The column oven temperature was set to 50 °C during sample loading and data acquisition. The LC was equipped with two mobile phases: solvent A (2% ACN and 0.2% FA, in water) and solvent B (80% ACN and 0.2% FA, in water). All solvents were of UHPLC grade (Honeywell, Charlotte, NC, USA). Peptides were directly loaded onto the analytical column with a maximum flow rate that would not exceed the set pressure limit of 950 bar (usually around 0.5 – 0.6 µL min^{-1}) and separated on the analytical column by

running a 105 min gradient of solvent A and solvent B at a flow rate of 300 nL/min (start with 3% (v/v) B, gradient 3% to 6% (v/v) B for 5 min, gradient 6% to 29% (v/v) B for 70 min, gradient 29% to 42% (v/v) B for 15 min, gradient 42% to 100% (v/v) B for 5 min and 100% (v/v) B for 10 min). The mass spectrometer was controlled by the Orbitrap Fusion Lumos Tune Application and operated using the Xcalibur software. The MS settings for the different experiments are provided in Table 3.1.

Table 3.1. MS settings for whole proteome analysis

Project	MS	general	MS1	MS2	MS2	MS3	Comments; special settings
ACE_0796	Lumos	Xcalibur v4.5.445.18 Tune v3.5.3881.18 Gradient: 105 min	Analyzer: FT Res.: 120000 SR: 375 - 1800 AGC: Standard AcT: 50 ms RF: 30 SF: -- DDM: CT/3sec	Analyzer: IT Res./ScR: -/rapid SR: Auto AGC: 300 AcT: auto CS: +2 to +7 IsM: Q IsW: 1.6 Frag.: sHCD NCE: 25, 30, 45			classic high low experiment: MS1 in Orbitrap at high resolution and data dependent MS2 in Iontrap. Dynamic exclusion enabled (exclude after n times=1; Exclusion duration (s)= 20; mass tolerance= ± 10ppm)

							intensity threshold: 5.0e³ Spray Voltage: +2300 V ion transfer tube Temp.: 230 °C

Note: FT= Fourier Transform (Orbitrap); IT= Iontrap; Q= Quadrupol; Res.= max. Resolution at 200 m/z (Lumos) or 400 m/z (Elite) [FWHM (full width at half maximum)]; ScR= scan rate for measurements in the IT; SR= scan range [m/z]; AGC= automatic gain control, max number of acquired ions per measurement; AcT= max. Ion acquisition time [ms]; CS= charge states used for fragmentation; IsM= Isolation mode (Q or IT), MS2 isolation and further is only done in IT; IsW= Isolation window [m/z], value followed by scan mode the isolation is based on (MS1, MS2 …) Frag.= Fragmentation method; HCD= Higher-energy collisional dissociation; CID= Collision-induced dissociation; ETD= Electron-transfer dissociation; EThcD= Electron-Transfer/Higher-Energy Collision Dissociation; sHCD= stepped HCD; NCE= normalized collision energy; cycles: number of MSn recorded or max cycle time; RF= RF Lens [%]; SF= Source Fragmentation [V]; DDM: Data dependent Mode (cycle time in seconds, CT/[s] or number of scans, NS); NS= Number of data dependent scans

3.5.13. Data processing and analysis

RAW spectra were submitted to an Andromeda (Cox et al. 2011) search in MaxQuant (2.0.3.0) using the default settings (Cox and Mann 2008). Label-free quantification and match-between-runs was activated (Cox et al. 2014). The MS/MS spectra data were searched against the Uniprot *A. thaliana* reference proteome UP000006548_3702_20231009_OPPG.fasta (one protein per gene; 27449 entries) and the project specific database ACE_0796_SOI_v01.fasta (2 entries). All searches included a contaminants database search (as implemented in MaxQuant, 245 entries). The contaminants database contains known MS contaminants and was included to estimate the level of contamination. Andromeda searches allowed oxidation of

methionine residues (16 Da) and acetylation of the protein N-terminus (42 Da). Carbamidomethylation on Cystein (57) was selected as static modification. Enzyme specificity was set to “Trypsin/P”. The instrument type in Andromeda searches was set to Orbitrap and the precursor mass tolerance was set to ±20 ppm (first search) and ±4.5 ppm (main search). The MS/MS match tolerance was set to ±0.5 Da. The peptide spectrum match FDR and the protein FDR were set to 0.01 (based on target-decoy approach). For protein quantification unique and razor peptides were allowed. Modified peptides were allowed for quantification. The minimum score for modified peptides was 40. Label-free protein quantification was switched on, and unique and razor peptides were considered for quantification with a minimum ratio count of 2. Retention times were recalibrated based on the built-in nonlinear time-rescaling algorithm. MS/MS identifications were transferred between LC-MS/MS runs with the “match between runs” option in which the maximal match time window was set to 0.7 min and the alignment time window set to 20 min. The quantification is based on the “value at maximum” of the extracted ion current. At least two quantitation events were required for a quantifiable protein. Further analysis and filtering of the results was done in Perseus v1.6.10.0. (Tyanova et al. 2016). Comparison of protein group quantities (relative quantification) between different MS runs is based solely on the LFQ’s as calculated by MaxQuant, MaxLFQ algorithm (Cox et al. 2014).

3.5.14. Data availability

The mass spectrometry proteomics data for the on-bead digestions have been deposited to the ProteomeXchange Consortium via the PRIDE (Vizcaíno et al. 2016) partner repository (https://www.ebi.ac.uk/pride/archive/) with the dataset identifier PXD061382.

3.5.15. Accession numbers

Sequence data from this manuscript is available in the Arabidopsis Genome Initiative database under these accession numbers: *DIN1*, AT4G35770; *DIN6*, AT3G47340; *PYL5*, AT5G05440; *BGAL4*, AT5G56870; *UBC21*, AT5G25760; *UBQ10*, AT4G05320.

Acknowledgements

We thank the IGC Plant Facility (Vera Nunes) for excellent plant management. This work was supported by Fundação para a Ciência e a Tecnologia grants UIDB/04551/2020 (DOI 10.54499/UIDB/04551/2020), UIDP/04551/2020 (DOI 10.54499/UIDP/04551/2020, GREEN-IT-Bioresources for Sustainability), LA/P/0087/2020 (LS4FUTURE Associated Laboratory), PTDC/BIA-FBT/4942/2020, PD/BD/150239/2019, and by the Max Planck Society.

3.6. References

Avidan O, Martins MCM, Feil R, Lohse M, Giorgi FM, Schlereth A, Lunn JE, and Stitt M. Direct and indirect responses of the Arabidopsis transcriptome to an induced increase in trehalose 6-phosphate. Plant Physiol. 2024:**196**(1):409–431. https://doi.org/10.1093/plphys/kiae196

Avidan O, Moraes TA, Mengin V, Feil R, Rolland F, Stitt M, and Lunn JE. In vivo protein kinase activity of SnRK1 fluctuates in Arabidopsis rosettes during light-dark cycles. Plant Physiol. 2023:**192**(1):387–408. https://doi.org/10.1093/plphys/kiad066

Avonce N, Mendoza-Vargas A, Morett E, and Iturriaga G. Insights on the evolution of trehalose biosynthesis. BMC Evol Biol. 2006:**6**(1):109. https://doi.org/10.1186/1471-2148-6-109

Baena-González E and Lunn JE. SnRK1 and trehalose 6-phosphate – two ancient pathways converge to regulate plant metabolism and growth. Curr Opin Plant Biol. 2020. https://doi.org/10.1016/j.pbi.2020.01.010

Baena-González E, Rolland F, M. Thevelein J, and Sheen J. A central integrator of transcription networks in plant stress and energy signalling. Nature. 2007:**448**:938–942.

Belda-Palazón B, Adamo M, Valerio C, Ferreira LJ, Confraria A, Reis-Barata D, Rodrigues A, Meyer C, Rodriguez PL, and Baena-González E. A dual function of SnRK2 kinases in the regulation of SnRK1 and plant growth. Nat Plants. 2020:**6**(11):1345–1353. https://doi.org/10.1038/s41477-020-00778-w

Belda-Palazón B, Costa M, Beeckman T, Rolland F, and Baena-González E. ABA represses TOR and root meristem activity through nuclear exit of the SnRK1 kinase. Proceedings of the National Academy of Sciences. 2022:**119**(28). https://doi.org/10.1073/pnas.2204862119

Blanford J, Zhai Z, Baer MD, Guo G, Liu H, Liu Q, Raugei S, and Shanklin J. Molecular mechanism of trehalose 6-phosphate inhibition of the plant metabolic sensor kinase SnRK1. Sci Adv. 2024:**10**(20). https://doi.org/10.1126/sciadv.adn0895

Broeckx T, Hulsmans S, and Rolland F. The plant energy sensor: evolutionary conservation and divergence of SnRK1 structure, regulation, and function. J Exp Bot. 2016:**67**(22):6215–6252. https://doi.org/10.1093/jxb/erw416

Cabib E and Leloir LF. The biosynthesis of trehalose phosphate. American Society for Biochemistry and Molecular Biology. 1958.

Chantranupong L, Wolfson RL, and Sabatini DM. Nutrient-Sensing Mechanisms across Evolution. Cell. 2015:**161**(1):67–83. https://doi.org/10.1016/j.cell.2015.02.041

Clough SJ and Bent AF. Floral dip: a simplified method for Agrobacterium-mediated transformation of Arabidopsis thaliana. The Plant Journal. 1998:**16**(6):735–743. https://doi.org/10.1046/j.1365-313x.1998.00343.x

Cox J, Hein MY, Luber CA, Paron I, Nagaraj N, and Mann M. Accurate Proteome-wide Label-free Quantification by Delayed Normalization and Maximal Peptide Ratio Extraction, Termed MaxLFQ. Molecular & Cellular Proteomics. 2014:**13**(9):2513–2526. https://doi.org/10.1074/mcp.M113.031591

Cox J and Mann M. MaxQuant enables high peptide identification rates, individualized p.p.b.-range mass accuracies and proteome-wide protein quantification. Nat Biotechnol. 2008:**26**(12):1367–1372. https://doi.org/10.1038/nbt.1511

Cox J, Neuhauser N, Michalski A, Scheltema RA, Olsen J V., and Mann M. Andromeda: A Peptide Search Engine Integrated into the MaxQuant Environment. J Proteome Res. 2011:**10**(4):1794–1805. https://doi.org/10.1021/pr101065j

Crozet P, Margalha L, Butowt R, Fernandes N, Elias CA, Orosa B, Tomanov K, Teige M, Bachmair A, Sadanandom A, et al. SUMOylation represses SnRK1 signaling in Arabidopsis. Plant Journal. 2016. https://doi.org/10.1111/tpj.13096

Crozet P, Margalha L, Confraria A, Rodrigues A, Martinho C, Adamo M, Elias CA, and Baena-GonzÃ¡lez E. Mechanisms of regulation of SNF1/AMPK/SnRK1 protein kinases. Front Plant Sci. 2014:**5**(May):1–17. https://doi.org/10.3389/fpls.2014.00190

Delorge I, Figueroa CM, Feil R, Lunn JE, and Van Dijck P. Trehalose-6-phosphate synthase 1 is not the only active TPS in Arabidopsis thaliana. Biochemical Journal. 2015. https://doi.org/10.1042/bj20141322

Fichtner F and Lunn JE. The Role of Trehalose 6-Phosphate (Tre6P) in Plant Metabolism and Development. Annu Rev Plant Biol. 2021:**72**(1):737–760. https://doi.org/10.1146/annurev-arplant-050718-095929

Gibson DG, Smith HO, Hutchison CA, Venter JC, and Merryman C. Chemical synthesis of the mouse mitochondrial genome. Nat Methods. 2010:**7**(11):901–903. https://doi.org/10.1038/nmeth.1515

Gibson DG, Young L, Chuang R-Y, Venter JC, Hutchison CA, and Smith HO. Enzymatic assembly of DNA molecules up to several hundred kilobases. Nat Methods. 2009:**6**(5):343–345. https://doi.org/10.1038/nmeth.1318

Gutierrez-Beltran E and Crespo JL. Compartmentalization, a key mechanism controlling the multitasking role of the SnRK1 complex. J Exp Bot. 2022:**73**(20):7055–7067. https://doi.org/10.1093/jxb/erac315

Hughes CS, Moggridge S, Müller T, Sorensen PH, Morin GB, and Krijgsveld J. Single-pot, solid-phase-enhanced sample preparation for proteomics experiments. Nat Protoc. 2019:**14**(1):68–85. https://doi.org/10.1038/s41596-018-0082-x

Jeong E-Y, Seo PJ, Woo JC, and Park C-M. AKIN10 delays flowering by inactivating IDD8 transcription factor through protein phosphorylation in Arabidopsis. BMC Plant Biol. 2015:**15**(1):110. https://doi.org/10.1186/s12870-015-0503-8

Jossier M, Bouly JP, Meimoun P, Arjmand A, Lessard P, Hawley S, Grahame Hardie D, and Thomas M. SnRK1 (SNF1-related kinase 1) has a central role in sugar and ABA signalling in Arabidopsis thaliana. Plant Journal. 2009:**59**(2):316–328. https://doi.org/10.1111/j.1365-313X.2009.03871.x

Kelley JB and Paschal BM. Fluorescence-based quantification of nucleocytoplasmic transport. Methods. 2019:**157**:106–114. https://doi.org/10.1016/j.ymeth.2018.11.002

Livak KJ and Schmittgen TD. Analysis of Relative Gene Expression Data Using Real-Time Quantitative PCR and the 2−ΔΔCT Method. Methods. 2001:**25**(4):402–408. https://doi.org/10.1006/meth.2001.1262

Lunn JE. Gene families and evolution of trehalose metabolism in plants. Functional Plant Biology. 2007:**34**(6):550. https://doi.org/10.1071/FP06315

Lunn JE, Delorge I, Figueroa CM, Van Dijck P, and Stitt M. Trehalose metabolism in plants. The Plant Journal. 2014:**79**(4):544–567. https://doi.org/10.1111/tpj.12509

Mair A, Pedrotti L, Wurzinger B, Anrather D, Simeunovic A, Weiste C, Valerio C, Dietrich K, Kirchler T, Nägele T, et al. SnRK1-triggered switch of bZIP63

dimerization mediates the low-energy response in plants. Elife. 2015. https://doi.org/10.7554/eLife.05828

Margalha L, Elias A, Belda-Palazón B, Peixoto B, Confraria A, and Baena-González E. HOS1 promotes plant tolerance to low-energy stress via the SnRK1 protein kinase. Plant Journal. 2023:**115**(3). https://doi.org/10.1111/tpj.16250

Meijering E, Jacob M, Sarria J -C. F, Steiner P, Hirling H, and Unser M. Design and validation of a tool for neurite tracing and analysis in fluorescence microscopy images. Cytometry Part A. 2004:**58A**(2):167–176. https://doi.org/10.1002/cyto.a.20022

Mergner J, Frejno M, List M, Papacek M, Chen X, Chaudhary A, Samaras P, Richter S, Shikata H, Messerer M, et al. Mass-spectrometry-based draft of the Arabidopsis proteome. Nature. 2020:**579**(7799):409–414. https://doi.org/10.1038/s41586-020-2094-2

Muralidhara P, Weiste C, Collani S, Krischke M, Kreisz P, Draken J, Feil R, Mair A, Teige M, Müller MJ, et al. Perturbations in plant energy homeostasis prime lateral root initiation via SnRK1-bZIP63-ARF19 signaling. Proceedings of the National Academy of Sciences. 2021:**118**(37). https://doi.org/10.1073/pnas.2106961118

Nelson BK, Cai X, and Nebenführ A. A multicolored set of *in vivo* organelle markers for co-localization studies in Arabidopsis and other plants. The Plant Journal. 2007:**51**(6):1126–1136. https://doi.org/10.1111/j.1365-313X.2007.03212.x

Nunes C, Primavesi LF, Patel MK, Martinez-Barajas E, Powers SJ, Sagar R, Fevereiro PS, Davis BG, and Paul MJ. Inhibition of SnRK1 by metabolites: Tissue-dependent effects and cooperative inhibition by glucose 1-phosphate in combination with trehalose 6-phosphate. Plant Physiology and Biochemistry. 2013:**63**:89–98. https://doi.org/10.1016/j.plaphy.2012.11.011

Paul MJ, Watson A, and Griffiths CA. Linking fundamental science to crop improvement through understanding source and sink traits and their integration for yield enhancement. J Exp Bot. 2020:**71**(7):2270–2280. https://doi.org/10.1093/jxb/erz480

Pedrotti L, Weiste C, Nägele T, Wolf E, Lorenzin F, Dietrich K, Mair A, Weckwerth W, Teige M, Baena-González E, et al. Snf1-RELATED KINASE1-Controlled C/S $_1$ -bZIP Signaling Activates Alternative Mitochondrial Metabolic Pathways to Ensure Plant Survival in Extended Darkness. Plant Cell. 2018:**30**(2):495–509. https://doi.org/10.1105/tpc.17.00414

Peixoto B and Baena-González E. Management of plant central metabolism by SnRK1 protein kinases. J Exp Bot. 2022:**73**(20):7068–7082. https://doi.org/10.1093/jxb/erac261

Peixoto B, Moraes TA, Mengin V, Margalha L, Vicente R, Feil R, Höhne M, Sousa AGG, Lilue J, Stitt M, et al. Impact of the SnRK1 protein kinase on sucrose

homeostasis and the transcriptome during the diel cycle. Plant Physiol. 2021:**187**(3):1357–1373. https://doi.org/10.1093/plphys/kiab350

Rahmani F, Hummel M, Schuurmans J, Wiese-Klinkenberg A, Smeekens S, and Hanson J. Sucrose Control of Translation Mediated by an Upstream Open Reading Frame-Encoded Peptide. Plant Physiol. 2009:**150**(3):1356–1367. https://doi.org/10.1104/pp.109.136036

Ramon M, Dang TVT, Broeckx T, Hulsmans S, Crepin N, Sheen J, and Rolland F. Default Activation and Nuclear Translocation of the Plant Cellular Energy Sensor SnRK1 Regulate Metabolic Stress Responses and Development. Plant Cell. 2019:**31**(7):1614–1632. https://doi.org/10.1105/tpc.18.00500

Ramon M, De Smet I, Vandesteene L, Naudts M, Leyman B, Van Dijck P, Rolland F, Beeckman T, and Thevelein JM. Extensive expression regulation and lack of heterologous enzymatic activity of the Class II trehalose metabolism proteins from Arabidopsis thaliana. Plant Cell Environ. 2009. https://doi.org/10.1111/j.1365-3040.2009.01985.x

Rappsilber J, Mann M, and Ishihama Y. Protocol for micro-purification, enrichment, pre-fractionation and storage of peptides for proteomics using StageTips. Nat Protoc. 2007:**2**(8):1896–1906. https://doi.org/10.1038/nprot.2007.261

Sanagi M, Aoyama S, Kubo A, Lu Y, Sato Y, Ito S, Abe M, Mitsuda N, Ohme-Takagi M, Kiba T, et al. Low nitrogen conditions accelerate flowering by modulating the phosphorylation state of FLOWERING BHLH 4 in *Arabidopsis*. Proceedings of the National Academy of Sciences. 2021:**118**(19). https://doi.org/10.1073/pnas.2022942118

Schluepmann H, Pellny T, van Dijken A, Smeekens S, and Paul M. Trehalose 6-phosphate is indispensable for carbohydrate utilization and growth in Arabidopsis thaliana. Proceedings of the National Academy of Sciences. 2003. https://doi.org/10.1073/pnas.1132018100

Shen W, Reyes MI, and Hanley-Bowdoin L. Arabidopsis Protein Kinases GRIK1 and GRIK2 Specifically Activate SnRK1 by Phosphorylating Its Activation Loop. Plant Physiol. 2009:**150**(2):996–1005. https://doi.org/10.1104/pp.108.132787

Tian L, Xie Z, Lu C, Hao X, Wu S, Huang Y, Li D, and Chen L. The trehalose-6-phosphate synthase TPS5 negatively regulates ABA signaling in Arabidopsis thaliana. Plant Cell Rep. 2019:**38**(8):869–882. https://doi.org/10.1007/s00299-019-02408-y

Tsai AYL and Gazzarrini S. AKIN10 and FUSCA3 interact to control lateral organ development and phase transitions in Arabidopsis. Plant Journal. 2012. https://doi.org/10.1111/j.1365-313X.2011.04832.x

Tyanova S, Temu T, Sinitcyn P, Carlson A, Hein MY, Geiger T, Mann M, and Cox J. The Perseus computational platform for comprehensive analysis of (prote)omics data. Nat Methods. 2016:**13**(9):731–740. https://doi.org/10.1038/nmeth.3901

Vandesteene L, Ramon M, Le Roy K, Van Dijck P, and Rolland F. A single active trehalose-6-P synthase (TPS) and a family of putative regulatory TPS-like proteins in arabidopsis. Mol Plant. 2010. https://doi.org/10.1093/mp/ssp114

Van Leene J, Eeckhout D, Gadeyne A, Matthijs C, Han C, De Winne N, Persiau G, Van De Slijke E, Persyn F, Mertens T, et al. Mapping of the plant SnRK1 kinase signalling network reveals a key regulatory role for the class II T6P synthase-like proteins. Nat Plants. 2022:**8**(11):1245–1261. https://doi.org/10.1038/s41477-022-01269-w

Vizcaíno JA, Csordas A, del-Toro N, Dianes JA, Griss J, Lavidas I, Mayer G, Perez-Riverol Y, Reisinger F, Ternent T, et al. 2016 update of the PRIDE database and its related tools. Nucleic Acids Res. 2016:**44**(D1):D447–D456. https://doi.org/10.1093/nar/gkv1145

Vogel G, Fiehn O, Jean-Richard-dit-Bressel L, Boller T, Wiemken A, Aeschbacher RA, and Wingler A. Trehalose metabolism in Arabidopsis: occurrence of trehalose and molecular cloning and characterization of trehalose-6-phosphate synthase homologues. J Exp Bot. 2001:**52**(362):1817–1826. https://doi.org/10.1093/jexbot/52.362.1817

Weiste C, Pedrotti L, Selvanayagam J, Muralidhara P, Fröschel C, Novák O, Ljung K, Hanson J, and Dröge-Laser W. The Arabidopsis bZIP11 transcription factor links low-energy signalling to auxin-mediated control of primary root growth. PLoS Genet. 2017:**13**(2):e1006607. https://doi.org/10.1371/journal.pgen.1006607

Wiese A, Elzinga N, Wobbes B, and Smeekens S. A conserved upstream open reading frame mediates sucrose-induced repression of translation. Plant Cell. 2004:**16**(7):1717–29. https://doi.org/10.1105/tpc.019349

Xiang C, Han P, Lutziger I, Wang K, and Oliver DJ. A mini binary vector series for plant transformation. Plant Mol Biol. 1999:**40**(4):711–717. https://doi.org/10.1023/A:1006201910593

Yadav UP, Ivakov A, Feil R, Duan GY, Walther D, Giavalisco P, Piques M, Carillo P, Hubberten HM, Stitt M, et al. The sucrose-trehalose 6-phosphate (Tre6P) nexus: Specificity and mechanisms of sucrose signalling by. J Exp Bot. 2014. https://doi.org/10.1093/jxb/ert457

Zacharaki V, Ponnu J, Crepin N, Langenecker T, Hagmann J, Skorzinski N, Musialak-Lange M, Wahl V, Rolland F, and Schmid M. Impaired KIN10 function restores developmental defects in the *Arabidopsis trehalose 6-phosphate synthase1 (tps1)* mutant. New Phytologist. 2022:**235**(1):220–233. https://doi.org/10.1111/nph.18104

Zhai Z, Keereetaweep J, Liu H, Feil R, Lunn JE, and Shanklin J. Trehalose 6-Phosphate Positively Regulates Fatty Acid Synthesis by Stabilizing WRINKLED1. Plant Cell. 2018:**30**(10):2616–2627. https://doi.org/10.1105/tpc.18.00521

Zhang Y, Primavesi LF, Jhurreea D, Andralojc PJ, Mitchell RAC, Powers SJ, Schluepmann H, Delatte T, Wingler A, and Paul MJ. Inhibition of SNF1-Related Protein Kinase1 Activity and Regulation of Metabolic Pathways by Trehalose-6-Phosphate. Plant Physiol. 2009:**149**(4):1860–1871. https://doi.org/10.1104/pp.108.133934

3.7. Supplementary Information

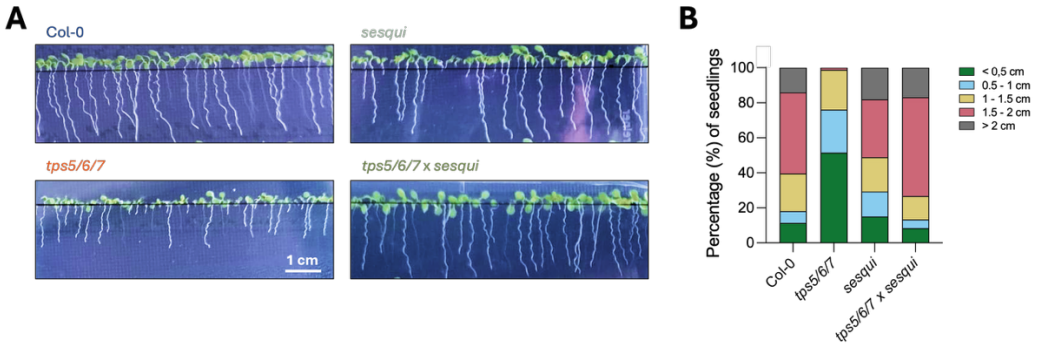

Supplementary Figure 3.1. Root growth variability in Col-0, *tps5/6/7*, *sesqui* and *tps5/6/7 x sesqui* seedlings.
(**A**) Representative images of 7-d old seedlings of Col-0, *tps5/6/7*, and segregating populations from *sesqui* and *tps5/6/7 x sesqui* mutants, grown vertically on 0.5× MS medium under long-day conditions (16 h light, 110 µmol m^{-2} s^{-1}, 22 °C / 8 h dark, 18 °C), prior to transfer for root growth assays. Scale bar 1 cm. (**B**) Quantification of the distributions of root lengths in seedlings shown in (A) (*n*=1; 133-163 seedlings per genotype). Each bar corresponds to a specific genotype, and the different colored segments represent the percentage of seedlings whose root lengths fall within defined intervals: < 0.5 cm (green), ≥ 0.5 and < 1 cm (blue), ≥ 1 and < 1.5 cm (yellow), ≥ 1.5 and < 2 cm (pink), ≥ 2 cm (grey).

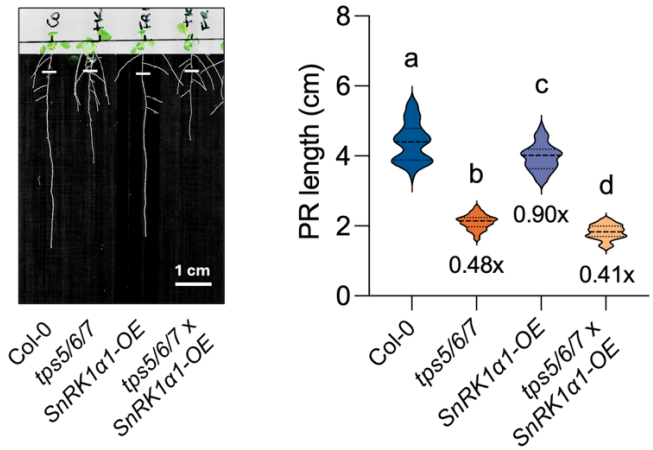

Supplementary Figure 3.2. Impact of *SnRK1α1* overexpression on root growth in the *tps5/6/7* background.
Left, representative images of 14-d old Col-0, *tps5/6/7*, *SnRK1α1-OE* and *tps5/6/7 x SnRK1α1-OE* seedlings grown vertically on 0.5× MS medium for 7 d and transferred to fresh 0.5× MS plates for 7 d. Scale bar 1 cm. *Right*, quantification of PR length, measured from the white mark to the root tip (*n*=3; 38-56 seedlings per genotype). The upper and lower horizontal lines represent the first and third quartiles, respectively. The middle horizontal dashed line indicates the median. Different letters indicate statistically significant differences between genotypes ($p<0.05$, one-way ANOVA with Tukey HSD test).

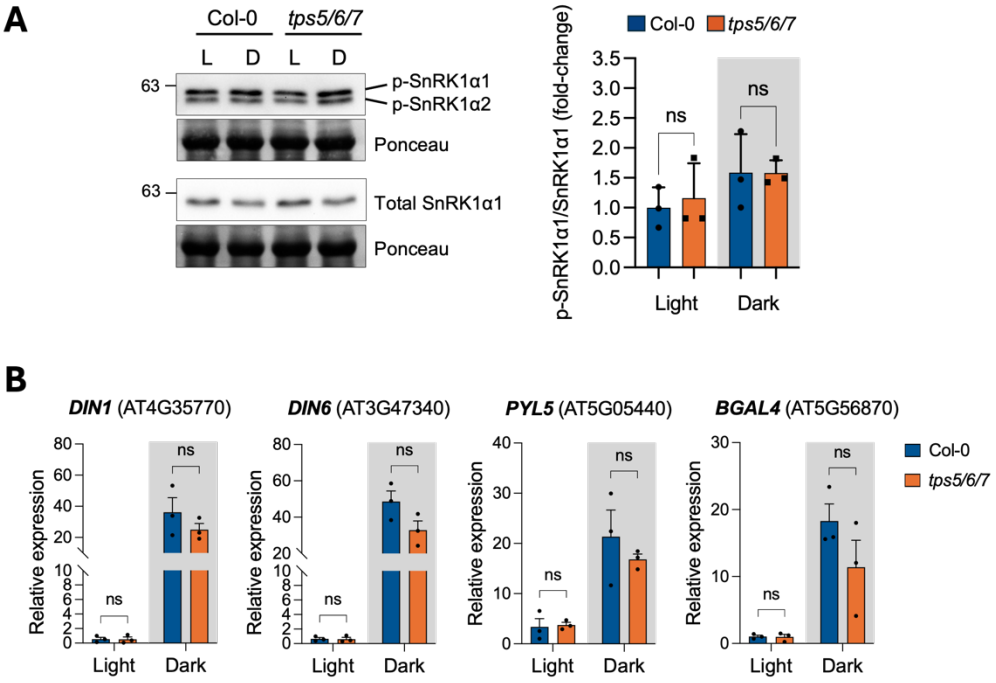

Supplementary Figure 3.3. Impact of TPS5/6/7 depletion on SnRK1α1 T-loop phosphorylation and on the basal expression of SnRK1-regulated genes.
(**A**) *Left*, Representative immunoblots showing SnRK1α T-loop phosphorylation (p-SnRK1α1 and p-SnRK1α2) and total SnRK1α1 levels detected, respectively, with anti-phosphoAMPK (p-AMPK) and anti-SnRK1α1 antibodies. Proteins were extracted from 14d-old Col-0 and *tps5/6/7* seedlings, either maintained in the light (L) or transferred to darkness (D) at ZT2 for 4 h and harvested at ZT6. *Right*, Quantification of SnRK1α1 T-loop phosphorylation, presented as the p-SnRK1α1/SnRK1α1 ratio. Bars show the mean of 3 independent experiments (error bars, SD). Asterisks indicate significant differences between genotypes (p<0.05; two tailed unpaired t-test). (**B**) qPCR analysis of *DIN1*, *DIN6*, *PYL5* and *BGAL4* expression in 14d-old Col-0 and *tps5/6/7* seedlings, either maintained in the light (L) or transferred to darkness (D) at ZT3 for 5 h and harvested at ZT8. Values denote expression relative to the ZT8 time point (light) of the Col-0 line. Bars show the mean of 3 independent experiments (error bars, SEM). Asterisks indicate significant differences between genotypes (p<0.05; two tailed unpaired t-test).

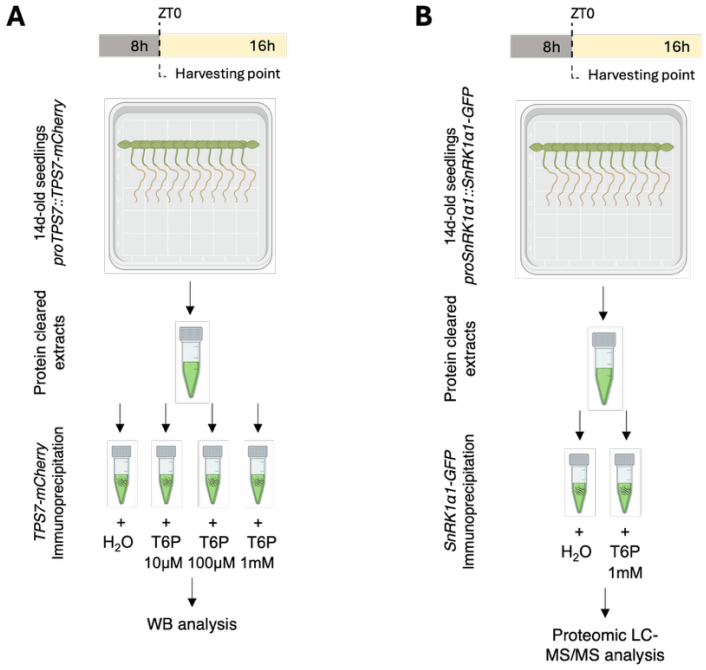

Supplementary Figure 3.4. Experimental set-up for assessing the TPS7-SnRK1α1 interaction.
Cleared protein extracts from 14d-old *proTPS7::TPS7-mCherry* (**A**) or *proSnRK1α1::SnRK1α1-GFP* (**B**) seedlings, harvested at EN, were aliquoted and incubated with ChromoTek RFP- or GFP-Trap® Magnetic Agarose beads, respectively, in the absence (H_2O control) or presence of the indicated concentrations of T6P. (**A**) Immunoprecipitated mCherry-tagged TPS7 and co-immunoprecipitated SnRK1α1 were assessed by immunodetection (Figure 3.4A-B). (**B**) Proteins interacting with GFP-tagged SnRK1α1 were identified by MS/MS analyses (Figure 3.4C). Created with Biorender.com.

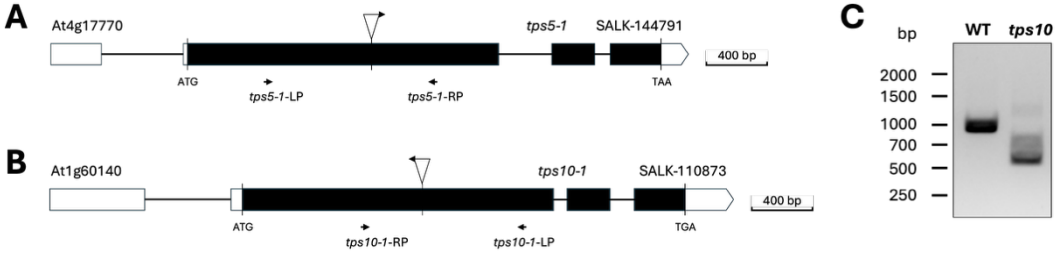

Supplementary Figure 3.5. *tps5* and *tps10* T-DNA insertional mutants.
Schematic representation of the insertion sites of the *tps5* (**A**) and *tps10* (**B**) T-DNA mutants used in this study. The ATG start codon and TAA/TGA stop codons are indicated. Exons are shown as black boxes, introns as black lines, and the T-DNA insertion site as a triangle above the gene diagram. Scale bar: 400 bp. (**C**) Confirmation of *tps10* mutant identity by genotyping using T-DNA left border and gene-specific primers (LP and RP, indicated in **B**). The *tps5* mutant was previously described (Tian et al., 2019).

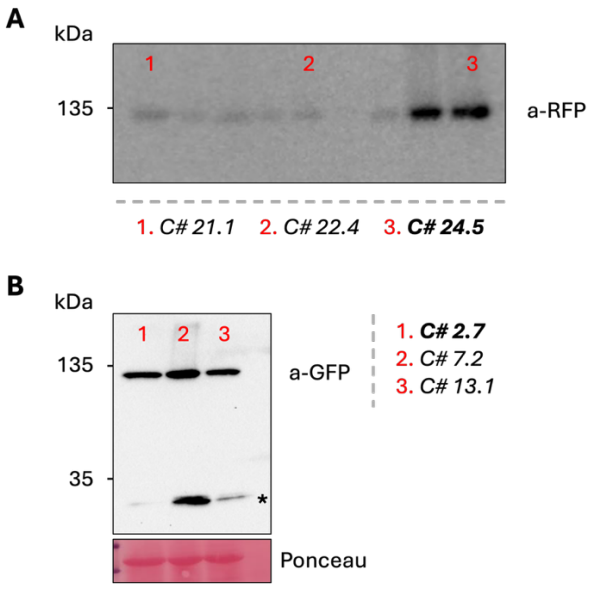

Supplementary Figure 3.6. Levels of TPS5 in *proTPS5::TPS5-mCherry* and TPS10 in *proTPS10::TPS10-mTurquoise* plants.
(**A**) Immunoblot detection of TPS5-mCherry in *proTPS5::TPS5-mCherry* complementation lines (*C#21.1*, *C#22.4*, *C#24.5*). (**B**) Immunoblot detection of TPS10-mTurquoise in *proTPS10::TPS10-mTurquoise lines* (*C#2.7*, *C#7.2*, *C#13.1*). Anti-RFP and anti-GFP antibodies were used to detect the respective fusion proteins. The asterisk in (**B**) marks degradation products, likely free mTurquoise. Lines in bold (*C#24.5* for TPS5 and *C#2.7* for TPS10) were used for TPS-SnRK1α1 interaction analyses (Figure 3.4D).

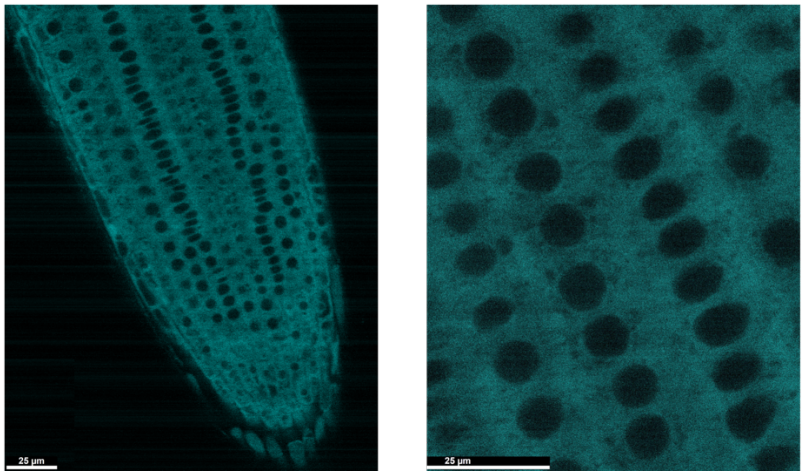

Supplementary Figure 3.7. Subcellular localization of TPS7-mCherry.
Representative fluorescence microscopy images of the root meristem of Arabidopsis seedlings stably expressing *TPS7-mCherry* (line C#6.3). Scale bar: 25 µm.

Supplementary Table 3.1. Primers, Plant lines and Antibodies.
List of all primers, plant lines and antibodies used in this study.

Supplementary Table 3.1. Primers, Plant lines and Antibodies			
Genotyping primers	**Name**	**Sequence (5' => 3')**	
tps5-1 (SALK-144791)	*tps5-1*-LP	TGATCGTTCTTTATGGCAAGC	
	tps5-1-RP	GCATTTGCTTCTCTGCTTCTG	
tps6-1 (GK-362A03)	*tps6-1*-LP	TGCATCAGCTACTGCATCAAC	
	tps6-1-RP	AGTGTGTGCCTACGTTTTTGC	
tps7-1 (GK-341E02)	*tps7-1*-LP	TTCACTGCCTGACCACCTAAG	
	tps7-1-RP	GCTGGAGTATTACGGGAGGAC	
tps10-1 (SALK-110873)	*tps10-1*-LP	TTGCTCTCTTGCTCGATCTTC	
	tps10-1-RP	TGTCATGCTGCTGTAGAATGC	
snrk1α1-3 (GABI_579_E09)	*snrk1α1-3*-LP	CCAGCATAATAGAGAACGAAGC	
	snrk1α1-3-RP	TTGACCCATCAAATAATACACGAA	
snrk1α2-2 (WiscDsLox384F5)	*snrk1α2-2*-LP	CGTAGTGATCCACATGTGCAG	
	snrk1α2-2-RP	GATTGCAGACTTTGGGTTGAG	
T-DNA primer SALK	LBb1.3	ATTTTGCCGATTTCGGAAC	
T-DNA primer GABI-Kat	o8409 (GABI LB)	ATATTGACCATCATACTCATTGC	
T-DNA primer WISC	T-DNA-Wis	AACGTCCGCAATGTGTTATTAAGTTGTC	
Cloning primers	**Name**	**Sequence (5' => 3')**	**Description**
proTPS5::gTPS5-mCherry	pCB302_5_C_Fw	TCGCCGGAGTGGGCTGCAGGAATTCCCG	Cloning to pCB302 vector
	pCB302_5_C_Rev	TGCAGTTACTGGGGGATCCACTAGTTCTAGAG	
	ProTPS5_C_Fw	TGGATCCCCCAGTAACTGCAGTAGTTAAG	
	ProTPS5+gTPS5_C_Rev	CCTTGCTCACAAACAGATCTTTAGTTGGAAC	
	mCherry_C_Fw	AGATCTGTTTGTGAGCAAGGGCGAGGAG	
	mCherry_C_Rev	TCACAAATCCTTACTTGTACAGCTCGTCCATG	
	TermTPS5_C_Fw	GTACAAGTAAGGATTTGTGAACGAAAGTTTTAGTG	
	TermTPS5_C_Rev	CCTGCAGCCCACTCCGGCGATACGGATTC	
proTPS10::gTPS10-mTurquoise	pCB302_10_C_Fw	CCCGACGATCGGGCTGCAGGAATTCCCG	Cloning to pCB302 vector
	pCB302_10_C_Rev	AACAATCAAAGGGGGATCCACTAGTTCTAGAG	
	ProTPS10_C_Fw	TGGATCCCCCTTTGATTGTTTGTTTTACTATTTTTTTTATCGAC	
	ProTPS10+gTPS10_C_Rev	CCTTGCTCACTACCACGCTTTCGAAGGAG	
	mTurquoise_C_Fw	AAGCGTGGTAGTGAGCAAGGGCGAGGAG	
	mTurquoise_C_Rev	CTCTGATTTCTTACTTGTACAGCTCGTCCATG	
	TermTPS10_C_Fw	GTACAAGTAAGAAATCAGAGATCAACGGGG	
	TermTPS10_C_Rev	CCTGCAGCCCGATCGTCGGGTTCCATGG	
qRT-PCR primers	**Name**	**Sequence (5' => 3')**	
DIN1	FqDIN1	CAGAGTCGGATCAGGAATGG	
	RqDIN1	ATTTGACCGCTCTCACAACC	
DIN6	FqDIN6	AACTTGTCGCAAGATCAAGG	
	RqDIN6	GGAACACGTGCCTCTAGTCC	
PYL5	FqPYL5	GGTCACCGGTGCAACTCC	
	RqPYL5	CGCGTGGATCATCTGCACC	
BGAL4	FqBGAL4	CAAGAAGATGCTCCTGGTCC	
	RqBGAL4	AGCTCCAAGCGATGTAACGG	
UBC21	FqUBC21	CTGCGACTCAGGGAATCTTCTAA	
	RqUBC21	TTGTGCCATTGAATTGAACCC	
UBQ10	FqUBQ10	GGCCTTGTATAATCCCTGATGAATAAG	
	RqUBQ10	AAAGAGATAACAGGAACGGAAACATAGT	

Supplementary Table 3.1. Primers, Plant lines and Antibodies

Plant line	Line ID	Reference
tps5-1	SALK_144791	Tian et al., 2019 Plant Cell Reports
tps6-1	GK-362A03	This study
tps7-1	GK-341E02	This study
tps10-1	SALK_110873	This study
tps5/7	SALK_144791/GK-341E02	This study
tps5/6/7	SALK_144791/GK-362A03/GK-341E02	This study
TPS5-mCherry	*proTPS5::gTPS5-mCherry* (SALK_144791 background)	This study
TPS7-mCherry	*proTPS7::gTPS7-mCherry* (GK-341E02 background)	This study
TPS10-mTurquoise	*proTPS10::gTPS10-mTurquoise* (SALK_110873 background)	This study
snrk1α1-3	GABI_579E09	Mair et al., 2015 eLife
tps7/snrk1α1-3	GK-341E02/GABI_579E09	This study
tps5/7/snrk1α1-3	SALK_144791/GK-341E02/GABI_579E09	This study
tps5/6/7/snrk1α1-3	SALK_144791/GK-362A03/GK-341E02/GABI_579E09	This study
sesquia2	GABI_579E09 (-/-) x WiscDsLox384F5 (+/-)	Belda-Palazón et al., 2020 Nature Plants
tps5/6/7/sesquia2	SALK_144791/GK-362A03/GK-341E02/GABI_579E09 (-/-) x WiscDsLox384F5 (+/-)	This study
SnRK1α1-OE	*35S::SnRK1α1*	Jossier et al., 2009
tps7/SnRK1α1-OE	GK-341E02/*35S::SnRK1α1*	This study
tps5/6/7/SnRK1α1-OE	SALK_144791/GK-362A03/GK-341E02/*35S::SnRK1α1*	This study
NLS-ACC	*pro35S:NLS-ratAcc-GFP-2xHA*	Muralidhara et al., 2021 PNAS
tps5/6/7/NLS-ACC	SALK_144791/GK-362A03/GK-341E02/pro35S:NLS-ratAcc-GFP-2xHA	This study
SnRK1α1-GFP	*ProSnRK1α1::gSnRK1α1-GFP::terSnRK1α1*	Crozet et al., 2016 The Plant Journal
tps5/6/7/SnRK1α1-GFP	*SALK_144791/GK-362A03/GK-341E02/ProSnRK1α1::gSnRK1α1-GFP::terSnRK1α1*	This study

Supplementary Table 3.1. Primers, Plant lines and Antibodies

Antibody - short name	Antibody - full description	Source	Company	Product number		Dilution	Dilution buffer
Anti-p-ACC	Anti Phospho-Acetyl-CoA Carboxylase (Ser79)	Commercial	Cell Signaling	#3661	Rabbit polyclonal	1:1000	1% (w/v) non-fat dry milk in 1x TBS
Anti-GFP	GFP Mouse IgG Monoclonal Antibody	Commercial	Roche	11814460001	Mouse monoclonal	1:1000	1% (w/v) non-fat dry milk in 1x TBS
Anti-RFP	RFP Mouse IgG2c Monoclonal Antibody	Commercial	Chromotek	[6G6]	Mouse monoclonal	1:1000	1% (w/v) non-fat dry milk in 1x TBS
Anti-SnRK1α1	Anti-SnRK1α1	Custom-made	Cocalico	Belda-Palazón et al., 2020 Nature Plants	Rabbit polyclonal	1:4000	1% (w/v) non-fat dry milk in 1x TBS
Anti-p(T172)-AMPKα	Anti Phospho-AMPKalpha (Thr172) (40H9)	Commercial	Cell Signaling	#2535	Rabbit monoclonal	1:1000	5% (w/v) BSA in 1x TBS
Anti-rabbit	Peroxidase Affinipure goat anti-rabbit IgG	Commercial	Jackson Immuno Research	111035144	Goat polyclonal	1:10000	1% (w/v) non-fat dry milk in 1x TBS
Anti-mouse	Peroxidase Affinipure goat anti-mouse IgG	Commercial	Jackson Immuno Research	115035146	Goat polyclonal	1:10000	1% (w/v) non-fat dry milk in 1x TBS

CHAPTER 4

General Discussion and Future Perspectives.

4.1. TPS5/6/7 proteins are novel regulators of the SnRK1 kinase

Sugar homeostasis underpins metabolic and energetic stability across all domains of life. This is especially critical for sessile autotrophs like plants, which must continuously balance photosynthetic carbon production in source tissues with the heterotrophic demands of non-photosynthetic organs, while simultaneously adapting to fluctuating environmental conditions (Smith and Stitt 2007). In most plants, sucrose serves as both the principal end-product of photosynthesis and the primary transported form of carbon and energy, distributed via the phloem from source to sink tissues where it fuels biosynthetic processes and growth (Lunn 2016). The coordinated regulation of sucrose production, transport, storage and utilization relies on sophisticated sensing mechanisms that monitor and respond to sucrose availability throughout the plant (Smith and Stitt 2007; Miret et al. 2024). Among these mechanisms, trehalose 6-phosphate (T6P) has emerged as a pivotal signaling metabolite that not only reflects the internal sucrose status but also actively regulates sucrose levels (Yadav et al. 2014; Figueroa and Lunn 2016; Baena-González and Lunn 2020), thereby profoundly influencing metabolism, growth, and development (Fichtner and Lunn 2021; Göbel and Fichtner 2023). T6P exerts its regulatory influence, in part, by inhibiting the conserved energy-sensing kinase SNF1-related protein kinase 1 (SnRK1) (Zhang et al. 2009; Nunes et al. 2013; Zhai et al. 2018; Avidan et al. 2024; Blanford et al. 2024). In actively growing tissues, sucrose-driven T6P accumulation inhibits the catalytic activity of SnRK1, relieving its repression of anabolic processes and enabling resource investment in growth and development. Conversely, when sucrose is limited, falling T6P levels lift SnRK1 inhibition, enabling the kinase to activate catabolic pathways that mobilize energy reserves while simultaneously restraining energy-intensive growth (Baena-González and Lunn 2020). Despite robust evidence for T6P-dependent SnRK1 regulation, the precise molecular mechanisms of T6P perception and subsequent SnRK1 inhibition remain unresolved.

In this thesis, I identified a group of catalytically inactive T6P synthase (TPS) proteins, TPS5/6/7, as essential mediators of T6P-dependent regulation of SnRK1 activity. Arabidopsis plants lacking TPS5/6/7 exhibit modified growth and development including severe root growth defects and delayed flowering, alongside a complex metabolic signature consistent with impaired sugar utilization and defective T6P signaling. My work further indicates that these phenotypes stem from aberrant SnRK1 activity in the absence of TPS5/6/7, as they are rescued by the loss of SnRK1 function. Crucially, I demonstrated that T6P enhances the physical interaction between TPS-II proteins and SnRK1 in a highly specific and dose-dependent manner. Together, these findings support a model in which TPS5/6/7 may act as T6P sensors, inhibiting SnRK1 activity under sucrose-replete conditions to promote biosynthetic processes and growth.

4.2. The TPS5/6/7-SnRK1 axis regulates plant growth and development

Plant growth and development, driven by the generation of new cells and cellular growth and modification of existing ones, are resource and energetically demanding processes that require tight coordination between sugar/energy sensing pathways to ensure adequate resource allocation (Amthor et al. 2019; Fernie et al. 2020). Multiple lines of evidence indicate that T6P and SnRK1 antagonistically regulate plant growth and development, with elevated T6P levels and reduced SnRK1 activity being required to activate biosynthetic processes and growth in response to sucrose availability (Göbel and Fichtner 2023).

In Chapter 2, we showed that loss of TPS7, or combined loss of TPS5/7 or TPS5/6/7, delays flowering and reduces primary root growth, with the *tps5/6/7* mutant exhibiting the most severe phenotypes, despite accumulating substantially higher levels of T6P and sucrose than Col-0. In Chapter 3, we demonstrated that the flowering delays in *tps7* and *tps5/7* mutants were fully rescued by loss of SnRK1α1, while the root growth defects of the *tps5/6/7* mutant were nearly fully rescued by the *sesquiα*

mutation (*snrk1α1*$^{-/-}$*/snrk1α2*$^{-/+}$*).* Due to time constraints, we were unable to assess whether the flowering phenotype in *tps5/6/7* is alleviated by the *snrk1α1* or *sesquiα* mutations, making this an important question for future investigation. In any case, these findings suggest that T6P is unable to exert its growth-promoting effects in the absence of TPS5/6/7, and that SnRK1 operates downstream of these proteins. The persistence of growth and developmental defects despite elevated T6P levels implies that SnRK1 becomes unresponsive to T6P in the *tps5/6/7* mutant, and that the unchecked SnRK1 activity is a primary driver of the observed phenotypes. Notably, a recent study showed that *snrk1α1* alleles harboring mutations in the catalytic domain C-lobe can rescue both flowering and embryogenesis defects in *tps1-2* plants (Zacharaki et al. 2022). This further supports the idea that a lack of T6P – real, as in *tps1-2*, or perceived, as in *tps5/6/7* mutants – leads to aberrant SnRK1 activity that ultimately suppresses growth and development.

Importantly, despite the near-complete rescue of root growth defects in the *tps5/6/7* mutant by the *sesquiα* mutations, residual growth inhibition suggests that either additional SnRK1-independent mechanisms contribute to the phenotype, or that full suppression of SnRK1 activity may require the complete loss of both SnRK1α1 and SnRK1α2. Nonetheless, we were unable to retrieve a viable *tps5/6/7/snrk1α1*$^{-/-}$ */snrk1α2*$^{-/-}$ mutant, consistent with previous reports that complete loss of both catalytic α-subunits of SnRK1 is not viable (Baena-González et al. 2007) and may be embryo lethal (Ramon et al. 2019). This finding reinforces the idea that while SnRK1α acts predominantly as a growth repressor under conditions of energy limitation, it is nevertheless also essential for normal plant growth (Margalha et al. 2019; Baena-González and Lunn 2020).

Although my findings provide compelling evidence for the involvement of TPS-II proteins in the T6P-dependent regulation of SnRK1, including the observation that T6P promotes the physical interaction between TPS-II proteins and SnRK1α1, further experiments are needed to determine whether this effect is mediated by direct binding of T6P to the TPS-II proteins themselves, to SnRK1, or to both. In particular, it remains to be established whether T6P interacts with the conserved, predicted T6P-binding

residues within the phosphatase-like domain of Class II TPS proteins (Lunn 2007). This could be tested, for example, using microscale thermophoresis to assess direct binding between T6P and fluorescently labeled TPS-II proteins – either wild-type or variants carrying point mutations in the predicted T6P-binding residues. If TPS-II proteins do bind T6P, the anticipated dissociation constant (Kd) for wild-type proteins would likely fall within the low to mid micromolar range, consistent with the known affinity of SnRK1α for T6P (32 ± 6 μM) (Zhai et al. 2018) and the physiological T6P concentrations in plant cells (Lunn et al. 2006). In contrast, if the predicted residues are essential for T6P recognition, point mutations at these positions would be expected to abolish binding or cause a substantial reduction in affinity (e.g., a markedly higher Kd), thereby supporting their role in T6P sensing. However, it is also possible that these predicted residues do not represent the actual T6P-binding interface in TPS-II proteins. Thus, structure-guided mutagenesis, informed by *in silico* docking approaches (e.g., CHAI Discovery), could help identify alternative binding pockets and refine the design of binding assays.

Provided that T6P binding and the implicated residues are demonstrated, subsequent experiments should determine whether disrupting this interaction also abrogates the association between TPS-II proteins and SnRK1, and whether this, in turn, affects SnRK1 activity, as T6P-dependent binding might occur for functions unrelated to SnRK1 regulation. This could be explored using co-immunoprecipitation (Co-IP) assays with either in vitro-synthesized or transiently expressed TPS-II proteins – both wild-type and T6P-binding-deficient variants – in the presence and absence of T6P, to assess whether disruption of T6P binding impairs their physical association with SnRK1. To determine whether such impaired interaction translates into altered SnRK1 activity*, in vitro* kinase assays could be conducted using recombinant SnRK1 and a known substrate such as the AMARA peptide (Jossier et al. 2009), in the presence of wild-type or mutant TPS-II proteins across a physiological T6P concentration gradient. If TPS-II proteins function as T6P-dependent regulators of SnRK1, one would expect wild-type TPS-II to modulate SnRK1 activity in a T6P-responsive manner, whereas mutants deficient in T6P binding should fail to do so. Additionally, to establish physiological relevance, T6P-binding-deficient TPS5/6/7

variants should be introduced into *tps5/6/7* mutant plants to assess their ability to rescue the developmental and metabolic defects. Failure of these variants to complement the mutant phenotypes, together with the biochemical evidence, would provide conclusive proof that T6P perception by TPS-II proteins is mechanistically required for SnRK1 inhibition and essential for their in vivo function.

Alternatively, it is possible that T6P binding to SnRK1 itself promotes interaction with TPS-II proteins. For example, if TPS-II proteins exhibit significantly weaker T6P binding than SnRK1 (i.e., a higher Kd) or continue to interact with SnRK1 despite mutations disrupting T6P binding, this would suggest that T6P-induced conformational changes in SnRK1, rather than direct T6P binding to TPS-II, drive complex formation. To explore this possibility, a similar mutagenesis approach could be applied to SnRK1, targeting residues previously identified as essential for T6P binding (Blanford et al. 2024). Generating T6P-binding-deficient SnRK1 variants would allow reciprocal experiments to test whether T6P-mediated interactions with TPS-II proteins require T6P recognition by one or both partners. If these SnRK1 mutants fail to interact with TPS-II in the presence of T6P, or exhibit altered T6P-sensitive kinase activity, it would support the model that T6P acts as a molecular bridge coordinating the interaction and regulatory function of TPS-II and SnRK1.

Finally, while C-terminally tagged TPS7-mCherry fully complemented the *tps7* mutant, the N-terminal mCherry-TPS7 fusion only partially restored the mutant's delayed flowering phenotype. This suggests that the N-terminal tag interferes with TPS7 function, potentially by reducing its interaction with SnRK1. However, although cross-linking MS/MS experiments have revealed the TPS7 and SnRK1α residues involved in the interaction (Van Leene et al. 2022), it is unclear how this might be altered by the N-terminal tag. Furthermore, it is unclear whether these interactions induce changes in SnRK1 activity e.g. by blocking substrate access, stabilizing an autoinhibited state or other. As such, future structural predictions and molecular docking simulations combined with functional complementation assays, using truncated or domain-specific versions of TPS-IIs, will be instrumental in identifying the regions necessary for SnRK1 interaction and regulatory function.

4.3. The *tps5/6/7* metabolic phenotype: a product of SnRK1 misregulation and maladaptive compensation

T6P is indispensable for sucrose utilization and growth in actively growing tissues of *Arabidopsis thaliana* (Schluepmann et al. 2003). In addition to this role, T6P significantly influences photoassimilate partitioning, with inducible increases in T6P during the day redirecting carbon flux from sucrose production toward the synthesis of organic and amino acids (Figueroa et al. 2016; Avidan et al. 2023, 2024). It also inhibits starch mobilization at night, thereby tuning carbon export from the leaf to match the nocturnal demand for sucrose to support growth (Martins et al. 2013; dos Anjos et al. 2018; Ishihara et al. 2022). Through these coordinated actions, T6P integrates central carbon and nitrogen metabolism, maintaining sucrose homeostasis while providing key biosynthetic precursors required for cell division and expansion (Fichtner et al. 2017).

Our results show that loss of TPS5/6/7 leads to the accumulation of sucrose, T6P, and other soluble sugars, accompanied by a general depletion of amino acids. These metabolic imbalances are further exacerbated under conditions that enhance carbon availability, such as higher light intensities. In contrast, changes in glycolytic intermediates are relatively minor, while alterations in organic acids are more complex, generally elevated in shoots but reduced in roots tips. Intriguingly, these patterns deviate from the expected metabolic signature of elevated T6P (as described above), and the responses of *tps5/6/7* to increased carbon availability, whether through high light or sucrose supplementation, do not consistently align with those observed in Col-0. While in Col-0 increased carbon availability promotes growth, sugar levels remain relatively stable, and branched-chain and other amino acids increase. In the *tps5/6/7* mutant, on the other hand, increased carbon availability does not promote growth and leads to sugar hyperaccumulation and amino acid depletion. Surprisingly, and despite the marked rescue of *tps5/6/7* growth defects by the *snrk1α* loss-of-function mutations, the metabolic profile of the mutant does not correspond to a typical starvation response either, where an overall depletion of carbon reserves activates

SnRK1 (Baena-González et al. 2007; Mair et al. 2015; Nukarinen et al. 2016; Pedrotti et al. 2018; Ramon et al. 2019). Consistent with this, BCAA levels are reduced in the mutant, rather than elevated as would be expected when SnRK1 drives their accumulation through protein degradation for subsequent catabolism as alternative energy substrates (Gibon et al. 2006; Chen et al. 2017; Pedrotti et al. 2018; Huang et al. 2019). While seemingly contradictory, these results likely reflect a far more complex regulatory landscape, in which the loss of TPS5/6/7 uncouples T6P-dependent sugar sensing from SnRK1 activity – consistent with the enhanced interaction between TPS-IIs and SnRK1 by T6P – while leaving other sugar-responsive pathways operational. This leads to an atypical metabolic state that diverges from both canonical T6P- and SnRK1-mediated responses, making it difficult to disentangle primary effects from secondary or compensatory changes.

In any case, the observed metabolic and phenotypic features of *tps5/6/7* strongly suggest that the primary effects stem from disrupted coordination between sucrose availability and its utilization, likely due to SnRK1 imposing a growth brake. Consequently, sucrose produced throughout the day accumulates but is not effectively consumed, leading to elevated T6P levels. Increased T6P, paradoxically, might also negatively impact plant growth, despite its usual role as a growth-promoting signal (Schluepmann et al. 2012). For example, seedlings grown on trehalose-supplemented media exhibit growth arrest due to a tenfold accumulation of T6P, a phenotype that can be reversed by expressing an *E. coli* T6P-hydrolase to break down the excess T6P (Schluepmann et al. 2004). In this context, the growth impairment was later attributed to T6P-mediated inhibition of SnRK1 activity, as seedlings overexpressing SnRK1α1 were able to grow on trehalose-supplemented media (Delatte et al. 2011). In *tps5/6/7*, however, growth impairment is exacerbated by SnRK1α1 overexpression and rescued by SnRK1 loss, indicating that aberrant SnRK1 activity, rather than its inhibition by T6P, drives the growth defects.

Another example where excessive T6P has been reported to impair growth comes from transgenic potato plants expressing the *E. coli OtsA* gene specifically in their tubers (Debast et al. 2011). Notably, the reduction in tuber yield was

accompanied by increased respiration rates, suggestive of high metabolic activity (Debast et al. 2011). This raises the possibility that the increased respiration observed in *tps5/6/7*, as indicated by higher O_2 consumption rates, may partly result from the elevated T6P levels in the mutant. The high abundance of other sugars may further contribute to this, as night-time leaf respiration in wheat, pea, and spinach has been shown to correlate strongly with carbohydrate concentrations accumulated during the preceding photoperiod (Azcón-Bieto et al. 1983). However, increased O_2 consumption in the *tps5/6/7* mutant was also observed after 24 hours of darkness, when T6P and sugar levels are presumably much lower. Together with the observation that the respiratory response to sucrose is less pronounced in *tps5/6/7* compared to Col-0, this suggests that alternative pathways for energy production (e.g. BCAA catabolism) might be activated in the mutant (see Section 2.4.3 for more details). While highly speculative, if all these mechanisms converge in an uncoordinated manner, it could result in a surplus of respiratory substrates and potential over-reduction of the mitochondrial electron transport chain. Consequently, this may increase single-electron leakage, thereby promoting reactive oxygen species (ROS) formation and ultimately causing cellular damage (Rhoads et al. 2006). Although we currently lack direct evidence to confirm this scenario, the observed accumulation of proline, GABA, and dehydroascorbate in the *tps5/6/7* mutant (Supplementary Table 2.1) is consistent with the activation of antioxidant defense mechanisms aimed at mitigating ROS accumulation and oxidative stress (Hasanuzzaman et al. 2019; Khan et al. 2021; Renzetti et al. 2024). This hypothetical scenario illustrates how elevated sugars, increased T6P, and dysregulated SnRK1 activity could interact maladaptively, generating a metabolically imbalanced state that culminates in allostatic overload – a condition where the cumulative burden of compensatory responses and unresolved primary defects further exacerbates the impairment of growth (Goldstein and McEwen 2002; McEwen and Wingfield 2003; McEwen 2004; Sonmez et al. 2023).

Such maladaptive interactions might also underlie the altered regulation of PEPC and NR in the *tps5/6/7* mutant. Work from Figueroa et al. (2016) demonstrated that a transient rise in T6P triggers the post-translational activation of PEPC and NR. However, in *tps5/6/7*, the phosphorylation status of PEPC in roots and, to some extent,

the activation state of NR in shoots do not align with the expected effects associated with elevated T6P. In the case of NR, a 3.5-fold increase in T6P levels was shown to enhance NR activity by 42% at ZT6 (Figueroa et al. 2016). By comparison, NR activity in *tps5/6/7* rosettes increased by only 9% at the same time point. Although direct comparison is limited by the absence of T6P measurements for *tps5/6/7* rosettes, T6P levels in shoots of *tps5/6/7* seedlings at the EN are already 1.8-fold higher than those in Col-0, with this difference presumably increasing during photosynthetic activity. If so, this may indicate a diminished sensitivity of NR to T6P in the mutant, resulting in weaker activation than expected, though still higher than that observed in Col-0. One possible explanation for this attenuated response is that the effects of T6P on NR may be partially mediated through SnRK1. While SnRK1 phosphorylates NR and facilitates its binding to 14-3-3 proteins, leading to NR inactivation (McMichael Jr et al. 1995; Moorhead et al. 1996), elevated carbohydrate levels in the mutant likely counteract this inhibition, as sugars are known to stimulate NR activity (Kaiser et al. 2002; Iglesias-Bartolomé et al. 2004). Moreover, hexose phosphates may inhibit SnRK1 activity independently of T6P, as supported by both *in vitro* and correlative *in vivo* evidence (Nunes et al. 2013; Avidan et al. 2023). Therefore, sugars could regulate NR activity through both SnRK1-dependent and -independent mechanisms, which may explain the complex and attenuated NR activation observed in the mutant.

For PEPC, a direct connection to SnRK1 remains less clearly established. Nonetheless, the high Ser^{11} phosphorylation of PEPC in an inducible *snrk1α1/α2* mutant (Nukarinen et al. 2016) suggests that either PEPC itself or its upstream kinase (PEPCK) may be subject to inhibition by SnRK1. This is consistent with the reduced Ser^{11} phosphorylation of PEPC in the *tps5/6/7* mutant. Such control could potentially disturb the carbon flux between glycolysis and the TCA cycle, thereby increasing dependence on alternative carbon sources like amino acids.

Collectively, these interpretations represent our working framework for reconciling the complex metabolic and physiological phenotypes of the *tps5/6/7* mutant. However, caution is needed, given that the current data capture only a single time point at the end of the night (EN), which limits our ability to fully understand the

temporal dynamics of the mutant's metabolism. Given the well-established diurnal regulation of central metabolites and signaling pathways, it is possible that the differences observed at EN reflect time-specific effects rather than general metabolic defects. For example, the reduced BCAA levels observed in the *tps5/6/7* mutant at EN might result from diminished nuclear SnRK1 activity at that specific time – as SnRK1 promotes the expression of genes involved in BCAA catabolism (Pedrotti et al. 2018) – rather than reflecting a persistent depletion throughout the diel cycle. Similarly, the apparent depletion of other amino acids could stem from enhanced utilization or impaired synthesis during the night, with levels potentially recovering during the day due to light-driven nitrogen assimilation (reviewed in Sathee et al. 2025). Furthermore, T6P levels are typically low at EN and peak late in the light period, when T6P-mediated inhibition of SnRK1 activity is presumably more pronounced (Peixoto et al. 2021; Avidan et al. 2023). Consequently, direct effects of T6P on SnRK1 are likely stronger during the day, while observations made at EN may represent downstream or delayed metabolic consequences of altered SnRK1 activity earlier in the photoperiod. Thus, to obtain a more comprehensive understanding of the mutant's metabolic behavior, time-resolved metabolite profiling across the full day-night cycle will be essential.

Another important limitation of our study is that the rescue of the *tps5/6/7* growth phenotype by the *snrk1α* loss-of-function mutations has so far only been assessed at the phenotypic level, without examining the accompanying metabolic changes. As a result, it remains unclear whether the metabolic alterations observed in *tps5/6/7* plants, such as elevated respiration or changes in sugar and amino acid levels, are also reversed in the *tps5/6/7/sesquiα* mutant. For instance, the increased respiration rate in *tps5/6/7* could be independent of SnRK1 and instead be primarily driven by elevated T6P levels, as suggested by similar findings in *OtsA*-expressing potato tubers (Debast et al. 2011). If so, the growth rescue conferred by SnRK1 loss may not reflect a restoration of metabolic homeostasis, but rather the removal of a growth-repressive SnRK1 signal acting downstream of T6P. However, it is also possible that SnRK1 loss indirectly alters T6P accumulation (Peixoto et al. 2021), complicating interpretation of the metabolic rescue. Hence, future metabolic analyses should also include both *tps5/6/7* crosses with SnRK1 gain- and loss-of-function lines

and inducible SnRK1 manipulation in the mutant background to clarify the specific contributions of SnRK1 and T6P to these phenotypes and distinguish primary effects from secondary metabolic adaptations.

4.4. TPS5/6/7 impacts differently nuclear and non-nuclear SnRK1 functions

Recent proteomic analyses identified TPS-II proteins as SnRK1 interactors, with in vitro and transient assays further suggesting that they are negative regulators of SnRK1 (Van Leene et al. 2022). Here, we provide genetic validation of this relationship and demonstrate through immunoprecipitation assays that T6P enhances the binding of TPS-II proteins to SnRK1. Presumably, this enables plants to tailor SnRK1 activity to cellular carbohydrate levels, ensuring metabolic responses and growth align with carbon availability. Intriguingly, despite the expectation that loss of TPS5/6/7 would uniformly enhance SnRK1 activity, the emerging picture is more nuanced, with nuclear and non-nuclear SnRK1 functions exhibiting seemingly opposing responses in the *tps5/6/7* mutant.

In the context of SnRK1 nuclear functions, our results show that loss of TPS5/6/7 reduces both p-ACC phosphorylation and SnRK1 nuclear localization. These findings appear to contradict two observations from Van Leene et al. (2022): First, that activation of SnRK1 target promoters in tobacco BY2 protoplasts was significantly reduced when cells co-transfected with SnRK1α1 and its activating kinase SnAK were additionally co-transfected with TPS5 or TPS7. Second, that TPS-II proteins reduced the nuclear accumulation of SnRK1α1-GFP in transiently transformed *N. benthamiana* leaves. This divergence likely reflects differences in the experimental systems used as cell-based or transient overexpression assays may not fully capture the physiological context and regulatory complexity present in intact plants. On the other hand, while constitutive loss-of-function mutants offer valuable systemic insights, their pleiotropic nature can trigger compensatory adaptations that

obscure direct regulatory mechanisms, as exemplified by the complex metabolic profile of the *tps5/6/7* mutant.

Regardless, our results show that the lack of TPS5/6/7 disrupts the nuclear-to-cytoplasmic distribution of SnRK1, as evidenced by reduced nuclear localization of SnRK1α1-GFP in the *tps5/6/7* mutant background (Figure 3.3A). This effect may occur through indirect mechanisms, possibly related to the overaccumulation of soluble sugars, as discussed in Chapter 3. Another, non-mutually exclusive mechanism underlying this redistribution may involve changes in SnRK1 complex composition – a factor not addressed in Van Leene's transient assays. Although SnRK1α1 can function independently of its regulatory subunits (Ramon et al. 2019), TPS-II proteins have been shown to interact with all SnRK1 subunits (Van Leene et al. 2022). This raises the possibility that, in their native context, TPS-II proteins influence the assembly of the SnRK1 complex. In their absence, as in the *tps5/6/7* mutant, alterations in complex composition – such as stronger association between SnRK1α1 and myristoylated β-subunits (Ramon et al. 2019) – could reduce SnRK1α1 nuclear localization and target gene induction. This could be tested, for example, through co-immunoprecipitation analyses to determine changes in SnRK1 complex assembly between Col-0 and *tps5/6/7* plants.

Although nuclear SnRK1 activity appears diminished in *tps5/6/7* seedlings, we cannot rule out a context-dependent increase that was not captured due to differences in timing or tissue specificity. Nonetheless, the rescue of root growth defects by *snrk1α* mutations suggests that elevated non-nuclear SnRK1 activity is the more likely driver of the growth impairment in this mutant. This is perhaps not surprising, given the well-established cytoplasmic functions of SnRK1, particularly in the phosphorylation/regulation of numerous proteins, including metabolic enzymes (Broeckx et al. 2016; Cho et al. 2016; Nukarinen et al. 2016) and TOR (Belda-Palazón et al. 2020, 2022). Interestingly, two independent studies showed that plants exposed to unexpectedly low irradiance for a single light period exhibited growth restriction the following day, even after normal light conditions were restored and sugar levels had increased (Moraes et al. 2019; Avidan et al. 2023). This response similarly correlated

with reduced nuclear SnRK1 activity and elevated non-nuclear SnRK1 activity at the end of the night (Avidan et al. 2023), further supporting the idea that the non-nuclear functions of SnRK1 may play a predominant role in mediating growth repression under certain contexts. However, despite our efforts, the specific non-nuclear SnRK1 activities driving the *tps5/6/7* phenotype remain unresolved and warrant further investigation. To directly test whether non-nuclear SnRK1 activity is enhanced in the *tps5/6/7* mutant, one approach would be to cross it with a cytosolic p-ACC reporter line (Avidan et al. 2023) and monitor phosphorylation of both nuclear and cytosolic reporters across the diel cycle and under stress conditions. Alternatively – or in parallel – crossing *tps5/6/7* with a Separation of Phases-based Activity Reporter of Kinase (SPARK) sensor could enable real-time, *in vivo* visualization of tissue-specific and dynamic changes in cytosolic SnRK1 activity (Safi et al. 2023).

However, while these approaches would provide valuable insight into the spatial and temporal dynamics of SnRK1 activity, they would likely yield only a broad overview with limited mechanistic resolution of the specific non-nuclear pathways or targets involved. Therefore, future research should also aim to dissect these mechanisms more deeply. One promising direction would be to investigate in further depth the interplay between SnRK1 and TOR in the *tps5/6/7* background, given their well-established antagonistic roles in growth regulation (Margalha et al. 2019; Artins et al. 2024) and recent evidence linking T6P to the coordinated inhibition of SnRK1 and activation of TOR (Morales-Herrera et al. 2023). This line of investigation is further motivated by our observation that, in *tps5/6/7* roots, both RPS6 phosphorylation and total RPS6 protein levels are substantially less responsive to sucrose supplementation than in Col-0, although the relative phosphorylation status of RPS6 did not provide clear evidence of altered TOR activity. It is important to note, however, that RPS6 phosphorylation is an indirect readout of TOR activity, and that while RPS6 expression is likely influenced by T6P (Avidan et al. 2024), its abundance may also be affected by other unresolved metabolic cues. Therefore, an inducible *tps5/6/7* knockdown, in which sugar and T6P levels initially remain unchanged, could provide clearer insights into TOR activity. Alternatively, more direct assays could be performed. First, TOR activity could be investigated using chemical inhibitors (e.g. AZD8055), measuring

primary root growth as a physiological readout (as in Belda-Palazón et al. 2020). If TOR signaling is already repressed in the *tps5/6/7* mutant, as we hypothesize, a reduced sensitivity to the inhibitor – reflected by attenuated root growth inhibition – would be expected. Second, TOR activity could be monitored by measuring the phosphorylation status of the direct TOR substrate, S6 kinase (S6K) or of RAPTOR1B, a core TOR complex component that interacts with and is phosphorylated by SnRK1α1 (Nukarinen et al. 2016; Belda-Palazón et al. 2020). Further supporting this approach, TPS-II proteins were recently shown to interact with FCS-like zinc finger (FLZ) proteins (Van Leene et al. 2022), which act as plant-specific scaffolds mediating the crosstalk between SnRK1 and TOR/RAPTOR1B (Jamsheer K et al. 2018b, 2018a; Feng et al. 2025). This raises the possibility that TPS-II proteins may influence growth either directly by modulating SnRK1 activity and/or indirectly, by affecting its interaction with TOR/RAPTOR1B through FLZ proteins.

Notably, an inducible *tps5/6/7* line would not only help clarify whether altered TOR signaling contributes to the growth restriction observed in the mutant but would also offer a powerful tool to dissect which SnRK1-related mechanisms are affected by loss of TPS5/6/7. While very early phosphorylation events may be difficult to capture due to the slower kinetics of inducible silencing, previous studies (e.g.,Nukarinen et al. 2016) have shown that phosphoproteomic profiling of inducible SnRK1 loss-of-function lines can reveal meaningful shifts in SnRK1 signaling. Similarly, inducible *tps5/6/7* silencing could enable medium-resolution, time-resolved phosphoproteomic and interactomic analyses (the latter contingent on SnRK1 being tagged) to identify key downstream SnRK1 responses before major compensatory changes emerge.

To further explore SnRK1-dependent mechanisms beyond TOR, and taking advantage of already available tools, an informative approach would be to immunoprecipitate SnRK1 from both Col-0 and *tps5/6/7* plants in the presence and absence of T6P. Subsequent MS/MS analysis of the pulled-down complexes could reveal differences in interacting proteins, including potential alterations in SnRK1 subunit assembly that may contribute to its altered subcellular localization and activity in the mutant, as proposed earlier in this discussion.

Taken together, the effects of TPS5/6/7 loss on SnRK1 signaling under both basal and stress-inducing conditions suggest that these proteins may physically sequester a specific pool of SnRK1 – likely defined by subcellular localization or association with distinct signaling complexes – rather than exerting global control over SnRK1 activity. Supporting this, TPS-II proteins have been shown to localize outside the nucleus when transiently expressed in tobacco leaves (Van Leene et al. 2022), a localization pattern we also confirmed for mCherry-tagged TPS7 in stable Arabidopsis lines (Chapter 3). These observations point to TPS-II proteins acting predominantly on a non-nuclear SnRK1 pool, which they may selectively sequester to perform two critical functions: under sucrose-replete conditions, TPS5/6/7 would maintain SnRK1 in an inactive state to prevent growth suppression, whereas during energy deficit, a decline in T6P levels would render this pool responsive, enabling its release and subsequent activation of SnRK1-dependent stress responses.

Interestingly, this mode of regulation resembles that of SnRK2 proteins, which selectively sequester a dedicated, ABA-responsive pool of SnRK1 to modulate its activity (Belda-Palazón et al. 2020, 2022). Together, these examples suggest plants have evolved an arsenal of context-specific SnRK1 regulators that differentially control distinct kinase pools to fine-tune signaling outputs. Moreover, in both cases, suppression of SnRK1 – whether via SnRK2s in response to ABA or via TPS-IIs in response to carbon status – is consistent with the view that SnRK1, unlike Snf1 and AMPK which are activated by low energy levels, is active by default and must be actively suppressed when energy and carbon supplies are abundant (Ramon et al. 2019).

4.5. TPS5/6/7 are required for proper sucrose-T6P coupling

Despite broad acceptance of the sucrose-T6P nexus model in explaining sucrose homeostasis, the mechanism by which rising sucrose levels drive T6P accumulation remains unresolved. Based on inhibitor studies in Arabidopsis, sucrose-induced T6P accumulation is transcription-independent but requires de novo protein

synthesis (Yadav et al. 2014). However, the protein(s) responsible for this response have yet to be identified. More recently, *tps1-1* complementation studies implicated TPS1 in this process (Fichtner et al. 2020). While *tps1-1* mutants complemented with either AtTPS1 or OtsA (under AtTPS1 regulatory elements) were rescued through embryogenesis, only the TPS1-complemented line maintained a strong correlation between T6P and sucrose. In contrast, T6P and sucrose levels correlated poorly in the OtsA-complemented line, indicating that functional properties of TPS1 apart from its catalytic activity are required for coupling sucrose to T6P (Fichtner et al. 2020). Meanwhile, SnRK1α has also been proposed to play a role in linking T6P levels to the sucrose status. Work by Peixoto et al. (2021), using SnRK1α gain- and loss-of-function mutants, showed that although T6P accumulation tracked diel sucrose dynamics, the relationship between the two was altered in the mutants. Specifically, *SnRK1α1-OE* plants accumulated disproportionately higher T6P levels than Col-0 for a given sucrose concentration, whereas *sesquiα2* mutants displayed the opposite trend. Presumably, this could reflect a compensatory adjustment of T6P to buffer changes in SnRK1α activity, though the underlying regulatory set points remain unclear.

Interestingly, in *tps5/6/7* mutants, T6P levels also increased disproportionately relative to sucrose (1.6-fold higher in shoots at EN), resembling the pattern observed in *SnRK1α1-OE* plants (1.4-fold higher in rosettes at EN) (Peixoto et al. 2021). Although diel cycle measurements will be needed to determine whether the sucrose-T6P relationship in *tps5/6/7* mutants is disrupted or shifted to a new state, the disproportionate increase in T6P relative to sucrose was consistent across all mutant tissues and became more pronounced under high light conditions, reaching up to 4.1-fold higher in shoots at EN. Consequently, T6P:sucrose ratios were elevated in the mutant across all tissues and conditions compared to Col-0. This raises the possibility that TPS5/6/7 might also contribute to the mechanism coupling sucrose to T6P, ensuring precise regulation of T6P synthesis and/or degradation to prevent overaccumulation. Alternatively, given that SnRK1α1 overexpression leads to elevated T6P levels (Peixoto et al. 2021), the increased T6P:sucrose ratio in *tps5/6/7* mutants may stem from deregulated SnRK1 activity.

Nevertheless, it is currently unclear whether and how the sucrose status is relayed via TPS5/6/7 to regulate T6P levels. It is possible that these proteins respond directly to sucrose or indirectly to other metabolic derivatives such as G6P and/or UDPG, which serve as precursors for T6P biosynthesis (Cabib and Leloir 1958; Avonce et al. 2006). If this is the case, the regulatory mechanism could involve modulation of TPS1 activity, changes in T6P turnover via TPP proteins, or indirect effects through crosstalk with SnRK1, potentially acting in concert. Among these, a role involving TPS-II-mediated regulation of TPP proteins appears less likely at present, given the lack of evidence for direct interaction between TPS-IIs and TPPs. In contrast, a role for TPS-IIs, including TPS5/6/7, in modulating TPS1 activity is supported by multiple observations, although direct experimental validation is still lacking. First, TPS-II proteins share conserved domain architecture with the yeast regulatory proteins TSL1 and TPS3 (non-catalytic subunits of the trehalose biosynthetic complex in *Saccharomyces cerevisiae*) (Avonce et al. 2010). These subunits are required for the stability and function of yeast TPS1, the sole catalytically active TPS in yeast (Reinders et al. 1997; Bell et al. 1998; Chen et al. 2022), suggesting that analogous regulatory interactions may exist in plants. Second, physical interactions between rice TPS-I and TPS-II proteins have been demonstrated using yeast two-hybrid and bimolecular fluorescence complementation assays (Zang et al. 2011), supporting the possibility of conserved protein-protein interactions. Third, *TPS5/6/7* promoters are active in the same phloem tissues where a GFP-TPS1 fusion protein localizes (Ramon et al. 2009; Fichtner et al. 2020), indicating overlapping expression domains that could permit functional interaction *in vivo*. Interestingly, complementation of the *tps1-1* mutant with a truncated variant of TPS1 lacking the N-terminal extension resulted in elevated T6P:sucrose ratios, largely driven by increased T6P (Fichtner et al. 2020). The N-terminal extension of TPS1 harbors a putative autoinhibitory domain, and mutations in this region have been shown to relieve inhibition, leading to increased TPS activity in yeast complementation assays (Van Dijck et al. 2002). These findings suggest that the N-terminal region contributes to regulating TPS1 activity and balancing T6P production with available sucrose,

potentially providing a mechanism through which interacting proteins such as TPS5/6/7 could exert control.

Given the increased T6P:sucrose ratios observed in both *tps5/6/7* and *SnRK1α1-OE* lines, it is also plausible that SnRK1 and TPS5/6/7 operate in a feedback loop to maintain T6P homeostasis, with SnRK1 promoting T6P synthesis and TPS5/6/7 acting to prevent its overaccumulation. A simple mechanistic framework could involve T6P-sensitive formation of TPS5/6/7-SnRK1 complexes that modulate TPS1 activity in response to the cellular sugar status. In this model, elevated T6P levels under high sucrose conditions would promote complex formation between TPS5/6/7 and SnRK1, thereby sequestering SnRK1 and reducing its capacity to activate TPS1. Conversely, when sucrose and T6P levels decline, these complexes would dissociate, freeing SnRK1 to enhance TPS1 activity, although T6P production would remain limited until the availability of its substrates, G6P and UDPG, both regulated by sucrose, increases. Such a model would also be consistent with the elevated T6P:sucrose ratios observed in *SnRK1α1-OE* plants (Peixoto et al. 2021), where the increased abundance of SnRK1 may exceed the buffering capacity of TPS5/6/7 proteins. As a result, the excess unsequestered SnRK1 could lead to greater activation of TPS1, driving higher T6P synthesis. While SnRK1-dependent phosphorylation of TPS1 has not yet been reported experimentally, predictive analysis using the *in silico* tool PhosMoS (Carianopol et al. 2020) identifies multiple potential SnRK1 target sites within TPS1, supporting the plausibility of this regulatory interaction. It is important to note, however, that while this model provides a plausible framework for regulating T6P homeostasis in response to internal sugar status, it does not address how sucrose levels are initially sensed or transduced.

4.6. Concluding remarks

The functions of TPS-II proteins have remained puzzling due to their non-catalytic nature (Vogel et al. 2001; Ramon et al. 2009; Vandesteene et al. 2010; Delorge et al. 2015), yet their strong evolutionary conservation and indeed family

expansion in the green lineage (Avonce et al. 2006; Yang et al. 2012) argues for fundamental biological importance. We propose these proteins function as regulatory nodes that relay T6P signals to SnRK1 to modulate its activity, thereby coordinating metabolic and growth responses. Three lines of evidence support this model: (1) the metabolic and phenotypic traits of *tps5/6/7* mutants, (2) the SnRK1-dependence of these phenotypes, and (3) the specific, dose-dependent T6P enhancement of TPS-II–SnRK1α1 interactions.

Remarkably, T6P-enhanced interactions occurred with all TPS-II isoforms except TPS5 (see Chapter 3 Discussion for details), revealing a conserved molecular mechanism across the family. However, the inability of TPS8-10 to fully compensate for the loss of TPS5-7 suggests additional functional specialization, consistent with the tightly regulated expression patterns and stimulus-specific responsiveness of TPS-II genes (Ramon et al. 2009; Tian et al. 2019; Persyn et al. 2024; Vishal et al. 2024). This differential regulation suggests that, while all TPS-II proteins share the core role of T6P-SnRK1 signal transduction, individual members have likely diversified to modulate SnRK1 through temporal (developmental stage-specific) and spatial (tissue-specific) control, creating a responsive signaling network that integrates both metabolic status (via T6P) and external cues.

Further elucidating the precise roles of TPS-II proteins across tissues, developmental stages, and environmental conditions will be essential for a comprehensive understanding of T6P-SnRK1 signaling. Such insights are particularly valuable given the translational potential of this pathway for crop improvement (Paul et al. 2018; Griffiths et al. 2025). Indeed, modulation of T6P signaling, whether via transgenic approaches, natural genetic variation, or chemical intervention with plant-permeable T6P analogs, has been associated with improved yield and stress resilience in major cereals (Bailey-Serres et al. 2019; Paul et al. 2020). Additionally, several TPS-II genes have been linked to source- and sink-related yield traits in wheat and maize (Hufford et al. 2012; Lyra et al. 2021). Thus, integrating TPS-II gene manipulation with chemical modulation of T6P could allow precise control of the T6P-

SnRK1 pathway, offering a powerful strategy to enhance crop resilience and yield stability in variable environments.

Overall, this thesis advances our understanding of how plants integrate carbon status with growth regulation by uncovering the regulatory roles of catalytically inactive TPS-II proteins within the T6P-SnRK1 signaling pathway. These findings lay the groundwork for future studies to explore the molecular mechanisms and physiological relevance of this network across plant tissues, developmental stages, and environmental conditions.

4.7. References

Amthor JS, Bar-Even A, Hanson AD, Millar AH, Stitt M, Sweetlove LJ, and Tyerman SD. Engineering Strategies to Boost Crop Productivity by Cutting Respiratory Carbon Loss. Plant Cell. 2019:**31**(2):297–314. https://doi.org/10.1105/tpc.18.00743

Artins A, Martins MCM, Meyer C, Fernie AR, and Caldana C. Sensing and regulation of C and N metabolism – novel features and mechanisms of the TOR and SnRK1 signaling pathways. The Plant Journal. 2024:**118**(5):1268–1280. https://doi.org/10.1111/tpj.16684

Avidan O, Martins MCM, Feil R, Lohse M, Giorgi FM, Schlereth A, Lunn JE, and Stitt M. Direct and indirect responses of the Arabidopsis transcriptome to an induced increase in trehalose 6-phosphate. Plant Physiol. 2024:**196**(1):409–431. https://doi.org/10.1093/plphys/kiae196

Avidan O, Moraes TA, Mengin V, Feil R, Rolland F, Stitt M, and Lunn JE. In vivo protein kinase activity of SnRK1 fluctuates in Arabidopsis rosettes during light-dark cycles. Plant Physiol. 2023:**192**(1):387–408. https://doi.org/10.1093/plphys/kiad066

Avonce N, Mendoza-Vargas A, Morett E, and Iturriaga G. Insights on the evolution of trehalose biosynthesis. BMC Evol Biol. 2006:**6**(1):109. https://doi.org/10.1186/1471-2148-6-109

Avonce N, Wuyts J, Verschooten K, Vandesteene L, and Van Dijck P. The Cytophaga hutchinsonii ChTPSP: First Characterized Bifunctional TPS–TPP Protein as Putative Ancestor of All Eukaryotic Trehalose Biosynthesis Proteins. Mol Biol Evol. 2010:**27**(2):359–369. https://doi.org/10.1093/molbev/msp241

Azcón-Bieto J, Lambers H, and Day DA. Effect of Photosynthesis and Carbohydrate Status on Respiratory Rates and the Involvement of the Alternative Pathway in Leaf Respiration. Plant Physiol. 1983:**72**(3):598–603. https://doi.org/10.1104/pp.72.3.598

Baena-González E and Lunn JE. SnRK1 and trehalose 6-phosphate – two ancient pathways converge to regulate plant metabolism and growth. Curr Opin Plant Biol. 2020. https://doi.org/10.1016/j.pbi.2020.01.010

Baena-González E, Rolland F, Thevelein JM, and Sheen J. A central integrator of transcription networks in plant stress and energy signalling. Nature. 2007:**448**(7156):938–942. https://doi.org/10.1038/nature06069

Bailey-Serres J, Parker JE, Ainsworth EA, Oldroyd GED, and Schroeder JI. Genetic strategies for improving crop yields. Nature. 2019:**575**(7781):109–118. https://doi.org/10.1038/s41586-019-1679-0

Belda-Palazón B, Adamo M, Valerio C, Ferreira LJ, Confraria A, Reis-Barata D, Rodrigues A, Meyer C, Rodriguez PL, and Baena-González E. A dual function of SnRK2 kinases in the regulation of SnRK1 and plant growth. Nat Plants. 2020:**6**(11):1345–1353. https://doi.org/10.1038/s41477-020-00778-w

Belda-Palazón B, Costa M, Beeckman T, Rolland F, and Baena-González E. ABA represses TOR and root meristem activity through nuclear exit of the SnRK1 kinase. Proceedings of the National Academy of Sciences. 2022:**119**(28). https://doi.org/10.1073/pnas.2204862119

Bell W, Sun W, Hohmann S, Wera S, Reinders A, De Virgilio C, Wiemken A, and Thevelein JM. Composition and Functional Analysis of the Saccharomyces cerevisiae Trehalose Synthase Complex. Journal of Biological Chemistry. 1998:**273**(50):33311–33319. https://doi.org/10.1074/jbc.273.50.33311

Blanford J, Zhai Z, Baer MD, Guo G, Liu H, Liu Q, Raugei S, and Shanklin J. Molecular mechanism of trehalose 6-phosphate inhibition of the plant metabolic sensor kinase SnRK1. Sci Adv. 2024:**10**(20). https://doi.org/10.1126/sciadv.adn0895

Broeckx T, Hulsmans S, and Rolland F. The plant energy sensor: evolutionary conservation and divergence of SnRK1 structure, regulation, and function. J Exp Bot. 2016:**67**(22):6215–6252. https://doi.org/10.1093/jxb/erw416

Cabib E and Leloir LF. The biosynthesis of trehalose phosphate. American Society for Biochemistry and Molecular Biology. 1958.

Carianopol CS, Chan AL, Dong S, Provart NJ, Lumba S, and Gazzarrini S. An abscisic acid-responsive protein interaction network for sucrose non-fermenting

related kinase1 in abiotic stress response. Commun Biol. 2020:**3**(1):145. https://doi.org/10.1038/s42003-020-0866-8

Chen A, Vargas-Smith J, Tapia H, and Gibney PA. Characterizing phenotypic diversity of trehalose biosynthesis mutants in multiple wild strains of Saccharomyces cerevisiae. G3 (Bethesda). 2022:**12**(11). https://doi.org/10.1093/g3journal/jkac196

Chen L, Su Z-Z, Huang L, Xia F-N, Qi H, Xie L-J, Xiao S, and Chen Q-F. The AMP-Activated Protein Kinase KIN10 Is Involved in the Regulation of Autophagy in Arabidopsis. Front Plant Sci. 2017:**8**. https://doi.org/10.3389/fpls.2017.01201

Cho HY, Wen TN, Wang YT, and Shih MC. Quantitative phosphoproteomics of protein kinase SnRK1 regulated protein phosphorylation in Arabidopsis under submergence. J Exp Bot. 2016:**67**(9):2745–2760. https://doi.org/10.1093/jxb/erw107

Debast S, Nunes-Nesi A, Hajirezaei MR, Hofmann J, Sonnewald U, Fernie AR, and Börnke F. Altering trehalose-6-phosphate content in transgenic potato tubers affects tuber growth and alters responsiveness to hormones during sprouting. Plant Physiol. 2011:**156**(4):1754–71. https://doi.org/10.1104/pp.111.179903

Delatte TL, Sedijani P, Kondou Y, Matsui M, de Jong GJ, Somsen GW, Wiese-Klinkenberg A, Primavesi LF, Paul MJ, and Schluepmann H. Growth Arrest by Trehalose-6-Phosphate: An Astonishing Case of Primary Metabolite Control over Growth by Way of the SnRK1 Signaling Pathway. Plant Physiol. 2011:**157**(1):160–174. https://doi.org/10.1104/pp.111.180422

Delorge I, Figueroa CM, Feil R, Lunn JE, and Van Dijck P. Trehalose-6-phosphate synthase 1 is not the only active TPS in Arabidopsis thaliana. Biochemical Journal. 2015. https://doi.org/10.1042/bj20141322

dos Anjos L, Pandey PK, Moraes TA, Feil R, Lunn JE, and Stitt M. Feedback regulation by trehalose 6-phosphate slows down starch mobilization below the rate that would exhaust starch reserves at dawn in Arabidopsis leaves. Plant Direct. 2018. https://doi.org/10.1002/pld3.78

Feng L, Li X, Zheng X-A, Zheng Z, Liu Q-R, Liu C, Zhu Q-L, Shen W, Yang C, Li H, et al. SnRK1 and TOR: central regulators of autophagy in plant energy stress responses. aBIOTECH. 2025. https://doi.org/10.1007/s42994-025-00218-3

Fernie AR, Bachem CWB, Helariutta Y, Neuhaus HE, Prat S, Ruan Y-L, Stitt M, Sweetlove LJ, Tegeder M, Wahl V, et al. Synchronization of developmental, molecular and metabolic aspects of source–sink interactions. Nat Plants. 2020:**6**(2):55–66. https://doi.org/10.1038/s41477-020-0590-x

Fichtner F, Barbier FF, Feil R, Watanabe M, Annunziata MG, Chabikwa TG, Höfgen R, Stitt M, Beveridge CA, and Lunn JE. Trehalose 6-phosphate is involved in triggering axillary bud outgrowth in garden pea (*Pisum sativum* L.). The Plant Journal. 2017:**92**(4):611–623. https://doi.org/10.1111/tpj.13705

Fichtner F and Lunn JE. The Role of Trehalose 6-Phosphate (Tre6P) in Plant Metabolism and Development. Annu Rev Plant Biol. 2021:**72**(1):737–760. https://doi.org/10.1146/annurev-arplant-050718-095929

Fichtner F, Olas JJ, Feil R, Watanabe M, Krause U, Hoefgen R, Stitt M, and Lunn JE. Functional Features of TREHALOSE-6-PHOSPHATE SYNTHASE1, an Essential Enzyme in Arabidopsis. Plant Cell. 2020:**32**(6):1949–1972. https://doi.org/10.1105/tpc.19.00837

Figueroa CM, Feil R, Ishihara H, Watanabe M, Kölling K, Krause U, Höhne M, Encke B, Plaxton WC, Zeeman SC, et al. Trehalose 6–phosphate coordinates organic and amino acid metabolism with carbon availability. The Plant Journal. 2016:**85**(3):410–423. https://doi.org/10.1111/tpj.13114

Figueroa CM and Lunn JE. A Tale of Two Sugars: Trehalose 6-Phosphate and Sucrose. Plant Physiol. 2016:**172**(1):7–27. https://doi.org/10.1104/pp.16.00417

Gibon Y, Usadel B, Blaesing OE, Kamlage B, Hoehne M, Trethewey R, and Stitt M. Integration of metabolite with transcript and enzyme activity profiling during diurnal cycles in Arabidopsis rosettes. Genome Biol. 2006:**7**(8):R76. https://doi.org/10.1186/gb-2006-7-8-R76

Göbel M and Fichtner F. Functions of sucrose and trehalose 6-phosphate in controlling plant development. J Plant Physiol. 2023:**291**:154140. https://doi.org/10.1016/j.jplph.2023.154140

Goldstein DS and McEwen B. Allostasis, Homeostats, and the Nature of Stress. Stress. 2002:**5**(1):55–58. https://doi.org/10.1080/102538902900012345

Griffiths CA, Xue X, Miret JA, Salvagiotti F, Acevedo-Siaca LG, Gimeno J, Reynolds MP, Hassall KL, Halsey K, Puranik S, et al. Membrane-permeable trehalose 6-phosphate precursor spray increases wheat yields in field trials. Nat Biotechnol. 2025. https://doi.org/10.1038/s41587-025-02611-1

Hasanuzzaman M, Bhuyan MHMB, Anee TI, Parvin K, Nahar K, Mahmud J Al, and Fujita M. Regulation of Ascorbate-Glutathione Pathway in Mitigating Oxidative Damage in Plants under Abiotic Stress. Antioxidants. 2019:**8**(9):384. https://doi.org/10.3390/antiox8090384

Huang X, Zheng C, Liu F, Yang C, Zheng P, Lu X, Tian J, Chung T, Otegui MS, Xiao S, et al. Genetic Analyses of the Arabidopsis ATG1 Kinase Complex Reveal Both Kinase-Dependent and Independent Autophagic Routes during Fixed-Carbon Starvation. Plant Cell. 2019:**31**(12):2973–2995. https://doi.org/10.1105/tpc.19.00066

Hufford MB, Xu X, van Heerwaarden J, Pyhäjärvi T, Chia J-M, Cartwright RA, Elshire RJ, Glaubitz JC, Guill KE, Kaeppler SM, et al. Comparative population genomics of maize domestication and improvement. Nat Genet. 2012:**44**(7):808–811. https://doi.org/10.1038/ng.2309

Iglesias-Bartolomé R, González CA, and Kenis JD. Nitrate reductase dephosphorylation is induced by sugars and sugar-phosphates in corn leaf segments. Physiol Plant. 2004:**122**(1):62–67. https://doi.org/10.1111/j.1399-3054.2004.00375.x

Ishihara H, Alseekh S, Feil R, Perera P, George GM, Niedźwiecki P, Arrivault S, Zeeman SC, Fernie AR, Lunn JE, et al. Rising rates of starch degradation during daytime and trehalose 6-phosphate optimize carbon availability. Plant Physiol. 2022:**189**(4):1976–2000. https://doi.org/10.1093/plphys/kiac162

Jamsheer K M, Sharma M, Singh D, Mannully CT, Jindal S, Shukla BN, and Laxmi A. FCS-like zinc finger 6 and 10 repress SnRK1 signalling in Arabidopsis. The Plant Journal. 2018a:**94**(2):232–245. https://doi.org/10.1111/tpj.13854

Jamsheer K M, Shukla BN, Jindal S, Gopan N, Mannully CT, and Laxmi A. The FCS-like zinc finger scaffold of the kinase SnRK1 is formed by the coordinated actions of the FLZ domain and intrinsically disordered regions. J Biol Chem. 2018b:**293**(34):13134–13150. https://doi.org/10.1074/jbc.RA118.002073

Jossier M, Bouly JP, Meimoun P, Arjmand A, Lessard P, Hawley S, Grahame Hardie D, and Thomas M. SnRK1 (SNF1-related kinase 1) has a central role in sugar and ABA signalling in Arabidopsis thaliana. Plant Journal. 2009:**59**(2):316–328. https://doi.org/10.1111/j.1365-313X.2009.03871.x

Kaiser WM, Weiner H, Kandlbinder A, Tsai C, Rockel P, Sonoda M, and Planchet E. Modulation of nitrate reductase: some new insights, an unusual case and a potentially important side reaction. J Exp Bot. 2002:**53**(370):875–882. https://doi.org/10.1093/jexbot/53.370.875

Khan MIR, Jalil SU, Chopra P, Chhillar H, Ferrante A, Khan NA, and Ansari MI. Role of GABA in plant growth, development and senescence. Plant Gene. 2021:**26**:100283. https://doi.org/10.1016/j.plgene.2021.100283

Lunn JE. Gene families and evolution of trehalose metabolism in plants. Functional Plant Biology. 2007:**34**(6):550. https://doi.org/10.1071/FP06315

Lunn JE. Sucrose Metabolism. In. Encyclopedia of Life Sciences. (Wiley), pp. 1–9. https://doi.org/10.1002/9780470015902.a0021259.pub2

Lunn JE, Feil R, Hendriks JHM, Gibon Y, Morcuende R, Osuna D, Scheible W-R, Carillo P, Hajirezaei M-R, and Stitt M. Sugar-induced increases in trehalose 6-phosphate are correlated with redox activation of ADPglucose pyrophosphorylase and higher rates of starch synthesis in *Arabidopsis thaliana*. Biochemical Journal. 2006:**397**(1):139–148. https://doi.org/10.1042/BJ20060083

Lyra DH, Griffiths CA, Watson A, Joynson R, Molero G, Igna A, Hassani-Pak K, Reynolds MP, Hall A, and Paul MJ. Gene-based mapping of trehalose biosynthetic pathway genes reveals association with source- and sink-related yield traits in a spring wheat panel. Food Energy Secur. 2021:**10**(3). https://doi.org/10.1002/fes3.292

Mair A, Pedrotti L, Wurzinger B, Anrather D, Simeunovic A, Weiste C, Valerio C, Dietrich K, Kirchler T, Nägele T, et al. SnRK1-triggered switch of bZIP63 dimerization mediates the low-energy response in plants. Elife. 2015:**4**. https://doi.org/10.7554/eLife.05828

Margalha L, Confraria A, and Baena-González E. SnRK1 and TOR: modulating growth–defense trade-offs in plant stress responses. J Exp Bot. 2019:**70**(8):2261–2274. https://doi.org/10.1093/jxb/erz066

Martins MCM, Hejazi M, Fettke J, Steup M, Feil R, Krause U, Arrivault S, Vosloh D, Figueroa CM, Ivakov A, et al. Feedback Inhibition of Starch Degradation in Arabidopsis Leaves Mediated by Trehalose 6-Phosphate. Plant Physiol. 2013. https://doi.org/10.1104/pp.113.226787

McEwen BS. Protection and Damage from Acute and Chronic Stress: Allostasis and Allostatic Overload and Relevance to the Pathophysiology of Psychiatric Disorders. Ann N Y Acad Sci. 2004:**1032**(1):1–7. https://doi.org/10.1196/annals.1314.001

McEwen BS and Wingfield JC. The concept of allostasis in biology and biomedicine. Horm Behav. 2003:**43**(1):2–15. https://doi.org/10.1016/S0018-506X(02)00024-7

McMichael Jr RW, Bachmann M, and Huber SC. Spinach Leaf Sucrose-Phosphate Synthase and Nitrate Reductase Are Phosphorylated/Inactivated by Multiple Protein Kinases in Vitro. Plant Physiol. 1995:**108**(3):1077–1082. https://doi.org/10.1104/pp.108.3.1077

Miret JA, Griffiths CA, and Paul MJ. Sucrose homeostasis: Mechanisms and opportunity in crop yield improvement. J Plant Physiol. 2024:**294**:154188. https://doi.org/10.1016/j.jplph.2024.154188

Moorhead G, Douglas P, Morrice N, Scarabel M, Aitken A, and MacKintosh C. Phosphorylated nitrate reductase from spinach leaves is inhibited by 14-3-3 proteins and activated by fusicoccin. Current Biology. 1996:**6**(9):1104–1113. https://doi.org/10.1016/S0960-9822(02)70677-5

Moraes TA, Mengin V, Annunziata MG, Encke B, Krohn N, Höhne M, and Stitt M. Response of the Circadian Clock and Diel Starch Turnover to One Day of Low Light or Low CO_2. Plant Physiol. 2019:**179**(4):1457–1478. https://doi.org/10.1104/pp.18.01418

Morales-Herrera S, Jourquin J, Coppé F, Lopez-Galvis L, De Smet T, Safi A, Njo M, Griffiths CA, Sidda JD, Mccullagh JSO, et al. Trehalose-6-phosphate signaling regulates lateral root formation in Arabidopsis thaliana. Proceedings of the National Academy of Sciences. 2023:**120**(40). https://doi.org/10.1073/pnas.2302996120

Nukarinen E, Ngele T, Pedrotti L, Wurzinger B, Mair A, Landgraf R, Börnke F, Hanson J, Teige M, Baena-Gonzalez E, et al. Quantitative phosphoproteomics reveals the role of the AMPK plant ortholog SnRK1 as a metabolic master regulator under energy deprivation. Sci Rep. 2016:**6**(August):1–19. https://doi.org/10.1038/srep31697

Nunes C, Primavesi LF, Patel MK, Martinez-Barajas E, Powers SJ, Sagar R, Fevereiro PS, Davis BG, and Paul MJ. Inhibition of SnRK1 by metabolites: Tissue-dependent effects and cooperative inhibition by glucose 1-phosphate in combination with trehalose 6-phosphate. Plant Physiology and Biochemistry. 2013:**63**:89–98. https://doi.org/10.1016/j.plaphy.2012.11.011

Paul MJ, Gonzalez-Uriarte A, Griffiths CA, and Hassani-Pak K. The Role of Trehalose 6-Phosphate in Crop Yield and Resilience. Plant Physiol. 2018:**177**(1):12–23. https://doi.org/10.1104/pp.17.01634

Paul MJ, Watson A, and Griffiths CA. Linking fundamental science to crop improvement through understanding source and sink traits and their integration for yield enhancement. J Exp Bot. 2020:**71**(7):2270–2280. https://doi.org/10.1093/jxb/erz480

Pedrotti L, Weiste C, Nägele T, Wolf E, Lorenzin F, Dietrich K, Mair A, Weckwerth W, Teige M, Baena-González E, et al. Snf1-RELATED KINASE1-Controlled C/S_1-bZIP Signaling Activates Alternative Mitochondrial Metabolic Pathways to Ensure

Plant Survival in Extended Darkness. Plant Cell. 2018:**30**(2):495–509. https://doi.org/10.1105/tpc.17.00414

Peixoto B, Moraes TA, Mengin V, Margalha L, Vicente R, Feil R, Höhne M, Sousa AGG, Lilue J, Stitt M, et al. Impact of the SnRK1 protein kinase on sucrose homeostasis and the transcriptome during the diel cycle. Plant Physiol. 2021:**187**(3):1357–1373. https://doi.org/10.1093/plphys/kiab350

Persyn F, Smagghe W, Eeckhout D, Mertens T, Smorscek T, De Winne N, Persiau G, Van De Slijke E, Crepin N, Gadeyne A, et al. A Nitrogen-specific Interactome Analysis Sheds Light on the Role of the SnRK1 and TOR Kinases in Plant Nitrogen Signaling. Molecular & Cellular Proteomics. 2024:**23**(10):100842. https://doi.org/10.1016/j.mcpro.2024.100842

Ramon M, Dang TVT, Broeckx T, Hulsmans S, Crepin N, Sheen J, and Rolland F. Default Activation and Nuclear Translocation of the Plant Cellular Energy Sensor SnRK1 Regulate Metabolic Stress Responses and Development. Plant Cell. 2019:**31**(7):1614–1632. https://doi.org/10.1105/tpc.18.00500

Ramon M, De Smet I, Vandesteene L, Naudts M, Leyman B, Van Dijck P, Rolland F, Beeckman T, and Thevelein JM. Extensive expression regulation and lack of heterologous enzymatic activity of the Class II trehalose metabolism proteins from Arabidopsis thaliana. Plant Cell Environ. 2009. https://doi.org/10.1111/j.1365-3040.2009.01985.x

Reinders A, Bürckert N, Hohmann S, Thevelein JM, Boller T, Wiemken A, and De Virgilio C. Structural analysis of the subunits of the trehalose-6-phosphate synthase/phosphatase complex in *Saccharomyces cerevisiae* and their function during heat shock. Mol Microbiol. 1997:**24**(4):687–696. https://doi.org/10.1046/j.1365-2958.1997.3861749.x

Renzetti M, Funck D, and Trovato M. Proline and ROS: A Unified Mechanism in Plant Development and Stress Response? Plants (Basel). 2024:**14**(1). https://doi.org/10.3390/plants14010002

Rhoads DM, Umbach AL, Subbaiah CC, and Siedow JN. Mitochondrial Reactive Oxygen Species. Contribution to Oxidative Stress and Interorganellar Signaling. Plant Physiol. 2006:**141**(2):357–366. https://doi.org/10.1104/pp.106.079129

Safi A, Smagghe W, Gonçalves A, Wang Q, Xu K, Fernandez AI, Cappe B, Riquet FB, Mylle E, Eeckhout D, et al. Phase separation-based visualization of protein–protein interactions and kinase activities in plants. Plant Cell. 2023:**35**(9):3280–3302. https://doi.org/10.1093/plcell/koad188

Sathee L, R S, Barman D, Adavi SB, Jha SK, and Chinnusamy V. Nitrogen at the crossroads of light: integration of light signalling and plant nitrogen metabolism. J Exp Bot. 2025:**76**(3):803–818. https://doi.org/10.1093/jxb/erae437

Schluepmann H, Berke L, and Sanchez-Perez GF. Metabolism control over growth: a case for trehalose-6-phosphate in plants. J Exp Bot. 2012:**63**(9):3379–3390. https://doi.org/10.1093/jxb/err311

Schluepmann H, van Dijken A, Aghdasi M, Wobbes B, Paul M, and Smeekens S. Trehalose Mediated Growth Inhibition of Arabidopsis Seedlings Is Due to Trehalose-6-Phosphate Accumulation. Plant Physiol. 2004:**135**(2):879–890. https://doi.org/10.1104/pp.104.039503

Schluepmann H, Pellny T, van Dijken A, Smeekens S, and Paul M. Trehalose 6-phosphate is indispensable for carbohydrate utilization and growth in Arabidopsis thaliana. Proceedings of the National Academy of Sciences. 2003. https://doi.org/10.1073/pnas.1132018100

Smith AM and Stitt M. Coordination of carbon supply and plant growth. Plant Cell Environ. 2007. https://doi.org/10.1111/j.1365-3040.2007.01708.x

Sonmez MC, Ozgur R, and Uzilday B. Reactive oxygen species: Connecting eustress, hormesis, and allostasis in plants. Plant Stress. 2023:**8**:100164. https://doi.org/10.1016/j.stress.2023.100164

Tian L, Xie Z, Lu C, Hao X, Wu S, Huang Y, Li D, and Chen L. The trehalose-6-phosphate synthase TPS5 negatively regulates ABA signaling in Arabidopsis thaliana. Plant Cell Rep. 2019:**38**(8):869–882. https://doi.org/10.1007/s00299-019-02408-y

Vandesteene L, Ramon M, Le Roy K, Van Dijck P, and Rolland F. A single active trehalose-6-P synthase (TPS) and a family of putative regulatory TPS-like proteins in arabidopsis. Mol Plant. 2010. https://doi.org/10.1093/mp/ssp114

Van Dijck P, Mascorro-Gallardo JO, De Bus M, Royackers K, Iturriaga G, and Thevelein JM. Truncation of Arabidopsis thaliana and Selaginella lepidophylla trehalose-6-phosphate synthase unlocks high catalytic activity and supports high trehalose levels on expression in yeast. Biochem J. 2002:**366**(Pt 1):63–71. https://doi.org/10.1042/BJ20020517

Van Leene J, Eeckhout D, Gadeyne A, Matthijs C, Han C, De Winne N, Persiau G, Van De Slijke E, Persyn F, Mertens T, et al. Mapping of the plant SnRK1 kinase signalling network reveals a key regulatory role for the class II T6P synthase-like

proteins. Nat Plants. 2022:**8**(11):1245–1261. https://doi.org/10.1038/s41477-022-01269-w

Vishal B, Krishnamurthy P, and Kumar PP. Arabidopsis class II TPS controls root development and confers salt stress tolerance through enhanced hydrophobic barrier deposition. Plant Cell Rep. 2024:**43**(5):115. https://doi.org/10.1007/s00299-024-03215-w

Vogel G, Fiehn O, Jean-Richard-dit-Bressel L, Boller T, Wiemken A, Aeschbacher RA, and Wingler A. Trehalose metabolism in Arabidopsis: occurrence of trehalose and molecular cloning and characterization of trehalose-6-phosphate synthase homologues. J Exp Bot. 2001:**52**(362):1817–1826. https://doi.org/10.1093/jexbot/52.362.1817

Yadav UP, Ivakov A, Feil R, Duan GY, Walther D, Giavalisco P, Piques M, Carillo P, Hubberten HM, Stitt M, et al. The sucrose-trehalose 6-phosphate (Tre6P) nexus: Specificity and mechanisms of sucrose signalling by. J Exp Bot. 2014. https://doi.org/10.1093/jxb/ert457

Yang H-L, Liu Y-J, Wang C-L, and Zeng Q-Y. Molecular evolution of trehalose-6-phosphate synthase (TPS) gene family in Populus, Arabidopsis and rice. PLoS One. 2012:**7**(8):e42438. https://doi.org/10.1371/journal.pone.0042438

Zacharaki V, Ponnu J, Crepin N, Langenecker T, Hagmann J, Skorzinski N, Musialak-Lange M, Wahl V, Rolland F, and Schmid M. Impaired KIN10 function restores developmental defects in the *Arabidopsis trehalose 6-phosphate synthase1 (tps1)* mutant. New Phytologist. 2022:**235**(1):220–233. https://doi.org/10.1111/nph.18104

Zang B, Li H, Li W, Deng XW, and Wang X. Analysis of trehalose-6-phosphate synthase (TPS) gene family suggests the formation of TPS complexes in rice. Plant Mol Biol. 2011:**76**(6):507–522. https://doi.org/10.1007/s11103-011-9781-1

Zhai Z, Keereetaweep J, Liu H, Feil R, Lunn JE, and Shanklin J. Trehalose 6-Phosphate Positively Regulates Fatty Acid Synthesis by Stabilizing WRINKLED1. Plant Cell. 2018:**30**(10):2616–2627. https://doi.org/10.1105/tpc.18.00521

Zhang Y, Primavesi LF, Jhurreea D, Andralojc PJ, Mitchell RAC, Powers SJ, Schluepmann H, Delatte T, Wingler A, and Paul MJ. Inhibition of SNF1-Related Protein Kinase1 Activity and Regulation of Metabolic Pathways by Trehalose-6-Phosphate. Plant Physiol. 2009:**149**(4):1860–1871. https://doi.org/10.1104/pp.108.133934